THE DIRECT AND INDIRECT TRANSMISSION OF VIBRATIONAL ENERGY IN BUILDING STRUCTURES

A THESIS SUBMITTED FOR THE DEGREE OF

DOCTOR OF PHILOSOPHY

IN THE UNIVERSITY OF ASTON IN BIRMINGHAM

BARRY MARSHALL GIBBS, BSc MA

The Department of Building

1974

To my father and the

memory of my mother

SUMMARY

A description is given of an alternative method of analysis of noise transmission in buildings. This method incorporates power flow techniques and has the advantage in that a unified approach is possible to both the direct and indirect transmission paths. The method is therefore equally applicable to transmission between rooms which are adjacent or several rooms or floors apart. The first configuration only lies within the range of classical theories.

In this analysis, the building is regarded as an assembly of plate elements. Vibrational energy flows to and from each plate across common structural junctions in a manner analogous to heat transfer between bodies at different temperatures, and can also flow to and from the enclosed air volumes. The solution of sets of simultaneous energy-balance equations gives the steady-state vibrational energy of each plate at a structural junction. The pressure wave energy, generated within a room by plate (or wall) vibrations, is also predicted.

The vibrational energies are predicted from the modal density, loss factor, coupling loss factor, and radiation loss factors, which are assessed theoretically and experimentally. Numerical calculations, involving a computer, yield values of the transmission coefficients of bending, longitudinal, and transverse waves at cross-junctions, T-junctions and corners of reinforced concrete plates.

The theory is compared with measurements involving quarter-scale models over a frequency range of measurement of 400 Hz - 12.5 KHz. Power-flow theory can be used in the mid and high frequencies, but at low frequencies, modal densities become too small.

Investigations are made on the effect of increasing the dissipative loss factor of plates by means of a layer of sand-bitumin mixture.

In measurements on the transmission between two rectangular rooms sharing one junction, agreement with theory is found except at low frequencies and a simplified theory, in which only bending wave transmissions are considered, gives adequate agreement with experiment.

INDEX

ACKNOWLEDGEMENTS

The author wishes to express his deep appreciation of the help given by Dr C L S Gilford in this project and in the preparation of the thesis; for his inductive attitude, constant involvement, and advice given throughout long discussions. Gratitude is also expressed to Professor A W Pratt for the interest displayed and encouragement given.

Members of the technical staff gave valuable assistance in the preparation of experiments; Mr B Bull, Mr R Davis, and Mr A Stratford in the concrete laboratory, Mr W Gibbons and Mr R Newman in the wood-work shop, and Mr E Parsons and Mr S Tandy in the metal-work shop.

Thanks are given to Mr M Clark and Mr M Ellett for the expertise and enthusiasm displayed in the acoustics laboratory, to Mr D Hill for the preparation of the photographic plates and to Miss L Averall for typing this thesis.

The work was carried out during a Research Assistantship in the Department of Building.

CHAPTER 1

SOUND TRANSMISSION IN BUILDINGS

1.1 Introduction

In the development of new building materials and constructional methods, priority is usually given to the increase of the ratio of mechanical strength to weight of the structural components in the building. This improvement is often, unfortunately, allied to a decrease in desirable acoustical characteristics. Pre-stressed concrete, although stronger than that cast 'in situ', is less efficient in absorbing vibrational energy (Putt 1970). Sounds are thus more readily propagated throughout the structure. High rise buildings can be considered as a two or three dimensional array of rooms, any one of which can contain the source of noise. Noise is defined as undesired sound.

The Acoustician, concerned with noise reduction in buildings, must therefore have an understanding of the processes involved in the generation, propagation and dissipation of sound energy in both air and in the solid structure. His solution to the problem cannot be at the expense of the mechanical strength of the material and of the structure. Various accepted methods of analysis and solution of the problem of noise transmission in buildings are now described. Alternative approaches, not so readily accepted, are listed, including a suggested method of analysis by the author.

Sound can be transmitted from any one point to another in a building. In airborne sound transmission the point of origin and reception are in air while impact sound transmission involves the generation of sound directly into the solid structure. The structure then transmits and radiates sound into the receiving enclosed air volume.

The shortest path between the source point (or room) and the receiving point (or room) is the direct path which is often interrupted by one or more intervening partition walls. All other paths are termed indirect or flanking paths which involve propagation as structure-borne sound, sometimes over appreciable distances.

Calculation of sound transmission between source and receiver involves the measurement of sound pressure level difference $(L_1 - L_2)$ in decibels. If the sound source and receiver are room volumes a spatial average of the mean square sound pressure is taken. The British Standard recommendation BS 2750 (1956) suggests that the level difference be normalized by taking into account the sound absorption of the receiver room. The normalized level difference is expressed as,

$$D_N = (L_1 - L_2) + 10 \log_{10}(A_o/A) \qquad \ldots\ldots\ldots 1.1$$

where A is the receiver room absorption and Ao is a reference, taken to be 10 m^2 at all frequencies.

The most common source-receiver configuration is that of adjacent rooms separated by a partition wall. The insulating characteristic of this wall is expressed as a sound transmission coefficient τ which is the ratio of sound power radiated into the receiver room to

that falling on the source room side of the partition. The sound reduction index (s.r.i.) or transmission loss (T.L.) is thus derived,

$$\text{T.L.} = \text{s.r.i.} = 10 \log_{10} 1/\tau = 10 \log_{10} E_1/E_2 \quad \ldots\ldots\ldots 1.2$$

E_1/E_2 is the ratio of sound energies of the two rooms. In field measurements, the transmission loss is calculated from,

$$\text{T.L.} = L_1 - L_2 + 10 \log_{10} (S/A) \quad \ldots\ldots\ldots 1.3$$

S is the area of the partition and A is the absorption, in the same units, of the receiver room.

Impact sound transmission measurements are absolute, the sound source consisting of impacts produced by hammers, of mass 500 grams, falling through a height of 40 mm. Normally, there are five hammers falling at a rate of 10 per second. The resultant received sound pressure level is normalised as in airborne sound transmission measurements. Thus,

$$L_N = L_2 + 10 \log_{10} (Ao/A) \quad \ldots\ldots\ldots 1.4$$

In both impact and airborne sound measurements the signal at the receiving microphone is filtered to one third octave bandwidth about any central frequency.

By use of these standard methods and calculations, comprehensive lists of transmission characteristics of many wall and floor types have been produced. In this country, information on field measurements has been published by the Building Research Station (1960), (now the Building Research Establishment), and notable

contributions are to be found abroad, such as in the publications of the National Bureau of Standards of the USA (1964). These and other reports, along with many laboratory measurements of partition walls are primarily concerned with direct transmission. In the field measurements, the source and receiver rooms are either vertically or horizontally adjacent. The information is not applicable to situations when the source and receiver room may be separated by several floors or rooms. It is in this configuration that the indirect transmission paths assume greatest importance. Thus, in the following discussion a brief outline is given of the theoretical and experimental work produced on both direct and indirect sound transmission and on their relative importance in various sound source-receiver configurations.

1.2.1 Multiple leaf partitions and laminate constructions

In development of power flow theory to describe noise transmission in building structures, and in the quarter scale experiments, only single leaf homogeneous walls will be considered. Apart from simplifying the analysis, it is felt that this type of wall is representative of those existing in high rise buildings. However many problems of excessive noise transmission have been solved using multiple leaf partitions and sandwich constructions, and the literature provides examples of many notable contributions to the theoretical and experimental assessment of their sound transmission characteristics. Beranek and Work (1949) and London (1950) describe the transmission of reverberant sound through double walls. London's

solution involves a ray technique where continuity conditions need to be satisfied at each air-leaf boundary. The boundary conditions are that (a) the continuity of particle displacement in a direction perpendicular to the plate surface must be maintained, and (b) the equations of motion at each partition need to be satisfied. Experimental measurement by Brandt (1954), Peutz (1954), and Waterhouse (1954) show discrepancies with values predicted using the methods of London even when the theory is modified by a dissipation factor R. This parameter is incorporated into the expression of mechanical impedance per unit area of panel to give,

$$z = 2R/\cos\theta + i\omega m \qquad \ldots\ldots\ldots 1.5$$

Where θ is the angle of incidence of the impinging pressure wave and m is the mass per unit area of the leaf. The resistive term R attempts to account for insulation values higher than those predicted from mass law theory at low frequencies. It is used to take into account all losses, compressional, flexural and by radiation and also losses at the edge of the panel.

If some dissipative material fills the air gap between the two leaves the problem can be solved by the use of impedance methods. Beranek and Work (1949) have made calculations and measurements of several types of wall and acoustical blankets. Experiment by Ford, Lord and Williams (1967) have indicated the effectiveness of introducing absorbent linings, even in quite small quantities.

Mulholland, Parbrook, and Cummings (1967) use multiple reflection theory to assess the effect of leaves which are absorbent on their

inner surfaces. By empirically assigning a value of absorption coefficient to these inner surfaces, agreement is obtained between the theory, which assumes the plates to be infinite in area, and measured values. A development of this method (1968) takes into account the finiteness of the plate, and of the effect of sound absorption at the edge of the air space between finite panels. Agreement with measurement is best when total absorption is assumed to occur at the edges.

Where many acoustic and mechanical modes exist, White and Powell (1965) employ statistical energy analysis techniques when calculating the transmission of random sound through rectangular double walls. In this technique, described in Chapter 2, a thermal analogy is drawn with the vibrational power flow between the first panel, the cavity, and the second panel. Sharp and Beauchamp (1969) produce a matrix recurrence relation which describes the general case of multiple leaf and of laminate constructions. This general equation is easily reduced to describe double or triple leaf partitions.

Kurtze and Watters (1959) suggest a sandwich construction in which the two outer leaves enclose a core of softer material. The resultant laminate is more susceptible to shear wave propagation than to the generation of the slower bending waves. The coincidence frequency can therefore be shifted several octaves to a higher frequency, allowing the transmission loss to obey the mass law over the full frequency range of interest. Coincidence, in which the structural wavelength matches that of the airborne sound wavelength, results in a dip in the transmission loss of the partition. Ford, Lord, and

Walker (1967) show that in this type of laminate, an undesirable resonance results from a dilational mode of vibration which depends upon the core stiffness and the mass of the leaves. It is shown that the core stiffness can be optimised to allow a theoretical mass law response to exist throughout the full frequency range. The mass law is described in section 1.2.2 which deals with single leaf panels.

Finally, Sewell (1970) derived the exact, two-dimensional, solution of the transmission of reverberant sound through a double partition in a rigid baffle. Donato (1972) successfully restates the classical approach and Price and Crocker (1970) produce impressive experimental results by the use of statistical energy analysis.

1.2.2 Single leaf partitions

The classical method of calculating the transmission loss of a single leaf wall is to assume the wall to have negligible stiffness and compressibility. For sound incident at an angle θ, the well used expression for transmission loss is,

$$T.L._{\theta} = 10 \log_{10} (1 + \frac{Z\cos\theta}{2\rho c})^2 \qquad \ldots\ldots\ldots 1.6$$

where Z is the mechanical impedance of the partition which, in this case, is given by,

$$Z = i\omega m \qquad \ldots\ldots\ldots 1.7$$

where m is the mass per unit area. Thus, the wall is assumed to have

mass reactance only. On integrating equation 1.6 over a suitable angular range a mean or random transmission loss is obtained in terms of the transmission loss at normal incidence. Cremer (1942) suggests that in real situations the angle of integration does not exceed 80^{o}. The expression relating the random transmission loss to that at normal incidence is,

$$T.L._{random} = T.L_{o} - 10 \log_{10} (0.23\ T.L_{o}) \qquad .....1.8$$

This theory is known as the mass law and concludes that the transmission loss of a simple partition increases by 6 dB for every doubling of frequency or of the mass per unit area. However, this law does not hold to arbitrarily high frequencies. Cremer (1942), Brillouin (1952), and Goselle (1953) argue that at the critical coincidence frequency of the panel the radiation characteristics alter dramatically. This causes a decrease in the value of transmission loss. A correction to equation 1.7 due to panel stiffness gives,

$$Z = i\omega m \left[1 - \left(\frac{\nu}{\nu_c} \sin^2\theta \right)^2 \right] \qquad ..... 1.9$$

where ν_c is the critical coincidence frequency. If the internal dissipative losses of the material are considered, a further correction gives,

$$Z = i\omega m \left[1 - \left(\frac{\nu}{\nu_c} \sin^2\theta \right)^2 \right] + \omega m \eta \left(\frac{\nu}{\nu_c} \sin^2\theta \right)^2 \qquad ..... 1.10$$

where η is the internal loss factor of the material.

An often used description of the frequency dependence of transmission loss is given by Watters (1959). The frequency range of interest is

divided into three regions. The first region extends from the basic resonance of the panel to the coincidence frequency. Here the wall obeys the mass law and the gradient of the curve is given as 6dB/octave. The central region is a plateau which results from coincidence and extends over two or three octaves. The third region has a gradient of approximately 10dB/octave. Gosële (1968) gives experimental results of panels, which are large compared to the bending wavelength, that illustrate the plateau region and subsequent slope of the third region.

In order to develop the theory of partition walls it is necessary to assess the effect of edge conditions. The finite panel theory must also take into account the finiteness of the source and receiver rooms. Sewell (1970) gives a complete solution of the transmission of reverberant sound through a partition surrounded by an infinite rigid baffle. Solutions are given for panels having free, simply supported, and clamped edges and it is shown that above the critical frequency, edge conditions do not affect the result.

However, if vibrational energy flows from the panel to the side walls then edge conditions will affect the transmission loss above, as well as below, coincidence. Heckl (1960) shows that only if less energy is transmitted into the side walls than is absorbed by internal friction, does the insulation remain independent of the boundary conditions.

By assuming all surfaces with the exception of the partition as being hard (i.e. having no velocity) Josse and Lamure (1964) treat a

theoretical model of two rectangular rooms separated by a simply supported wall. The transmission is expressed as a coupling between the panel modes and the room modes. Below the critical frequency the transmission loss is shown to depend upon wall dimensions and the values given are less than those predicted using the mass law. At higher frequencies the transmission loss becomes independent of panel and room dimensions.

In similar work Nilsson (1971) draws the same conclusions for the frequency range above the critical frequency. At lower frequencies a simply supported panel gives a transmission loss 3 dB higher than that of a clamped panel.

In measurements, Gosële (1965) discusses the influence of geometry (and of flanking transmission) on the laboratory measurement of transmission loss. It is shown that if the panel is set in a niche in the transmission suite aperture a lower transmission loss is measured than when no niche is present. Utley (1968), by comparing measurements of low frequency transmission loss from different laboratories indicates that the measurements are influenced by an unspecified room parameter. Kihlman (1970) in experiments, shows the influence of boundary conditions on the measured transmission loss and draws two conclusions.

(1) Below the critical frequency the mode pattern of the panel is important; this in turn is influenced by the way in which the panel is connected to the opening frame. The baffling effect also appears important.

(2) Above the critical frequency the total loss factor (i.e. internal and edge losses) is the important factor.

So far the discussion has been confined to airborne sound transmission of walls and floors. A brief mention must be made of the impact-noise isolation of floor structures and, more specifically, their relationship with the airborne transmission loss. Heckl and Rathe (1963) apply the principle of reciprocity in deriving a relation which allows the calculation of impact noise from the transmission loss or vice versa. It is argued that if both are known then some estimate of sound leakage and flanking is possible. It is shown that the sum of the two standard measurements, L_N and T.L., is independent of the properties of the floor. Vér (1971) extends the theory into the frequency range below the critical frequency by considering both the resonant and forced response of the floor.

As a summary the factors influencing the transmission loss of partitions can be listed as follows.

(1) The material density, expressed as the mass per unit area of the wall.
(2) The flexural stiffness.
(3) The dissipative loss factor of the material.
(4) The damping at the edge of the partition. This results from the flow of vibrational energy into the side walls.
(5) The source room/receiver room geometry which affects the modal distribution and coupling of the bending wave field

on the partition and the pressure wave fields within the rooms.

When dealing with multi-leaf panels, additional considerations are necessary.

(6) The distribution of mass of the leaves.

(7) The depth of the cavity.

(8) The absorption and stiffness characteristics of the filling material.

An understanding and assessment of these parameters and their effect on the transmission loss still does not allow the acoustician to predict with confidence the performance of party walls and partitions in real situations. The problem of flanking transmission has yet to be assessed and a general understanding is necessary of indirect transmission which becomes important at appreciable distances from the noise source.

1.3 Indirect Transmission

In investigations of indirect transmission the theoretical and experimental assessment has taken two forms.

(1) When calculating the transmission loss of a wall in buildings, an attempt has been made to introduce a correction to the predicted values due to flanking transmission. In measurements several authors have attempted to separate the direct from the indirect

contribution in order to calculate the former in field conditions.

(2) At greater distances from the sound source the effect of single partitions becomes less important. All wall and floor surfaces contribute to the propagation, dissipation, and radiation of sound energy within the building and it is important to assess the decrease with distance from the sound source, of the vibrational amplitude of the surfaces. It is the bending (or flexural) vibrational modes of wall and floor surfaces which couple most effectively with the room modes. Therefore calculations of bending wave energy at distances from the source will yield useful information on expected airborne sound energies in distant receiver rooms.

The investigation can thus be considered as that into near field and far field effects and both are now discussed in more detail.

1.3.1 Near Field Indirect Transmission

Several of the techniques of field measurement of transmission loss of walls in the presence of flanking paths are given in a review by Burd (1968). They are listed as follows.

(1) London (1941) suggests the use of source and receiver microphone as close to the partition surfaces as possible without touching and using high level sound

sources.' It is then assumed that the flanking paths introduce large energy losses due to diffraction and it then becomes possible to measure the sound pressure level difference of the partition alone. This method is limited to certain configurations and could not be adopted as a general technique in the field.

(2) In work by Ward (1963) and by Utley and Mulholland (1967) the sound pressure level produced by radiation from a surface is shown to be related to the vibration amplitude of that surface. The surface is assumed to be radiating above the critical frequency and thus to have the characteristics of a piston radiator, i.e. the surface vibration is assumed to be co-phased. Thus, knowing the vibration amplitude of the partition, and assuming that this surface only transmits the energy, the sound pressure level can be calculated. A measure of the contribution of flanking transmission is then possible in the supercritical frequency range. Utley and Mulholland argue that by applying a correction for the proportion of the area of the waves on a panel which are in phase at low frequency, the method can be used in measuring transmission loss of a panel in the frequency region in which the influence of the mass law is predominant.

(3) Raes (1955) suggests a pulse-method when measuring transmission loss in unfinished buildings. Analogous to structural or space insulation a 'time insulation' is introduced by making the direct path between source

room and receiver room microphones as short as possible, relative to all other paths. By using a sound pulse at the source it is possible that the direct contribution will arrive at the receiver microphone up to 10 milliseconds earlier than the contributions from other paths. Difficulties in this method become apparent when it is required to measure the sound transmission as a function of frequency. The pulse width cannot be too small since the equivalent steady-state bandwidth is too large. The pulse width cannot be too large since path separation then becomes difficult. The problem is further complicated if one takes into account the dispersive nature of bending waves. The frequency dependence of the wave velocity results in an alteration in the pulse shape as it propagates through the structure.

(4) Burd (1964) developed a method, proposed by Goff (1955), in which the cross-correlation function of a noise signal $f_1(t)$ is produced by analogue means. The receiver room microphone signal $f_2(t)$ results from the contribution of many paths. The running cross-correlation function for a delay time τ may be expressed approximately as,

$$\phi_{21}(\tau) = \lim_{T\to\infty} \frac{1}{T} \int_0^T f_1(t) f_2(t-\tau)\, dt,$$

where T is the integrating time of the equipment. On plotting the function against delay time a series of peaks is seen, corresponding to the different transmission paths. The disadvantages of this method

are the same as those of the pulse method. It is impossible to differentiate between the contributions of different paths which have the same delay time, and filtering of the signal limits the time resolution between paths.

(5) A method suggested by Meyer, Parkin, Oberst and Purkis (1951) could find application in both near field and far field measurements. In this technique it is assumed that the same sound energy will radiate from a wall or floor if the same bending wave pattern is reproduced, no matter by which method. Thus airborne excitation of the source room might be simulated by mechanical drivers exciting the party wall, side walls and floors etc. On removing the drivers the separate contributions of each flanking path are estimated. The technique is valid in the supercritical frequency region. Here the acoustically and mechanically excited fields are both composed of free bending waves. The limitation of the method is in the complexity of simulation technique which would quickly be unsurmountable for configurations more complicated than that or a receiver room adjacent to the source room. It is imagined that a fair degree of expertise would also be required in setting up the experiment. However, the authors are able to conclude that the contribution of direct and indirect transmission is equal when the partition transmission loss is 49 dB. The indirect transmission is negligible for a 40 dB partition. The method was

used with some success by Purkis and Parkin (1952) in assessing the indirect transmission with joist and solid floors.

(6) A simpler method of assessing flanking transmission in flats for both airborne and impact sound is given by Eijk and Kasteleyn (1955). The simplifying assumption is made that the airborne sound transmission over more than one storey is due to flanking transmission only. The transmission loss due to flanking transmission between two rooms directly over each other is determined by subtracting from the transmission loss over two storeys the flanking transmission loss per storey. In laboratory measurements of high transmission loss walls, Hudson and Mulholland (1971) use the same process of subtraction in the measurement of the airborne flanking path between the source and receiver rooms of a transmission suite. The path through the instrument area adjacent to the two rooms is assessed by measurement of the transmission loss between the instrument area and the source room, and then between the instrument area and the receiver room. The values are then expressed as corrections to the measured transmission loss of the partition.

All analysis techniques described have attempted, by various methods, to separate the direct from the indirect contribution to the transmission loss of partitions in configurations where the source

and receiver rooms are close together. In situations where the sound source and receiver are several rooms or floors apart the contributions from the indirect transmission predominate, and different methods of analysis become necessary.

1.3.2 Far Field Indirect Transmission

Several authors have made notable additions to the theories of Cremer (1949) on structure-borne sound in buildings. Analyses of the propagation and transmission of sound through various structural junctions have been made by Cremer (1953), Budrin and Nikiforov (1964), Zabarov (1968, 1970), Kihlman (1970), and Bhattacharya, Mulholland, and Crocker (1971). A full discussion of their theories and experiment is given in section 3.4 which deals with the transmission of vibrational energy through plates forming cross-junctions, corners etc.

An analysis of indirect sound transmission must include a description of the various structural wave forms by which sound propagates throughout a building. They can be listed as follows.

(1) In solids which extend appreciable distances in all directions a pure longitudinal (or extensional) wave can be generated in which the particle velocity is in the direction of propagation. In general, structural dimensions are seldom such that this wave type propagates over any appreciable distance.

(2) Structural elements, more often than not, have cross-sectional dimensions small compared with the wavelength of vibration. The particle velocity in the direction of propagation is accompanied by Poisson expansions and contractions perpendicular to it. These quasi-longitudinal waves are slower than the pure wave and in solids which are finite in two dimensions, as in a rod, the wave velocity is further reduced.

(3) Shear waves, which are slower than longitudinal waves, exist in solids of both finite and infinite dimensions. Here, the particle velocity is perpendicular to the direction of propagation. As is described in section 3.6 on the reflection and transmission of waves at a junction, it is necessary to assume the generation of a special form of shear wave. This is the transverse wave in which the particle velocity is parallel to the plane of the plate or wall in which it travels.

(4) The most important wave form in structure-borne sound propagation is the bending (or flexural) wave which occurs in rods and plates of relatively small transverse dimensions. This wave is propagated as a curvature along the structure.

(5) Torsional waves result from particle rotation about the neutral axis of the section and are found in rods and beams.

(6) In relatively thick structures, Rayleigh waves may be

generated in which only the surface (and layers adjacent) are deformed.

The waveforms listed under 2, 3, and 4 form the main contribution to structure-borne sound. Section 3.6 gives a mathematical formulation of the generation, propagation, reflection and transmission of these waves in structures and it is shown that, depending upon the nature of the structural discontinuity, each of the three wave forms is capable of generating the other two.

Field measurement of structure-borne sound is confined to bending waves which, as stated previously, are the most efficient radiators of sound energy from walls and floors. Westphal (1956) uses continuous excitation and pulse signals in measuring the decrease in bending wave energy with increase of distance from sound sources in tall flats. Measurements by Martin and Müller (1956) on an eight-storey building have illustrated the importance of junctions, in the dissipation of sound energy at distances from the sound source. By taking a mean value of bending wave energy on each surface, contours are constructed which indicate the frequency dependence of the decrease of sound energy with increased distance. The decrease is more marked with increase in frequency. Westphal (1957) in field measurement, and by constructing an electrical analogue, is able to show that in steel framework, high-rise buildings, structure-borne sound is strongly attenuated in the vertical direction.

It is interesting to note that in measurements of Meyer, Parkin, Oberst, and Purkis (1951) and in the contour measurements of Martin

and Müller (1956) it is seen that the decrease with increased distance in mean bending energy of each wall and floor is more marked at higher frequencies but the decrease across any one surface becomes less. This is the result of a more reverberant (diffuse) bending wave field being generated on each surface at the higher frequencies. As the number of modes within the measurement bandwidth increases the spatial variation in the amplitude of vibration becomes less and a single value of bending wave energy level can more readily be assigned to the surface. It is this factor which prompted the author to attempt to apply statistical energy analysis techniques and power flow theory to the propagation of sound in buildings.

1.4 Summary

In both direct and indirect noise transmission in buildings, some sound energy is dissipated in the building material and some in the air volumes enclosed, not forgetting the surface absorption in the rooms. Reflection of bending, quasi-longitudinal, and transverse waves occur at structural discontinuities such as changes in cross-section, junctions, changes in material etc. and, most importantly, the effect must be considered of the large impedance mismatch which occurs at the boundary between the air and the wall surface.

In the following discussion, the above parameters are calculated and, by power flow techniques the transmission of vibrational energy

through building structures is predicted. Experiments are devised, using quarter-scale models, which establish the validity of the method over part of the frequency range of interest i.e. 100 Hz to 3.15 KHz. It is hoped by this method that a unified approach to direct and indirect noise transmission is possible.

CHAPTER 2

POWER-FLOW METHODS

2.1 Introduction

Technological developments within the last decade have resulted in increased strength:mass ratios in structural elements and, at the same time, have produced more powerful sources of random vibrations. In the Aero-Space industry it must be possible for the effect of acoustic and turbulent boundary layer excitation on the mechanical vibrational response of a space vehicle to be calculated (Ungar and Scharton 1967). Gas circulators in carbon dioxide cooled nuclear reactors can produce 10^4 Watts of acoustic power in gases at pressures of thirty atmospheres (Fahy 1969). The cooling element structures may therefore be subjected to sound pressure levels of up to 180 dB. Many more problems exist where structures respond to wide bands of noise and the need arises to predict fairly accurately the degree of the response.

The low frequency vibrational response of structures having simple geometry can be assessed adequately by classical techniques. They generally involve the determination of the shapes of several low order modes and the calculation of their individual response to a specified type of excitation. The total response is then obtained by superposition of all the responses. At higher frequencies, and with broad bandwidths, many vibrational modes may be involved and the determination of mode shapes, associated natural frequencies, and modal responses becomes complicated. In practical structures

a complete mathematical description of the geometry, boundary conditions, and elastic properties becomes difficult and the large amount of data generated makes interpretation intractable.

To circumvent these problems an analytical technique was evolved in which the time-average of the response of a complex structure (and its distribution over the structure) when excited by noise of various bandwidths, could be calculated, using easily obtainable parameters. These techniques require a knowledge of the density with respect to frequency of the vibrational modes, the internal losses of the structural materials, their sound radiation characteristics, and the mechanical coupling existing between parts of the structure (Ungar and Scharton 1967). Equations in terms of these parameters, analogous to equations of heat flow in thermodynamics, were derived to describe vibrational power flow between structures. This technique for evaluating vibrational power flow is known as statistical energy analysis (S.E.A).

Lyon and Maidanik (1962) first considered the vibrational power flow between randomly excited coupled oscillators in a study of acoustically induced excitation of simple structures. The equations of motion of two oscillators are expressed and the power flow between them derived in terms of time-averaged second moments of these equations. The oscillators are assumed to be coupled through inertia, through stiffness, and through a mechanism which could be either conservative or dissipative.

Expressing the two equations,

$$\ddot{x}_1 + \beta_1 \dot{x}_1 + \omega_1^2 x_1 + A\ddot{x}_2 + B_2\dot{x}_2 + Cx_2 = f_1 \qquad \ldots\ldots\ldots 2.1$$

$$\ddot{x}_2 + \beta_2 \dot{x}_2 + \omega_2^2 x_2 + A\ddot{x}_1 + B_1\dot{x}_1 + Cx_1 = f_2 \qquad \ldots\ldots\ldots 2.2$$

f_i is the force on the ith oscillator and x_i is the resultant displacement. It is seen that the mass, damping, and spring terms of equation 2.1 are modified by including an inertial coupling A, a coupling B_2, and a spring coupling C. When B_1 and B_2 are equal, the coupling is dissipative, and when equal and opposite the coupling is conservative. In addition, the sources f_1 and f_2 are assumed to be statistically independent and to have 'flat' power spectra compared to the admittance spectra of the two oscillators.

From equation 2.2 the effective force f_1^2 produced on oscillator 2 from the coupled motion of oscillator 1 is written,

$$f_1^2 = -A\ddot{x}_1 - B_1\dot{x}_1 - Cx_1 \qquad \ldots\ldots\ldots 2.3$$

The time-average power is therefore,

$$j_{12} = \langle f_1^2 \dot{x}_2 \rangle = -A\langle \ddot{x}_1 \dot{x}_2 \rangle - B_1 \langle \dot{x}_1 \dot{x}_2 \rangle - C\langle x_1 \dot{x}_2 \rangle \qquad \ldots\ldots 2.4$$

To evaluate the moments in equation 2.4 an 8 x 8 matrix is produced by multiplying equations 2.1 and 2.2 by the displacements and velocities x_1, $\dot{x}_1$, x_2, $\dot{x}_2$ and then averaging. The determinant of the matrix is evaluated by assuming that the coupling terms are small. Thus,

$$|A| << 1; \quad |C| << \omega_1^2, \omega_2^2 ; \quad |B| << \beta_1, \beta_2$$

On evaluating the moments and remembering that with conservative coupling the energy dissipation in the system is independent of the

coupling, equation 2.5 is written as,

$$j_{12} = -j_{12} = g_{12}(e_1 - e_2) \qquad \ldots\ldots 2.5$$

where

$$g_{12} = \left[A^2(\beta_1\omega_2^4+\beta_2\omega_1^4+\beta_1\beta_2(\beta_1\omega_2^2+\beta_2\omega_1^2)\right]+(B^2-2AC)$$

$$\times(\beta_1\omega_2^2+\beta_2\omega_1^2)+C^2(\beta_1+\beta_2)\Big]\Big/\Big[(\omega_1^2-\omega_2^2)^2+(\beta_1+\beta_2)(\beta_1\omega_2^2+\beta_2\omega_1^2)\Big]$$

and where e_1 is the unperturbed energy in the ith oscillator. The assumption is made that the coupling term is small and that the actual energy level in a coupled oscillator is little different from that in an uncoupled oscillator.

If the coupling is dissipative then the equality in 2.5 does not hold. The two oscillator system becomes a three component system where the coupling dissipates power at a rate given by,

$$j_{diss.} = B\langle(\dot{x}_1 + \dot{x}_2)^2\rangle \qquad \ldots\ldots 2.6$$

The important conclusion of the derivation is that, in conservative coupling, the vibrational power flow can be regarded as analogous to a heat flow resulting from energy (or temperature) difference in the oscillators.

In extending the theory to describe power flow between two groups of oscillators, several assumptions were necessary. The modes need to be well separated (in frequency space), internal losses must be small, and the response must be linear. It is then possible to show that, in a given bandwidth, the average power flow from one oscillator set to the second set is proportional to the difference in the average

energy of the oscillators of the two sets. Lyon and Maidanik found application of the formulated theory in predicting the response of a baffled, simply supported aluminium beam in a reverberant sound field.

Lyon (1963) and then Eichler (1965) applied the techniques in describing noise reduction of rectangular metal boxes placed in reverberant sound fields. Lyon assumed one box surface only as being flexible whereas Eichler considered the response of all surfaces. The analyses are essentially the same. Both authors were at pains to stress the frequency regions of application of S.E.A. At low frequency (below the fundamental resonances) the box panels and enclosed air are assumed pure stiffnesses and the noise reduction, defined as ten times the logarithm of the ratio of the mean square pressure in the surrounding sound field to that in the enclosed field, is expressed in terms of the acoustic compliance and wall compliance. At intermediate frequencies the box walls assume a resonant behaviour but the enclosed air remains a stiffness which loads the wall reactively. The box walls and the surrounding sound field can therefore be considered as two ensembles of oscillators (or two sub-systems) between which power flows. At the lower limit of this frequency region the wall modes are sufficiently well spaced to be considered separately. At the upper limit of this range multimodal averaging becomes necessary. In the high frequency region in which the enclosed air volume becomes resonant the analysis is that of a three sub-system configuration, i.e. the enclosed air volume, the box walls, and the surrounding reverberant sound field. In the intermediate and high frequency regions the

S.E.A. techniques were applied with success. Eichler, in describing modal and multimodal power balance, introduces the concept of coupling loss factor and derives a law equating the product of coupling loss factor and modal density in sub-systems. An oscillator, or mode, is supplied with power Π_i and attains an average energy e_i. A parameter $\emptyset$ is introduced such that the energy dissipated internally is expressed as $e_i\emptyset_i$ and that lost through coupling to the second mode as $e_i\emptyset_i^j$. Power $e_j\emptyset_j^i$ returns from the second mode. The modal energy balance is written,

$$e_i \sum_j \emptyset_i^j - \sum_{j \neq i} e_j \emptyset_j^i = \Pi_i \qquad \ldots\ldots\ldots 2.7$$

Reducing all generator powers and loss factors to zero and assuming a general law of thermodynamics, namely, that in two isolated, lossless systems interacting with each other, their mean energies are in proportion to their number of degrees of freedom, i.e. $e_i = e_j$, equation 2.7 becomes

$$\emptyset_i^j = \emptyset_j^i \qquad \ldots\ldots\ldots 2.8$$

If several modes exist within the bandwidth, multimodal averaging is necessary. By discarding correlations between the modal energies and their coupling it is possible to express double averaging in the derivation as the product of two simple averages. The power balance equation 2.7 becomes,

$$\omega E \sum_{r_s} \eta_r^s - \omega \sum_{s \neq r} E_s \eta_s^r = \Pi_r \qquad \ldots\ldots\ldots 2.9$$

where the power is supplied to the rth sub-system. The coupling loss factor η_r^s has now been defined such that the power flowing from

sub-system r to sub-system s is given by $\omega E_r \eta_r^s$. The internal power loss in the rth sub-system is expressed by a similar expression $\omega E_r \eta_r^r$ (or $\omega E_r \eta_r$) where η_r^r (or η_r) is the dissipative loss factor of the structural material. E_r is the energy stored in the rth sub-system, averaged over time and unit bandwidth. Similarly, the equality 2.8 is modified to,

$$n_r \eta_r^s = n_s \eta_s^r \qquad \ldots\ldots\ldots 2.10$$

That is, the products of modal density and coupling loss factor in coupled sub-systems are equal. The simplicity of the theoretical model is apparent but Eichler stresses the limitations to its practical application. As stated by Lyon and Maidanik (1962), the sub-systems are assumed linear, loosely and conservatively coupled, and the bandwidth must be small compared to its centre frequency.

As well as the fluid-structure interaction, Lyon and Eichler (1964) apply S.E.A. techniques to structure-structure couplings, the structural elements investigated being a plate with a cantilevered beam and a plate with a cantilevered plate. The primary variable is the modal energy and the structures are described by their modal densities, masses, and loss-factors. The coupling loss factor of the plate-beam structure is derived by consideration of moment impedances and that of the two plate structure by solving the bending wave equation for the boundary conditions existing at the junction. Agreement between theory and experiment, in the case of broad-band excitation, is good.

Lyon and Scharton (1965) considered a three element structure

consisting of two aluminium plates connected by a narrow aluminium strip of equal thickness. On exciting one of the plates, bending wave fields resulted on all three structural components. In addition, torsional waves are generated on the connecting beam and the technique of analysis needed modification in order to account for the possible change of wave type when vibrational energy passed from one structure to another. Two approaches were considered.

(1) If the flexural and torsional modes on the connecting beam are considered uncoupled, the transmission of vibrational energy from the source plate to the other plate has two components or paths. One path is that of bending waves on plate 1 generating bending waves on the beam which, in turn, produce a bending wave field on plate 2. A second possible path results when the plate 1 bending field generates torsional waves on the beam which then generate a bending wave on plate 2. The two components are considered separately, the resultant bending wave field on plate 2 being the sum of the two contributions.

(2) If the two wave types on the beam are considered coupled only one possible path is assumed, which is described by an effective coupling loss factor. Assuming that the two wave modes are well coupled then, in any frequency band, they will come to equilibrium at the same modal energy. The total energy in the beam can be expressed as,

$$E_t = (n_f + n_t)E_m$$

where E_m is the averaged energy per mode, and n_f and n_t are the flexural and torsional modal densities respectively. The effective coupling loss factor is thus given as,

$$\eta_r^s(\text{eff.}) = \frac{n_f \eta_r^s(\text{flex.}) + n_t \eta_r^s(\text{tor.})}{n_f + n_t}$$

Using equality 2.10 the power flow, within, a unit bandwidth from the ith to the (i + 1)th sub-system is expressed as,

$$\Pi_i^{i+1} = \omega \eta_i^{i+1} n_i \left[\frac{E_i}{n_i} - \frac{E_{i+1}}{n_{i+1}} \right] \quad \ldots\ldots\ldots 2.11$$

add the power lost internally by,

$$\Pi_i = \omega \eta_i E_i$$

E_i is the energy stored in the ith sub-system. The ratio of the bending wave energies of the two plates could thus be expressed in terms of the derived coupling and internal loss factors. Agreement between theory and experiment was fair, even when the number of modes within a bandwidth was low.

Newland (1966) has shown that the coupling loss factor, so far defined, and the expression 2.10 can give rise to anomalous results if misapplied. Taking the example of the plate-beam-plate structure of Lyon and Scharton (1965), two equalities are assumed to hold simultaneously, namely,

$$\eta_2^3 = \eta_2^1$$
$$\eta_3^2 = \eta_1^2 \qquad \ldots\ldots\ldots 2.12$$

where the source plate is considered the first sub-system, the connecting beam the second, and the receiving plate as the third sub-system. Newland points out that both equalities in 2.12 can only be true if the modal densities of the plates are equal (as was, in fact, the case in Lyon's experiment). The weakness of the coupling loss factor as defined in equation 2.11 is, it is argued, that it depends not only upon the coupling itself but also on the properties of the coupled sub-systems. Newland (1966) produces an alternative factor dependent upon the total number of modes coupled.

The derivation employs a perturbation technique and the first case considered is that of two oscillators coupled through a small, purely elastic link. Expanding the model to describe power flow between two sets of oscillators coupled inertially and through stiffness, a coupling factor is derived by which the power flow is expressed in terms of the frequency shifts of the oscillators caused by the coupling, and of the modal densities of both sub-systems (Newland 1968). As with the derivation of Lyon, it is necessary to assume conservative, loose coupling, and the ratio of bandwidth to centre frequency must be small. In addition, the mode widths must be smaller than the band-width by an order of magnitude. Newland's coupling factor is written,

$$\delta_i^{i+1} = 2\pi\, \omega^{-1} n_i \langle \Delta\omega_i \rangle \cdot \langle \Delta\omega_{i+1} \rangle \qquad \ldots\ldots\ldots 2.13$$

where $\langle \Delta\omega_i \rangle$ is the average difference between the natural angular frequency in the coupled and uncoupled states. The power flow equation 2.11 becomes,

$$\Pi_i^{i+1} = \frac{\pi n_i n_{i+1}}{2\omega^2} \delta_i^{i+1} \left[\frac{E_i}{n_i} - \frac{E_{i+1}}{n_{i+1}} \right] \qquad \ldots\ldots\ldots 2.14$$

The two coupling factors are related by the expression,

$$\eta_i^{i+1} = \frac{\pi n_{i+1}}{2\omega^2} \delta_i^{i+1} \qquad \ldots\ldots\ldots 2.15$$

The modal densities are with respect to angular frequency.

It appears that there are two quite distinct definitions of coupling factor and it must be assumed that two answers will result from the analysis of any one problem. By considering coupled beams, Khabbaz (1970) indicated the discrepancy in the value of the two coupling factors. Newland's value, obtained by considering the frequency shift due to coupling is about five times that of Lyon, derived by consideration of the amplitude of the transmitted wave across the coupling of the beams when a travelling bending wave is incident upon it. Crandall and Lotz (1971, 1973) investigated the same problem of connected beams and divided the approach into that of weak and strong coupling. In the case of weak coupling, the two methods give the same value of coupling factor and it is only in strong coupling that the difference occurs. This, they argue, results from the misapplication of both the frequency shift method of Newland and the travelling wave method of Lyon. Both methods are limited to weakly coupled sub-systems.

Scharton and Lyon (1968) have shown that the proportionality between time-average power flow and the difference in the time-average energies of two linearly coupled oscillators is independent of the strength of the coupling if the oscillator energies are correctly defined. The analysis is extended to the case of a group of linear oscillators, all having the same natural frequencies and internal losses, and all experiencing identical mass and spring coupling. Gersch (1969) and Davies (1972, 1973) have further considered the coupled oscillator and coupled oscillator ensemble problem. Gersch, by using matrix inversion, obtains exact solutions for average power flow between two oscillators in terms of second moment computations. Davies indicates that by suitable definition of the modal coupled energy the power flow and energy difference of S.E.A. can be preserved for the case of strong coupling. His results are applied to the problem of two beams coupled by a rotational spring of arbitrary strength. Work by Mercer, Rees, and Fahy (1971) employs a perturbation analysis in developing expressions for the energy flow between two oscillators connected by weak, conservative coupling, where one oscillator is subject to transient excitation.

When deciding on a definition of coupling loss factor, ease of application must be considered a priority. The parameter suggested in a letter by Lyon and Scharton (1966) has the important advantage in that it can enter the energy balance equation on the same basis as that of the dissipative loss factor. The total loss of a sub-system is therefore simply related to the sum of the two loss factors times the total energy of the sub-system. Newland's frequency shift

method may pose problems in experimental assessment. In considering weak couplings only the experimenter is presented with the difficulty of measuring the corresponding small shift in frequency. Conversely, larger frequency shifts will be allied to stronger couplings which lie outside the region of validity of Newland's theory. If power flow techniques are to be applied to problems of noise transmission in buildings, we see from the above that the following limitations and requirements must be considered.

(1) The coupling loss factors between structures and between structures and the surrounding (or enclosed) air need careful definition.

(2) The bandwidth of interest should be wide enough to contain several of the structural or room modes.

(3) Internal loss factors of the structural material must be assumed low.

(4) The bandwidth of interest, as well as that on any mode must be small compared to the centre frequency.

(5) In order to apply S.E.A. techniques, with special reference to equations 2.10 and 2.11, the coupling must be assumed small.

(6) The vibrational fields generated on structures and in room volumes are assumed diffuse.

Only an approximation to the above conditions is possible when dealing with real problems of noise transmission in buildings.

However, the attractive simplicity of power flow techniques invites the question of whether regions of validity exist in which these methods can be applied meaningfully. The following sections will be concerned with the application of some of the techniques described to problems involving building structures such as the junction of reinforced concrete plates (walls and floors) and the sound radiation characteristics of plates forming surfaces of a rectangular room. It is hoped to show in this thesis that such considerations will allow a unified approach to the problem of direct and indirect sound transmission in buildings.

2.2 Applications in Building Structures

Little theoretical and experimental work has been done in applying power flow and S.E.A. techniques to the structure-structure and structure-fluid vibrational energy flows in noise transmission through buildings. This brief description of previous work includes experiments which, although outside the area of building acoustics, has relevance to the matter in hand.

Structure-fluid interactions have been investigated more fully than structure-structure power flows. Fahy (1969) was concerned with the determination of the radiation characteristics below the critical frequency of a thin flexible panel forming one side of a box, the dimensions of which were not large compared to the acoustic wavelength, and where the sound field in the enclosed volume could not be assumed diffuse. As with Bhattacharyan and Crocker (1969/70), it is shown that the coupling between the plate bending modes and

and the room modes is most efficient when certain simple relationships concerning modal numbers are obeyed. Above the critical frequency, Kihlman (1967) argues that the radiation from a standing, sinusoidal wave shape on a room wall is, on the average, the same as that obtained from the same wave radiating into semi-infinite space. The assessment of sub-critical and super-critical radiation characteristics of plates is discussed in section 3.1, dealing with structure-fluid coupling.

S.E.A. techniques have been successfully applied by Crocker and Price in investigating the radiation and transmission characteristics of single panels (1969) and double panels (1970) forming a partition between the two rooms of a transmission suite. In the case of the single panel partition, the source room, panel, and receiver room are considered as a three sub-system configuration with, in the case of loudspeaker axcitation of the source room, sound power flowing from the first sub-system (source room) to the second (panel), and from the second to the third (receiver room). If sound leakage exists between the rooms it constitutes an extra coupling (or transmission path) between the first and third sub-systems. A double leaf partition between rooms is described by an extra two sub-systems; the second leaf and the enclosed volume in the partition. In both partitions considered, energy balance equations using equation 2.11, are produced and, on solution, the ratios of the bending energy fields on the plate and the sound pressure energies in the rooms are given. Although successfully applied, as with previous work, the panels investigated were thin (in this case, aluminium) and had high critical coincidence frequencies. The radiation characteristics

investigated were, in general, in the sub-critical region and the bending waves were considered the only form of vibrational energy on the plates.

When real building structures are analysed, the thickness of walls and floors encountered does not allow the use of some of the thin plate approximations described, to arbitrarily high frequencies. The bending wave velocities and critical coincidence frequencies are lower than found on thin metal plates. As well as bending waves, other wave types must be considered. They include longitudinal and shear waves. In investigating the propagation of structure-borne sound via cross-junctions of concrete plates of thickness ranging from 50 mm to 200 mm Kihlman (1967) considered both longitudinal and transverse shear waves as well as bending waves. As shown by Cremer (1948), an incident bending wave at a junction of semi-infinite plates will generate, in the far field, not only bending waves but longitudinal and, in the case of oblique incidence, transverse waves. The transverse wave arises from the need to preserve continuity of displacement across the junction of the plates when a bending or longitudinal wave is incident obliquely. It has the properties of a shear wave with the additional characteristic of having its particle displacement in the plane of the plate. Appendix I describes more fully the generation of these waves. Cremer was able to consider numerically the transmission of energy at junctions for simple cases. Kihlman's theoretical and experimental investigation was concerned mainly with the effect of concrete floors on the sound transmission of light concrete partitions. By use of energy balance equations, the structure-borne sound

transmissions of cross-junctions were predicted. Agreement between theory and experiment was good. The methods employed in the following sections are derived, in some cases, from the work of Cremer (1948), Kihlman (1967), and Lyon and Eichler (1964) and reference to their work is made in the sections on power-flow models and the assessment of power flow parameters.

2.3 Limitations of power flow techniques in sound transmission in buildings

In this chapter, simple parameters are defined, energy balance equations generated, and vibrational energy ratios calculated for the case of structure-borne sound transmission through junctions of concrete plates and for the sound radiation characteristics of concrete plates forming rectangular rooms. In the latter case, S.E.A. will be applied. It is necessary however to gauge the limitations of these techniques when applying them to building structures.

The considerations are listed as follows.

(1) In this description of power flow to and from finite systems it is convenient to consider the vibrational fields generated as being diffuse. The fields of interest are sound pressure fields in rectangular rooms and bending, longitudinal and transverse wave fields on rectangular reinforced concrete plates.

In the frequency range of 100 Hz to 3.15 kHz the pressure fields of small rectangular rooms have high modal densities.

Even at the lower end of the frequency range, where the eigenfrequencies are well separated, a one-third octave bandwidth still contains several modes. Using the low frequency modification of Dah You Maa (1938) to the standard room modal density equation,

$$n_r = \frac{4\pi V}{c_o^3} \nu^2 \left(1 + \frac{S c_o}{8V} \frac{1}{\nu} + \frac{L c_o^2}{8\pi V} \frac{1}{\nu^2}\right) \qquad \ldots\ldots\ldots 2.16$$

where V, S, L are the volume, surface area, and sum of the dimensions of the rectangular room respectively, and c_o is the sound wave velocity (taken as 344 m/sec), it is possible to calculate the number of modes within a third octave bandwidth for any room dimension at a frequency Assuming dimensions of 2 m x 3 m x 4 m, the modal density at 100 Hz is calculated as 0.16 modes/Hz, and at 1 kHz the value is 8.33 modes/Hz. Therefore, within a one-third octave bandwidth there are 4 modes at 100 Hz, 266 at 500 Hz and 1,983 modes at 1 kHz. Thus the modal density increases rapidly with frequency and, over most of the frequency range of interest, can be assumed to be large enough to allow the sound field to be considered diffuse.

Wave velocities encountered in structural vibrations are much higher than that of airborne sound and, in the case of bending waves, are dispersive. This dispersion results in a modal density which is independent of frequency. Hart and Shah (1970) give a derivation of bending wave modal density resulting in the expression,

$$n(\nu) = \frac{S\sqrt{3}}{h c_L} \qquad \ldots\ldots\ldots 2.17$$

where S, h, c_L, are the plate area, thickness, and longitudinal wave velocity, respectively. For a concrete plate of dimensions 4 m x 3 m x 0.15 m and a longitudinal wave velocity of 4,193 m/sec, the modal density is calculated, using equation 2.17, as 3.305×10^{-2} modes/Hz. This gives a modal spacing of approximately 30 Hz. Therefore, within a one-third octave bandwidth, 1 mode occurs at 100 Hz, 8 modes at 1 kHz, and 24 modes at 3.15 kHz. It would appear that only at mid and high frequencies can appreciable numbers of modes be assumed to exist within a bandwidth. However, the conclusion reached by Lyon and Scharton (1965) from experiments on the plate-beam-plate structure was that S.E.A. methods were successful, even when few modes are present. Reasonable results were obtained when only one torsional mode existed on the connecting beam. Kihlman (1967) was also confronted with the need to consider few modes and was led to look at the modal distribution as an additional pointer. It was argued that, if the number of modes within a band-width is low, a high variation in response of a finite system would be expected. However, if the mode distribution, with respect to frequency, is smooth, an average response, averaged over the bandwidth, will, in many cases, agree with values obtained assuming a higher modal density or ideally diffuse field. In bending wave fields on rectangular plates, extreme

variations in modal distribution do not occur and the assumption of a diffuse field may be assumed valid at the lower frequencies.

The assumption of high modal densities for airborne sound in rectangular rooms and bending wave fields on rectangular concrete plates appears reasonable. The same cannot be said about longitudinal and transverse wave fields. The wave velocities measured are much higher, with a correspondingly lower modal density at lower frequencies. It will be shown in Section 3.2.3 that if equation 2.16 is modified to describe non-dispersive waves in a two dimensional finite system, the following expression for longitudinal wave modal density results.

$$n_L(\nu) = \frac{2\pi S}{c_L^2}\nu + \frac{(L_x + L_y)}{c_L} \qquad \ldots\ldots\ldots 2.18$$

where S, L_x, L_y are the plate area, length, and breadth respectively. For a plate of dimensions 4 m x 3 m x 0.15m and a wave velocity of 4,193 m/sec the modal densities are 2.098×10^{-3} modes/Hz at 100 Hz, 5.958×10^{-3} modes/Hz at 1 kHz, and 1.518×10^{-2} modes/Hz at 3.15 kHz. Therefore, in a one-third octave bandwidth, only 1 mode is predicted at 1 kHz, and 11 modes are predicted at 3.15 kHz. Longitudinal wave modal density is therefore appreciable at high frequencies only. The transverse wave velocity lies somewhere in value between that of longitudinal waves and bending waves and like the former is non-dispersive. The

modal density will therefore be greater than that of longitudinal waves and, being non-dispersive, will increase with frequency.

To summarise, it would appear valid to assume high modal densities, and hence diffuse fields, over most of the frequency range of 100 Hz to 3.15 kHz, when dealing with airborne sound waves and bending waves. However, in the case of longitudinal and transverse waves, the region of validity is confined to the upper part of the frequency range. A fuller description of the modal densities of the various wave types is given in section 3.2 and section 6.4.

(2) The assumption is made that the vibrational wavelengths on concrete plates are not large compared to the plate dimensions. This results from the theoretical assessment of the coupling loss factors of finite plates, where the length of the junction is assumed infinite when deriving the mechanical impedence of the junction. Kihlman (1967) observes that it is at least required that the wavelength should not be greater than twice the smallest plate dimension (excluding thickness). This condition is obeyed by bending waves which, at the lowest frequency of 100 Hz are still of the same order of magnitude as the length of junction. A concrete plate of dimensions 4 m x 3 m x 0.15 m has a bending wavelength of approximately 3.4 m at 100 Hz. For longitudinal waves of velocity 4,193 m/sec the wavelength assumes the same order

of magnitude as the plate dimensions at a frequency of 1.25 kHz where λ_L is approximately 3.35 m. For transverse waves of velocity 2,481 m/sec, the frequency is 800 Hz where λ_T is approximately 3.1 m. Therefore, over the frequency-range of interest, the bending waves can be thought of as equal to or smaller than the plate dimensions; whereas this is true only at high frequencies for longitudinal waves, and, at mid and high frequencies for transverse waves.

(3) Edge losses other than at the junction of the plates are assumed small.

(4) Although longitudinal, or more correctly, quasi-longitudinal waves on plates radiate some sound energy into the surrounding air, bending waves are much more efficient in this respect. They will therefore be thought of as the only structural vibration to couple efficiently with room modes. Transverse waves will have no sound radiation characteristics since their particle displacement is in the plane of the plate.

(5) The bending, longitudinal, and transverse wave modes generated on a concrete plate are considered uncoupled. Therefore, three vibrational fields exist upon a plate each of which can be analysed separately. As stated in (4)

bending waves are the most important structural vibration to the acoustician and will thus be investigated more thoroughly than other wave types.

(6) It is assumed that mechanical excitation of the concrete plates initially generates a bending wave field only. This appears reasonable when one considers the relative ease with which bending waves are excited in rods (section 5.3) and plates (section 6.4).

2.4.1 Power Flow in Structural Junctions

In this section, energy balance equations are produced for cross-junctions, T-junctions, and corners of finite plates. By simple analysis, or by numerical methods, involving a computer, the vibrational energies on each plate, relative to the bending wave energy on the mechanically excited (or source) plate, are calculated. The following notation is adopted.

(1) The vibrational energy of a plate E, is suffixed by b, l or t, describing the bending, longitudinal, and transverse components of the field, respectively.

(2) The coupling loss factor η is defined as such that the power flow from the bending wave field on the ith plate to the longitudinal wave field on the jth plate is written as,

$$\Pi_{ib}^{jl} = \omega \eta_{ib}^{jl} E_{ib} \qquad \ldots\ldots\ldots 2.19$$

where E_{ib} is the total bending wave energy on the ith plate, and ω is the angular frequency. As a further example of this nomenclature, consider the power flow from the bending wave field on the jth plate to that on the ith plate. This is written,

$$\Pi_{jb}^{ib} = \omega \eta_{jb}^{ib} E_{jb} \qquad \ldots\ldots\ldots 2.20$$

(3) The internal loss factor is defined as in convention such that the bending wave energy dissipated on the ith plate in a unit bandwidth is expressed as,

$$\Pi_{ib} = \omega \eta_b E_{ib} \qquad \ldots\ldots\ldots 2.21$$

A longitudinal loss factor η_l , and transverse loss factor η_t are similarly incorporated in the energy balance equations. At this point sound radiation losses are not considered separately, but as a small addition to the bending wave internal losses.

2.4.2 Some General Considerations

Before describing specific cases of plates coupled to form junctions, it might be advantageous to analyse a generalised, simplified power flow model and from it draw some basic conclusions.

Consider a sub-system coupled to (n - 1) sub-systems the latter being independent of each other (Fig 2.1(a)). Assume that the first sub-system (the source) is excited to a vibrational energy level E_1 in the steady state. Some of the energy is dissipated internally and some transfers to each of the other sub-systems. Further, assume that all coupling loss factors are equal and all internal loss factors are equal. By simplifying the expressions in 2.19 to 2.20, the energy balance equation for the rth sub-system is given by,

$$\omega E_r(\eta_r + \eta_r') = \omega E_1 \eta_1^r \qquad \ldots\ldots\ldots 2.22$$

The L.H.S of the equation describes the energy dissipated and transferred, and the R.H.S describes energy gain. The angular frequency ω is common to both sides of the equation and can be ignored in this and all subsequent equations. Assuming the equalities,

$$\eta_1' \ldots\ldots \eta_r' \ldots\ldots \eta_n' = \eta_{diss.}$$

$$\eta_1^2 \ldots\ldots \eta_1^r \ldots\ldots \eta_1^n = \eta_2' \ldots\ldots \eta_r' \ldots\ldots \eta_n' = \eta_{coupl} \qquad \ldots\ldots\ldots 2.23$$

equation 2.22 gives the vibrational energy ratio,

$$\frac{E_r}{E_1} = \frac{\eta_{coupl.}}{\eta_{diss.} + \eta_{coupl.}} = \frac{1}{1 + \eta_{diss.}/\eta_{coupl.}} \qquad \ldots\ldots\ldots 2.24$$

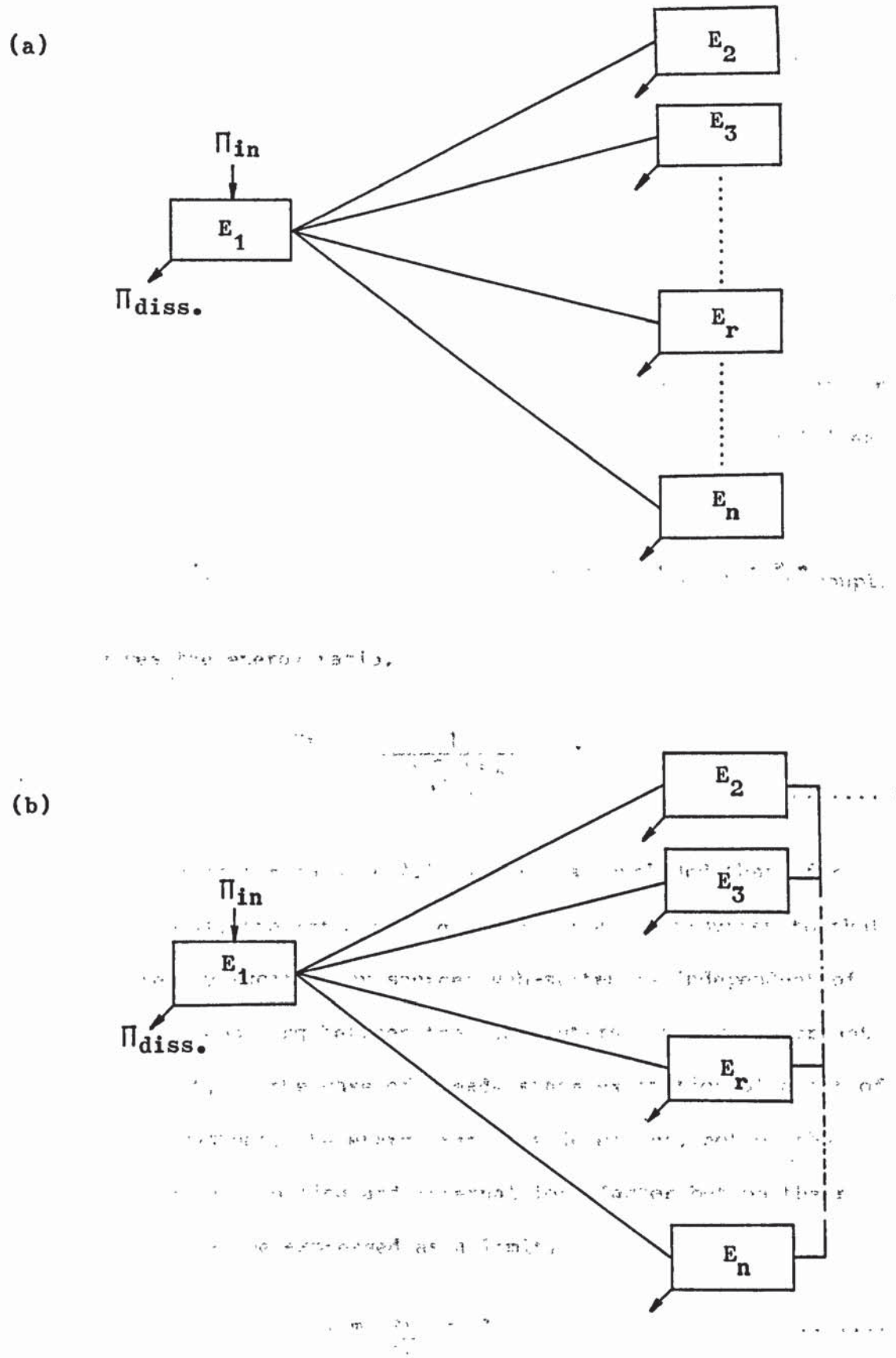

Generalised power flow diagram for n coupled subsystems.

(a) Subsystems coupled to the excited subsystem.

(b) All subsystems coupled to each other.

The problem can be extended by allowing each sub-system to be coupled to each other (Fig 2.1(b)). The energy balance equation for the rth sub-system, in the steady state, becomes,

$$Er(\eta_r + \sum_{\substack{s=1 \\ s\neq r}}^{n} \eta_r^s) = \sum_{\substack{s=1 \\ s\neq r}}^{n} Es\eta_s^r \qquad \ldots\ldots\ldots 2.25$$

If the equalities in 2.23 are used, each sub-system, other than the source, will have the same energy level. Equation 2.25 simplifies to,

$$Er(\eta_{diss} + (n-1)\eta_{coupl.}) = (n-2)Er\eta_{coupl.} + E_1\eta_{coupl.}$$

which gives the energy ratio,

$$\frac{Er}{E_1} = \frac{1}{1 + \frac{\eta diss.}{\eta coupl.}} \qquad \ldots\ldots\ldots 2.26$$

Equation 2.26 is the same as 2.24 and it is concluded that, for the given model, the ratio of the energy of any sub-system to that of the directly excited (or source) sub-system is independent of the degree of coupling between the sub-systems. A more important result is that, in the case of steady state excitation of a set of coupled sub-systems, the energy ratio is dependent, not on the actual values of coupling and internal loss factor but on their ratio. This can be expressed as a limit,

$$\lim_{\eta_{diss}/\eta_{coupl.} \to 0} \frac{Er}{E_1} = 1 \qquad \ldots\ldots\ldots 2.27$$

2.5 Cross Junction of Finite Plates

The junction of four plates (Fig 2.2(a)) is assumed perfectly rigid and to have dimensions negligibly small compared to its length. It can be thought as the intersection of two plates, in which case, plate 1 has the same dimensions as plate 3, and plate 2 has the same as that of plate 4. This symmetry will be used often in simplifying the energy balance equations.

2.5.1 Bending Wave Fields

If, as is likely, at low frequencies, or for the case of thin plates, bending waves are considered the only form of vibrational energy, the flow diagram (Fig 2.2(b)) is simplified by disregarding the longitudinal and transverse components. Further simplification results from assuming that the vibrational fields on plate 4 are equal to those on plate 2. Therefore, no power flows between them.

As described earlier, energy balance equations are produced for each plate in which the L.H.S describes the energy flowing from or dissipated in a plate, and the R.H.S describes energy flowing back to the plate from the connected, or coupled plates. Thus for the bending wave field on plate 2,

$$E_{2b}(\eta_b + \eta_{2b}^{1b} + \eta_{2b}^{3b}) = E_{1b}\eta_{1b}^{2b} + E_{3b}\eta_{3b}^{2b} \quad \ldots\ldots\ldots 2.28$$

On plate 3,

$$E_{3b}(\eta_b + \eta_{3b}^{1b} + 2\eta_{3b}^{2b}) = E_{1b}\eta_{1b}^{3b} + 2E_{2b}\eta_{2b}^{3b} \quad \ldots\ldots\ldots 2.29$$

(a)

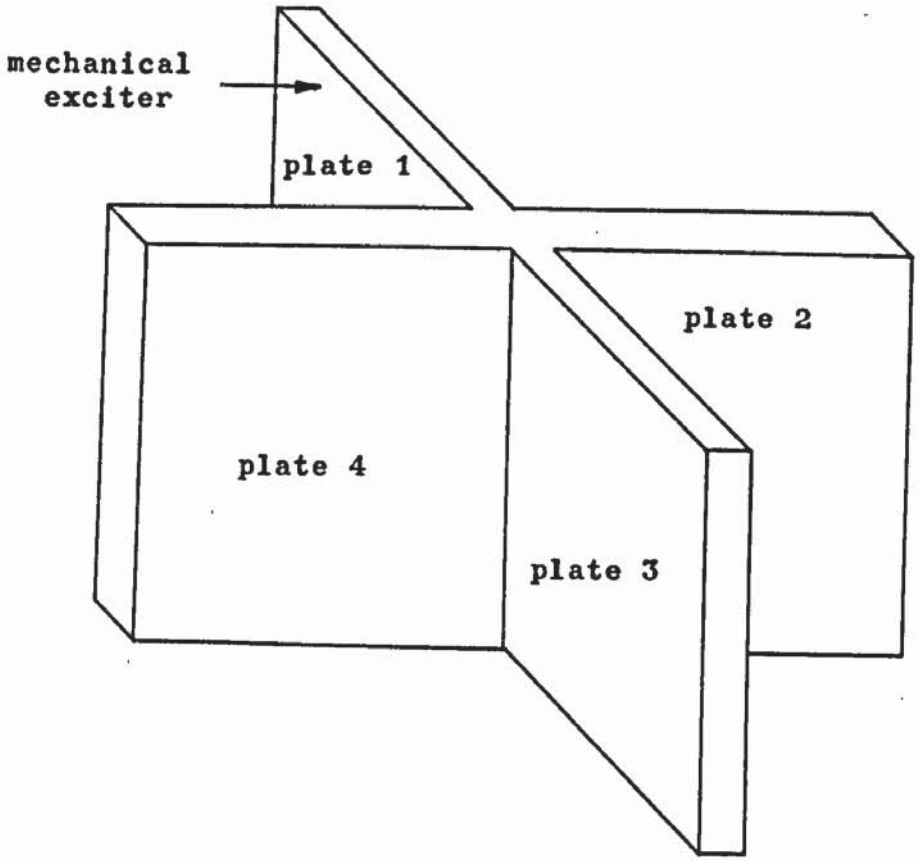

(b)

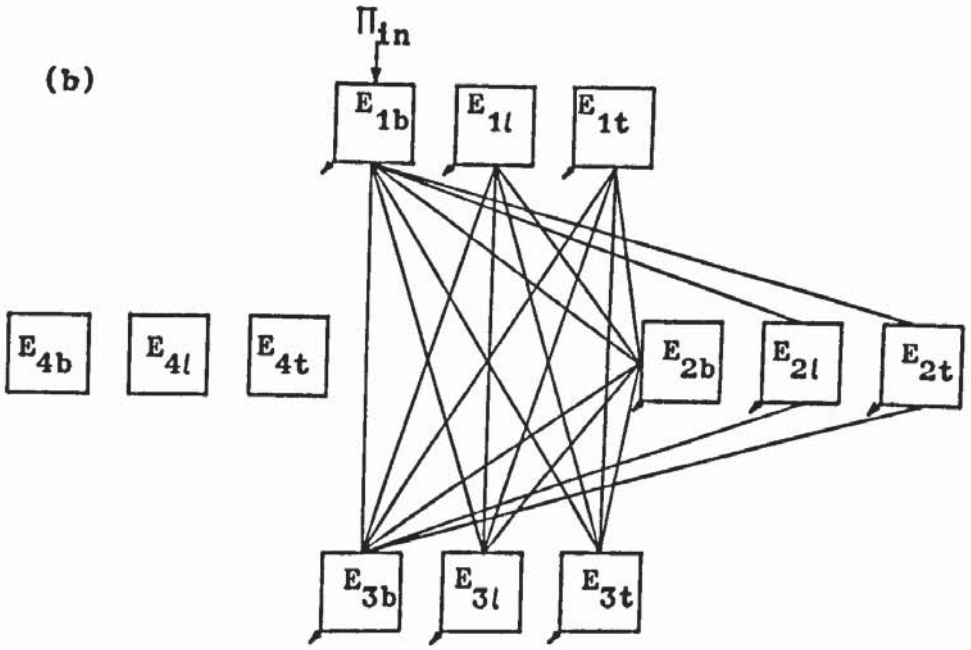

(a) Cross-junction of four finite plates, one of which is mechanically excited into bending vibration.

(b) Associated power flow diagram.

From equations 2.28 and 2.29 the bending wave energies on plate 2 and plate 3 are expressed in terms of that on plate 1. By simple manipulation, and by use of the equalities,

$$\eta_{3b}^{2b} = \eta_{1b}^{2b}$$

$$\eta_{2b}^{3b} = \eta_{2b}^{1b}$$

$$\eta_{3b}^{1b} = \eta_{1b}^{3b} \qquad \text{..... 2.30}$$

the energy ratio for plate 2 is given as,

$$\frac{E_{2b}}{E_{1b}} = \frac{\eta_{1b}^{2b} + \dfrac{\eta_{1b}^{2b} \cdot \eta_{1b}^{3b}}{\eta_b + 2\eta_{2b}^{2b} + \eta_{1b}^{3b}}}{\eta_b + 2\eta_{2b}^{1b} - \dfrac{2\eta_{1b}^{1b} \cdot \eta_{1b}^{2b}}{\eta_b + 2\eta_{2b}^{2b} + \eta_{1b}^{3b}}} \qquad \text{..... 2.31}$$

and, for plate 3,

$$\frac{E_{3b}}{E_{1b}} = \frac{\eta_{1b}^{3b} + \dfrac{2\eta_{1b}^{2b} \cdot \eta_{1b}^{1b}}{\eta_b + 2\eta_{2b}^{2b}}}{\eta_b + \eta_{1b}^{3b} + 2\eta_{1b}^{2b} - \dfrac{2\eta_{1b}^{1b} \cdot \eta_{1b}^{2b}}{\eta_b + 2\eta_{2b}^{2b}}} \qquad \text{..... 2.32}$$

2.5.2 Non-diffuse Longitudinal and Transverse Fields

In section 2.3 it has been shown that, at low frequencies and mid frequencies, the longitudinal and transverse fields generated cannot be thought diffuse. Kihlman (1967) argues further that although bending waves may produce longitudinal and transverse waves at the junction of plates the fields generated suffer appreciable edge losses at low frequencies. Therefore these non-reverberant fields are not involved in the reverse power flow but rather act as energy sinks. Thus, the L.H.S of equations 2.28 and 2.29 have additional power loss terms describing the transformation at the junction of bending waves into longitudinal and transverse waves which dissipate energy through internal and edge losses.

For the bending wave field on plate 2, equation 2.28 becomes,

$$E_{2b}(\eta_b + 2\eta_{2b}^{1b,l,t}) = E_{1b}\eta_{1b}^{2b} + E_{3b}\eta_{1b}^{2b} \quad \ldots\ldots\ldots 2.33$$

and for plate 3,

$$E_{3b}(\eta_b + 2\eta_{1b}^{2b,l,t} + \eta_{1b}^{3b}) = E_{1b}\eta_{1b}^{3b} + 2E_{2b}\eta_{2b}^{1b} \quad \ldots\ldots\ldots 2.34$$

The notation in equations 2.33 and 2.34 has been altered to shorten the expressions. The loss factor describing the transformation of bending waves on the ith plate to bending, longitudinal, and transverse waves on the jth plate $\eta_{ib}^{jb,l,t}$ is such that,

$$\eta_{ib}^{jb,l,t} = \eta_{ib}^{jb} + \eta_{ib}^{jl} + \eta_{ib}^{jt}$$

The energy ratios in equations 2.31 and 2.32 become,

$$\frac{E_{2b}}{E_{1b}} = \frac{\eta_{1b}^{2b} + \eta_{1b}^{2b}.\eta_{1b}^{3b} \,/\, (\eta_b + 2\eta_{1b}^{2b,l,t} + \eta_{1b}^{3b,l,t})}{\eta_b + 2\eta_{2b}^{1b,l,t} - 2\eta_{1b}^{2b}.\eta_{2b}^{1b} \,/\, (\eta_b + 2\eta_{1b}^{2b,l,t} + \eta_{1b}^{3b,l,t})} \quad \ldots\ldots 2.35$$

and,

$$\frac{E_{3b}}{E_{1b}} = \frac{\eta_{1b}^{3b} + 2\eta_{1b}^{2b}.\eta_{2b}^{1b} \,/\, (\eta_b + 2\eta_{2b}^{1b,l,t})}{\eta_b + 2\eta_{1b}^{2b,l,t} + \eta_{1b}^{3b,l,t} - 2\eta_{1b}^{2b}\eta_{2b}^{1b} \,/\, (\eta_b + 2\eta_{2b}^{1b,l,t})} \quad \ldots\ldots 2.36$$

2.5.3 Diffuse Vibrational Fields

At high frequencies, the wave fields other than bending wave fields can also be considered diffuse. Reverse power flow must now be taken into account. Thus, the 'paths' shown in the flow diagram (Fig 2.1(b)) are all two-directional and more terms are added to the L.H.S and R.H.S of the equations 2.28 and 2.29. Not all possible paths have been considered in this modification e.g. the transmission from longitudinal and transverse waves on plate 1 to similar wave types on plate 2. These paths are described by relatively small coupling loss factors and yield small energy transfer. The resultant fields are therefore considered secondary. The validity of these assumptions is seen in section 4.4 and Appendix III where numerical values of related parameters are given.

For the bending wave field on plate 2,

$$E_{2b}(\eta_b + 2\eta_{2b}^{1b,l,t}) = E_{1b}\eta_{1b}^{2b} + E_{1l}\eta_{1l}^{2b} + E_{1t}\eta_{1t}^{2b} + E_{3b}\eta_{1b}^{2b} + E_{3l}\eta_{1l}^{2b} + E_{3t}\eta_{1t}^{2b} \quad \ldots\ldots 2.37$$

and plate 3 gives,

$$E_{3b}(\eta_b + 2\eta_{1b}^{2b,l,t} + \eta_{1b}^{3b,l,t}) = E_{1b}\eta_{1b}^{3b} + E_{1l}\eta_{1l}^{3b} + E_{1t}\eta_{1t}^{3b} + 2E_{2b}\eta_{2b}^{1b} + 2E_{2l}\eta_{2l}^{1b} + 2E_{2t}\eta_{2t}^{1b} \quad \ldots 2.38$$

Equations 2.37 and 2.38 have terms involving longitudinal and transverse energies on all three plates; the energy balance equations for longitudinal energy are,

$$E_{1l}(\eta_l + 2\eta_{1l}^{2b} + \eta_{1l}^{3b,l,t}) = 2E_{2b}\eta_{2b}^{1l} + E_{3b}\eta_{1b}^{3l} + E_{3l}\eta_{1l}^{3l} + E_{3t}\eta_{1t}^{3l} \quad \ldots 2.39$$

$$E_{2l}(\eta_l + 2\eta_{2l}^{1b}) = E_{1b}\eta_{1b}^{2l} + E_{3b}\eta_{1b}^{2l} \quad \ldots 2.40$$

$$E_{3l}(\eta_l + 2\eta_{1l}^{2b} + \eta_{1l}^{3b,l,t}) = 2E_{2b}\eta_{2b}^{1l} + E_{1b}\eta_{1b}^{3l} + E_{1l}\eta_{1l}^{3l} + E_{1t}\eta_{1t}^{3l} \quad \ldots 2.41$$

and the transverse energies are,

$$E_{1t}(\eta_t + 2\eta_{1t}^{2b} + \eta_{1t}^{3b,l,t}) = 2E_{2b}\eta_{2b}^{1t} + E_{3b}\eta_{1b}^{3t} + E_{3l}\eta_{1l}^{3t} + E_{3t}\eta_{1t}^{3t} \quad \ldots 2.42$$

$$E_{2t}(\eta_t + 2\eta_{2t}^{1b}) = E_{1b}\eta_{1b}^{2t} + E_{3b}\eta_{1b}^{2t} \quad \ldots 2.43$$

$$E_{3t}(\eta_t + 2\eta_{3t}^{2b} + \eta_{1t}^{3b,l,t}) = 2E_{2b}\eta_{2b}^{1t} + E_{1b}\eta_{1b}^{3t} + E_{1l}\eta_{1l}^{3t} + E_{1t}\eta_{1t}^{3t} \quad \ldots 2.44$$

The equations 2.37 to 2.44 use the equalities 2.30 plus the following,

$$\eta_{3l}^{2b} = \eta_{1l}^{2b}$$

$$\eta_{3t}^{2b} = \eta_{1t}^{2b}$$

$$\eta_{3l}^{1l} = \eta_{1l}^{3l}$$

$$\eta_{3l}^{1t} = \eta_{1l}^{3t}$$

$$\eta_{3t}^{1l} = \eta_{1t}^{3l}$$

$$\eta_{3t}^{1t} = \eta_{1t}^{3t} \qquad \text{..... 2.45}$$

Equations 2.3 to 2.4 could, with lengthy manipulation, yield each plate energy in terms of the bending wave energy on plate 1. A more convenient method is that of expressing the equations as a matrix which can be inverted by use of a computer. Thus the matrix is defined as,

$$[A]\,[E] = [C] \qquad \text{..... 2.46}$$

which is expressed more fully as,

$$
\begin{bmatrix}
\eta_t+2\eta_{1\ell}^{2b}+\eta_{1\ell}^{3b\ell t} & 0 & -2\eta_{2b}^{1\ell} & 0 & 0 & -\eta_{1b}^{3\ell} & -\eta_{1}^{3\ell} & -\eta_{1t}^{3\ell} \\
0 & \eta_t+2\eta_{1t}^{2b}+\eta_{1t}^{3b\ell t} & -2\eta_{2b}^{1t} & 0 & 0 & -\eta_{1b}^{3t} & -\eta_{1\ell}^{3t} & -\eta_{1t}^{3t} \\
-\eta_{1\ell}^{2b} & -\eta_{1t}^{2b} & \eta_b+2\eta_{2b}^{1b\ell t} & 0 & 0 & -\eta_{1b}^{2b} & -\eta_{1\ell}^{2b} & -\eta_{1t}^{2b} \\
0 & 0 & 0 & \eta_t+2\eta_{2\ell}^{1b} & 0 & -\eta_{1b}^{2\ell} & 0 & 0 \\
0 & 0 & 0 & 0 & \eta_t+2\eta_{2t}^{1b} & -\eta_{1b}^{2t} & 0 & 0 \\
-\eta_{1\ell}^{3b} & -\eta_{1t}^{3b} & -2\eta_{2b}^{1b} & -2\eta_{2\ell}^{1b} & -2\eta_{2t}^{1b} & \eta_b+\eta_{1b}^{3b\ell t}+2\eta_{1b}^{3b\ell t} & 0 & 0 \\
-\eta_{1\ell}^{3\ell} & -\eta_{1t}^{3\ell} & -2\eta_{2b}^{1\ell} & 0 & 0 & 0 & \eta_t+\eta_{1\ell}^{3b\ell t}+2\eta_{1\ell}^{2b} & 0 \\
-\eta_{1\ell}^{3t} & -\eta_{1}^{3t} & -2\eta_{2b}^{1t} & 0 & 0 & 0 & 0 & \eta_t+\eta_{1t}^{3b\ell t}+2\eta_{1t}^{2b}
\end{bmatrix}
\begin{bmatrix} E_{1\ell} \\ E_{1t} \\ E_{2b} \\ E_{2\ell} \\ E_{2t} \\ E_{3b} \\ E_{3\ell} \\ E_{3t} \end{bmatrix}
=
\begin{bmatrix} 0 \\ 0 \\ \eta_{1b}^{2b} \\ \eta_{1b}^{2\ell} \\ \eta_{1b}^{2t} \\ \eta_{1b}^{3b} \\ \eta_{1b}^{3\ell} \\ \eta_{1b}^{3t} \end{bmatrix}
$$

(b) Matrix inversion,

$$[E] = [A]^{-1}[C]$$

will then yield all vibrational energies relative to the bending wave energy on plate 1. The numerical methods employed are discussed in Chapter 4.

2.6 T-Junctions of Finite Plates

The junction of three plates can be thought of as a large plate from which is cantilevered a smaller plate (Fig 2.3(a)). Either the large plate or the cantilevered plate can be mechanically excited, each giving different power flow diagrams. For the case where the large plate is excited (Fig 2.3(b)) the procedure of obtaining the energy ratios is the same as that for a cross-junction.

(a)

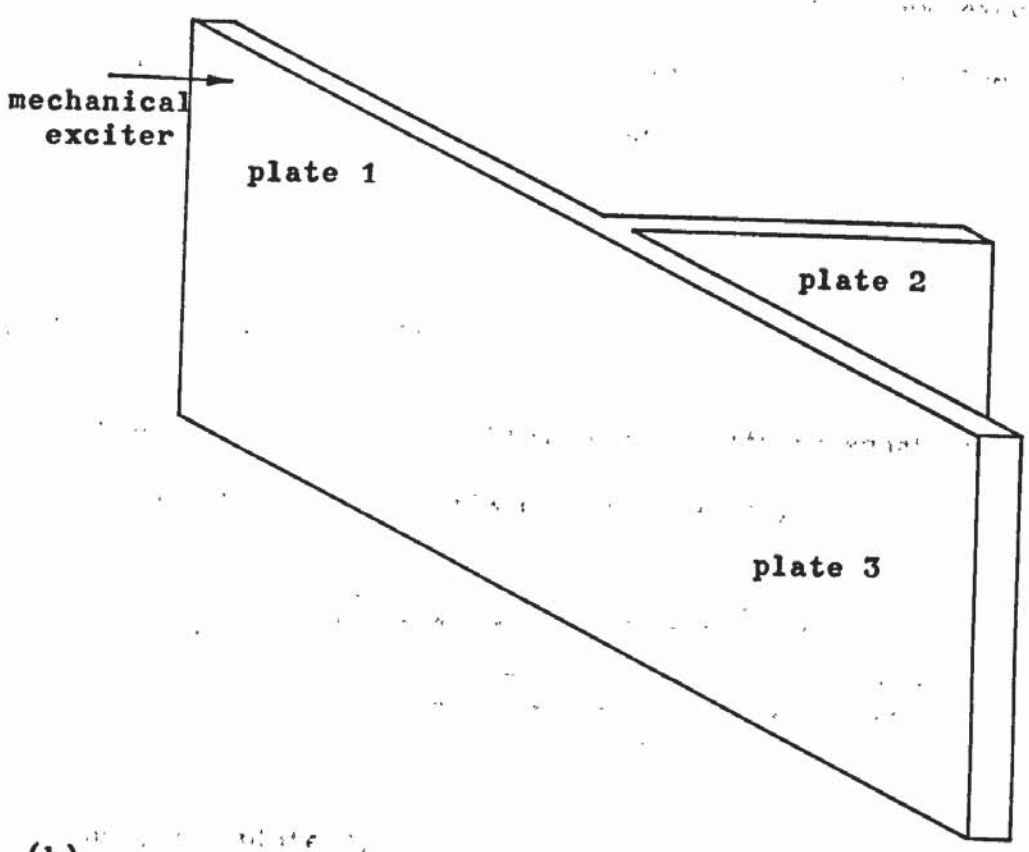

(b)

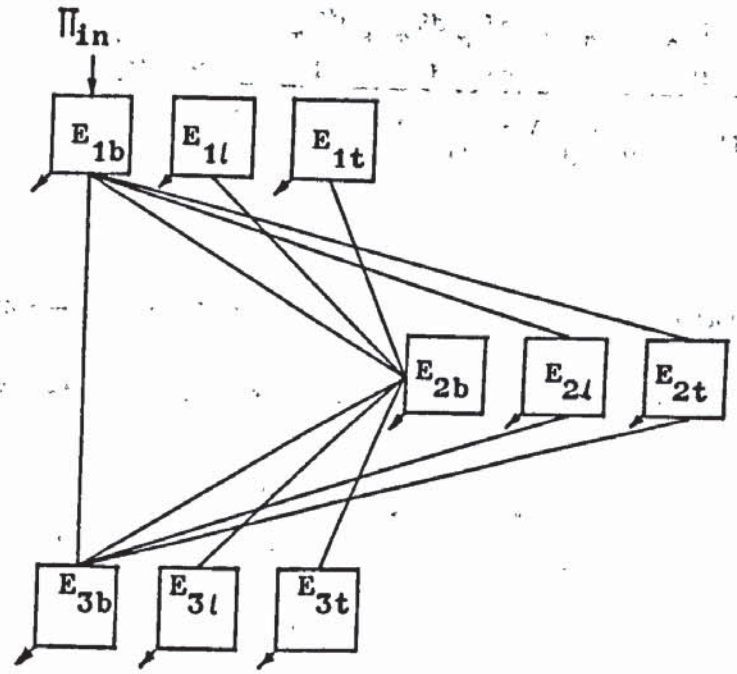

(a) T-junction where the large plate is mechanically excited into bending vibration.

(b) Power flow diagram.

Many of the energy balance equations are the same except that a factor of two is removed from some of the terms. The energy ratios will, therefore be stated directly.

2.6.1 Bending Wave Fields

The energy ratios are obtained by modifying equations 2.28 and 2.29. The energy on plate 2 is given by,

$$\frac{E_{2b}}{E_{1b}} = \frac{\eta_{1b}^{2b} + \eta_{1b}^{2b}.\eta_{1b}^{3b} / (\eta_b + \eta_{1b}^{2b} + \eta_{1b}^{3b})}{\eta_b + 2\eta_{2b}^{1b} - \eta_{1b}^{2b}.\eta_{2b}^{1b} / (\eta_b + \eta_{1b}^{2b} + \eta_{1b}^{3b})} \quad \ldots\ldots 2.47$$

and, for plate 3,

$$\frac{E_{3b}}{E_{1b}} = \frac{\eta_{1b}^{3b} + \eta_{1b}^{2b}.\eta_{2b}^{1b} / (\eta_b + \eta_{2b}^{1b})}{\eta_b + \eta_{1b}^{2b} + \eta_{1b}^{3b} - \eta_{1b}^{2b}.\eta_{2b}^{1b} / (\eta_b + \eta_{2b}^{1b})} \quad \ldots\ldots 2.48$$

2.6.2 Non-diffuse Longitudinal and Transverse Fields

Equations 2.33 and 2.34 when altered, give for plate 2,

$$\frac{E_{2b}}{E_{1b}} = \frac{\eta_{1b}^{2b} + \eta_{1b}^{2b}.\eta_{1b}^{3b} / (\eta_b + \eta_{1b}^{2b,l,t} + \eta_{1b}^{3b})}{\eta_b + 2\eta_{2b}^{1b,l,t} - \eta_{1b}^{2b}.\eta_{2b}^{1b} / (\eta_b + \eta_{1b}^{2b,l,t} + \eta_{1b}^{3b})} \quad \ldots\ldots 2.49$$

and for plate 3,

$$\frac{E_{3b}}{E_{1b}} = \frac{\eta_{1b}^{3b} + \eta_{1b}^{2b}.\eta_{2b}^{1b} / (\eta_b + \eta_{2b}^{1b,l,t})}{\eta_b + \eta_{1b}^{2b,l,t} + \eta_{1b}^{3b} - \eta_{1b}^{2b}.\eta_{2b}^{1b} / (\eta_b + \eta_{2b}^{1b,l,t})} \quad \ldots\ldots 2.50$$

2.6.3 Diffuse Fields

$$\begin{bmatrix} \eta_l+\eta_{1l}^{2b} & 0 & -\eta_{2b}^{1l} & 0 & 0 & 0 & 0 & 0 \\ 0 & \eta_t+\eta_{1t}^{2b} & -\eta_{2b}^{1t} & 0 & 0 & 0 & 0 & 0 \\ -\eta_{1l}^{2b} & -\eta_{1t}^{2b} & \eta_b+2\eta_{2b}^{1b,l,t} & 0 & 0 & -\eta_{1b}^{2b} & -\eta_{1l}^{2b} & -\eta_{1t}^{2b} \\ 0 & 0 & 0 & \eta_l+2\eta_{2l}^{1b} & 0 & -\eta_{1b}^{2l} & 0 & 0 \\ 0 & 0 & 0 & 0 & \eta_t+2\eta_{2t}^{1b} & -\eta_{1b}^{2t} & 0 & 0 \\ 0 & 0 & -\eta_{2b}^{1b} & -\eta_{2l}^{1b} & -\eta_{2t}^{1b} & \eta_b+\eta_{1b}^{3b}+\eta_{1b}^{2b,l,t} & 0 & 0 \\ 0 & 0 & -\eta_{2b}^{1l} & 0 & 0 & 0 & \eta_l+\eta_{1l}^{2b} & 0 \\ 0 & 0 & -\eta_{2b}^{1t} & 0 & 0 & 0 & 0 & \eta_t+\eta_{1t}^{2b} \end{bmatrix} \begin{bmatrix} E_{1l} \\ E_{1t} \\ E_{2b} \\ E_{2l} \\ E_2 \\ E_3 \\ E_{3l} \\ E_3 \end{bmatrix} = \begin{bmatrix} 0 \\ 0 \\ \eta_{1b}^{2b} \\ \eta_{1b}^{2l} \\ \eta_{1b}^{2t} \\ \eta_{1b}^{3b} \\ 0 \\ 0 \end{bmatrix}$$

..... 2.51

The matrix describing the energy balance equations.

2.7.1 T-Junction Where Cantilevered Limb is Excited

Figure 2.4 illustrates this configuration with the associated power flow diagram. As in the analysis of the cross-junction, plate 4 vibrational fields are assumed equal to those on plate 2, and the energy balance equation need only be considered for plate 2. Adopting the procedure of the previous sections, initially, assume the bending wave fields only as reverberant. The energy ratio of plate 2 is, therefore,

$$\frac{E_{2b}}{E_{1b}} = \frac{\eta_{1b}^{2b}}{\eta_b + \eta_{2b}^{1b}} \qquad \text{..... 2.52}$$

Fig. 2.4

(a)

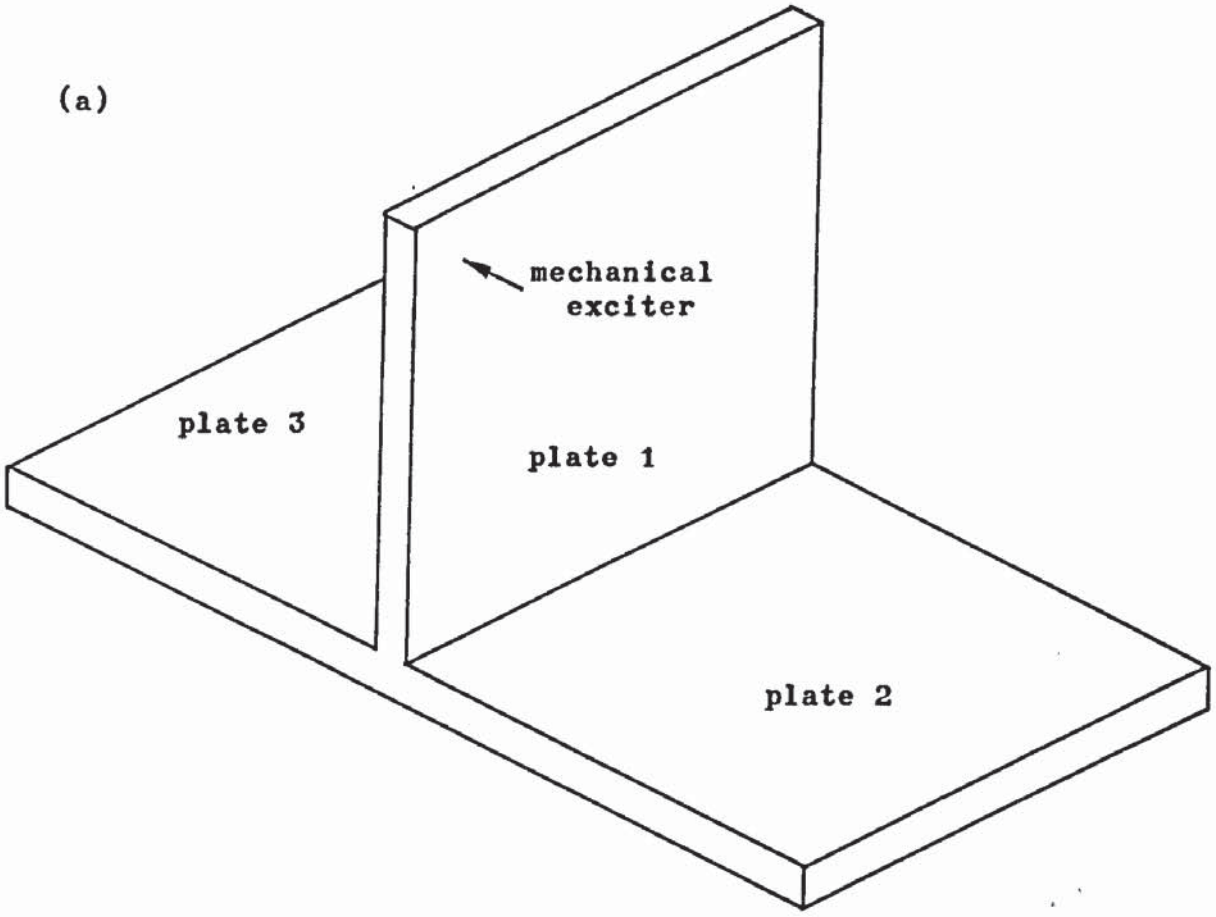

(b)

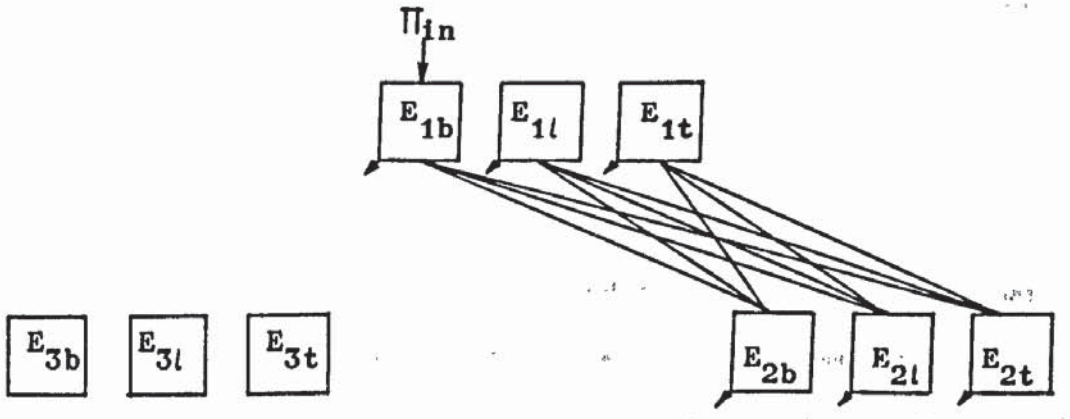

(a) T-junction in which the cantilevered plate is mechanically excited into bending vibration.

(b) Power flow diagram.

2.7.2 Non-diffuse Longitudinal and Transverse Fields

Equation 2.52 needs little modification and the ratio becomes,

$$\frac{E_{2b}}{E_{1b}} = \frac{\eta_{1b}^{2b}}{\eta_b + \eta_{2b}^{1b,l,t}} \qquad \ldots\ldots\ldots 2.53$$

2.7.3 Diffuse Longitudinal and Transverse Fields

The matrix describing this case is,

$$\begin{bmatrix} \eta+2\eta_l^{2b,l,t} & 0 & -2\eta_{2b}^{1l} & -2\eta_{2l}^{1l} & -2\eta_{2t}^{1l} \\ 0 & \eta_t+2\eta_{1t}^{2b,l,t} & -2\eta_{2b}^{1t} & -2\eta_{2l}^{1t} & -2\eta_{2t}^{1t} \\ -\eta_{1l}^{2b} & -\eta_{1t}^{2b} & \eta_b+\eta_{2b}^{1b,l,t} & 0 & 0 \\ -\eta_{1l}^{2l} & -\eta_{1t}^{2l} & 0 & \eta_l+\eta_{2l}^{1b,l,t} & 0 \\ -\eta_{1l}^{2t} & -\eta_{1t}^{2t} & 0 & 0 & \eta_t+\eta_{2t}^{1b,l,t} \end{bmatrix} \begin{bmatrix} E_{1l} \\ E_{1t} \\ E_{2b} \\ E_{2l} \\ E_{2t} \end{bmatrix} = \begin{bmatrix} 0 \\ 0 \\ \eta_{1b}^{2b} \\ \eta_{1b}^{2l} \\ \eta_{1b}^{2t} \end{bmatrix}$$

$\ldots\ldots\ldots 2.54$

2.8 Corner Junction of Finite Plates

Figure 2.5 gives the configuration and flow diagram of a corner junction. The energy ratios calculated are the same as in the previous section; when assuming bending waves as the only form of vibration, use equation 2.52, and when considering longitudinal and transverse fields as non-diffuse, use equation 2.53. It is necessary, of course, to incorporate the coupling loss factors of a corner junction into the equations.

Fig. 2.5

(a)

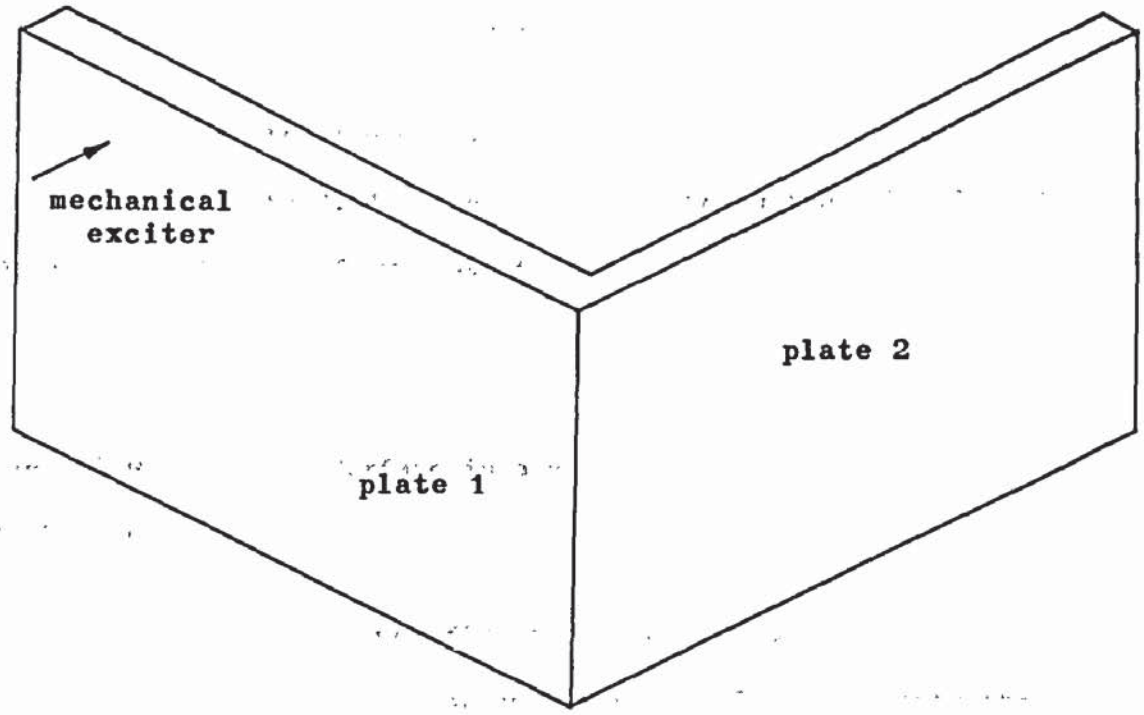

(b)

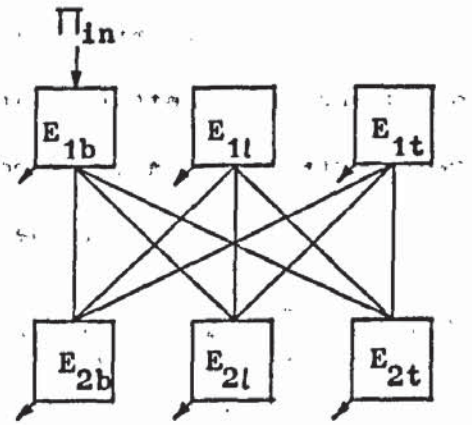

(a) Corner junction.

(b) Power flow diagram.

When all fields are assumed diffuse, the energy ratios result from a matrix similar to 2.54. The difference being that the elements containing a factor of two have this factor removed.

2.9 Power Flow Between a Surface in a Room and the Enclosed Air Volume

When dealing with the power flow from the bending wave field on a plate, forming one (or part of one) surface of a room, into the enclosed air volume, a coupling loss factor η_b^r describes the flow of energy from the plate and η_r^b describes the flow from the room to the plate. Thus, a vibrating panel radiating into a room where all other surfaces are assumed rigid (a fair assumption for the case of a scale model panel radiating into the receiver room from the aperture of a transmission suite), can be represented by the power flow diagram in Figure 2.6(b). There are two sources of power input; mechanical excitation of the plate and loudspeaker excitation of the room. From this diagram, two alternative energy balance equations result,

$$\omega E_b \eta_b + 2\omega E_b \eta_b^r = \omega E_r \eta_r^b + \Pi_{mech.} \quad \ldots\ldots\ldots 2.55$$

and,

$$\omega E_r \eta_r + \omega E_r \eta_r^b = \omega E_b \eta_b^r + \Pi_{acoust.} \quad \ldots\ldots\ldots 2.56$$

where η_b and η_r are the plate and room loss factors, respectively. Again, since the angular frequency ω is common to every term, it is disregarded. The factor of two in equation 2.55 indicates that

(a)

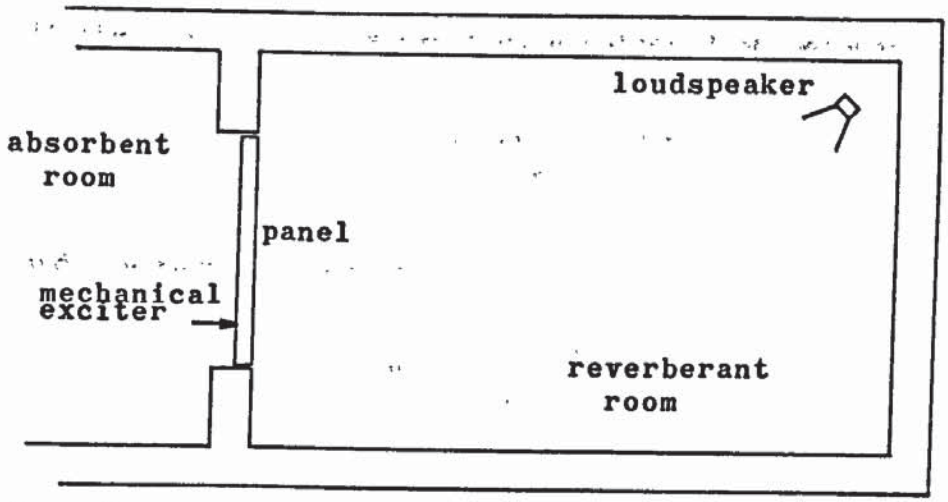

(b)

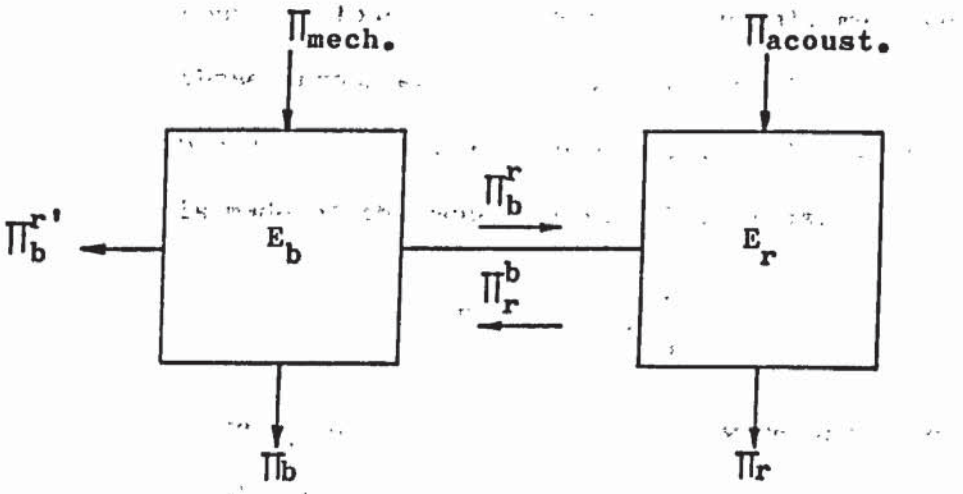

(a) Vibrating panel radiating into a reverberant room.

(b) Power flow diagram.

the plate is radiating into both the source and receiver rooms.

If the plate only, is excited, equation 2.56 becomes,

$$Er\eta_r + Er\eta_r^b = Eb\eta_b^r$$

and the resultant energy ratio is,

$$\frac{Er}{Eb} = \frac{\eta_b^r}{\eta_r + \eta_r^b} \qquad \text{..... 2.57}$$

In order to simplify this expression, use is made of the following considerations and assumptions.

(1) Because the modal densities of the bending wave fields and the pressure wave fields are appreciable (as discussed in sections 3.2.1 and 3.2.2), and because the coupling loss factors are, in general, much smaller than those encountered in structural coupling, the problem is brought within the range of S.E.A. In particular, use is made of the equality in 2.10. Thus,

$$n_r\eta_r^b = n_b\eta_b^r \qquad \text{..... 2.58}$$

where n_r and n_b are the pressure wave and bending wave modal densities, respectively.

(2) It will be shown in Chapter 3 that the coupling loss factor η_b^r is simply related to the radiation resistance of a plate. If a plate is suspended within a room then the radiation of sound is into 4π space. For a plate placed

in the aperture of a transmission suite, the radiation from each side of the plate is into 2π space. The assumption will be made that the coupling loss factor into 4π space is twice that into 2π space and unless stated, the latter will be used in this discussion. Therefore, in equation 2.55, the coupling loss factor η^{r}_{b} is the same as that in equation 2.56.

(3) When placed in the transmission suite aperture, the edge losses of the plate are assumed negligible.

(4) As well as the reverberant receiver room, the plate is coupled to the source room. This room is thought heavily damped (or in conventional terms, has a high average absorption coefficient), giving semi-free field conditions. Any power radiated into this room is therefore totally absorbed; none returning to the plate.

(5) Equation 2.57 contains a room loss factor term η_r which, although not the accepted method of describing the sound absorbing characteristics of a room, can be shown to be simply related to the classical expressions (section 3.3.2).

Using 2.58 in equation 2.57, gives,

$$\frac{Er}{Eb} = \frac{\eta^{r}_{b}}{\eta_r + \frac{n_b}{n_r}\eta^{r}_{b}} \qquad \ldots\ldots\ldots 2.59$$

If the only source of power is the loudspeaker, the equation 2.55 becomes,

$$Eb\eta_b + 2Eb\eta^r_b = Er\eta^b_r \qquad \ldots\ldots\ldots 2.60$$

which gives,

$$\frac{Eb}{Er} = \frac{\frac{nb}{nr}\eta^r_b}{\eta_b + 2\eta^r_b} \qquad \ldots\ldots\ldots 2.61$$

For both cases, the resultant energy ratios are seen to be dependent upon the internal loss factors of the plate and the room and the coupling loss factor between the bending wave field and the pressure field.

The description, so far, has been of an experimental rather than a field situation. In noise transmission in buildings, all wall and floor surfaces will radiate, and be excited by, airborne sound energy and the equivalent flow diagram involves many sub-systems. Also, structure-borne sound will flow between the plates making up the room surfaces. This more complex situation is investigated in Chapter 7 describing noise transmission between rooms. However, this simple model allows an experimental approximation and a resultant measurement of the radiation loss factor η^r_b (Chapter 6).

2.10 Summary

To summarise, by using power flow techniques and S.E.A., a unified approach to noise transmission in buildings is postulated. The vibrational energy flow between plates forming various structural junctions, and between plates and the surrounding air, have been investigated. Using energy balance equations, the relative vibrational energy for each wave type on each plate, and within the room volume, has been calculated in terms of simply defined parameters. These include the respective modal densities of each wave type, the internal loss factor of the material, and the coupling loss factor between each pair of sub-systems. It now remains to assess these parameters theoretically and experimentally.

CHAPTER 3

THEORETICAL ASSESSMENT OF POWER-FLOW PARAMETERS

The simplicity of application of power flow techniques in describing noise transmission has been shown in Chapter 2. The problem becomes more complicated when an attempt is made to define clearly the parameters used in the energy balance equations. Parameters such as the internal loss factor of a material and the modal density of a vibrational field are relatively easy to describe and to measure. However structure-fluid and structure-structure coupling loss factors demand a more detailed discussion. Along with the contributions of previous authors, this chapter is concerned with the theoretical assessment of structure-fluid coupling, modal density, loss factor, and structure-structure coupling which exist in buildings.

3.1 Structure-fluid and Sound Radiation from Plates

The sound radiation characteristics of a vibrating plate are influenced mainly by the efficiency of the coupling between the bending wave modes on the plate and the room modes. Before discussing the mechanism of this coupling a description is given of the sound radiation characteristics, if any, of other wave types which contribute to structure borne sound propagation.

3.1.1 Radiation characteristics of Structural Waves other than Bending Waves

In the generation and propagation of bending waves in structures,

PAGE NUMBERING AS ORIGINAL

near fields are produced at any discontinuity and, if a mechanical exciter is used, around the driver point. Heckl (1959) equates the radiation contribution of this near field on a plate to that of a piston type radiator of radius one-quarter of the bending wavelength. This contribution is independent of plate size and becomes less important at higher frequencies.

Quasi-longitudinal waves have a particle displacement normal to the surface of the plate due to lateral contraction described by the Poissons ratio. Sound can therefore be radiated into the surrounding medium, and is appreciable if the plate is surrounded by liquid of large acoustic impedance (Romanov 1969). However, in the case of air, this radiation is negligibly small, and abnormally large structural vibrational energies would be necessary before any appreciable radiation resulted.

Transverse shear waves which result from obliquely incident bending waves at a junction have their direction of propagation and particle displacement in the plane of the plate and therefore no sound radiation is possible.

The sound pressure field generated by a vibrating plate has near and far field components. Greene (1961) indicates that the near field results from the volume flow of air between adjacent areas which are vibrating out of phase. The sound pressure produced decays rapidly with distance (54.5 dB per wavelength for a plate with many nodal lines) and can therefore be ignored. In the following discussion therefore, the sound energy radiated by a

plate is that of the far field.

3.1.2 "Coincidence Effect"

The dispersive nature of bending waves results in the existence of frequencies where the bending wavelength, or a component of it, is equal to the airborne sound wavelength. This "matching" results in a sharp increase in sound energy transfer between plate and air and the phenomenon is known as coincidence. Cremer (1942) first developed a satisfactory concept of coincidence by describing an infinite plane pressure wave impinging upon an infinite plate (Fig 3.1). It is seen that the angle ϕ_o at which the sound waves incident on the plate are freely transmitted, is given by,

$$\phi_o = \sin^{-1} \frac{\lambda_o}{\lambda_b}$$

where $\frac{\lambda_o}{\lambda_b}$ is the ratio of pressure wavelength to plate bending wavelength.

The frequency at which coincidence occurs at an angle ϕ_o is given by,

$$\nu_c = 3^{\frac{1}{2}} C_o^2 / (\pi C_l h \sin^2\phi_o) \qquad \ldots\ldots\ldots 3.1$$

where C_l is the longitudinal wave velocity, C_o the airborne sound velocity, and h the plate thickness. It is seen that the coincidence frequency varies inversely as the square of the sine of the angle of incidence and that it cannot occur for plane waves normally incident. At grazing incidence (i.e. $\sin\phi_o = 1$) coincidence occurs at the lowest frequency possible for that particular plate thickness. This frequency is known as the critical coincidence frequency and is

Fig. 3.1

An infinite plane wave impinging upon an infinite plate.

(Cremer 1948)

given by,

$$\nu_c = 3^{\frac{1}{2}} C_o / (\pi C_l h) \qquad \ldots\ldots\ldots 3.2$$

Although Cremer's concept of coincidence assumes the plate to be infinite in area, the phenomenon is encountered in all transmission loss experiments. These measurements, involving finite plates, show that coincidence occurs at the frequency of grazing incidence (equation 3.2). However, Bhattacharya and Crocker (1969/70) argue that the agreement between the results of Cremer's infinite plate concept and finite plate measurements is accidental. It is further stated (Bhattacharya, Guy and Crocker 1971) that the coincidence effect of finite plates forming part of a rectangular enclosure is best approached by consideration of the modal character of the plate and room vibrations. Just as with Cremer's theory, Bhattacharya's concept gives the critical (or first) coincidence as occurring when the wave vector in the room is at the grazing angle of incidence, under conditions of maximum coupling and panel resonance. Subsequent coincidences occur at frequencies which obey the following condition

$$\frac{(\nu - \nu_{c/2})^2}{(\nu_{c/2})^2} - \frac{l^2}{(a.\nu_c/C_o)^2} = 1 \qquad \ldots\ldots\ldots 3.3$$

where $l = 0, 1, 2, \ldots\ldots$

l is the cavity mode number in the direction normal to the flexible plate and a is the room dimension in the same direction. The relationship between ν and l given by equation 3.3, has the form of a hyperbola. The critical coincidence ($l=0$) gives the maximum transmission of energy. The subsequent coincidences, given by

higher values of l, have a gradually reduced transmission.

The descriptions of coincidence by Cremer and by Bhattacharya are deceptively similar, and it is left to Yaneske (1972) to underline the fundamental differences between the two. Using the generalised concept of energy transfer between any load form and any shape of system displacement, Yaneske shows that a maximization condition corresponds to the load being present both 'at the right time' and 'at the right place' relative to the system displacement. The first condition is described as resonance and the second can be described by a term such as 'being coupled'. Since Cremer deals only with unbounded systems, resonance is automatic and the coincidence effect can be described solely by the condition in space which maximises the amplitude of the induced free wave in the system. Bhattacharya and Crocker use the term coincidence to describe several optimum conditions which must occur simultaneously. The condition of being 'at the right time' requires that the bending wave on the plate and the pressure field in the room must both be in a state of resonance. The condition of being 'at the right place' demands that the plate modes and the room modes are well coupled. The two conditions are separable and the need for them to be satisfied simultaneously shows that true coincidence in finite systems will rarely, if ever, occur.

Bhattacharya et al also point out that it is theoretically impossible to visualize coincidence in a finite plate unless it is backed by a cavity. This conclusion results from the fact that plane progressive pressure waves can only be assumed to match freely propagating bending waves on a plate. Conversely, standing waves in an enclosure

will generate standing waves on the plate. It is not possible to visualise the matching of a standing wave on a plate with a freely propagating wave in air.

3.1.3 Nomenclature

In the following discussion the parameter used most often is that of radiation loss factor η_{rad}. However, reference is now made to other parameters which have been used in describing sound radiation, and their relationship with each other. Gösele (1953) assesses the sound radiation effeciency of a vibrating plate by comparing the intensity radiated to that of a piston type radiator of the same area and vibrating with the same velocity amplitude. Thus if the sound intensity radiated by the piston is given by,

$$I_o = \frac{\rho_o c_o}{2} v^2 S$$

where v is the velocity amplitude, S the plate area, and $\rho_o c_o$ is the characteristic impedance of air, then the parameter s describing the radiation of the plate under observation is given by,

$$s = I/I_o$$

where I is the actual sound energy intensity radiated by the plate. The constant s is known as the sound radiation factor or efficiency of the vibrating surface and in general has a value near to or less than unity over most of the frequency range. Gösele shows that for an infinite plate the radiation factor becomes infinite at the coincidence frequency and then rapidly tends to unity for the higher frequencies. This well known expression for radiation is reproduced

below.

$$s = (1-(\lambda_o/\lambda_b)^2)^{-1/2} \qquad \lambda_b \geq \lambda_o$$

$$s = 0 \qquad \lambda_b < \lambda_o$$

..... 3.4

The simple expressions in 3.4 have been modified in two ways in order that the equation describes more realistically phenomena at the subcritical region.

(1) Gösele shows that if a finite plate is considered then the bending wave on it is a standing wave. Instead of being zero, the subcritical value of the radiation factor s will increase with increase of the ratio of bending wavelength to plate width, λ_b/a . Heckl (1959) appears to give an explanation of this increase by suggesting that the modal form of the plate bending wave field results in cancellation of all contributing vibrating areas adjacent to each other, except at the edges which give a resultant finite radiation. As the plate width decreases with respect to the wavelength, this edge effect assumes greater importance.

(2) Westphal (1954), by incorporating internal damping into the derivation (thus making Young's modulus complex) shows that the subcritical values of s increase with increase of internal loss factor of the plate.

In both modifications described the equations give a finite

value of s at coincidence.

Reference is often made to the radiation resistance Rrad of a structure in work on S.E.A. Examples are Lyon and Maidanik (1961) and Fahy (1969). Maidanik (1962) defines the radiation resistance as the sound power radiated by a panel divided by the mean square velocity of the panel, averaged on time and space. Thus,

$$Rrad = \frac{\Pi a}{\langle Vp^2 \rangle} \qquad \ldots\ldots\ldots 3.5$$

The related radiation loss factor is given by Fahy and Wee (1968) as,

$$\eta_{rad} = \frac{Rrad}{Mp\,\omega} \qquad \ldots\ldots\ldots 3.6$$

where Mp is the plate mass.

3.1.4 The modal behaviour of plates

A vibrating finite plate can be described as a two dimensional array of piston radiators which may reinforce or cancel each other, depending on whether two radiating surface elements are in phase or out of phase. Maidanik (1962) and Crocker and Price (1969) give comprehensive descriptions of this phenomenon.

The vibration modes of a finite plate can be divided into modes with resonance frequencies above critical coincidence and modes with those below. Crocker and Price describe the former as acoustically

fast (i.e. the bending wave velocity is greater than the speed of sound) and the latter as acoustically slow. A subsonic bending wave produces an airborne sound wave which because of its greater velocity, causes cancellation of the contributions of adjacent surface elements vibrating out of phase.

Figure 3.2 illustrates three important cases. When the bending wave speeds parallel to both edge directions are subsonic, the acoustic pressure generated by a phase element (or quarter wave cell) is cancelled everywhere except at the corners (Fig 3.2(a)). When a mode has a supersonic bending wave parallel to one edge and a subsonic wave parallel to the other edge, then cancellation will result everywhere except at the two edges (Fig 3.2(b)). The last case (Fig 3.2(c)) illustrates the surface mode which results when the bending wave is supersonic in both directions. Here, no cancellation occurs and the whole of the plate surface radiates sound energy.

3.1.5 Rectangular walls radiating into rectangular rooms

In section 3.1.2 it was mentioned that one of Bhattacharya's conditions for the occurrence of coincidence was the maximisation of coupling between plate and room modes. In work by Kihlman (1967), Fahy (1969), Bhattacharya and Crocker (1969/70) and Nilsson (1971) the coupling between the pressure wave modes in the room and the bending wave modes on the plate are evaluated. The plate can be part of or all of one wall surface, or the partition wall between two rooms.

Fig. 3.2

Wavelength relations and effective radiating areas for three modes. (Crocker and Price 1968).

The method adopted by each author is essentially the same and consists of calculating a coupling coefficient B_{qr}^{mn} between the room modes m,n (in the directions parallel to the plate edges) and the plate modes q,r. This coefficient is expressed as,

$$B_{qr}^{mn} = \frac{4}{bc} \int_0^c \int_0^b \sin \frac{q\Pi y}{b} \sin \frac{r\Pi z}{c} \cos \frac{m\Pi y}{b} \cos \frac{n\Pi z}{c} \, dy \, dz \quad \ldots\ldots\ldots 3.7$$

where b and c are the plate dimensions.

On evaluating this coefficient, Bhattacharya and Crocker show that certain combinations of room modes m,n and panel modes q,r give zero values to B_{mn}^{qr}. No coupling is then said to occur. For the conditions that do give coupling equation 3.7 reduces to,

$$B_{qr}^{mn} = \frac{4}{\Pi^2} \frac{4qr}{(m^2 - q^2)(n^2 - r^2)} \quad \ldots\ldots\ldots 3.8$$

Equation 3.8 gives maxima when,

$$m = q \pm 1$$
$$r = n \pm 1 \quad \ldots\ldots\ldots 3.9$$

Thus, a maximum results when the panel modes are closest to the room modes but have different parity.

Fahy (1969) further differentiates modal coupling into well coupled and proximate coupled modes. In the subcritical frequency range, he shows that the ($m = q \pm 1$, $r = n \pm 1$) type coupling is not normally possible. The most efficient coupling occurs between modes close in natural frequency (less than half the sum of their

bandwidths apart) and have the best available wave component match in directions parallel to the plate edges. The modes are then said to have maximum proximate coupling. In the supercritical frequency region the ($m = q \pm 1$, $r = n \pm 1$), well coupled modes predominate. Fahy's analysis is complicated by the statistics needed to describe quantitatively the contribution of each type of modal coupling.

The problem can be simplified by remembering that for the concrete plates investigated the radiation characteristics are those in the frequency region above critical coincidence where theory gives a radiation efficiency close to unity. Kihlman (1967), in calculating the average sound radiation from a wall with standing waves of sinusoidal shape, shows that, above critical coincidence, the radiation is on the average very nearly the same as that obtained from the same wave when radiating into a semi-infinite space. This conclusion was drawn by comparing results from calculations using wave analysis to those derived from simple energy methods.

3.1.6 Radiation loss factor and the effect of different boundary conditions

Although we are here primarily concerned with the supercritical frequency region of concrete plates, it may be of interest to calculate the radiation loss factor over the full audio frequency range. The calculation is that of Maidanik (1962) whose derivation, using a tranform method, is corroborated by Donato (1973) who uses

a direct derivation.

Experimental confirmation is given by Crocker and Price (1969). Although developed to explain the acoustic response of ribbed panels, the theory is applied successfully to simple panels forming partitions. The value of radiation loss factor $\eta_{rad}^{2\pi}$ into half space, of a plate of mass M_p, area S_p, and length of sides l_1, l_2 is given by,

$$\eta_{rad.}^{2\pi} = \frac{\rho_o c_o}{2\pi\rho\nu h} \begin{cases} (\lambda_c\lambda_a/S_p)\, 2(\nu/\nu_c)g_1 + (2(l_1+l_2)\lambda_c/S_p)g_2 & \nu < \nu_c \\ (l_1/\lambda_c)^{1/2} + (l_2/\lambda_c)^{1/2} & \nu = \nu_c \\ (1-\nu_c/\nu)^{-1/2} & \nu > \nu_c \end{cases} \quad \ldots\ldots 3.10$$

where $$g_1 = \begin{cases} (4/\pi^2)(1-\nu/\nu_c)/((\nu/\nu_c)^{1/2}(1-\nu/\nu_c)^{1/2}) & \nu < \nu_c/2 \\ 0 & \nu > \nu_c/2 \end{cases}$$

$$g_2 = (2\pi)^{-2}[(1-\nu/\nu_c)\ln[(1+(\nu/\nu_c)^{1/2})/(1-(\nu/\nu_c)^{1/2})] + 2(\nu/\nu_c)^{1/2}]/(1-\nu/\nu_c)^{3/2}$$

ρ_o and ρ are the air and plate densities respectively, λa is the acoustic wavelength, and λc is the coincidence wavelength of the panel. The plot of $\eta_{rad}^{2\pi}$ for a reinforced concrete plate of thickness 150 mm, is given by the solid line in Figure 3.3.

It is seen that the subcritical response and the value at critical coincidence are dependent upon the plate dimensions whereas the supercritical value is simply dictated by the ratio of the critical

coincidence frequency to the frequency of vibration. More specifically, Maidanik concludes that the subcritical coupling is proportional to the length of the plate's perimeter.

So far the plate has been assumed to be simply supported and that no near fields are produced at the plate edge. Both Maidanik (1962) and Smith (1964) show that at frequencies below coincidence the radiation contribution of near fields produced on free or rigidly clamped plates must be considered.

By considering an infinite beam-plate system, Maidanik shows that the radiation resistance (and therefore, the radiation loss factor) of a plate with boundaries which give rise to near fields is twice that of the simply supported plate when the frequency lies below coincidence. At higher frequencies, the near fields become progressively less important and the radiation resistance approaches the value of that of a simply supported plate. Thus, in Figure 3.3, the dotted line lying 3 dB above the solid line describes the radiation loss factor for free or clamped plates. It would be thought that experimental points will lie on the dotted line below coincidence frequency. Above coincidence the two lines would be expected to act as the envelope of experimental points, the tendency being to assume the values of the solid line at higher frequencies.

3.1.7 Summary

When describing the radiation characteristics of reinforced concrete plates, simple energy methods are used. The critical coincidence

Fig. 3.3

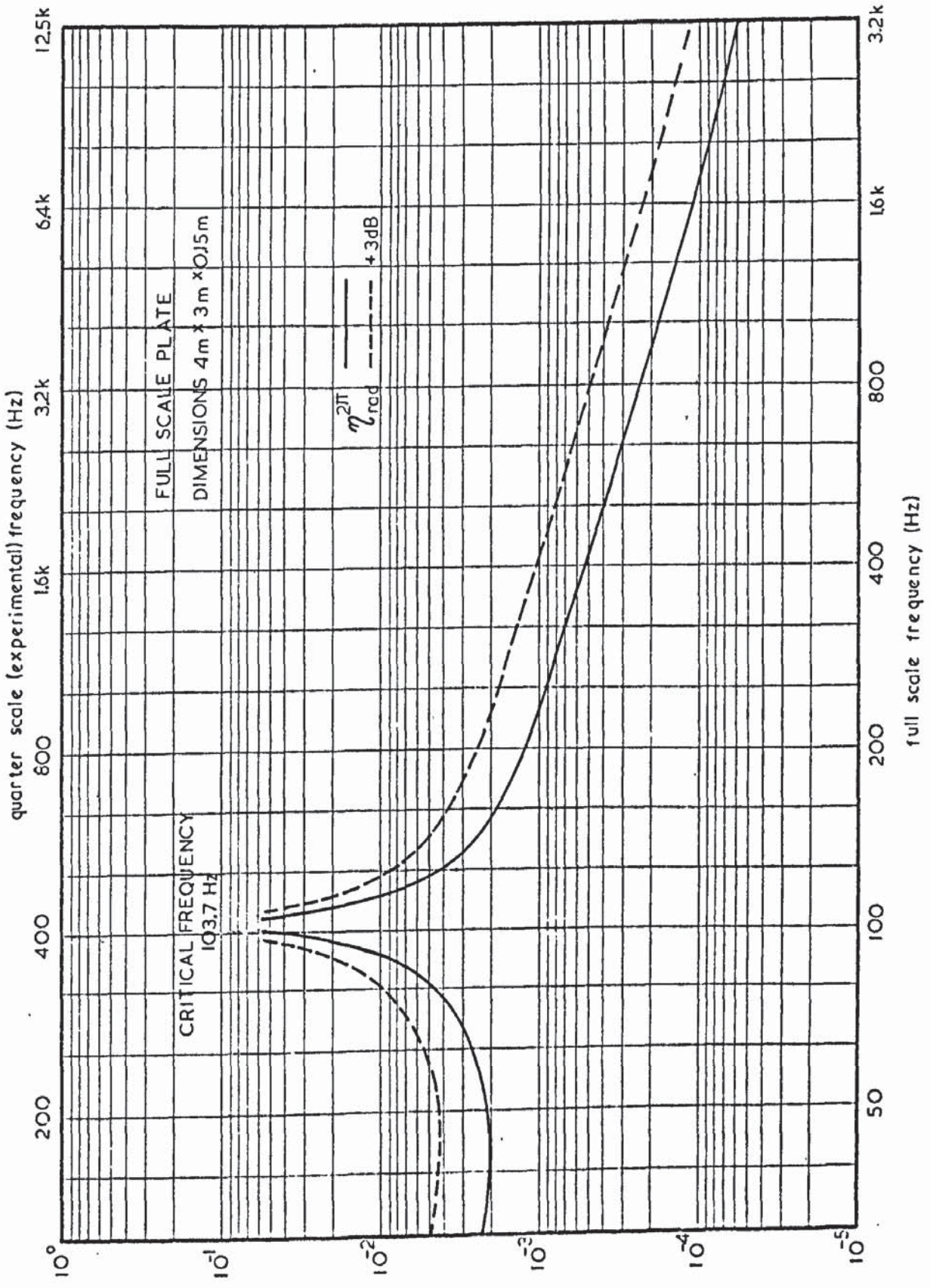
quarter scale (experimental) frequency (Hz)
12.5k
6.4k
3.2k
1.6k
800
400
200
FULL SCALE PLATE
DIMENSIONS 4m x 3m x 0.15m
$\eta^{2\pi}_{rad}$
+3dB
CRITICAL FREQUENCY
103.7 Hz
10^{0}
10^{-1}
10^{-2}
10^{-3}
10^{-4}
10^{-5}
3.2k
1.6k
800
400
200
100
50
full scale frequency (Hz)

frequency is thought to be the only observable coincidence and the modal characteristics of the plate and the room are ignored at supercritical frequencies. More specifically, the radiation of the plate is assumed independent of its situation, e.g. whether it forms part of a rectangular room, or is radiating into half-space. In the same frequency range, the effect of boundary conditions can be neglected. By these simplifications, the sound radiation into half-space from a vibrating plate can be expressed in terms of the radiation loss factor such that sound power flow Π_b^r from the bending wave field E_b on a plate, into a room is given by,

$$\Pi_b^r = \omega \eta_b^r E_b \qquad \ldots\ldots 3.11$$

where $$\eta_b^r = \eta_{rad}^{2\pi}$$

In this way the sound radiation characteristics of walls and floors making up rectangular rooms, can be introduced into the energy balance equations, described in Chapter 2, in the same way as the internal loss factors and the structural coupling loss factors.

3.2 Modal density

The modal density of some wave types has already been given in section 3 of Chapter 2, and it remains to give a description of the equations used in their calculation. The modal distributions of interest are those of pressure waves in rectangular rooms, and bending, longitudinal, and transverse waves on finite plates.

3.2.1 Pressure waves in rectangular rooms

Several authors have derived the expression giving the number N of modes, or eigentones in a rectangular room having frequencies less than a value ν . Morse and Ingard (1968) give the solution of the wave equation for the boundary condition that all surfaces are acoustically 'hard'. If ψ is the velocity potential, the sound wave equation is given as,

$$\nabla^2\psi - \frac{1}{c_o^2}\ddot{\psi} = 0$$

A solution of the wave equation can be written as,

$$\psi = \exp(-i\omega t)\cos\frac{l\pi x}{Lx}\cos\frac{m\pi y}{Ly}\cos\frac{n\pi z}{Lz} \qquad \ldots\ldots\ldots 3.12$$

where Lx, Ly, Lz are the room dimensions. The integers l, m, n are such that

$$4\pi^2\frac{\nu^2}{Co^2} = \frac{l^2\pi^2}{Lx^2} + \frac{m^2\pi^2}{Ly^2} + \frac{n^2\pi^2}{Lz^2} \qquad \ldots\ldots\ldots 3.13$$

For modes with frequencies less than ν , equation 3.13 becomes,

$$\frac{4\nu^2}{Co^2} > \frac{l^2}{Lx^2} + \frac{m^2}{Ly^2} + \frac{n^2}{Lz^2} \qquad \ldots\ldots\ldots 3.14$$

Thus, in(l, m, n) space, any point having positive integral co-ordinates represents an eigentone. The total number of eigentones below a frequency ν is given by the number of points in the positive octant of the ellipsoid represented by equation 3.14. The number of points equals the volume of this octant and therefore the number Np of eigentones having frequencies less than ν is given by,

$$Np = \frac{1}{8}\ \frac{4\pi}{3}\ \left(\frac{2Lx\nu}{Co}\right)\left(\frac{2Ly\nu}{Co}\right)\left(\frac{2Lz\nu}{Co}\right) = \frac{4\pi}{3}\ V\ \frac{\nu^3}{Co^3} \qquad \ldots\ldots\ 3.15$$

where V is the room volume.

The expression 3.15 is asymptotic in that the wavelength is assumed small compared to the room dimensions. Dah-You Maa (1939) shows that, at low frequencies, correcting terms need to be added to the expression. Points lying on the co-ordinate planes are shared between two octants and those on the axes by four octants. Therefore equation 3.15 is corrected by the addition of half the number of points on the co-ordinate planes and half the number on the axes. The equation becomes,

$$Np = \frac{4\pi}{3}\ V\ \frac{\nu^3}{Co^3} + \frac{\pi}{4}\ S\ \frac{\nu^2}{Co^2} + \frac{1}{2}\frac{\nu}{Co} \qquad \ldots\ldots\ 3.16$$

where S is the total surface area of the room, and L is the sum of the three room dimensions. The modal density is obtained on differentiating Np with respect to frequency. Thus,

$$n_p = \frac{dNp}{d\nu} = 4\pi V\ \frac{\nu^2}{Co^3} + \frac{\pi}{2}\ S\ \frac{\nu}{Co^2} + \frac{L}{2Co} \qquad \ldots\ldots\ 3.17$$

3.2.2 Bending waves on plates

The derivations of the vibrational modal densities on simple structural elements are described in a review by Hart and Shah (1971). For a simply supported rectangular plate the standing wave solution to the bending wave equation is expressed as,

$$\delta = \sin\left(\frac{p\pi x}{Lx}\right) \sin\left(\frac{q\pi y}{Ly}\right)$$

where the wave number K is related to the plate dimensions Lx, Ly

$$K^2 = \left[\left(\frac{p\pi}{Lx}\right)^2 + \left(\frac{q\pi}{Ly}\right)^2\right] \qquad \ldots\ldots\ldots 3.18$$

Thus, two component wave numbers are defined,

$$Kx = \frac{p\pi}{Lx} \quad \text{and} \quad Ky = \frac{q\pi}{Ly} \qquad \ldots\ldots\ldots 3.19$$

such that

$$\Delta Kx = \frac{\pi}{Lx} \quad \text{and} \quad \Delta Ky = \frac{\pi}{Ly}$$

for unit increments of p and q.

In K-space the number of resonant frequencies is given as,

$$N_b(\omega) = \frac{1}{\Delta K_x \Delta K_y} \iint_{S_p} dK_x\, dK_y \qquad \ldots\ldots\ldots 3.20$$

where Sp is the plate area.

The integral is evaluated using cylindrical co-ordinates and on assuming that the plate radius of gyration is $h/\sqrt{12}$.

Thus, $$N_b(\nu) = \frac{\sqrt{3}\, S_p}{c_l h}\, \nu$$

The modal density is therefore,

$$n_b(\nu) = \frac{dN_b(\nu)}{d\nu} = \frac{\sqrt{3}\, S_p}{c_l h} \qquad \ldots\ldots\ldots 3.21$$

The expression for modal density in 3.21 is that of thin plates. Using his universal dispersion curve Nelson (1971, 1972) shows that the modal density for plates which are not thin compared to bending wavelength, has a value larger than that predicted using thin plate theory. A correction factor Kp is incorporated and this is defined by the expression,

$$Kp = \frac{h\,K}{Cg/C_3}$$

where Cg/C_3 is the ratio of bending wave velocity to the surface (Rayleigh) wave velocity. The corrected modal density for bending waves on plates is then,

$$n_{corr.}(\upsilon) = n(\upsilon)\,Kp \qquad \ldots\ldots\ldots 3.22$$

It will be seen in measurements of bending wave modal density of model reinforced concrete plates (section 6.4) that the theory described by Hart and Shah is adequate in predicting experimental results.

3.2.3 Longitudinal and transverse waves on plates

The modal distribution of longitudinal and transverse waves on rectangular plates can be considered as a two dimensional analogy to that of pressure waves in rectangular rooms. This analogy is valid if the waves are thought non-dispersive, and on assuming that perfect reflection occurs at the plate edges. Thus, for longitudinal waves, the two dimensional analogy to expression 3.12 is given as,

$$\psi_l = \exp(-i\omega t) \cos \frac{m\pi y}{Ly} \cos \frac{n\pi z}{Lz} \qquad \ldots\ldots\ldots 3.23$$

where the plate lies in the x-y plane and has sides Ly, Lz. Similar to the derivation given by equations 3.12 to 3.14, the modes with frequencies less than a value ν are given by,

$$\frac{4\nu^2}{c_l^2} > \frac{m^2}{Ly^2} + \frac{n^2}{Lz^2} \qquad \ldots\ldots\ldots 3.24$$

Taking the positive quadrant, the total number of modes with frequency less than ν is,

$$N_l = \frac{1}{4} \pi \left(\frac{2Ly\nu}{c_l}\right)\left(\frac{2Lz\nu}{c_l}\right) = \pi Sp \frac{\nu^2}{c_l^2} \qquad \ldots\ldots\ldots 3.25$$

where Sp is the plate area. The modal density becomes,

$$n_l = \frac{dN_l}{d\nu} = 2\pi Sp \frac{\nu}{c_l^2} \qquad \ldots\ldots\ldots 3.26$$

Similarly, at low frequencies a correction can be added to equation 3.26 allowing for the points lying on the axes of intersection which have been halved. Equation 3.26 becomes,

$$N_l = \pi Sp \frac{\nu^2}{c_l^2} + (Lx + Lz) \frac{\nu}{c_l} \qquad \ldots\ldots\ldots 3.27$$

giving the modal density

$$n_l = \frac{dN_l}{d\nu} = 2\pi\ Sp \frac{\nu}{c_l^2} + \frac{(Lx + Lz)}{c_l} \qquad \ldots\ldots\ldots 3.28$$

The modal density for transverse waves is stated directly,

$$n_t = 2\pi\ Sp \frac{\nu}{Ct^2} + \frac{(Lx + Lz)}{Ct} \qquad \ldots\ldots\ldots 3.29$$

3.3 Loss factor

The following discussion on loss factor is primarily concerned with the internal dissipation of building materials, due to the effect of imperfect elasticity rather than the effects of applying damping to existing structures. Thus, work on the increased damping in sandwich structures containing one or more layers of viscoelastic material will not be considered. Neither will the effects of structural linkages such as rivets or bolts in steel plate be discussed. The increase in damping due to the attachment of a viscoelastic layer to the surface of a plate is analysed experimentally in section 6.6.2.

3.3.1 Definitions and nomenclature

So far, the internal dissipative loss factor η has been described in terms of the energy balance equations given in Chapter 2. In his description of the dynamic properties of viscoelastic material, Snowdon (1968) describes the concept of the complex elastic modulus. The strain is no longer simply related to the stress, but that the complex modulus $\bar{E}$ has a real component describing the storage modulus and an imaginary part describing the loss. The ratio of the imaginary to the real component is known as the loss factor. Other terms used are loss tangent or loss coefficient. Thus the complex modulus is written,

$$\bar{E} = E(1 + i\eta) \qquad \ldots\ldots 3.30$$

Internal losses in a building material such as reinforced concrete

can be caused by a variety of mechanisms involving the aggregate, cementing material, and reinforcing rods.

Kuhl and Kaiser (1952) show that the effect of crevices causes an increase of damping with increased vibration amplitude for brickwork but not for concrete. The increase of loss factor with increase in frequency is explained if it is assumed that 0.1% of the material consists of loose particles. However, as stated by Lazan, although information is available on metals and polymers, (Pisarenko, 1962), little is known of the physical micromechanisms in non-metallic materials.

As well as the internal loss factor there are several parameters which describe the dissipation of vibrational energy within a material. If the material, in the form of a bar, is excited into resonant vibration, the peak in the amplitude of vibration remains finite due to the internal damping present in all materials. As the damping increases the peak decreases and the bandwidth of half power points increases (Fig 3.4(a)). This magnification at resonance is described by the Q-factor which is calculated from the half power bandwidth ($\nu_2 - \nu_1$) in the expression,

$$Q = \frac{\nu_r}{(\nu_2 - \nu_1)}$$

where ν_r is the resonant frequency of the beam or system. The inverse value of the Q-factor gives the loss factor.

Instead of the steady state response, the transient response of a

Fig. 3.4

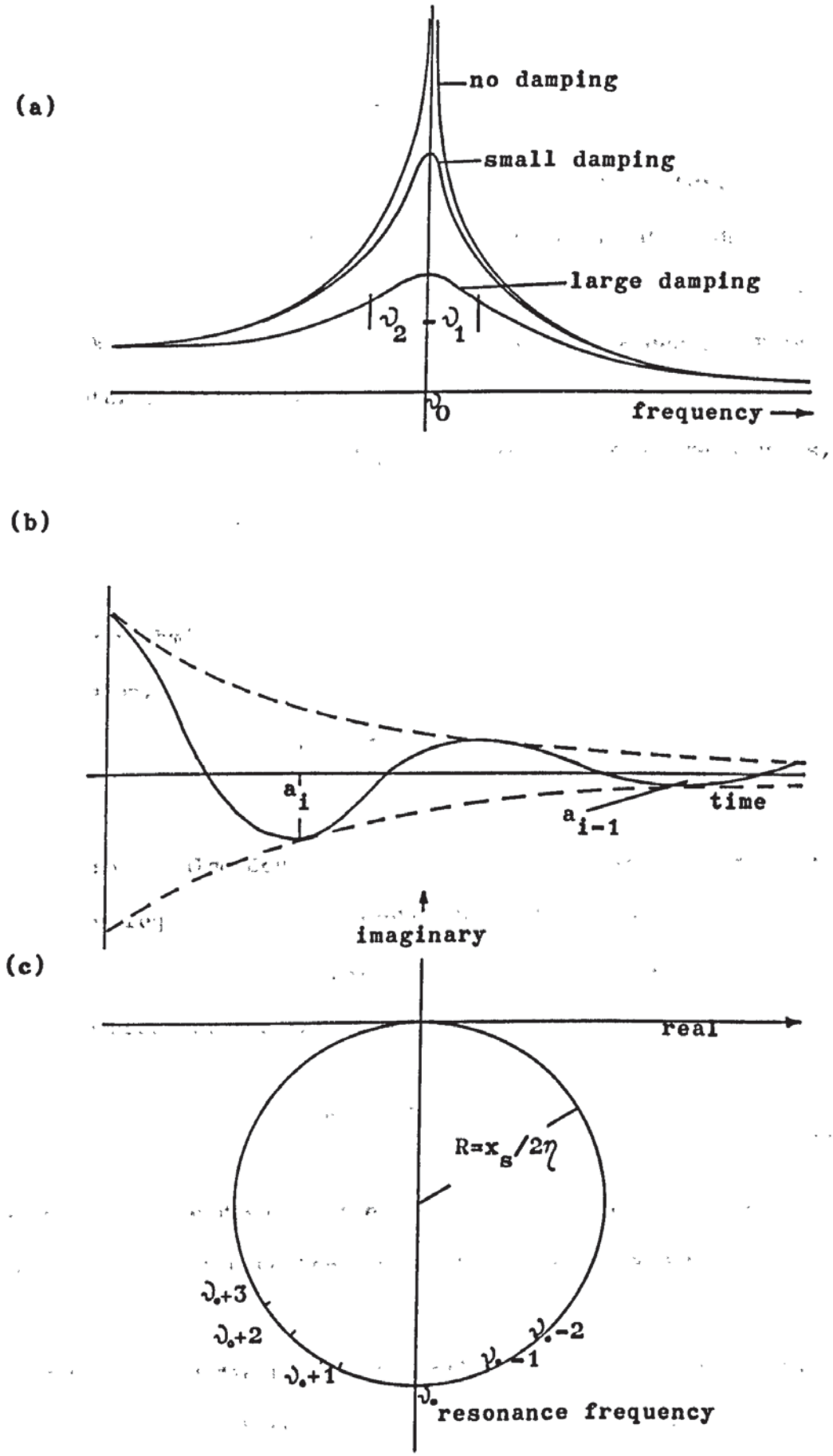

(a) Half power bandwidth method.

(b) Decay method.

(c) Admittance circle method.

system can be measured in calculation of loss factor. On removing the source of excitation the amplitude of vibration decays at a rate dictated by the internal losses. (Fig 3.4(b)). It is possible to talk of the logarithmic decrement δ of the decay. This parameter is calculated from the measurement of the ratio of successive amplitudes a_i/a_{i+1}. The well known expression is,

$$\delta = \ln \frac{a_i}{a_{i+1}} = \frac{1}{n} \ln \frac{a_i}{a_{i+n}}$$

The logarithmic decrement yields the loss factor by means of the expression,

$$\eta = \frac{\delta}{\pi}$$

The decay is also described by the reverberation time T which is the time required for the amplitude to decay to one thousandth of its initial value. The loss factor is derived from reverberation time by means of the expression

$$\eta = \frac{2.2}{\nu T} \qquad \ldots\ldots\ldots 3.31$$

where ν is the resonant frequency, or if noise of finite bandwidth is used, it is the centre frequency of the bandwidth.

From the argand diagram of the real and imaginary components of displacement, which results as the system passes through a resonance Kennedy and Pancu (1947) are able to calculate the loss factor (Fig 3.4(c)) of the system.

Consider a single-degree-of-freedom system subject to an alternating

force $F_o \exp(i\omega t)$

$$m\ddot{x} + c\dot{x} + Kx = F_o \exp(i\omega t)$$

where m is the mass, c is the viscous damping coefficient, and K the spring constant of the system. The displacement is assumed to be sinusoidal, thus

$$x = x_o \exp(i\omega t)$$

and the equation becomes

$$-\omega^2 m x_o + i\omega x_o c + K x_o = Fo$$

In a review of material damping by Bert (1973) it is shown that the stiffness term and the damping term can be combined to form a complex stiffness as follows.

$$\overline{K} = K + i\omega c = K(1 + i\eta)$$

From which

$$x_o = \frac{Fo}{(K - \omega^2 m) + i\eta K} \qquad \ldots\ldots\ldots 3.32$$

The accepted expression for natural frequency is,

$$\omega_o = \sqrt{\frac{K}{m}}$$

and if the force amplitude Fo is expressed in terms of the static deflection x_s then

$$Fo = \omega_o^2 m x_s$$

Substitution into equation 3.32 gives

$$x_o = \frac{x_s}{(1 - \frac{\omega^2}{\omega_o^2}) + \eta i}$$

On separating into real and imaginary components,

$$x_o = \frac{x_s}{(1 - \frac{\omega^2}{\omega_o^2})^2 + \eta^2} \left[(1 - \frac{\omega^2}{\omega_o^2}) - i\eta\right] \qquad \ldots\ldots\ldots 3.33$$

In this equation the angular frequency ω is the variable. To understand the shape of the argand diagram make the following substitutions.

$$\Omega^2 = \frac{\omega^2}{\omega_o^2}$$

$$\gamma = (1 - \Omega^2)$$

The real and imaginary parts of equation 3.33 can now be written,

$$X = \frac{x_s \gamma}{\gamma^2 + \eta^2} \qquad \ldots\ldots\ldots 3.34$$

$$Y = -\frac{\eta x_s}{\gamma^2 + \eta^2} \qquad \ldots\ldots\ldots 3.35$$

From 3.34 and 3.35,

$$X^2 + (Y + \frac{x_s}{\eta})^2 = (\frac{x_s}{\eta^2})^2 \qquad \ldots\ldots\ldots 3.36$$

This is the equation of a circle of radius $\frac{x_s}{2\eta}$ (Fig 3.4(c)), where the imaginary axis is cut at (0,0) and (0, $\frac{x_s}{\eta}$).

If the damping is measured by the rate with respect to frequency at which the response falls away from the peak then look at the rate of change of X with respect to Ω .

Thus,

$$\frac{dX}{d\Omega} = \frac{d}{d\Omega}\left(\frac{\gamma x_s}{\gamma^2+\eta^2}\right) = \frac{\partial\gamma}{\partial\Omega}\cdot\frac{d}{d\gamma}\left(\frac{\gamma x_s}{\gamma^2+\eta^2}\right)$$

Therefore

$$\frac{dX}{d\Omega} = -\frac{2x_s}{\eta^2} \qquad \ldots\ldots\ldots 3.37$$

Remembering that the radius of the circle is $\frac{x_s}{\eta}$, rearrange 3.37.

$$\eta = 2\frac{x}{\eta} \,/\, (dX/d\Omega)$$

$$\eta = 4 \times \text{RADIUS} \,/\, (dX/d\Omega)$$

The rate of change of real component of displacement is measured with respect to frequency as indicated in Figure 3.4(c).

The three methods of assessing loss factor were incorporated in experimental measurements of material constants described in section 5.6.

3.3.2 Room loss factor

In sections 2.9, 6.5.3.4, and 7.2 the sound pressure field within a room is considered a separate subsystem which is coupled to the bending modes generated on the enclosing room surface. As with other subsystems the room is assigned a loss factor which describes the energy dissipated within. Normal analyses of room absorption relate the average absorption of the room surfaces and the air volume to the resultant reverberation time. Eyring's formula (1930) is stated directly.

$$T = 0.162V/[4mV - S \log_e (1 - \bar{\alpha})] \quad \ldots\ldots 3.38$$

where m is the attenuation constant of air (in metres^{-1}), $\bar{\alpha}$ is the average absorption coefficient of the room surfaces, V the room volume, and S the surface area. It is seen that, without loss of consistency, the room loss factor η_r can be expressed in terms of the surface and air absorption. Using equations 3.31 and 3.38

$$\eta_r = \frac{13.58}{\upsilon V}[4mV - S \log_e (1 - \bar{\alpha})] \quad \ldots\ldots 3.39$$

Thus the room loss factor can be measured using reverberation techniques or predicted from values of average room and air absorption.

3.4 Transmission characteristics and structural coupling loss factor of junctions

The transmission and reflection of vibrational energy at structural discontinuities was first considered theoretically by Cremer (1948). He derived the mechanical impedance and the transmission and reflection characteristics of structures, such as rods, beams, and plates, when excited into vibration. The main results of this and other work is published in a book by Cremer and Heckl (1967).

Wave reflections in structures result from changes in cross-section, sperrmassen (descrete masses), changes in material, and changes in direction which occur at corners and other junctions. Cremer derives the amplitude of the reflected and transmitted waves by considering a simple travelling bending wave, or longitudinal wave, incident at

the discontinuity. The waves must satisfy the boundary conditions existing at the discontinuity. Thus, at a corner of two rods, it is necessary to assume continuity of vibration displacement, slope, bending moment, and shear force. Each boundary condition gives rise to an equation, and these sets of simultaneous equations allow the calculations of the various wave amplitudes. Complex structures give rise to many equations and the problem easily becomes intractable. Cremer deals numerically only with the simplest cases, and he produces little experimental verification. However, other authors were able to confirm much of the theory.

Exner and Böhme (1953) use models to investigate the frequency dependence of the reflection and transmission characteristics of thin elastic layers inserted into rods of duraluminium. The rod (40 mm cross-section and 1.7 m length) is excited at one end into bending or longitudinal vibration, depending upon the angle of the axis of the driver to that of the rod. The driver consists of a speech coil suspended in a magnetic field. The coil is attached to the test piece and a signal voltage applied across it. This is a common method of excitation and is referred to in section 5.4.

The other end of the duraluminium rod is damped by being inserted into sand. The reflected wave amplitude is reduced to a fraction of that which exists at a free termination. Over the frequency range investigated (200 Hz to 2 KHz), Exner shows that this fraction is less than one tenth. The rod can thus be considered semi-finite. The amplitudes of the waves produced on either side of the elastic layer were measured by means of accelerometer transducers and

results gave good agreement with the predictions of Cremer.

Similarly, experiments of Mugiono (1955) involved model aluminium bars of rectangular cross-section. These bars produced wave reflections by having one or two changes in cross-section. The measured amplitudes, again give good agreement with theory. Kurtze, Tamm, and Vogel (1955) studied the reflection and transmission of bending waves at the corner of two perspex rods; again thought of as semi-infinite by having their free-ends sand-damped. Theory on the alteration in the transmission characteristics at corners which results on inserting elastic layers at the corners was affirmed by experiment. Hinsch (1960) investigates the more complex problem of cross-junctions, using small rods of perspex and aluminium. From his results and conclusions an attempt is then made to determine the sound damping which occurs at structural joints in buildings, thus eliminating the need for field measurement. Budrin and Nikiforov (1964) give a numerical analysis much the same as that of Cremer and Hinsch. Heckl (1964) applies similar methods when investigating the vibration of grillages and other simple beam structures.

Further theory by Cremer (1954) considers the energy transfer, in the form of bending and longitudinal waves from a beam to a plate. Important, practical application of this work is seen in the need to assess the sound 'bridging' effect of short rods and the resultant alteration in impact sound insulation of floating floors and airborne sound insulation of lightweight double walls. Paul (1968), in experiments with bars and plates saw application of his results to buildings where vibrational energy in floors is transmitted by

supporting pillars.

Care is needed when applying the results and conclusions, from the simple theories and experiments described, to the more complicated situations existing in buildings. The areas of application are limited by the following factors.

(1) So far, the vibrational wave has been assumed to impinge on the discontinuity at normal incidence. This is true for the case of longitudinal and bending waves travelling along rods and beams. These structures are thought of as one- or two-dimensional systems and calculation is simplified. However the results and conclusions of this theory are easily misapplied to the three-dimensional structures in building. Here, waves on a plate, forming part of a junction, can impinge upon the junction at an oblique angle. Indeed, if the vibrational field on a plate is thought ideally diffuse, then all directions have equal probability of occurrence. The need to consider the angular average of the transmission characteristics of a junction, rather than the value at normal incidence, is analogous to the assessment of sound absorption coefficient of a room surface. The normal incidence absorption coefficient, as measured in an impedance tube, cannot be simply related to the reverberant absorption coefficient as measured in a diffuse sound field.

(2) In the calculations of Cremer et al of bending waves on bars

and plates it is assumed that bending wavelength is several times larger than the thickness of the structure. Thus the effects of rotatory inertia and sheer forces are neglected.

(3) The beams and plates are often assumed infinite or semi-infinite. Thus, at a junction of two or more rods, one reflection only is thought to occur as a result of an incident wave. The waves are thus considered free and progressive. If the rods were finite, reflections would occur at the free ends and the vibrational fields would be comprised of standing waves.

These discrepancies between the theoretical and experimental models and the situation existing in the field have not prevented attempts to apply results and conclusions of the former to the latter. Zaborov (1968, 1970) calculates the airborne sound insulation of wall constructions in the presence of flanking transmission by considering the contribution of each flanking path in terms of a transmission coefficient τ_{ij} , defined as the square of the ratio of the vibration velocity before and after the junction, i.e.

$$\tau_{ij} = \frac{v_j^2}{v_i^2}$$

Implicit in his argument is that in structure-borne sound propagation, energy losses occur only at discontinuities i.e. the losses are independent of the length of wall. Zaborov was able to draw the following conclusions concerning noise transmission.

(1) For the configurations investigated, the reduction in vibration level at a junction was predicted. Theory which admits to the existence of bending waves only gave essentially the same result as that of more complex theory in which longitudinal waves are included. The predictions differed by less than 1 dB.

(2) The increase in noise level in a room, with a single wall construction, caused by flanking transmission is approximately 1.5 dB to 2.5 dB. This corroborates the practice in the standards in several countries of subtracting 2 dB from the transmission loss of barriers measured in transmission suites to give the real loss in a building.

(3) The airborne sound transmission losses of multilayer wall constructions in buildings are considerably less than that measured in a transmission suite where no flanking transmission occurs. In many cases it was found that the value measured in the field is completely dependent upon the flanking transmission.

Therefore, by careful application of these results, useful design criteria might be formulated from the simple theories. However, it is argued that a closer theoretical approximation to real structures is necessary before drawing meaningful, and more generally applied, conclusions. This, subsequent authors have attempted to do.

Lyon and Eichler (1964) calculate a junction absorption coefficient

for a T-junction. This coefficient is defined by Heckl (1962) as the power absorbed at the junction, averaged over all angles of incidences, divided by the averaged incident power. The vibrational field is assumed diffuse. The calculation is simplified by assuming the plate thicknesses are equal and that the boundary conditions existing at the junction are satisfied by a free travelling bending wave. Quasi-stationary near fields, longitudinal and transverse waves are ignored. A relatively simple expression for the junction absorption coefficient results.

It is Cremer (1948) who first gives a solution to the case of an obliquely incident bending wave at a junction which takes into account the generation of other wave types. The boundary conditions are thus more correctly satisfied. The configurations considered are simple, thereby allowing numerical calculation. An example is the corner junction of two walls of equal thickness. By use of a computer Kihlman (1967, 1970) calculates the transmission at a cross-junction of finite, concrete plates for all angles of incidence. The frequency dependence of the angular averages are then produced.

Using methods similar to that of Cremer and Kihlman, a theoretical model of the vibration transmission at the junctions of infinite plates is now described. Transmission coefficients are defined and calculated, and, from them, the coupling loss factor is derived. Angular and frequency dependence of the transmission coefficients are illustrated and several plate configurations are investigated.

3.5 Assumptions in the derivation of structural coupling loss factor

3.5.1 The bending wave theory

In describing bending waves on plates or walls, classical (Kirchoff's) plate theory is employed. Thus, in figure 3.5, a bending wave on plate 1 is governed by the equation,

$$\nabla^4 \zeta_1 - K_{b1}^4 \zeta_1 = 0 \qquad \ldots\ldots\ldots 3.40$$

where ζ_1 is the displacement in the z-direction i.e. normal to the plate surface.

The wave number Kb_1 is defined by the relationship,

$$K_{b1} = \frac{h_1 \rho_1}{B_1} \omega^2 \qquad \ldots\ldots\ldots 3.41$$

where B_1 is the bending rigidity which, for a plate is given by,

$$B_1 = \frac{E_1 h_1^3}{12(1 - \mu_1^2)} \qquad \ldots\ldots\ldots 3.42$$

E_1 is Young's modulus, μ_1 is Poisson's ratio, h_1 is the plate thickness, and ρ_1 is the material density. Implicit in this derivation is that the time dependence of the equations can be expressed as $\exp(i\omega t)$.

The classical equation 3.40 cannot be assumed to hold to arbitrarily high audio frequencies. Timoshenko (1921) and Mindlin (1951) have shown that, at the higher frequencies, when the bending wavelength

Fig. 3.5

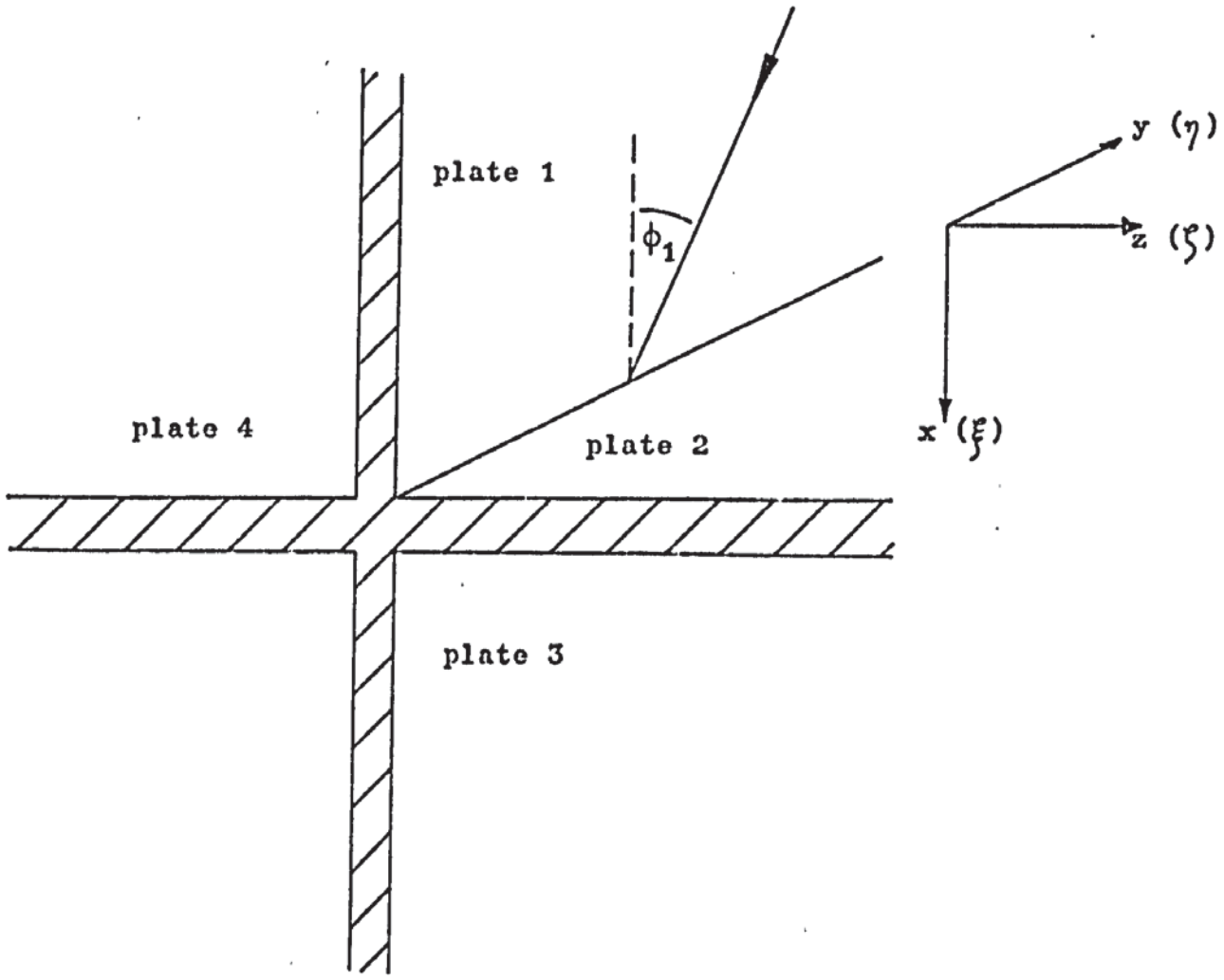

Cross junction of semi-infinite plates; bending wave incident.

assumes the same order of magnitude as the plate thickness, the effects of rotary inertia and, more importantly, shear must be considered. Cremer (1948) incorporates corrections for both effects in his modified bending wave equation which for present purposes can be expressed as,

$$\nabla^4 \zeta_1 - K_{b_1}^4 \zeta_1 + \frac{I}{A}(1 + 2(1+\mu_1)\epsilon) K_{b_1}^4 \nabla^2 \zeta_1 + \frac{2I^2}{A^2}(1+\mu_1)\epsilon \omega^4 \zeta_1 = 0 \quad \ldots\ldots 3.43$$

where I/A is the ratio of moment of inertia to cross-sectional area. The constant ϵ is known as the shearing distribution number and it results from the non-uniformity of the vertical shearing stress component over the plate cross-section. Its value is always greater than unity; for a circular cross-section it has a value of 1.18 and for a rectangular cross-section it has a value of 1.2.

The last term in equation 3.43 combines both corrections and can be ignored at frequencies where the separate corrections (the third term in the equation) first become appreciable. On substituting the values of the parameters into equation 3.43 the corrected bending wavelength is obtained from,

$$\lambda_{mod.} = \lambda_{b_1} \left[1 - 3.6 \left(\frac{h_1}{\lambda_{b_1}}\right)^2\right] \quad \ldots\ldots 3.44$$

for a plate of thickness h_1. If the cross-section is circular, the correction becomes,

$$\lambda_{mod.} = \lambda_{b_1} \left[1 - 10.04 \left(\frac{r_1}{\lambda_{b_1}}\right)^2\right] \quad \ldots\ldots 3.45$$

where r is the radius.

Wave velocity calculated using this corrected theory differs from that calculated using the simple theory by approximately 10% when the wavelength is six times the plate thickness. This somewhat arbitrary value is often quoted as a limit to the application of simple bending wave theory.

Figure 3.6 illustrates the calculated bending wavelength for reinforced concrete plates of thickness 150 mm and 200 mm. Both the simple theory and the corrected theory are shown and it is seen that the difference in predicted wavelengths is appreciable (approximately 10%) at a frequency of 1.4 KHz. Measurement of bending wavelength on specimen rods of building material (section 5.3) indicate that the corrected theory gives the best agreement between measured and predicted values. The assumption is therefore made in the derivation of coupling loss factor that the bending wave number Kb is that calculated using Cremer's modification to the simple theory.

3.5.2 Free bending waves

If a plate is excited over the whole of its surface by impinging airborne sound waves the bending wave field generated will consist of forced waves, the velocities of which are dictated by the airborne wave velocity and its angle of incidence at the plate. Below the critical coincidence frequency, therefore, the forced waves are propagated with velocities greater than those of free bending waves. Above the critical coincidence frequency, a diffuse airborne sound field will generate forced waves which will be propagated as free

Fig. 3.6

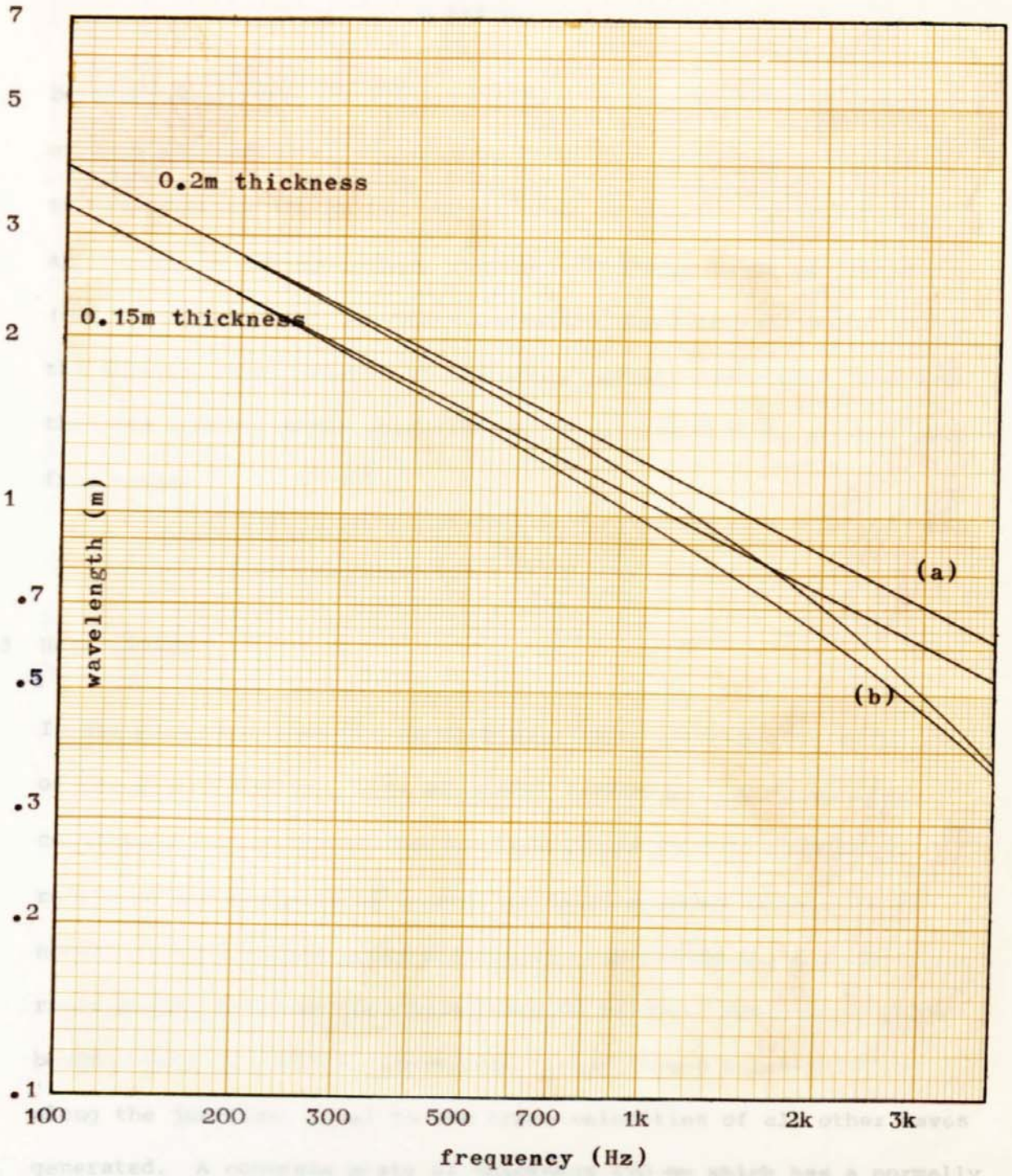

Bending wavelength for reinforced concrete plates.

$E = 4 \times 10^{10}$ N/m^2. $\rho = 2.5 \times 10^3$ kg/m^3. $\mu = 0.3$

(a) Simple bending wave theory.

(b) Cremer's modification.

bending waves. In section 6.5.4 the critical coincidence frequency of a reinforced concrete plate of thickness 200 mm is calculated to be approximately 80 Hz. For a plate of 150 mm the value is approximately 100 Hz. Thus, over the frequency range of interest (100 Hz to 3.15 KHz) the plate radiation characteristics lie within the supercritical range. It therefore appears reasonable to assume that the bending waves generated on the plates will be propagated as free waves.

3.5.3 Near fields

It has been seen that the bending wave equation (equation 3.40) is of the fourth degree. Even at normal incidence, the boundary conditions that exist at the junction cannot be satisfied by reflected and transmitted travelling bending waves alone. It is necessary to consider quasi-stationary near fields which decay rapidly with distance (see equation 3.46 below). When the incident bending wave is oblique, these near fields have a trace velocity along the junction, equal to the trace velocities of all other waves generated. A concrete plate of thickness 150 mm which has a normally incident bending wave has a calculated near field which decreases to one tenth of its amplitude at a distance of one metre at a frequency of 100 Hz. At 1KHz this distance is less than 150 mm. It is therefore assumed that these near fields do not contribute to the vibration energy level of the plate.

3.5.4 Mechanical impedance

So far, only the wave field in plates at a distance from the free and fixed edges have been described. The analysis becomes more complex at the edges, where forces and moments may be applied. Dyer (1960) uses Mindlin's plate equations in obtaining the impedance when a moment is applied to a small disc in the plane of the plate, the edge of which is infinite in extent. It is shown that classical theory may give erroneous results when the radius of the disc of application becomes smaller than the plate thickness. Similarly, Eichler (1964) uses classical theory when calculating the admittance of a semi-infinite plate excited by a stud attached to its edge. He concludes that more complex theory becomes necessary only if the width of the stud becomes smaller than the plate thickness. Kihlman (1967) argues that the method of Dyer might be of use in assessing the range of validity of classical theory, even when the plate edge is subjected to moments and forces along the whole length. This is possible, only if the phase is assumed to vary slowly along the edge.

The derivation of impedance (Appendix I) assumes the junction is of infinite length. Thus, application of these results to plates of finite dimensions is meaningful only if the junction is at least the same order of magnitude as the bending wavelength.

It therefore appears that application of simple bending wave theory has a frequency limit determined by conditions occuring at the plate edges as well as conditions at a distance from them.

3.6 Obliquely incident bending wave

The problem of a bending wave incident at the junction of four plates will now be considered. The plates are assumed semi-infinite and the junction line is thought to be of infinite length (fig 3.5). The cross-junction is thought to be the intersection of two infinite plates and therefore, plate 1 and plate 3 are assumed equal; and plates 2 and 4 are equal. This symmetry allows the following simplifications.

(1) The bending, longitudinal, and transverse wave fields on plates 2 and 4 are equal.

(2) The longitudinal and transverse fields of plates 1 and 3 are equal.

Internal dissipative losses are assumed small and at this stage are neglected.

Thus, consider an impinging bending wave, of unit amplitude, incident at an angle ϕ_1 to the junction normal (fig 3.5). The displacement in the z-direction on plate 1 is expressed as,

$$\zeta_1 = \exp(i\omega t)\exp(-iK_{b1}y\sin\phi_1)\left\{\exp(-iK_{b1}x\cos\phi_1) + T_{b1}\exp(iK_{b1}x\cos\phi_1) + T_{n1}\exp(K_{n1}x)\right\} \quad \ldots\ldots 3.46$$

The time dependent term, common to this and all subsequent expressions, will be assumed implicit and will, therefore, not be expressed. The first term inside the curled brackets describes the incident bending wave, the second term describes the reflected bending wave, and the last term is that of the quasi-stationary near field. The complex

coefficients Tb_1, Tn_1 describe the amplitude of these wave components. The wave number Kn_1 is expressed in terms of the progressive bending wave number Kb_1 by inserting the solution $\exp(-Kb_1 y \sin\phi_1)\ \exp(Kn_1 x)$ into the bending wave equation 3.40. This gives

$$Kn_1 = Kb_1 (1 + \sin^2\phi_1)^{\frac{1}{2}} \qquad \ldots\ldots\ldots 3.47$$

Similarly, the bending wave transmitted on plate 2 has the form,

$$\xi_2 = \exp(-iK_{b_2} y \sin\phi_2)\left\{T_{b_2} \exp(-iK_{b_2} z \cos\phi_2) + T_{n_2} \exp(-K_{n_2} z)\right\} \qquad \ldots\ldots 3.48$$

and, on plate 3.

$$\xi_3 = \exp(-iK_{b_3} y \sin\phi_3)\left\{T_{b_3} \exp(-iK_{b_3} x \cos\phi) + T_{n_3} \exp(-K_{n_3} x)\right\} \qquad \ldots\ldots 3.49$$

The first term on the right hand sides of 3.46, 3.48 and 3.49 describes the junction trace velocity which must be equal for all waves. That is, Snell's law is obeyed, giving,

$$Kb_1 \sin\phi_1 = Kb_2 \sin\phi_2 = Kb_3 \sin\phi_3 \qquad \ldots\ldots\ldots 3.50$$

In addition to the bending wave fields, longitudinal and transverse fields are generated in plates 2 and 4, and, to a lesser degree, in plates 1 and 3. It is again noted that the transverse waves (in which the direction of propagation is perpendicular to the direction of displacement, and both are parallel to plane of the plate surface) result from the need to satisfy the boundary conditions when the bending wave is obliquely incident.

In considering these waves it will be convenient, initially to

describe them using a single amplitude coefficient T_{lt}. Therefore, on plate 2 the displacement is given by,

$$\zeta_2 = \exp(-iKb_1 y \sin\phi_1)\, T_{lt2} \qquad \ldots\ldots\ldots 3.51$$

and on plate 3,

$$\xi_3 = \exp(-iKb_1 y \sin\phi_1)\, T_{lt3} \qquad \ldots\ldots\ldots 3.52$$

As in the expressions for the bending waves, the exponential term in equations 3.51 and 3.52 describes the trace velocity which is equal for all wave types. In the five expressions listed there are eight unknown amplitude coefficients of which five are of interest; namely Tb_1, Tb_2, Tb_3, T_{lt2}, T_{lt3}. By incorporating the boundary conditions at the junction, the amplitude coefficients will be calculated and hence the transmitted energy in that particular wave form. The boundary conditions are the continuity of displacement, bending wave slope, bending moment, and shear force. It would be more correct to describe the continuities as occuring at,

$$x = \pm \frac{h_2}{2}$$

$$z = \pm \frac{h_1}{2}$$

However, the plates will be assumed to have negligible thickness, thereby simplifying calculation.

3.6.1 Continuity of displacement

This condition is expressed as,

$$\xi_2\,(z)_{z=0} = \xi_3\,(x)_{x=0} \qquad \ldots\ldots\ldots 3.53$$

$$\zeta_1\,(x)_{x=0} = \zeta_2\,(z)_{z=0} = \zeta_3\,(x)_{x=0} \qquad \ldots\ldots\ldots 3.54$$

Substitution of the expressions 3.46-3.52 into equations 3.53 and 3.54 gives,

$$Tn_2 = T_{it3} - Tb_2 \qquad \ldots\ldots\ldots 3.55$$

$$Tn_1 = T_{it2} - 1 - Tb_1 \qquad \ldots\ldots\ldots 3.56$$

$$Tn_3 = T_{it2} - Tb_3 \qquad \ldots\ldots\ldots 3.57$$

This will allow the substitution and elimination of the near field coefficients in later equations.

3.6.2 Bending wave slope

At the junction the slopes of the bending waves are continuous. Thus,

$$\left(\frac{\partial \zeta_1}{\partial x}\right)_{x=0} = -\left(\frac{\partial \xi_2}{\partial z}\right)_{z=0} = \left(\frac{\partial \zeta_3}{\partial x}\right)_{x=0} \qquad \ldots\ldots\ldots 3.58$$

On substitution,

$$-iK_1\cos\phi_1 + iK_1\cos\phi_1 T_{b1} + K_{n1}T_{n1} = iK_2\cos\phi_2 T_{b2} + K_{n2}T_{n2} = -iK_1\cos\phi_1 T_{b3} - K_{n1}T_{n3} \qquad \ldots\ldots\ldots 3.59$$

For simplicity the suffix b of the bending wave number is not shown.

3.6.3 Bending moments

The sum of the bending moments about the y-axis is zero. The general expression for the bending moment at the edge of plate 1 is given by Timoshenko and Goodier (1951) as,

$$M_x = -B_1 \left(\frac{\partial^2 \zeta_1}{\partial x^2} + \mu_1 \frac{\partial^2 \zeta_1}{\partial y^2} \right)$$

The sum of the bending moments is therefore,

$$-B_1\left(\frac{\partial^2 \zeta_1}{\partial x^2} + \mu_1 \frac{\partial^2 \zeta_1}{\partial y^2}\right) - 2B_2\left(\frac{\partial^2 \xi_2}{\partial z^2} + \mu_2 \frac{\partial^2 \xi_2}{\partial y^2}\right) + B_1\left(\frac{\partial^2 \zeta_3}{\partial x^2} + \mu_1 \frac{\partial^2 \zeta_3}{\partial y^2}\right) = 0 \qquad \ldots\ldots\ldots 3.60$$

Substituting the five wave expressions into equation 3.60 gives,

$$B_1K_1^2\left[1 - (1 - \mu_1)\sin^2\phi_1\right] Tb_1 - B_1K_1^2\left[1 + (1 - \mu_1)\sin^2\phi_1\right] \times$$
$$Tn_1 + 2B_2\left[K_2^2 - (1 - \mu_2)K_1^2\sin^2\phi_1\right] Tb_2 - 2B_2\left[K_2^2 + (1 - \mu_2) \times\right.$$
$$\left. K_1^2\sin^2\phi_1\right] Tn_2 - B_1K_1^2\left[1 - (1 - \mu_1)\sin^2\phi_1\right] Tb_3 + B_1K_1^2\left[1 +\right.$$
$$\left.(1 - \mu_1)\sin^2\phi_1\right] Tn_3 + B_1K_1^2\left[1 - (1 - \mu_1)\sin^2\phi_1\right] = 0$$

$\ldots\ldots\ldots$ 3.61

3.6.4 Forces in the z-direction

At the junction of the plates forces will result from the linear movement found in the longitudinal and transverse waves and from the torsional moments in these plates.

The first type of force can be expressed by considering the impedance Z_{lt2} which relates the force F_{lt2} in the z-direction to the velocity $i\omega\zeta_2$.

The derivation of Z_{t2} is described in Appendix I.

The second type of force results from the bending experienced at the edge of a plate and is given by Timoshenko (1940) as,

$$Q_z = B_1\left(\frac{\partial^3 \zeta_1}{\partial x^3} + (2-\mu_1)\frac{\partial^3 \zeta_1}{\partial x\, \partial y^2}\right) \qquad \ldots\ldots\ldots 3.62$$

The statement that the total force in the z-direction equates to zero is expressed as,

$$Q_1 - Q_2 - 2F_{lt2} = 0 \qquad \ldots\ldots\ldots 3.63$$

Substitution of the wave expressions into 3.62 and 3.63 gives,

$$-iB_1K_1^3\cos\phi_1\,[\,1 + (1-\mu_1)\sin^2\phi_1\,]\,Tb_1 + B_1Kn_1K_1^2[\,1 - (1-\mu_1)\sin^2\phi_1\,]\,Tn_1 - iB_1K_1^3\cos\phi_1\,[\,1 + (1-\mu_1)\sin^2\phi_1]x\,Tb_3 + B_1Kn_1K_1^2\,[\,1 - (1-\mu_1)\sin^2\phi_1\,]\,Tn_3 + iB_1K_1^3\cos\phi_1 x\,[1 + (1-\mu_1)\sin^2\phi_1\,] - i2\omega z_{lt2}\,T_{lt2} = 0$$

$\ldots\ldots\ldots 3.64$

3.6.5 Forces in the x-direction

As well as a longitudinal and transverse wave resulting in plate 2 from the incident bending wave the transmitted bending in plate 2 will cause a longitudinal and transverse wave (say of third class) in plate 1 and plate 3. The addition of forces in the x-direction

gives zero. Remembering that the bending wave fields in plate 2 and plate 4 are equal and the longitudinal and transverse wave fields in plate 1 and plate 3 are equal, then

$$Q_2 - F_{lt3} = 0 \qquad \ldots\ldots 3.65$$

Substitution gives,

$$iB_2K_2\cos\phi_2\,[\,K_2^2 + (1-\mu_2)K_1^2\sin^2\phi_1\,]\,Tb_2 - B_2Kn_2\,[\,K_2^2 - (1-\mu_2)K_1^2\sin^2\phi_1\,]\,Tn_2 - i\omega Z_{lt3}\,T_{lt3} = 0 \qquad \ldots\ldots 3.66$$

$$\begin{bmatrix}
-(k_{n1}-ik\cos\phi_1) & (k_{n2}-ik_2\cos\phi_1) & 0 & k_{n1} & -k_{n2} \\
0 & -(k_{n2}-ik_2\cos\phi_1) & -(k_{n1}-ik_1\cos\phi_1) & k_{n1} & k_{n2} \\
2Bk_{11}^2 & 4Bk_{22}^2 & -2Bk_{11}^2 & 0 & -2B_2[k_2^2+(1-\mu)k_1^2\sin^2\phi_1] \\
\begin{matrix}-B_1k_1^2\{k_{n1}[1-(1-\mu_1)\sin^2\phi_1]+\\ ik_1\cos\phi_1[1+(1-\mu_1)\sin^2\phi_1]\}\end{matrix} & 0 & \begin{matrix}-B_1k_1^2\{k_{n1}[1-(1-\mu_1)\sin^2\phi_1]\\ +ik_1\cos\phi_1[1+(1-\mu_1)\sin^2\phi_1]\}\end{matrix} & \begin{matrix}2\{Bk_{n1}k_1^2[1-(1-\mu_1)\sin^2\phi_1\\ -i2\omega Z_{lt2}\}\end{matrix} & 0 \\
0 & \begin{matrix}B_2\{k_{n2}[k_2^2-(1-\mu_2)k_1^2\sin^2\phi_1]+\\ ik_2\cos\phi_1[k_2^2+(1-\mu_2)k_1^2\sin^2\phi_1]\}\end{matrix} & 0 & \begin{matrix}-\{Bk_{n2}[k_2^2-(1-\mu)k_1^2\sin^2\phi_1]\\ +i\omega Z_{lt3}\}\end{matrix} & 0
\end{bmatrix}
\begin{bmatrix} T_{b1} \\ T_{b2} \\ T_{b3} \\ T_{lt2} \\ T_{lt3} \end{bmatrix}
=
\begin{bmatrix} k_{n1} \\ 0 \\ -2B_1k_2^2 \\ \chi \\ 0 \end{bmatrix}$$

By substitution of the wave expressions into the boundary condition equations a set of simultaneous equations are obtained which allow the calculation of the unknown coefficients Tb_1, Tb_2, Tb_3, T_{lt2}, T_{lt3}. The set of equations can be expressed as the above matrix, where

$$\chi = B_1K_1^2\left\{K_{n1}[1-(1-\mu_1)\sin^2\phi_1] - iK_1\cos\phi_1[1+(1-\mu_1)\sin^2\phi_1]\right\}$$

To obtain the transmission coefficient at an angle of incidence it is necessary to calculate the energy intensities of the incident and transmitted waves. The general expression (Cremer, 1948) for the intensity (or power per unit length) of a bending wave impinging at an angle ϕ to the normal is given as,

$$I_{inc.}(\phi) = \tfrac{1}{2} M C_b V^2 \cos\phi \qquad \ldots\ldots\ldots 3.67$$

where C_b is the bending wave velocity, V is the transverse velocity amplitude, and M is the mass per unit area of the plate. If the wave is sinusoidal and of displacement amplitude T then,

$$V = i\omega T$$

Also make the substitution,

$$C_b = \frac{2\omega}{Kb}$$

The expression 3.67 now becomes,

$$I_{inc.}(\phi) = h\rho|T|^2\frac{\omega^3}{K_b}\cos\phi \qquad \ldots\ldots\ldots 3.68$$

where h. and ρ are the plate thickness and density respectively. Thus, on plate 1, a wave of unit amplitude, at an angle ϕ_1 has an intensity,

$$I_{inc}(\phi_1) = h_1\rho_1\left(\frac{\omega^3}{K_1}\right)\cos\phi_1 \qquad \ldots\ldots\ldots 3.69$$

The transmitted bending wave intensity on the ith plate is given by,

$$I_i(\phi_1) = h_i\rho_i\frac{\omega^3}{K_i}\left|T_{bi}\right|^2\cos\phi_i \qquad \ldots\ldots\ldots 3.70$$

The transmission coefficient $\gamma_l^i(\phi_1)$ is the ratio of the intensities in equations 3.69 and 3.70.

$$\gamma_l^i(\phi_l) = \frac{h_i \rho_i}{h_l \rho_l} \frac{K_l}{K_i} \frac{|T_{bi}|^2 \cos\phi_i}{\cos\phi_l} \qquad \ldots\ldots\ldots 3.71$$

The transmitted longitudinal and transverse wave energies incorporate the real part of the impedance Z_{lt} into the expression for intensity,

$$I_{lti}(\phi_1) = \frac{\omega^2}{2} R(Z_{lti}) |T_{lti}|^2 \qquad \ldots\ldots\ldots 3.72$$

The impedance Z_{lt} is derived in the appendix and for plate 1 is given as,

$$Z_{lt} = \frac{E_l h_l K_l^2}{\omega(1-\mu_l^2)K_t^4} \left[\frac{(K_t^2 - 2K_l^2\sin^2\phi_l)^2}{\sqrt{(K_l^2 - K_l^2\sin^2\phi_l)}} + 4K_l^2\sin^2\phi_l\sqrt{(K_t^2 - K_l^2\sin^2\phi_l)} \right]$$

$\ldots\ldots\ldots 3.73$

The two terms on the right hand side of equation 3.73 describe the subdivisions of energy into longitudinal and transverse components. The first term gives the energy transmitted as a longitudinal wave. Thus,

$$I_{li}(\phi_1) = \frac{\omega^2}{2} \frac{E_1 h_1 K_l^2}{\omega(1-\mu_1^2)K_t^2} \frac{(K_t^2 - 2K_1^2\sin^2\phi_1)^2}{\sqrt{(K_l^2 - K_1^2\sin^2\phi_1)}} |T_{lti}|^2$$

$\ldots\ldots\ldots 3.74$

The second term gives the transverse component of the transmitted energy,

$$I_{ti}(\phi_l) = \frac{\omega^2}{2} \frac{E_l h_l K_l^2}{\omega(1-\mu_1^2)K_t^2} 4K_l^2\sin^2\phi_l\sqrt{(K_t^2 - K_l^2\sin^2\phi_l)} |T_{lti}|^2$$

$\ldots\ldots\ldots 3.75$

When calculating the average transmission coefficient for each wave component, it is assumed that all angles of incidence have the same probability of occurrence. The general expression for the average transmission coefficient is written as,

$$\gamma_{i\,av.} = \frac{\frac{1}{\pi}\int_{-\pi/2}^{\pi/2} I_i(\phi_1)\, d\phi_1}{\frac{1}{\pi}\int_{-\pi/2}^{\pi/2} I_{inc}(\phi_1)\, d\phi_1} \qquad \ldots\ldots 3.76$$

The denominator of equation 3.76 can be readily integrated, and for transmitted bending waves,

$$\gamma_1{}^{i}{}_{av.} = \frac{h_i \rho_i k_1}{h_1 \rho_1 k_i} \int_0^{\pi/2} |\, T_{bi}\,|^2 \cos\phi_i \, d\phi_1 \qquad \ldots\ldots 3.77$$

The transmitted longitudinal and transverse waves are similarly expressed.

$$\gamma_1{}^{ilt}{}_{av.} = \frac{k_1}{2h_1 \rho_1 \omega} \int_0^{\pi/2} R(Z_{lti})\, |\, T_{lti}\,|^2 \, d\phi_1 \qquad \ldots\ldots 3.78$$

Equations 3.77 and 3.78 are calculated numerically and results are given in Chapter 4 and Appendix III of calculated transmission coefficients for various junctions of reinforced concrete plates.

3.7 Transmission of an incident longitudinal wave

As well as an incident bending wave at a junction the case of longitudinal and transverse waves must be assessed.

Consider an incident longitudinal wave at an angle ϕ_L, impinging at a junction of four plates. Bending, longitudinal and transverse waves will be generated on each plate. The problem is again simplified by lumping together the amplitudes of the resultant longitudinal and transverse waves on each plate. Also the vibrational fields on plate 4 are assumed equal to those on plate 2. Thus, the wave expressions on each plate are written as,

$$\xi_1 = \exp - iK_l y \sin\phi_l \; [\exp - iK_l x \cos\phi_l + T_{lt1}] \quad \ldots\ldots\ldots 3.79$$

$$\xi_2 = \exp - iK_l y \sin\phi_l \; [T_{b2} \exp - izK_2 \cos\phi_2 + T_{n2} \exp - K_{n2} z] \quad \ldots\ldots\ldots 3.80$$

$$\xi_3 = \exp - iK_l y \sin\phi_l \; [T_{lt3}] \quad \ldots\ldots\ldots 3.81$$

$$\zeta_2 = \exp - iK_l y \sin\phi_l \; [T_{lt2}] \quad \ldots\ldots\ldots 3.82$$

$$\zeta_3 = \exp - iK_l y \sin\phi_l \; [T_{b3} \exp - ixK_3 \cos\phi_3 + T_{n3} \exp - K_{n3} x] \quad \ldots\ldots\ldots 3.83$$

The wave expressions above are now incorporated into the following boundary condition equations.

3.7.1 Continuity equations

The continuity of displacement gives,

$$\xi_1 = \xi_2 = \xi_3 \quad \ldots\ldots\ldots 3.84$$

$$\zeta_1 = \zeta_2 \quad \ldots\ldots\ldots 3.85$$

On substitution equation 3.84 becomes

$$1 + T_{it1} = T_{b2} + T_{n2} = T_{it3} \qquad \ldots\ldots\ldots 3.86$$

and equation 3.85 becomes

$$T_{it2} = T_{b3} + T_{n3} \qquad \ldots\ldots\ldots 3.87$$

The continuity of bending slope gives,

$$\frac{\partial \xi_2}{\partial z} = -\frac{\partial \zeta_3}{\partial z} \qquad \ldots\ldots\ldots 3.88$$

which yields the equation,

$$-iK_2 \cos\phi_2 T_{b2} - K_{n2} T_{n2} = iK_3 \cos\phi_3 T_{b3} + K_{n3} T_{n3} \qquad \ldots\ldots\ldots 3.89$$

The bending moments at the junction sum to zero. This condition gives the equation,

$$-B_2 [K_2^2 \cos^2\phi_2 + \mu_2 K_i^2 \sin^2\phi_i] T_{b2} + B_2 [K_{n2}^2 - \mu_2 K_i^2 \times \sin^2\phi_i] T_{n2} + B_3 [K_3^2 \cos^2\phi_3 + \mu_3 K_i^2 \sin^2\phi_i] T_{b3} - B_3 \times [K_{n3}^2 - \mu_3 K_i^2 \sin^2\phi_i] T_{n3} = 0 \qquad \ldots\ldots\ldots 3.90$$

The sum of shear forces in the x-direction is zero. Thus,

$$i\omega Z_{i1} - i\omega Z_{it1} T_{it1} - i\omega Z_{it3} T_{it3} - i2B_2K_2 \cos\phi_2 [K_2^2 \cos^2\phi + (2 - \mu_2) K_i^2 \sin^2\phi_i] T_{b2} + 2B_2K_{n2} [K_{n2}^2 - (2 - \mu_2) \times K_i^2 \sin^2\phi_i] T_{n2} = 0 \qquad \ldots\ldots\ldots 3.91$$

Similarly for the forces in the z-direction.

$$i\omega Z_{lt2}\, T_{lt2} - i\, B_3 K_3 \cos\phi_3 \left[K_3^{\,2} \cos^2\phi_3 + (2 - \mu_3)\, K_l^{\,2} \sin^2\phi_l \right] \times T_{b3} + B_3 K_{n3} \left[K_{n3}^{\,2} - (2 - \mu_3)\, K_l^{\,2} \sin^2\phi_l \right] T_{n3} = 0 \quad \ldots\ldots 3.92$$

On eliminating the coefficients T_{n2}, T_{n3}, T_{lt1}, a matrix is produced representing the set of simultaneous equations.

$$\begin{bmatrix} 2B_2\{k_{n2}[k_{n2}^2-(2-\mu_2)k_l^2\sin^2\phi_l]+ ik_2\cos\phi_2[k_2^2\cos^2\phi_2+(2-\mu_2)k_l^2\sin^2\phi_l]\} & 0 & 0 & \{2B_2k_{n2}[k_{n2}^2-(2-\mu_2)k_l^2\sin^2\phi_l] - i2\omega Z_{lt3}\} \\ 0 & -B_l\{k_{nl}[k_{nl}^2-(2-\mu_l)k_l^2\sin^2\phi_l]+ ik_l\cos\phi_l[k_l^2\cos^2\phi_l+(2-\mu_l)k_l^2\sin^2\phi_l]\} & \{B_lk_{nl}[k_{nl}^2-(2-\mu_l)k_l^2\sin^2\phi_l] + i\omega Z_{lt2}\} & 0 \\ -(k_{n2}-ik_2\cos\phi_2) & -(k_{nl}-ik_l\cos\phi_l) & k_{nl} & k_{n2} \\ -2B_2k_2^2 & 2B_lk_l^2 & -B_l[k_{nl}^2-\mu_lk_l^2\sin^2\phi_l] & B_2[k_{n2}^2-\mu_2k_l^2\sin^2\phi_l] \end{bmatrix} \begin{bmatrix} T_{b2} \\ T_{b3} \\ T_{lt2} \\ T_{lt3} \end{bmatrix} = \begin{bmatrix} -i\omega(Z_{ll}-Z_{lt3}) \\ 0 \\ 0 \\ 0 \end{bmatrix}$$

$\ldots\ldots 3.93$

3.7.2 Transmission coefficient

The amplitude coefficients T_{b2}, T_{b3}, T_{lt2}, T_{lt3}, are obtained numerically by methods described in Chapter 4. The calculation of the transmission coefficients is essentially the same as that

described from an incident bending wave. The expressions are therefore stated directly.

The average coefficient for transmitted bending wave on the ith plate is given as,

$$\gamma_{1\iota}^{\ ib\ \text{av.}} = \frac{2h_i \rho_i}{K_\iota R(Z_{\iota t1})} \int_o^{\pi/2} \left| T_{bi} \right|^2 \cos\phi_i \, d\phi_\iota \qquad \ldots\ldots\ldots 3.94$$

For transmitted longitudinal and transverse waves,

$$\gamma_{1\iota}^{\ i\iota t\ \text{av.}} = \frac{1}{R(Z_{\iota t1})} \int_o^{\pi/2} \left| T_{\iota ti} \right|^2 R(Z_{\iota ti}) \, d\phi_\iota \qquad \ldots\ldots\ldots 3.95$$

If required, the contribution of the two wave components in equation 3.95 can be expressed separately.

The process for the calculation of the transmission of an incident transverse wave is essentially the same as that for incident bending and longitudinal waves, and is not to be described. Tables of calculated transmission coefficient for all three wave types are given in Appendix III.

3.8 Coupling loss factor

It remains to calculate the various coupling loss factors, introduced in Chapter 2, from the average transmission coefficients, derived in this chapter. So far the transmission of energy at a junction has been expressed as an absorption γ_{ib}^{jb} (Cremer 1948). Heckl (1962) when measuring the vibrational energy absorbed at the edge of a plate,

either by a strip of damping material, or by passage on to a connected plate, uses a reverberation time method analogous to that of room acoustics. The reverberation time is expressed in the form,

$$\frac{1}{T} = \frac{C_b}{13.8\pi S} \sum \gamma_i L_i + \frac{\omega\eta}{13.8} \qquad \ldots\ldots\ldots 3.96$$

where S is the plate area, C_b the bending wave velocity, and η the internal loss factor. The summation describes the contribution of each edge of length L_1 and absorption coefficient γ_i to the total absorption of the plate. Lyon and Eichler (1964) take the analysis further by expressing the first term of the R.H.S of equation 3.96 as a loss factor analogous to the internal loss factor in the second term. This loss factor is expressed as,

$$\eta_{1b}^{2b} = \frac{2}{\pi} \frac{L_1}{S_1} \frac{1}{K_{b1}} \gamma_{1b}^{2b} \qquad \ldots\ldots\ldots 3.97$$

for the case of bending wave energy on plate 1 generating bending wave energy on plate 2. The $\frac{1}{\pi}$ term results from the integration over the angle of incidence against the boundary. A coupling loss factor for an incident longitudinal wave can similarly be derived,

$$\eta_{1l}^{2b} = \frac{1}{\pi} \frac{L_1}{S_1} \frac{1}{K_l} \gamma_{1l}^{2b} \qquad \ldots\ldots\ldots 3.98$$

For an incident transverse wave,

$$\eta_{1t}^{2b} = \frac{1}{\pi} \frac{L_1}{S_1} \frac{1}{K_t} \gamma_{1t}^{2b} \qquad \ldots\ldots\ldots 3.99$$

The factor of two in equation 3.97 results from the fact that the bending wave group velocity is twice the value of the phase velocity.

3.9 The coupling loss factors for incident longitudinal and transverse waves

Equations 3.98 and 3.99 indicate that the coupling loss factor for incident longitudinal and transverse waves can be calculated if the appropriate transmission coefficient is known. A direct derivation of these transmission coefficients, using simple bending theory has been given in section 3.7. However two other methods of calculating the transmission coefficient and hence the coupling loss factor for these wave types are considered.

(1) Kihlman (1967), and, later Reichardt and Richter (1970) show that, for a wave obliquely incident at a junction, the transmission coefficient is independent of the direction of transmission, if the same trace is followed. Thus,

$$\gamma_1^2(\phi_1) = \gamma_2^1(\phi_2) \qquad \ldots\ldots\ldots 3.100$$

This is valid when one angle of incidence is considered. However, angle-averaged parameters are used in this present discussion and, in the case of plates of differing thicknesses the relation in equation 3.100 will not hold for all angles. If plate 1 is thicker than plate 2, a faster bending wave results on the former plate. The incident grazing angle on plate 1 will produce a smaller transmitted angle $\phi_{crit.}$ on plate 2. Therefore if a wave on plate 2 is incident at an angle larger than this critical angle $\phi_{crit.}$ then total reflection results and the equality in equation 3.100 breaks down. By means of reciprocity however, Kihlman

is able to show that the averaged coefficients can still be simply related. This is given by,

$$K_1 \gamma_1^2 = K_2 \gamma_2^1 \qquad \ldots\ldots\ldots 3.101$$

where K_1 and K_2 are the respective wave numbers of the plates. Thus, as an example, the transmission coefficient describing a longitudinal wave on plate 1, coupled to a bending wave on plate 2 is obtained by means of equation 3.101. Thus,

$$\gamma_{1l}^{2b} = \frac{K_{b2}}{K_l} \gamma_{2b}^{1l} \qquad \ldots\ldots\ldots 3.102$$

(2) If the modal densities of the longitudinal and transverse wave fields are appreciable then use may be made of the equality 2.10 which states that the products of the coupling loss factors and modal densities of coupled sub-systems are equal. Thus, if the coupling loss factor of a bending incident on plate 2 which generates a longitudinal wave on plate 3, is known, the reciprocal loss factor describing an incident longitudinal wave on plate 3 generating a bending wave on plate 2, can be calculated directly.

$$\eta_{3l}^{2b} = \frac{n_{b2}}{n_l} \eta_{2b}^{3l} \qquad \ldots\ldots\ldots 3.103$$

where n_{b2}/n_l = ratio of bending wave to longitudinal wave modal density.

The disadvantage of the second method described is that the longitudinal and transverse modal densities can only be thought large at the higher

frequencies in the range of interest. Both the above methods suffer the disadvantage that they can only describe transmissions involving bending waves. If it is desired that the coupling between longitudinal wave fields on plates be calculated it is necessary to use the methods described in section 3.7.

The next chapter gives numerical results calculated using all three methods, and it is seen that quite broad simplifications can still yield applicable results.

3.10 Summary

It is seen that by use of simple bending wave theory the structural coupling loss factor and structure-fluid coupling loss factor of coupled sub-systems can be calculated. These parameters, along with the ratio of modal densities of the coupled sub-systems, can now be entered into the energy balance equations described in Chapter 2, together with the internal loss factor of each sub-system.

CHAPTER 4

NUMERICAL ANALYSIS

The solution of power flow equations for coupled subsystems (Chapter 2) and that satisfying the boundary conditions existing at the junction of semi-infinite plates (Chapter 3) became intractable for the more complex configurations. The problem is circumvented by numerical methods, using a high speed digital computer. The model used at Aston University is an I.C.L. 1905E possessing a core size of 96K. The programming language used throughout this and other numerical analyses is 1900 Algol.

4.1 The solution of a set of linear equations

There are several numerical methods available for the solution of linear, simultaneous equations, such as those expressed as matrix 3.93. Possibly the most common method is Gauss' systematic elimination method. This method has many variants which differ in the way the matrices are stored, the order of elimination and method of reducing large rounding errors. For the problem at hand, it was felt that some accuracy in the calculations could be sacrificed in order to ensure that as short a computing time as possible resulted. In order to calculate transmission coefficient as a function of angle (in one degree increments) and of frequency (in third octave increments) the computation involves the solution of 1456 sets of simultaneous equations, each set represented by a 10 x 10 matrix. The elimination method chosen was that of Crout which was designed for the hand computation of small matrices. The method is illustrated

by means of the programme sub-routine given in Appendix II.

4.2 Integration of the transmission coefficient

Equations 3.33, 3.34, 3.55 and 3.56 give the integrals of the various transmission coefficients. The numerical integration was made possible by use of Simpson's rule given by

$$\int_{x_o}^{x_n} y(x)\,dx \sim (\Delta x/3)[y_o + 4y_1 + 2y_2 + 4y_3 + \cdots\cdots + 2y_{n-2} + 4y_{n-1} + y_n]$$

where Δx is the increment within the range $(x_n - x_o)$. As shown in Figures 4.1 - 4.10, the variation with angle of incidence of many of the calculated transmission coefficients is regular. Often, over much of the angular range, there is a monotonic decrease to zero at 90^o. A fairly large interval of one angular degree was thought adequate for the computation of the angular average. However the transmission coefficient γ_{1b}^{3b} displays a peak value, the sharpness of the peak being more pronounced at low frequencies (Fig 4.4). The angular increment was therefore altered to 0.2 degree at the lower frequencies, resulting in 450 increments in the range $0-\pi/2$. The reduction of increment resulted in a smooth curve of average value of γ_{1b}^{3b}, against frequency, without greatly increasing the computing time.

4.3 Discussion of results: The angular variation of transmission coefficient

The material constants used in the computation were obtained by

measurement. The experiments are described in Chapter 5 and the results are summarised in Table 5.1. In the case of reinforced concrete, all material constants can be assumed independent of frequency. The following values were used.

$$\text{Density } \rho = 2.5 \times 10^3 \text{ Kg/m}^3$$

$$\text{Young's modulus } E = 4.0 \times 10^{10} \text{ N/m}^2$$

$$\text{Poisson's ratio } \mu = 0.3$$

$$\text{Internal loss factor } \eta = 0.01$$

These constants, along with the plate thicknesses h_i, are the only input data necessary.

Figure 4.1 shows transmission coefficient as a function of incident angle at a frequency of 100 Hz, for the case of a bending wave incident at a junction of four semi-infinite plates. The transmission coefficients describing the change of wave type from the bending wave are expressed in a manner such that the longitudinal and transverse components are considered as one component. The transmission of energy into each wave type is detailed in the tables of Appendix III.

It can be seen that the coefficients differ greatly in characteristics, especially those involving bending components i.e. γ_{1b}^{2b} and γ_{1b}^{3b}. The latter has a sharp maximum and, at the angle where it occurs, the junction can be regarded as reflection-free. There is a corresponding dip in γ_{1b}^{2b} at the same angle above which it decays regularly to zero at an angle of 60°, where total reflection takes place. For the

Fig. 4.1

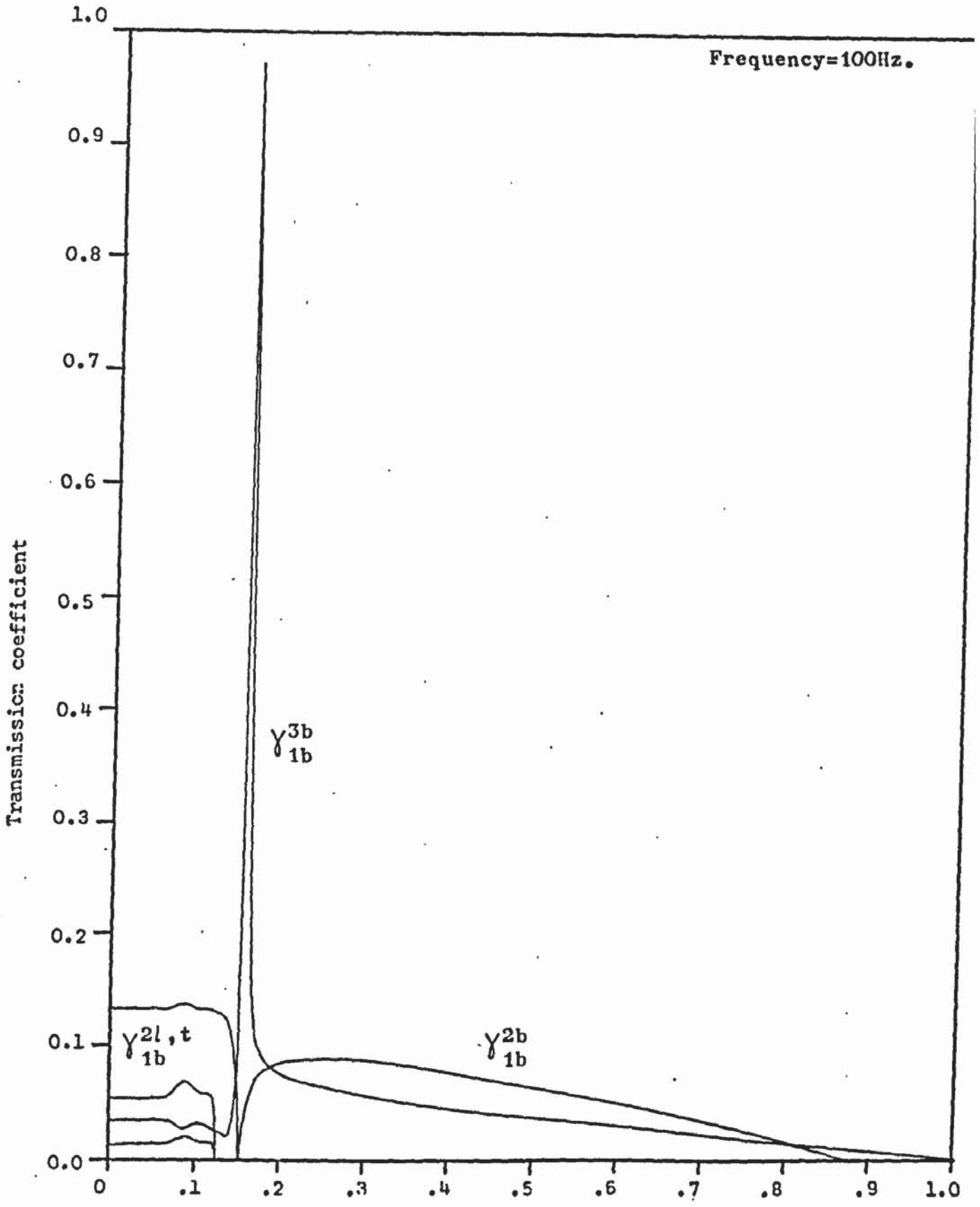

Transmission coefficient as a function of incident angle.

Cross-junction; $h_1 = 0.15m$ $h_2 = 0.2m$ $\mu_1 = \mu_2 = 0.3$

$E_1 = E_2 = 4 \times 10^{10}$ N/m^2 $\rho_1 = \rho_2 = 2.5 \times 10^3$ kg/m^3.

transmission coefficients describing the transfer from bending to longitudinal and transverse waves, the angle of total reflection is smaller; in this case, approximately 7^{o}.

Figure 4.2 illustrates the same transmission coefficients at a frequency of 1 KHz. The following changes are seen.

(1) The peak in γ_{1b}^{3b} occurs at a larger angle and is not as sharp as at the lower frequencies.

(2) A secondary dip, in γ_{1b}^{2b}, is much more conspicuous. This occurs at the angle at which the longitudinal component is totally reflected.

(3) The longitudinal and transverse components are totally reflected at a larger angle; in this case, approximately 25^{o}.

(4) The coefficient $\gamma_{1b}^{3l,t}$ increases in importance with frequency, but is still insignificant compared to other coefficients.

Figure 4.3 and Figure 4.4 best illustrate these trends as regards γ_{1b}^{2b} and γ_{1b}^{3b}. The gradual increase in angle with frequency of the occurrence of either peaks or dips in the bending wave coefficients results from the dispersive nature of the bending wave. At low frequencies, the bending wave velocities are much less than those of either longitudinal or transverse waves. Thus, Snell's law dictates that the angle of total reflection of the latter two wave types will be small, the critical angle corresponding to a sharp

Fig. 4.2

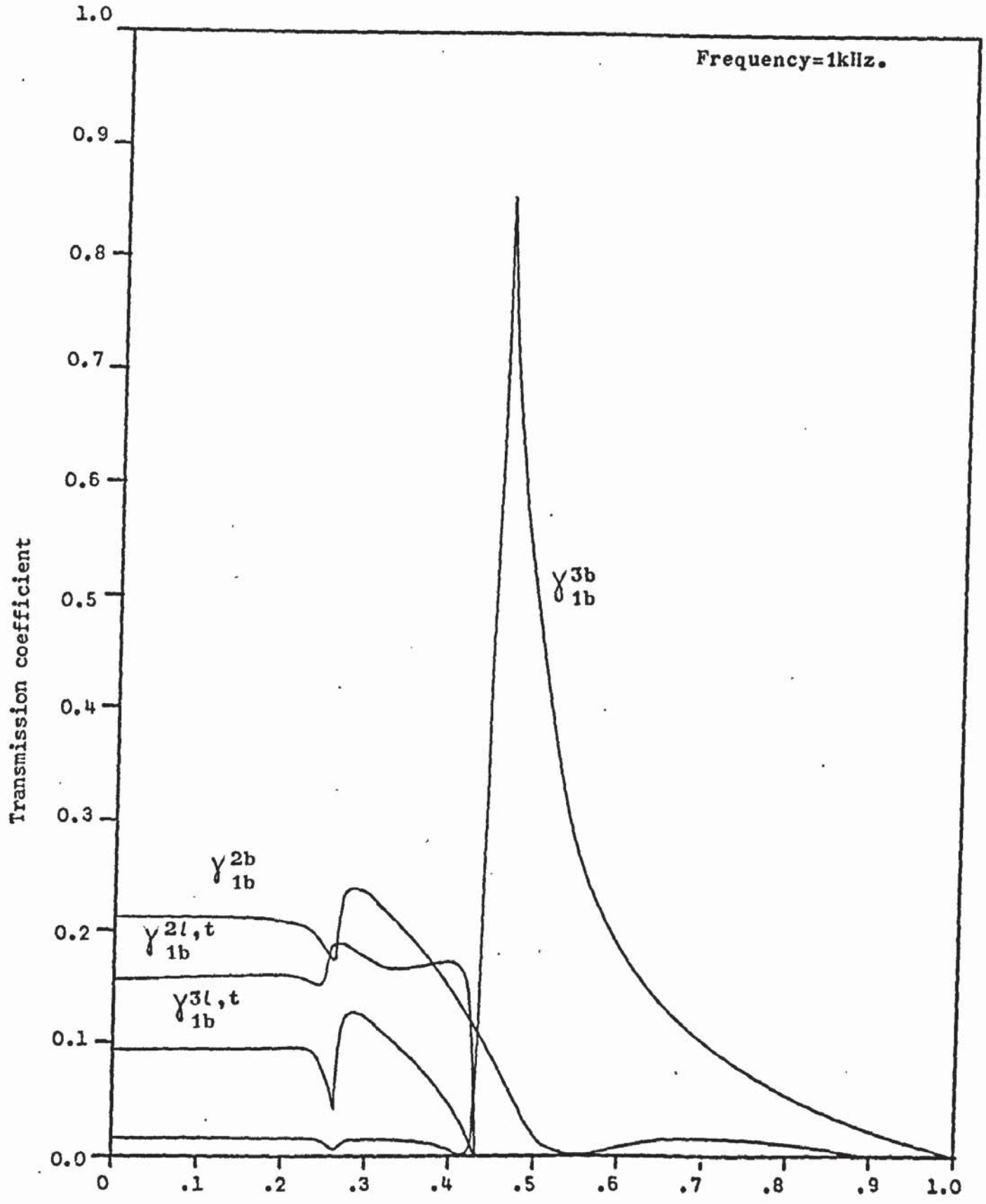

Transmission coefficient as a function of incident angle.

Cross-junction

$h_1 = 0.15m$ $h_2 = 0.2m$.

Fig. 4.3

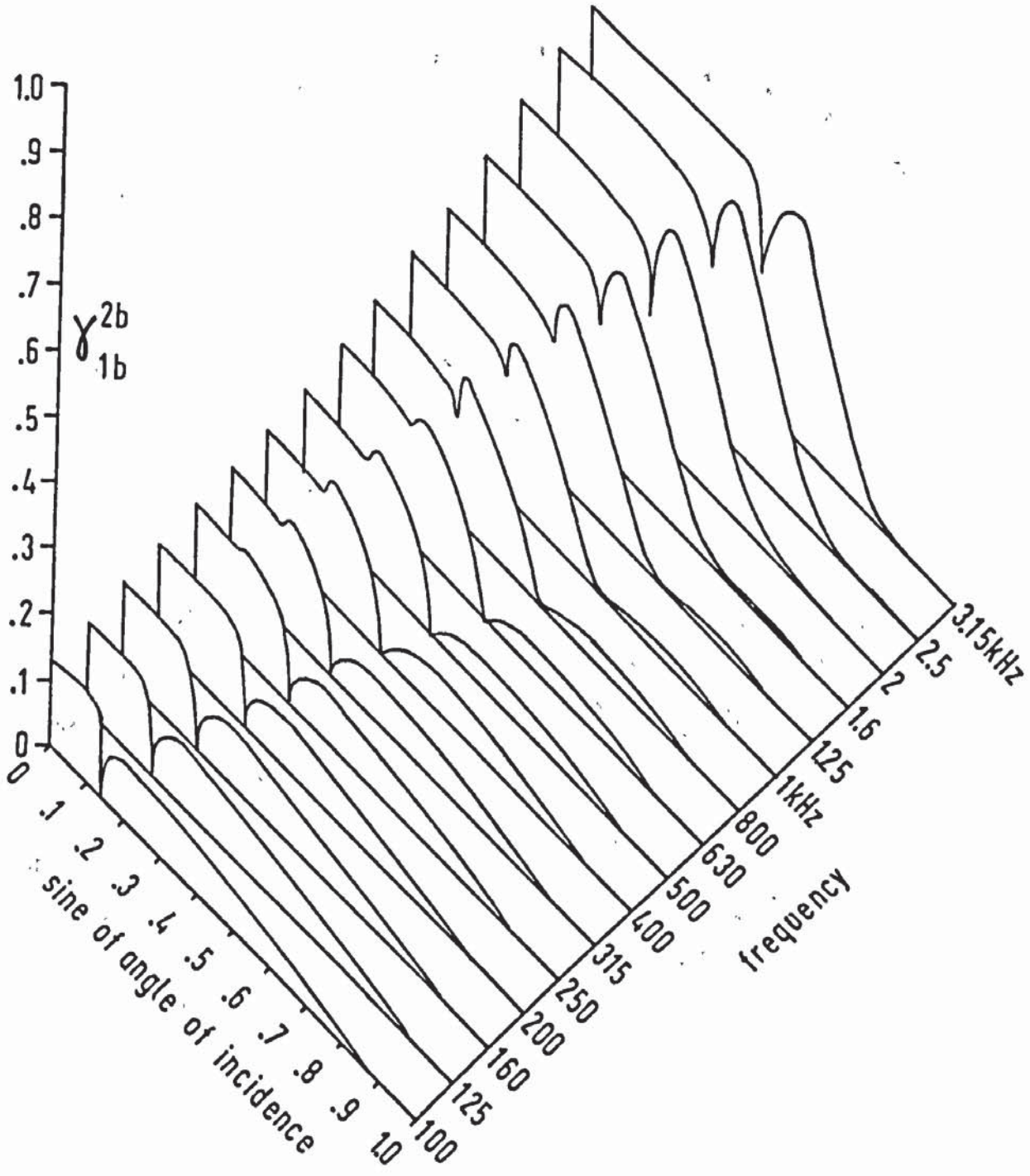

Transmission coefficient as a function of angle and frequency.

Cross-junction; $h_1 = 0.15m$ $h_2 = 0.2m$ $\mu_1 = \mu_2 = 0.3$

$E_1 = E_2 = 4 \times 10^{10}$ N/m^2 $\rho_1 = \rho_2 = 2.5 \times 10^3$ kg/m^3.

Fig. 4.4

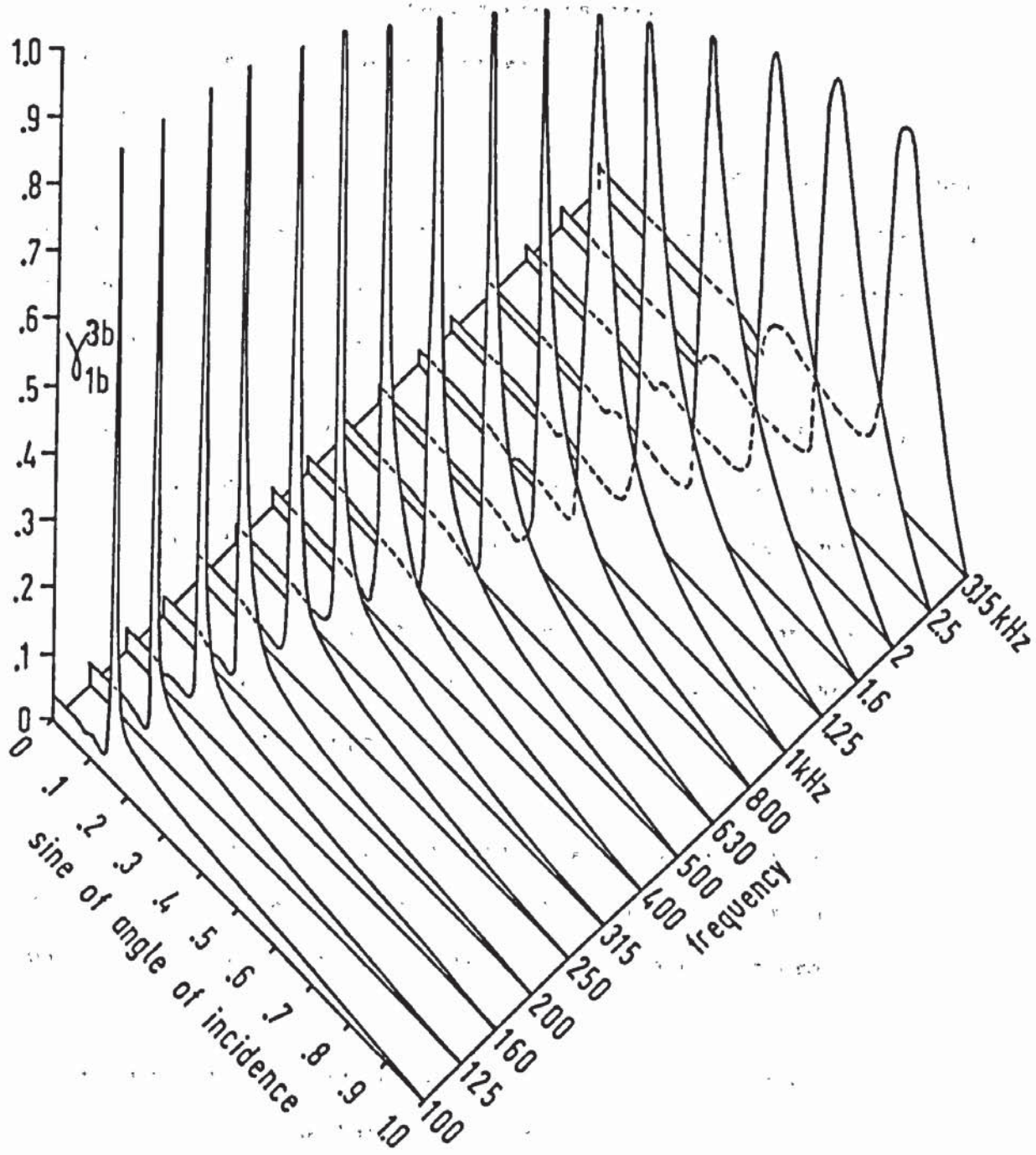

Transmission coefficient as a function of angle and frequency.

Cross-junction; h_1 = 0.15m h_2 = 0.2m

rise or fall in γ_{1b}^{3b} and γ_{1b}^{2b}, respectively. At higher frequencies, the frequency-dependent bending wave velocity is closer in value to (although still appreciably less than) that of other wave types. Thus, the critical angle will be larger and the contribution of the longitudinal and transverse components greater in the total energy transfer from one plate to another.

Figure 4.5 and Figure 4.6 give results for a bending wave incident at a T-junction at 100 Hz and 1KHz, respectively. Compared to the cross-junction, the coefficient γ_{1b}^{3b} assumes greater importance. The reasons for this are:-

(a) the impedance offered by a thick plate to an incoming wave on a thinner plate is greater than that offered by a thin plate to a wave on a thicker plate, and

(b) the junction contains only one limb at rightangles to the plate containing the incident wave. This farther reduces the impedance.

The coefficient $\gamma_{1b}^{3l,t}$ is negligibly small. This is to be expected since this coefficient is thought only to result from the bending wave field on plate 2 (and plate 4, in the case of a cross-junction).

Values are given in Figure 4.7 and Figure 4.8 for the case of a corner junction. The longitudinal and transverse components are illustrated separately. They show that the longitudinal coefficient has a maximum at normal incidence and, because it has the larger wave velocity, it has angle of total reflection smaller than that of

Fig. 4.5

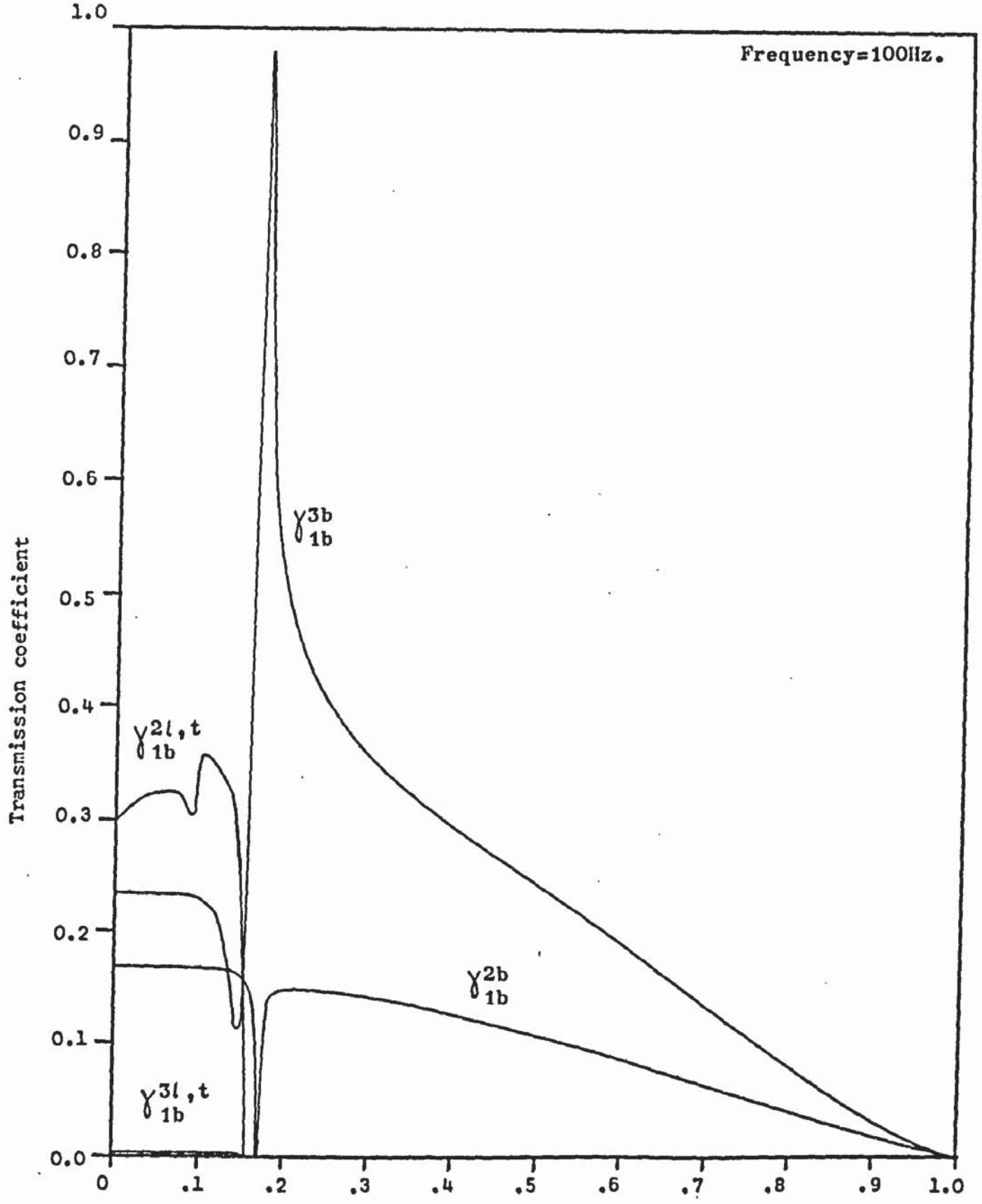

Transmission coefficient as a function of incident angle.

T-junction; $h_1 = 0.2m$ $h_2 = 0.15m$ $\mu_1 = \mu_2 = 0.3$

$E_1 = E_2 = 4 \times 10^{10}$ N/m^2 $\rho_1 = \rho_2 = 2.5 \times 10^3$ kg/m^3.

Fig. 4.6

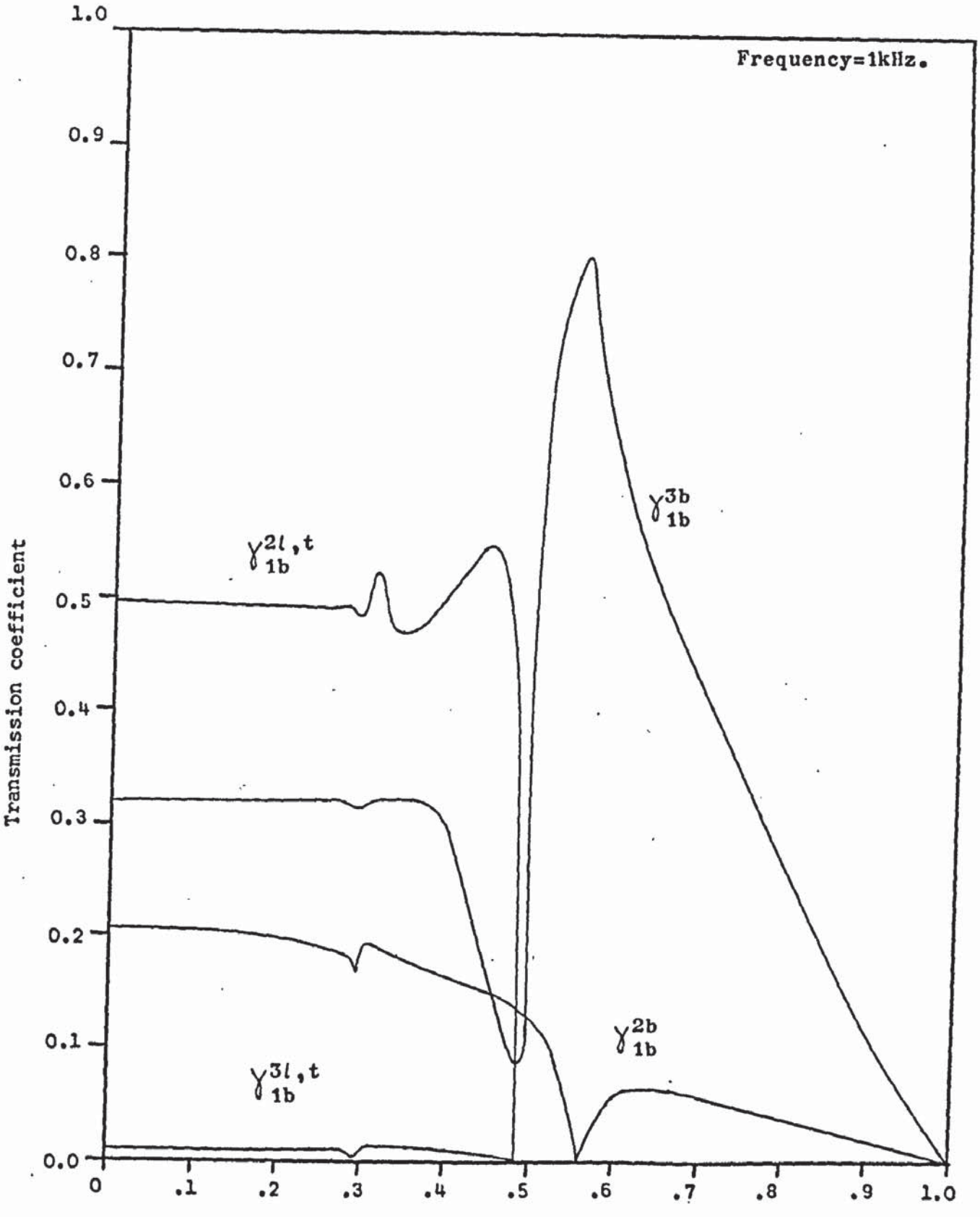

Transmission coefficient as a function of incident angle.

T-junction; $h_1 = 0.2m$ $h_2 = 0.15m$.

Fig. 4.7

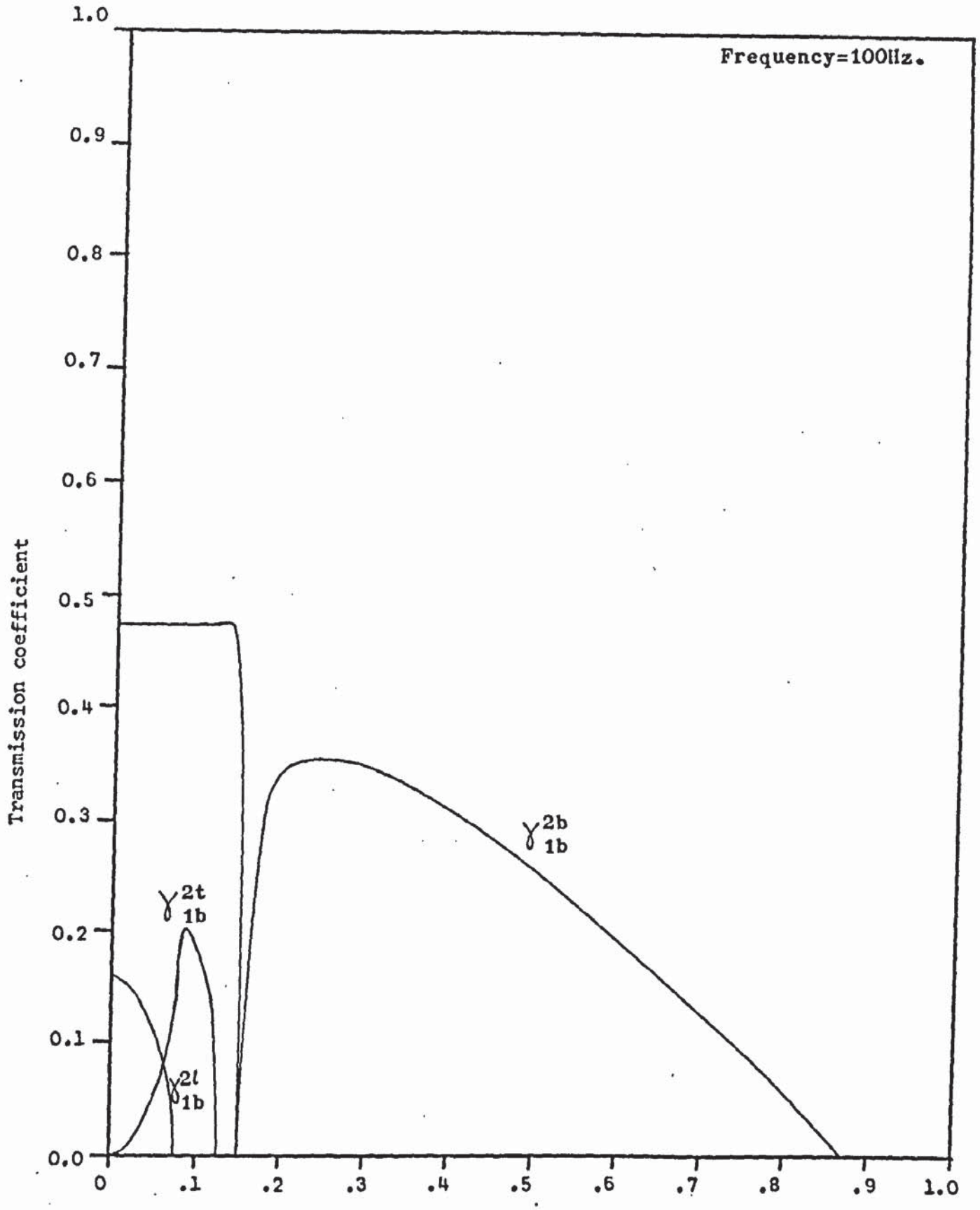

Transmission coefficient as a function of incident angle.

Corner junction; $h_1 = 0.15m$ $h_2 = 0.2m$ $\mu_1 = \mu_2 = 0.3$

$E_1 = E_2 = 4 \times 10^{10}$ N/m2 $\rho_1 = \rho_2 = 2.5 \times 10^3$ kg/m^3.

Fig. 4.8

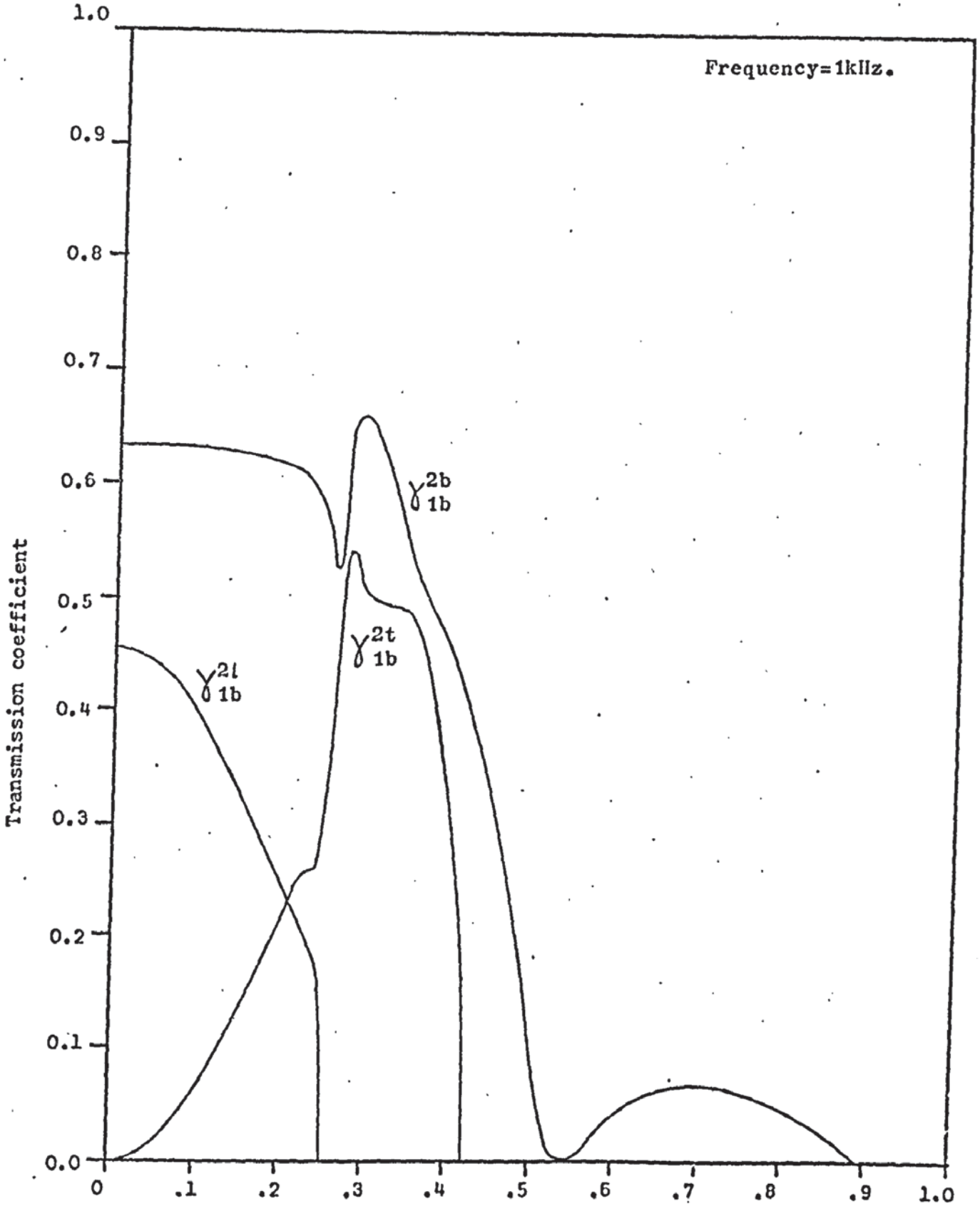

Transmission coefficient as a function of incident angle.

Corner junction; $h_1 = 0.15m$ $h_2 = 0.2m$.

the transverse wave. The latter increases from a zero value, at normal incidence, to a maximum where the longitudinal component is totally reflected, before dropping to zero at an angle corresponding to that of its own total reflection.

Calculations of the transmission coefficients which result when longitudinal and transverse waves are incident at a junction show them to be much more regular functions of the angle of incidence. Figure 4.9 illustrates the variation of coefficient when a longitudinal wave, of frequency 100 Hz, is incident at a cross-junction. Figure 4.10 illustrates the case at 1 KHz. The curves are smooth and either increase or decrease monotonically with angle. This would be expected since the incident longitudinal wave has the greatest velocity and therefore, according to Snell's law, no angle occurs such that total reflection results in any of the generated waves. The coefficient, indicating the transition from longitudinal to bending wave energy is small compared to other transitions, but increases in importance at the higher frequencies.

The curves given so far in this section are of coefficients which are proportional to the integrands given in equations 3.77, 3.78, 3.94 and 3.95. That is, the curves describe the energy generated at a junction, into the various waveforms, from an incident wave which is assumed to impinge at every angle to the normal with equal probability i.e. the incident field is diffuse. This approach is similar to that in most other branches of acoustics. Thus, on integrating these functions, an angularly averaged transmission coefficient will result which, it is felt, has physical significance

Fig. 4.9

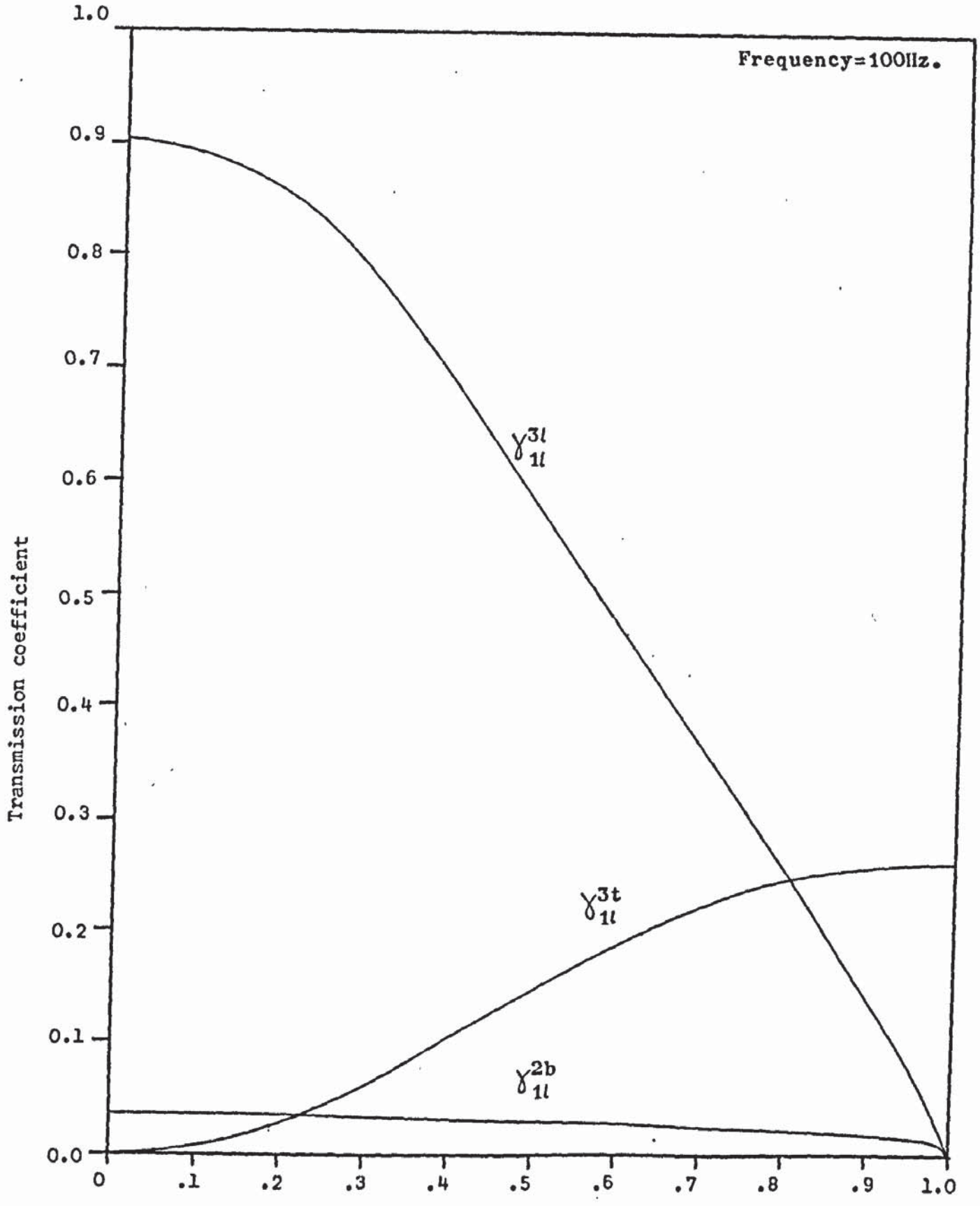

Transmission coefficient as a function of incident angle.

Cross-junction; $h_1 = 0.2m$ $h_2 = 0.15m$ $\mu_1 = \mu_2 = 0.3$

$E_1 = E_2 = 4 \times 10^{10}$ N/m^2 $\rho_1 = \rho_2 = 2.5 \times 10^3$ kg/m^3.

Fig. 4.10

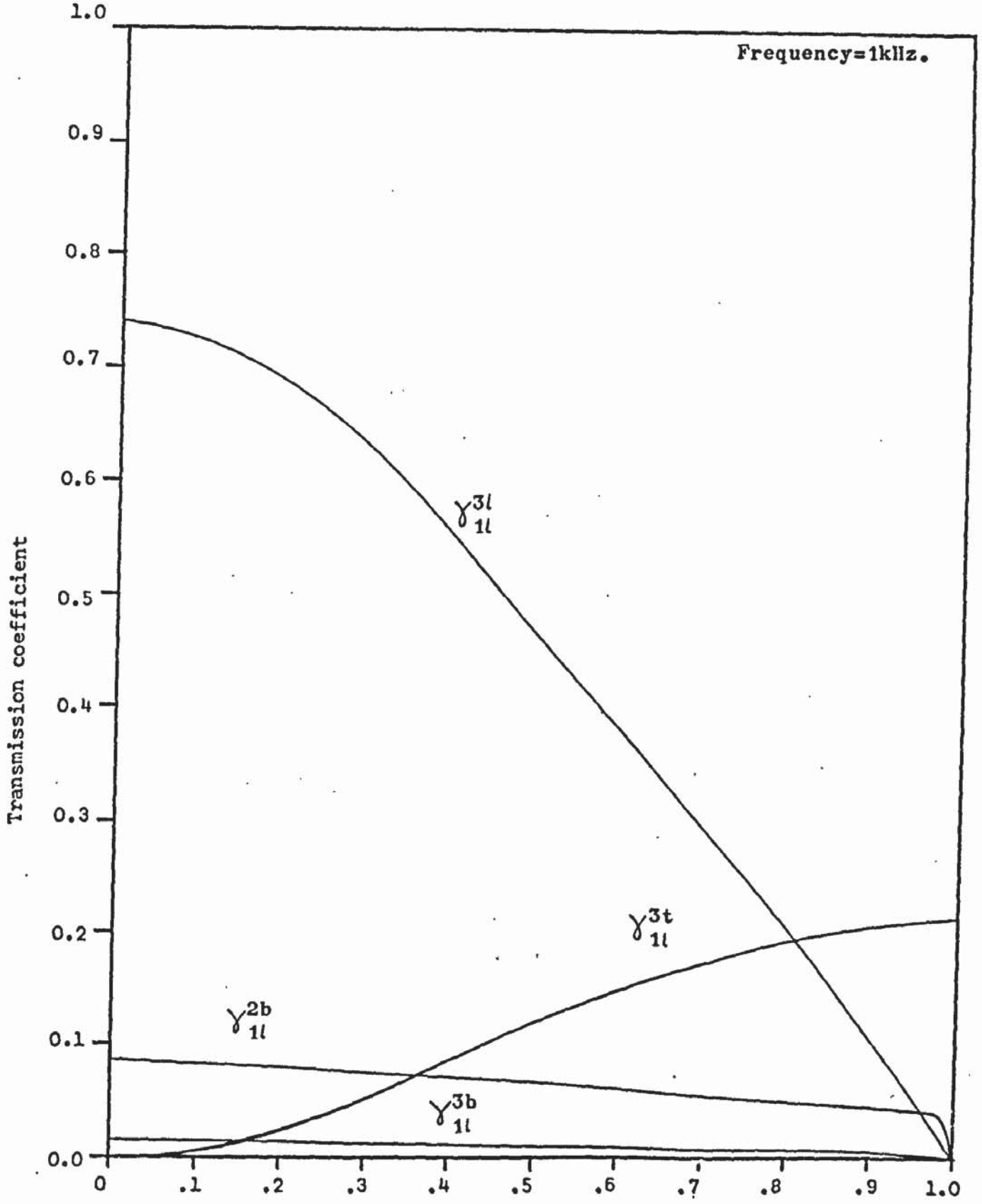

Transmission coefficient as a function of incident angle.

Cross-junction; $h_1 = 0.2m$ $h_2 = 0.15m$.

in the description of energy transfer at the junction of plates.

4.4 Variation of transmission coefficient with frequency

Figures 4.11 - 4.17 illustrate the variation with frequency of the angle-average transmission coefficients. Results were calculated for one-third octave frequency increments between 100 Hz and 3.15 kHz. Figure 4.11 gives a comparison of the coefficients calculated by simple bending wave theory and those calculated using Cremer's modifications. At low frequencies the two methods give results which do not differ. At frequencies above 400 Hz transmission coefficients obtained by Cremer's modified theory are higher than those calculated from simple bending wave theory. At 3.15 k the values of γ_{1b}^{3b} differ by approximately 10% of the higher value. The two values of $\gamma_{1b}^{2l,t}$ differ by approximately 40% of the higher value at the highest frequency. In subsequent graphs, the average transmission coefficients shown are those calculated using Cremer's modification.

Figures 4.11 - 4.13 give the average transmission coefficients for the case of a bending wave incident at a cross-junction, T-junction, and corner, respectively. In these, and most other, cases the variation with frequency of each, particular coefficient (for example $\gamma_{1b}^{2l,t}$) has the same trends, irrespective of the junction configuration. The following generalisations can therefore be made.

(1) Contrary to results given by Kihlman (1967), γ_{1b}^{2b} is seen to vary with frequency, albeit by a small amount. Over the range of 100 Hz - 3.15 kHz, the coefficient

Fig. 4.11

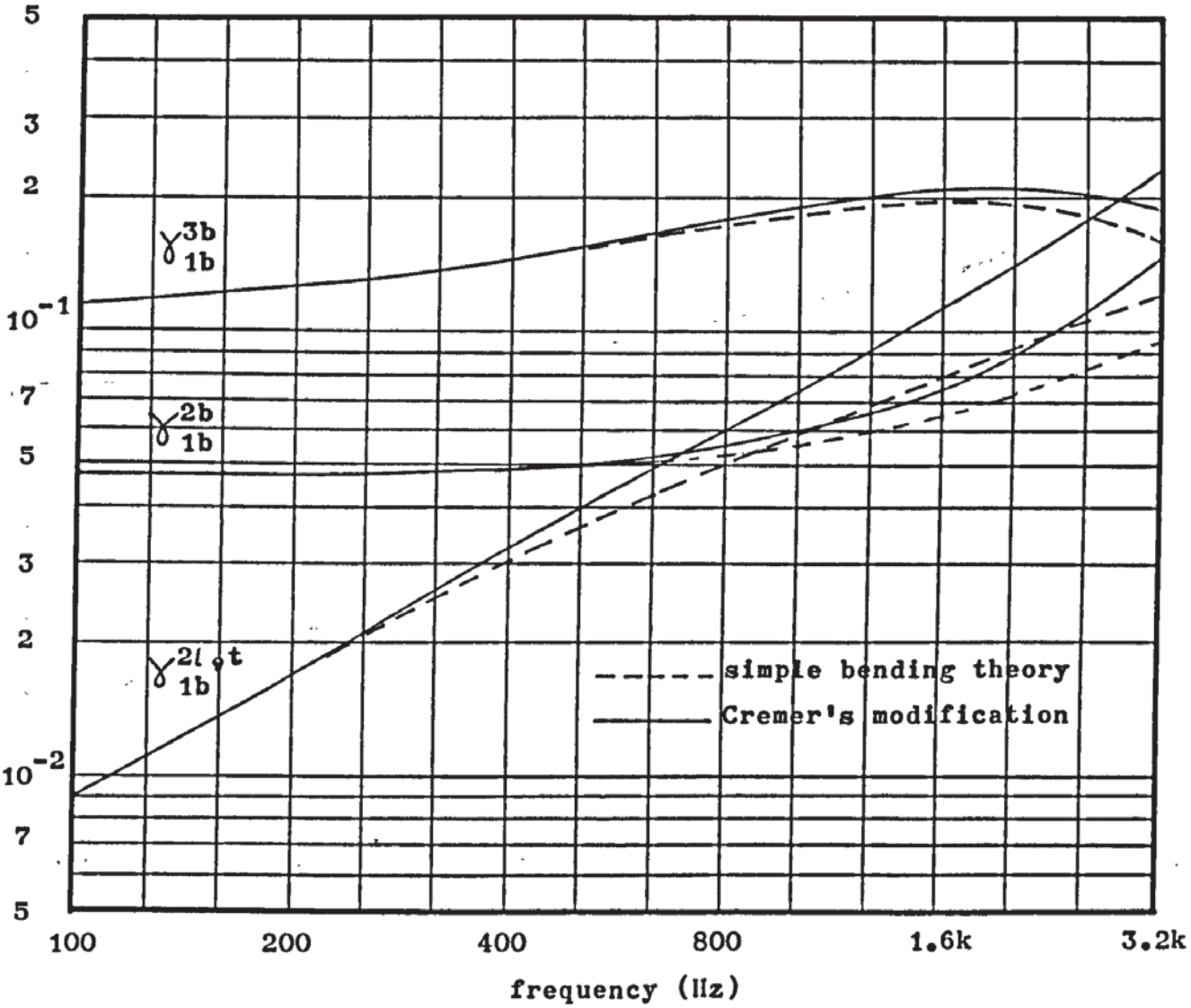

Transmission coefficient as a function of frequency.

Cross-junction; h_1 = 0.2m h_2 = 0.15m.

Fig. 4.12

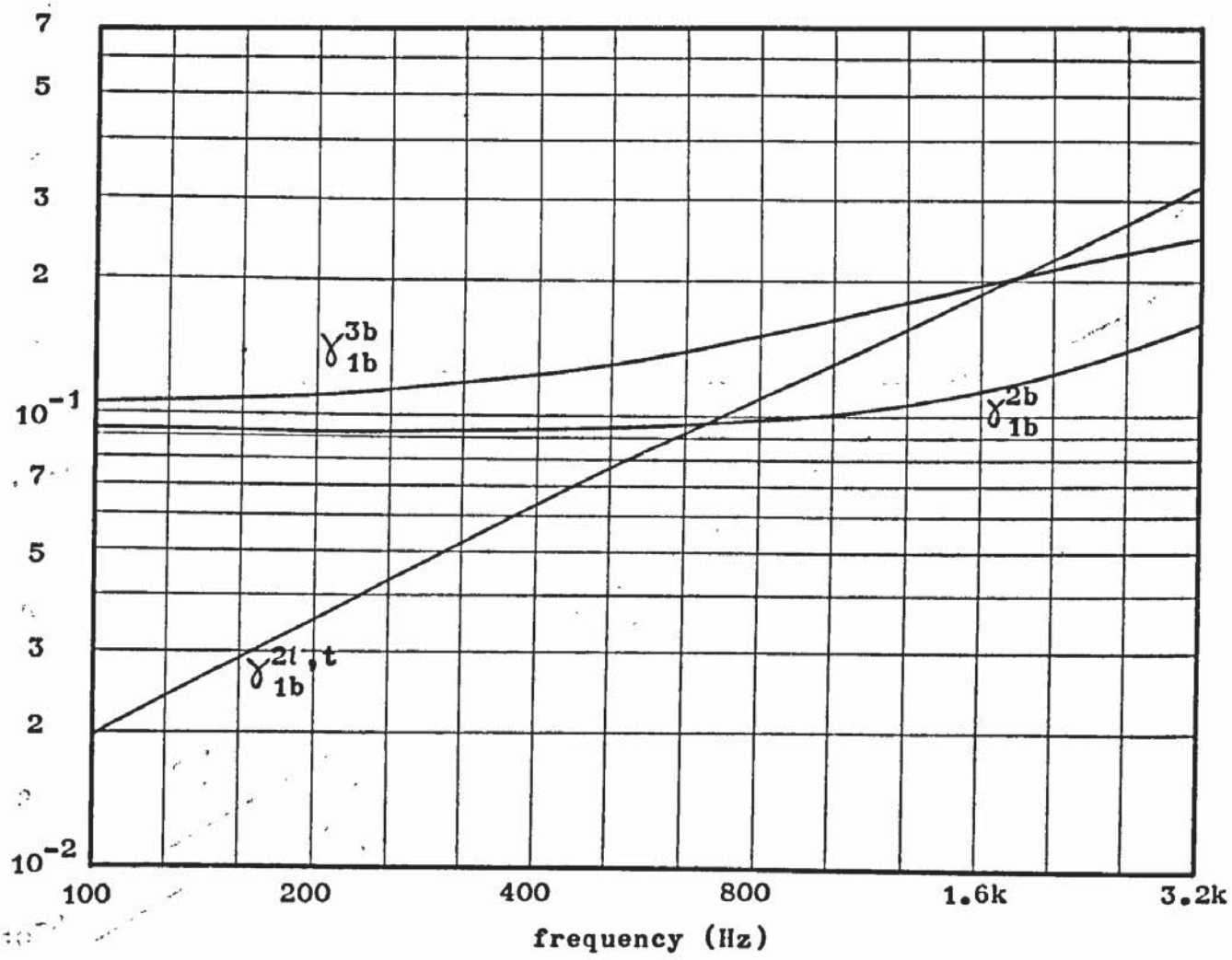

Transmission coefficient as a function of frequency.

T-junction; h_1 = 0.15m h_2 = 0.15m.

Fig. 4.13

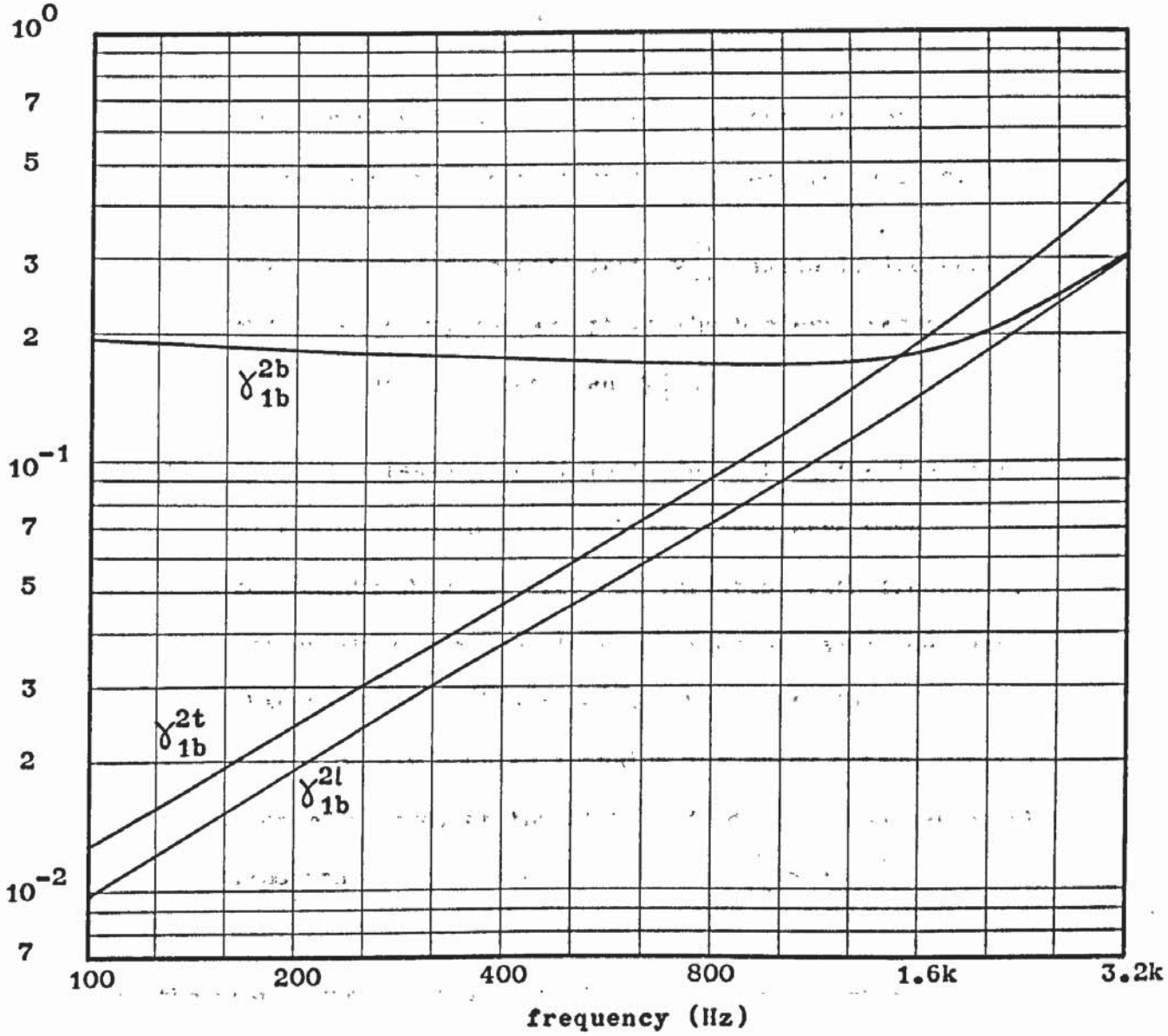

Transmission coefficient as a function of frequency.

Corner junction; h_1 = 0.2m h_2 = 0.15m.

increases by between 50% and 100%, the rate of increase being greatest at the higher frequencies.

(2) The transmission coefficient γ_{1b}^{3b} similarly increases with frequency, and except at the highest frequencies, assumes larger values than γ_{1b}^{2b}.

(3) The transmission coefficients describing the transfer of energy into longitudinal and transverse wave components show the greatest variation with frequency. Values at 100 Hz are often an order of magnitude less than those of γ_{1b}^{2b} and γ_{1b}^{3b}. The coefficient approximately doubles in value for every octave increment, and, at the highest frequency, assumes equal importance with the coefficients γ_{1b}^{2b} and γ_{1b}^{3b}.

In the graphs shown, values of $\gamma_{1b}^{3\,l,t}$ are not illustrated. In general this coefficient is an order of magnitude less than any other coefficient and can often be neglected in setting up the energy balance equations given in section 2.5. Some values are tabulated in Appendix III.

Using the same configurations of junctions with concrete plates of thicknesses 0.2 m and 0.15 m, results are given for the case of incident longitudinal and transverse waves. Figures 4.14 - 4.17 allow the following generalisation to be made.

(1) The coefficients vary greatly from each other, often by an order of magnitude. Thus, the largest contribution, in the case of a cross-junction, is

$\gamma_{1l}^{3l,t}$, the next two are γ_{1l}^{2b} and γ_{1l}^{3b}, and the least value is that of $\gamma_{1l}^{2l,t}$ which at 100 Hz is 28 dB less than the largest coefficient.

(2) The variation with frequency of coefficients, describing the generation of bending waves, is less than those describing the generation of other wave types.

It can be seen, that for reinforced concrete plates of not too dissimilar thicknesses, vibrational energy incident at a junction will transmit very efficiently into the other plates. The transmission coefficients calculated by Kihlman (1967) are very much lower in value for the cross-junctions investigated. The differences result from the greater impedances offered by the junction in Kihlman's model in which (a) the plate thicknesses differed by much greater amounts than that of the author (0.07 m - 0.15 m), and (b) the plates forming a junction were sometimes assumed to have different material constants. When plate thicknesses are considered which are of the same order as those considered by this author, then the results given by Kihlman (1967) give some agreement with those presented in this section and in Appendix III. (See Fig 5.11 and Table 9.24 in reference) Therefore, some attempt is now made to apply the results to real situations in which they can be compared with measurements.

4.5 Results for finite plate junctions

From the table of calculated transmission coefficients for junctions of semi-infinite plates (Appendix III) the associated structural

Fig. 4.14

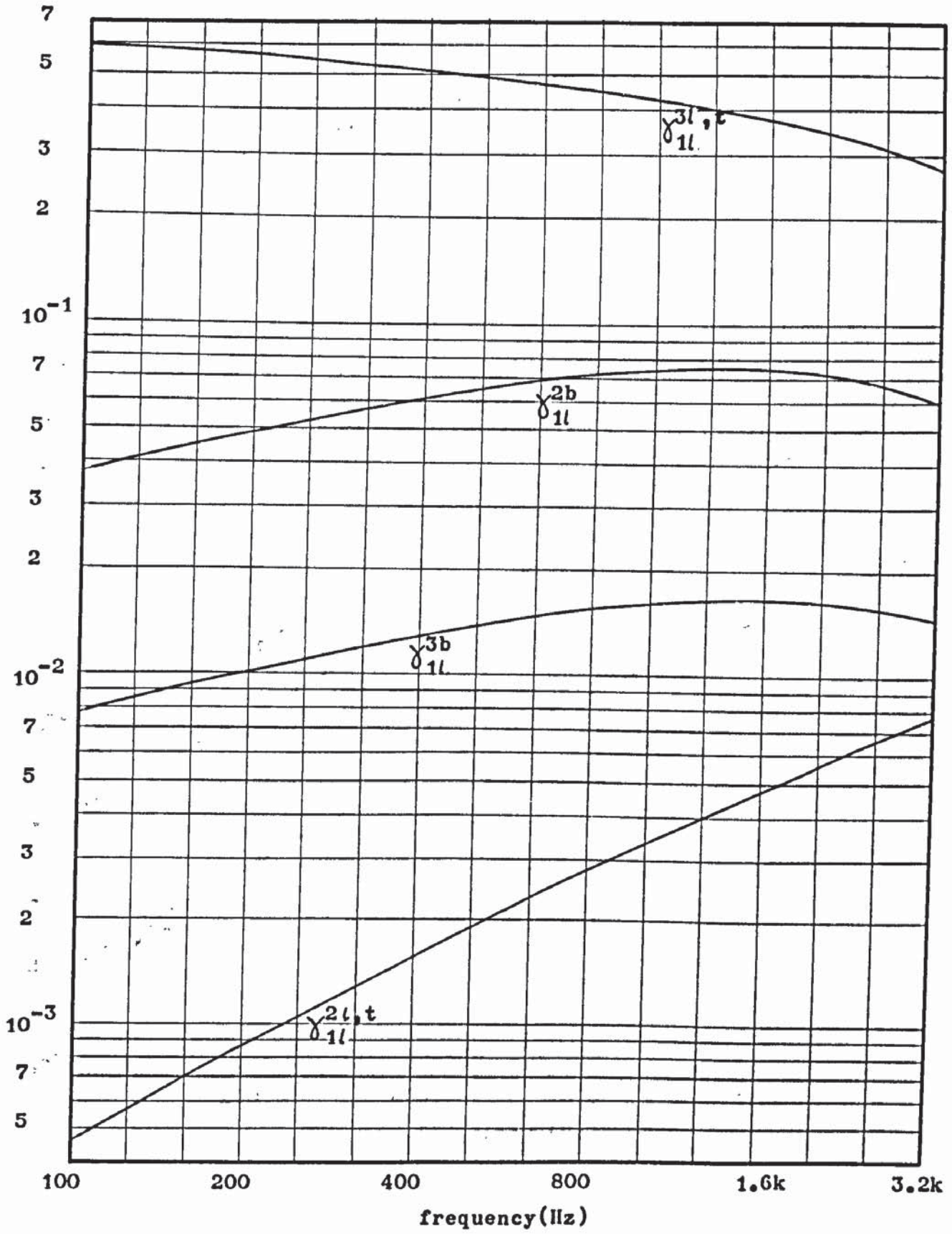

Transmission coefficient as a function of frequency.

Cross junction; $h_1 = 0.15m$ $h_2 = 0.2m$

Fig. 4.15

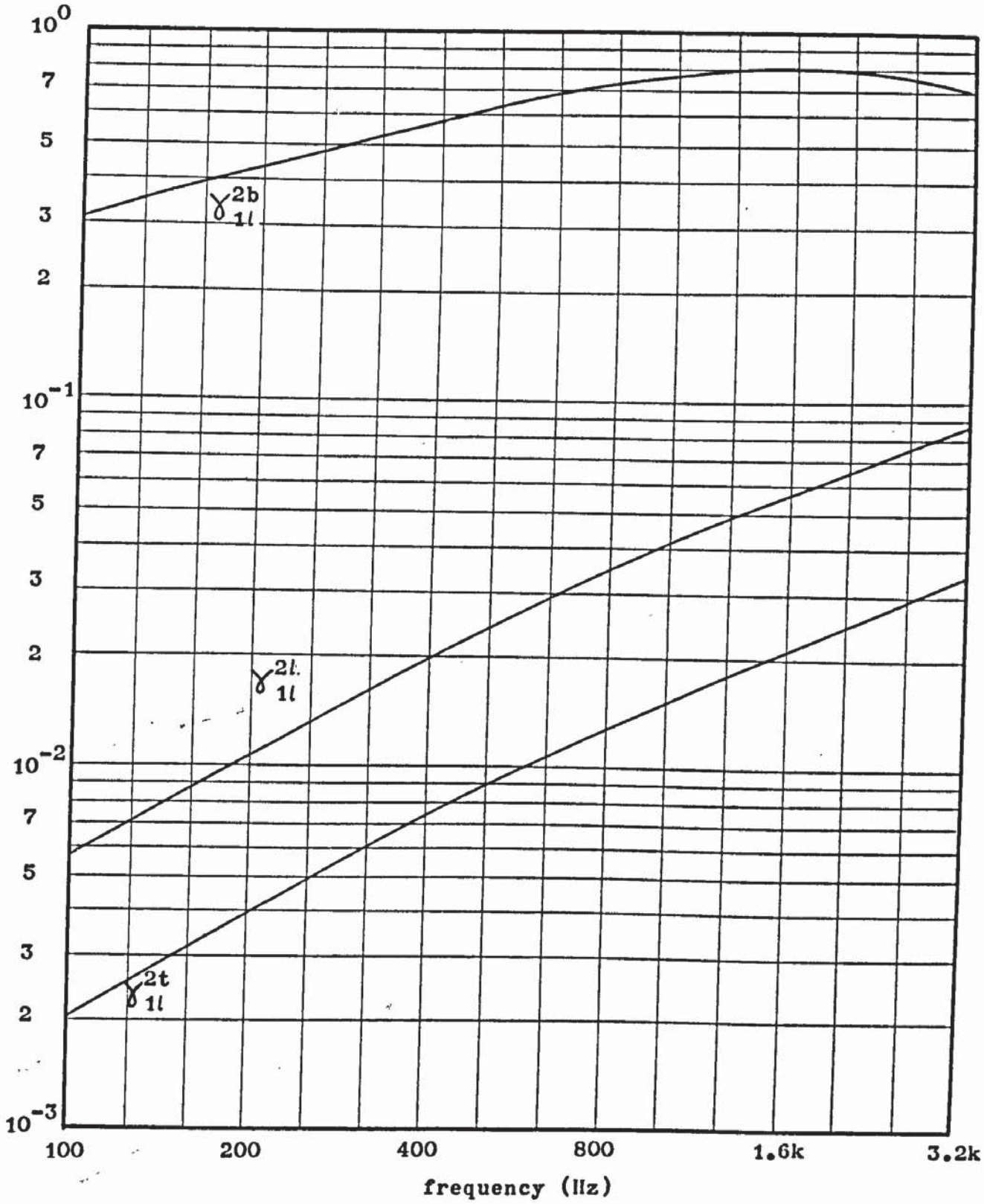

Transmission coefficient as a function of frequency.

Corner junction; h_1 = 0.2m h_2 = 0.15m

Fig. 4.16

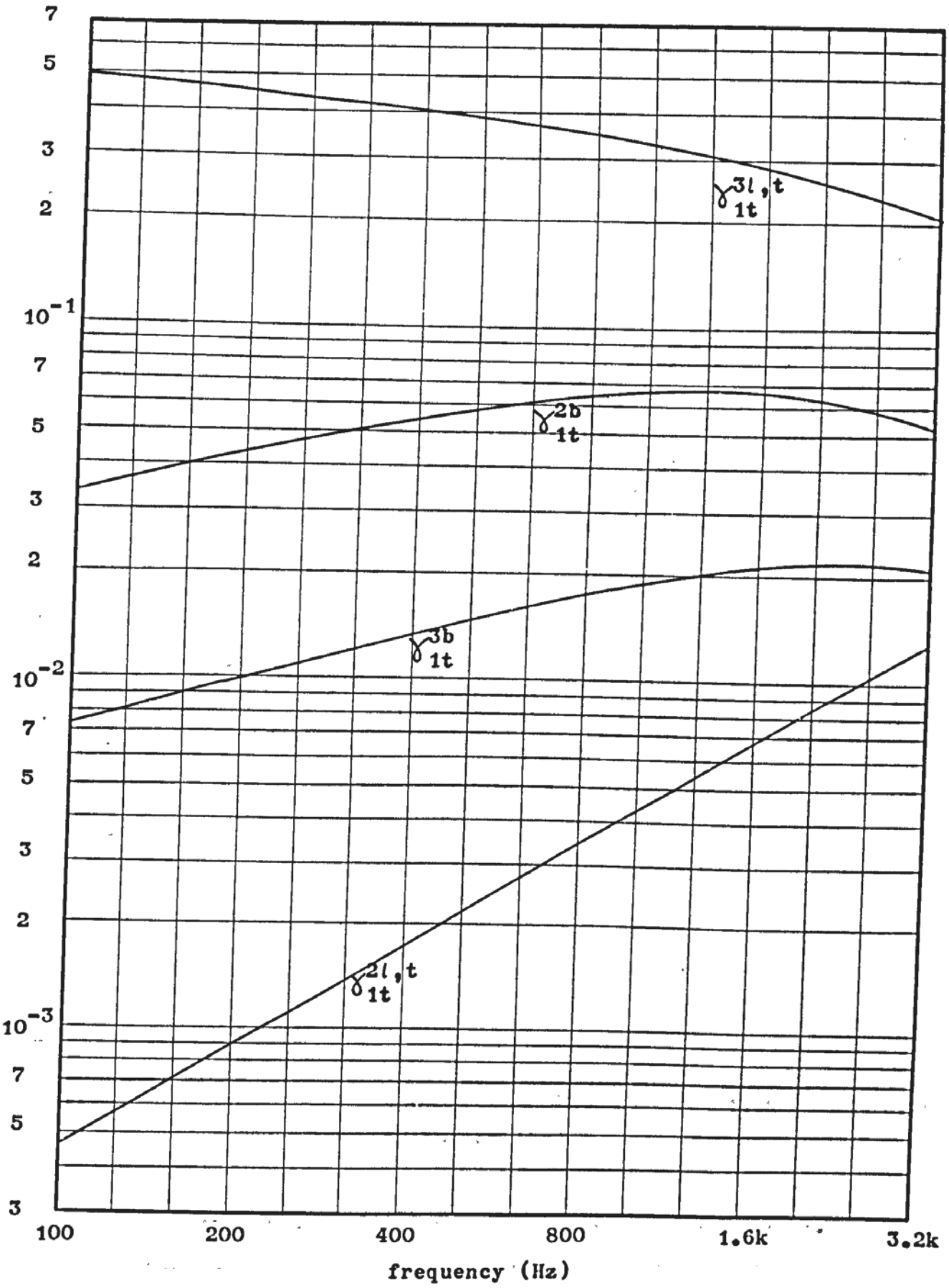

Transmission coefficient as a function of frequency.

Cross junction; $h_1 = 0.15m$ $h_2 = 0.2m$

Fig. 4.17

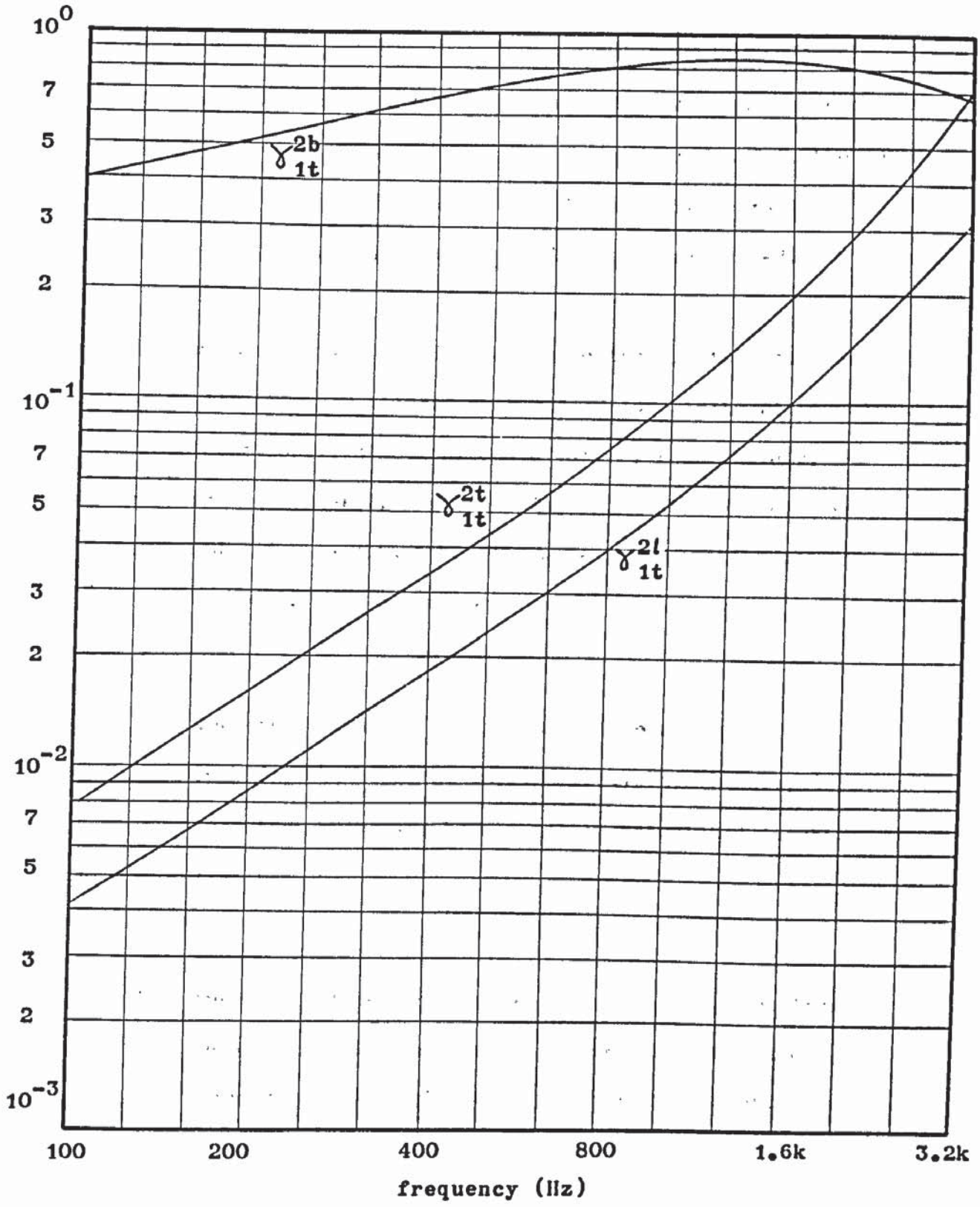

Transmission coefficient as a function of frequency.

Corner junction; $h_1 = 0.15m$ $h_2 = 0.2m$

coupling loss factors can be calculated as described in sections 3.8 and 3.9. The loss factors can now be introduced to the energy balance equations of sections 2.5 - 2.8 and the vibrational energy ratios for various plate configurations are calculated.

The calculations were carried out using the digital computer and results are shown in Figures 4.18 - 4.20 for finite plates forming a cross-junction, T-junction, and a corner, respectively. As described in Chapter 2, five methods of calculation have been postulated. The resultant bending wave energy ratios are given for all methods. The methods are listed as follows.

(a) The energy balance equations include all possible couplings between the three wave types, the coupling loss factors having been directly calculated (section 2.5.3).

(b) The longitudinal/transverse - bending couplings loss factors are calculated from the ratio of the wave numbers of the coupled wavetypes (section 3.9).

(c) The couplings in (b) can also be given from the ratio of the modal densities of the coupled wavetypes (section 3.9).

Fig. 4.18

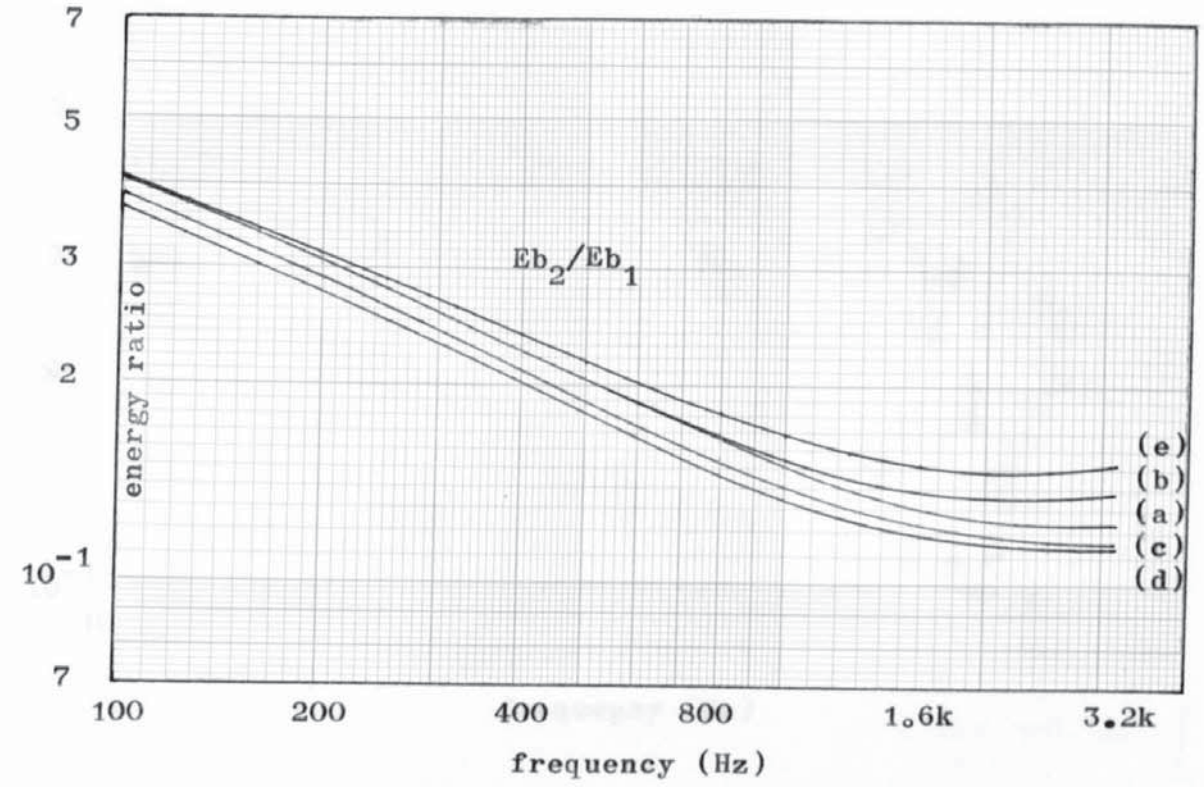

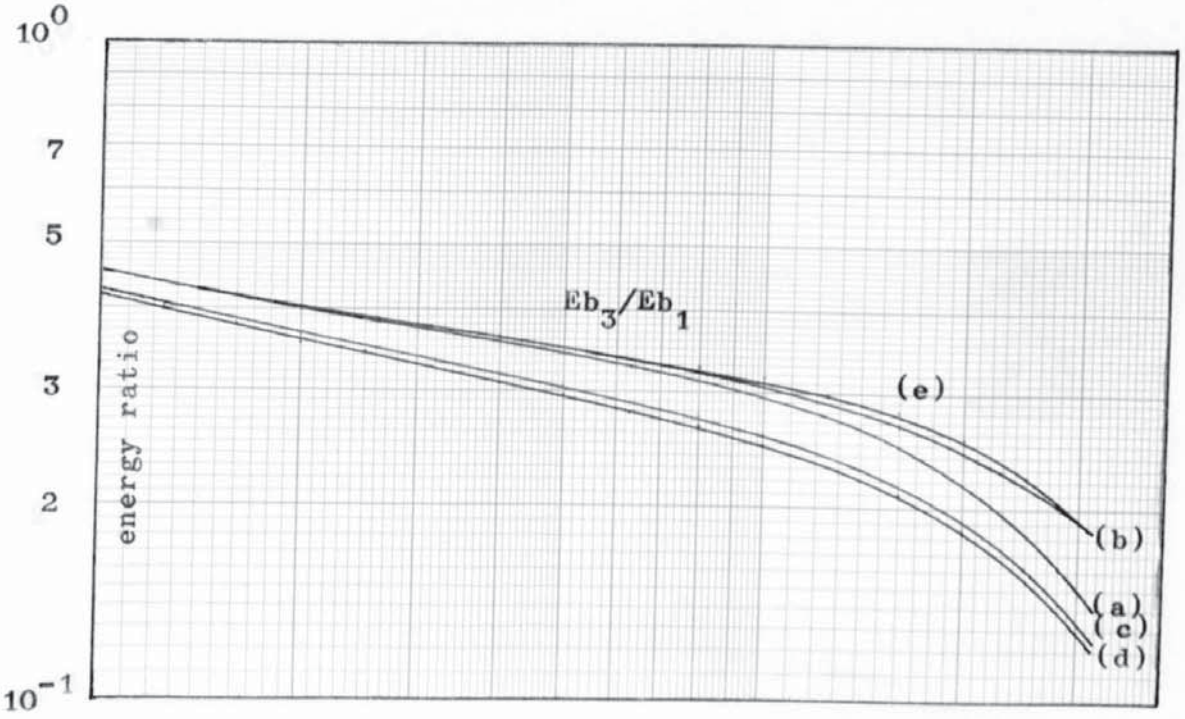

Bending energy ratios ; Cross junction of concrete plates.

Plate dimensions 4m x 3m, h_1 = 0.2m h_2 = 0.15m.

(a) All coupling coefficients directly calculated.

(b) Long/Tran - bending coefficients calculated from k-ratios.

(c) Long/Tran - bending coefficients derived from n-ratios.

(d) Bending - bending/long/tran. coupling coefficients only.

(e) Bending - bending coefficients only considered.

Fig. 4.19

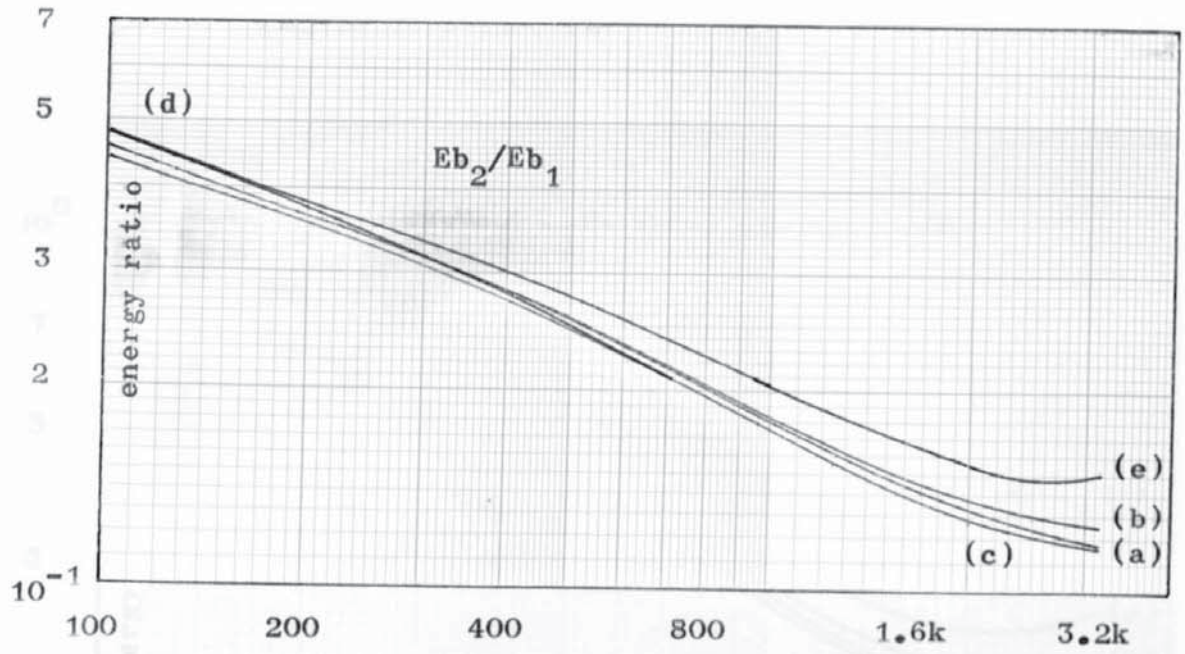

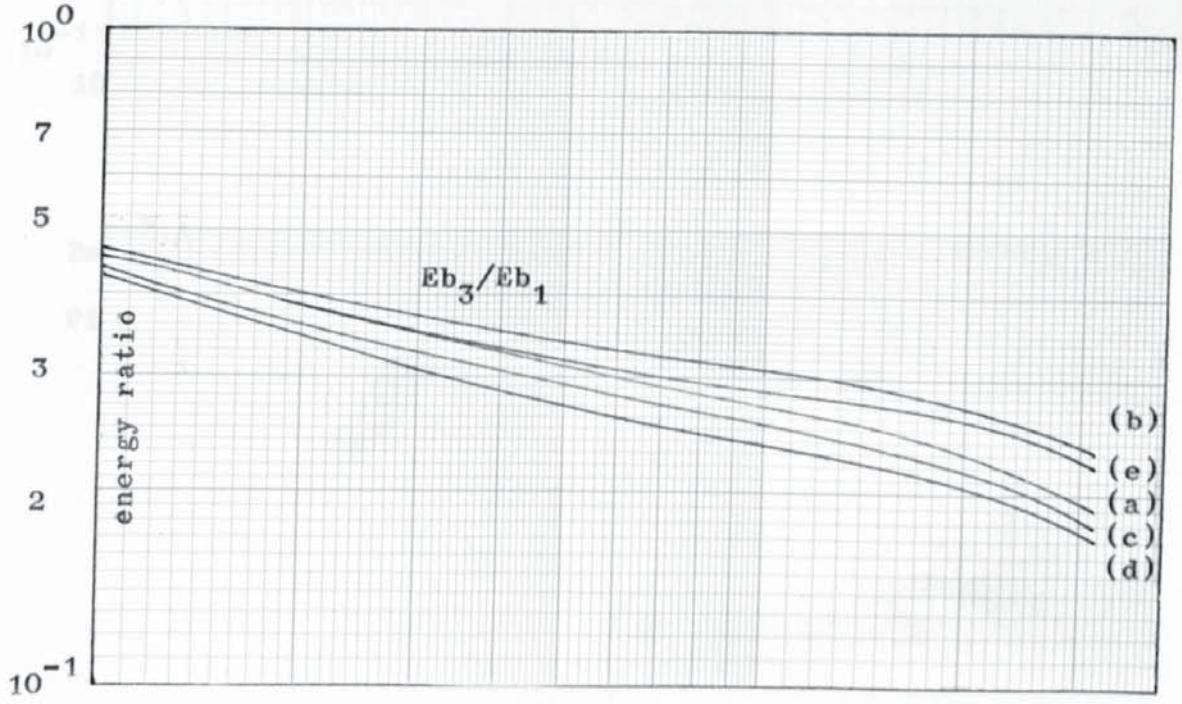

Bending energy ratios; T-junction of concrete plates.

Plate dimensions 4m x 3m, h_1 = 0.15m h_2 = 0.15m.

Fig. 4.20

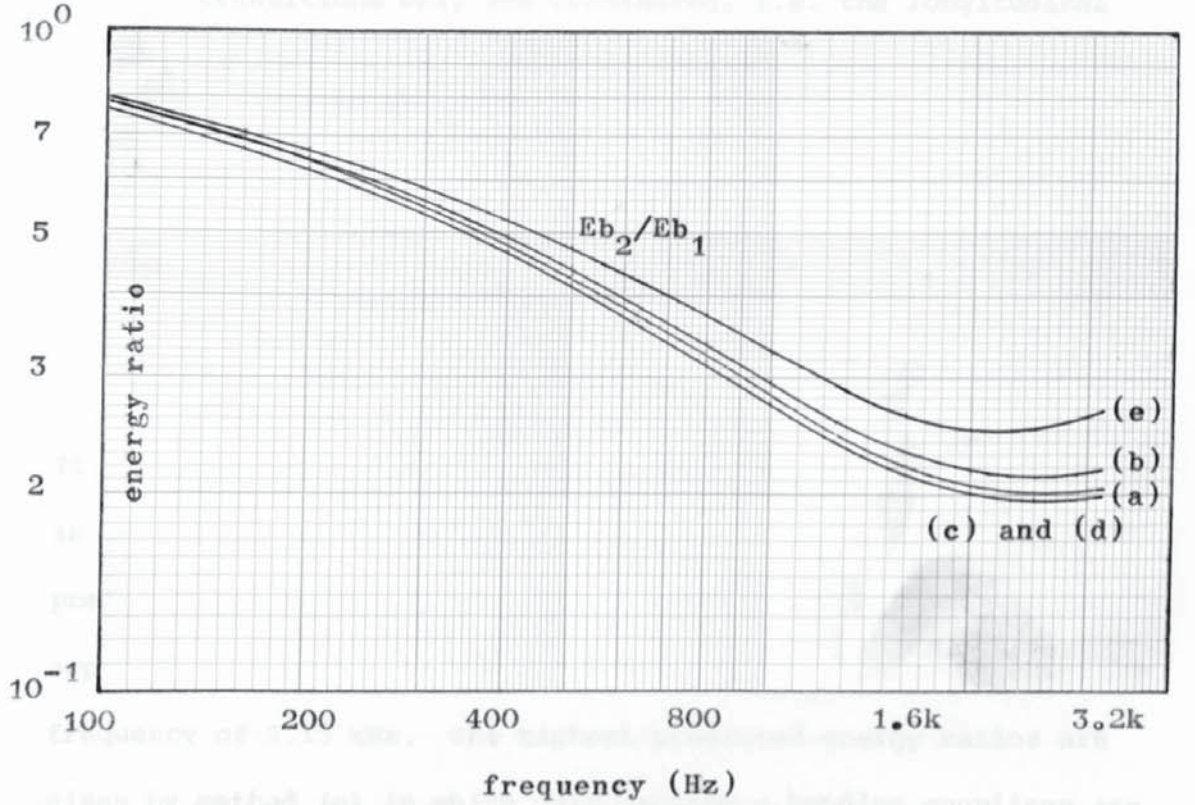

Bending energy ratios; Corner junction of concrete plates.

Plate dimensions 4m x 3m, h_1 = 0.2m h_2 = 0.15m

(d) The bending - bending/longitudinal/transverse wave transitions only are considered, i.e. the longitudinal and transverse fields are assumed non-diffuse (section 2.5.2).

(e) The bending - bending transitions only are considered (section 2.5.1).

It is seen in the examples given, that there is little difference in the calculated energy ratios using the five methods. The predictions lie within a band of 1 dB which is well within the expected experimental error. The maximum difference occurs at the frequency of 3.15 kHz. The highest predicted energy ratios are given by method (e) in which only bending - bending couplings are considered. Since this simple method gives values which differ from values produced by more exact theories, by an amount well within experimental error, it appears valid to include predictions using this model, alongside those of the more complex model (a), when comparing experiment with theory.

4.6 Further calculations and summary

In this chapter the principal transmission coefficients for cross- and T-junctions have been calculated. In Chapter 6 other coefficients will be calculated for comparison with experimental results. Similarly, calculations of radiation loss factor and modal spacing (or density) will be compared with experiment.

The results described in this chapter are summarised.

(1) Vibrational energy is transferred readily from one concrete plate to other concrete plates forming a junction; this is especially true if all plate thicknesses and material are equal or near equal. A reduction of energy flow results when the impedance, at the junction, is increased. This increase is possible by either introducing large thickness differences in the plates, and or assigning greatly differing material constants to each plate.

(2) In the finite systems investigated, consideration of wave types other than bending waves does not appreciably alter the predicted bending wave energy on each plate. It is thought however, that in more complex systems containing several junctions, at the higher frequencies the contribution of longitudinal and transverse components will become greater.

CHAPTER 5

SCALE MODELLING AND THE DYNAMIC CHARACTERISTICS OF BUILDING MATERIALS

5.1 Introduction

The experimental investigation of the theories described in Chapter 2 and Chapter 3, involved the use of quarter-scale models of the structural elements of interest. In acoustics, the use of models in predicting the response of full scale systems is a well established technique.

Harwood and Burd (1973) successfully predicted the acoustic response of studios and concert halls using models to a scale 1:8. Schoch and Feher (1952) use a large scale factor of between 1:20 and 1:30 when investigating sound transmission through single leaf partitions. Work by Kost (1967) involves the use of a scale factor of 1:35 in assessing the sound insulation of partition walls consisting of damped and undamped aluminium sheet. Ingemansson (1969) observes the effects of connections on the sound reduction of double walls. The scale factor in these experiments is 1:5. Schloss and Reader (1967) produce a direct comparison between the structural impedance and radiated sound of a full scale and quarter scale wooden structure in air and in water.

5.2 Similarity relations

The basis of scale modelling in acoustic experiments is the production

of a similarity relationship between the airborne or structural sound field in the original and in the model structures. If all linear dimensions are reduced by a ratio 1:n, then any mode of vibration of the prototype structure has its equivalent in the model, provided the frequency scale of the latter has been increased by a factor n . This is true only if the dynamic properties of the material, of which the structure is made, are independent of frequency.

Some examples of the dynamic response of structures are now considered. For wave velocities in rods and plates, the quasi-longitudinal wave velocity in a rod is given by,

$$C_{l2} = \sqrt{\frac{E}{\rho}}$$

and is seen to be independent of frequency. Therefore, the modal response of a rod set into longitudinal vibration is scaled correctly simply by shortening the rod by the required ratio. In the case of bending waves in plates the velocity is given by,

$$C_b = 2[h\omega]^{\frac{1}{2}} [E/12\rho(1 - \mu^2)]^{\frac{1}{4}}$$

The velocity is dependent upon the frequency and plate thickness. Thus, if the plate thickness is reduced by a factor n then the frequency must be increased by the same factor in order to ensure the same response. Therefore, in the case of bending waves, on rods and plates, all linear dimensions are reduced by a factor n to ensure correct scaling.

The critical coincidence frequency of a plate has been given by,

$$\nu_{crit} = \frac{3^{\frac{1}{2}} C_o^2}{\pi C_l h}$$

Again, geometric scaling by a factor n is accompanied by an increase in frequency of the same factor.

In power flow theory, reference is made to the modal densities of the vibrational fields; more specifically, the ratio of modal densities of coupled systems. The bending wave modal density with respect to frequency on a plate is given by,

$$n_b = \frac{3^{\frac{1}{2}} S_p}{C_l h}$$

Thus, a reduction in linear dimensions by a factor n will give a value of modal density reduced by the same factor. This appears contrary to the conditions required for true scaling. The apparent anomaly results from the definition of modal density which is given as the number of modes per Hz. In theory and experiment one is concerned with the number of modes involved in the response, within the bandwidth of interest. It is seen that the power flow equations, described in Chapter 2, are for a bandwidth of unit frequency. In this case, the modal density and number of modes per bandwidth have the same value. However, bandwidth is normally expressed as a fraction of the octave or as a percentage of the value of the centre frequency. Thus, in the case of third octave filtering, the bandwidth is approximately 23% of the centre frequency. Therefore, although the modal density decreases by a factor n, on increasing the frequency by this factor, the bandwidth increases by a factor n. The number of modes involved in the prototype and scale model thus remain the same

and the similarity relation is preserved. The same argument applies to longitudinal and transverse modal densities.

The discussion can be summarised by stating that, as in room acoustics, the structural vibration patterns of similar systems are affected only by the ratio of linear dimension to the vibrational wavelength, providing the dynamic characteristics of the materials are independent of frequency. This condition, along with the need to obtain values of the dynamic parameters, prompted a series of experiments concerned with the measurement of bending, longitudinal, and torsional wave velocities in some common materials.

5.3 Measurement of the material constants

Several authors have investigated the variation with frequency of complex elastic constants of building materials. Kuhl and Kaiser (1952) measure the absorption of structure-borne sound in walls with and without sand-filled cavities. Rupprecht (1958) considers the travelling wave as well as the standing wave conditions in investigations of the wave velocities and loss factors in rods of building material. The frequency range of measurement is 100 Hz to 10 kHz. Nöll extends the range from 5 kHz to 100 kHz when assessing the frequency dependence of complex elastic constants. His results seem to indicate that acoustic modelling with large scale factors (up to 30:1) appears possible.

The experimental procedure adopted is similar to that of Schmidt (1934). The complex Young's modulus and dynamic Poisson's ratio

of building materials are obtained by excitation of free-free rods of the material into bending, longitudinal, and torsional vibration, and then observing the resonances which occur on altering the driving frequency. By measuring the rate of decay in amplitude on removing the source of excitation, values of loss factor are obtained. The material of primary importance is reinforced concrete. However, results are given for brickwork and breeze-block.

5.4 Instrumentation

5.4.1 The driver

To excite the rods of building material into forced vibration it was necessary to have an efficient method of excitation which, at the same time, did not introduce additional losses into the system, i.e. there should be no contact between the driver and the specimen. The method adopted was that of cementing a speech coil (wound on a light aluminium former) to the rod and then introducing a magnetic field by means of a permanent magnet (Plate 5.1). An alternating current in the coil produces a force varying at the same frequency. The direction of the applied force, relative to the axis of the rod, determines the type of wave which will be produced. Figure 5.1 illustrates the driver positions required to excite quasi-longitudinal and bending waves in a freely suspended rod.

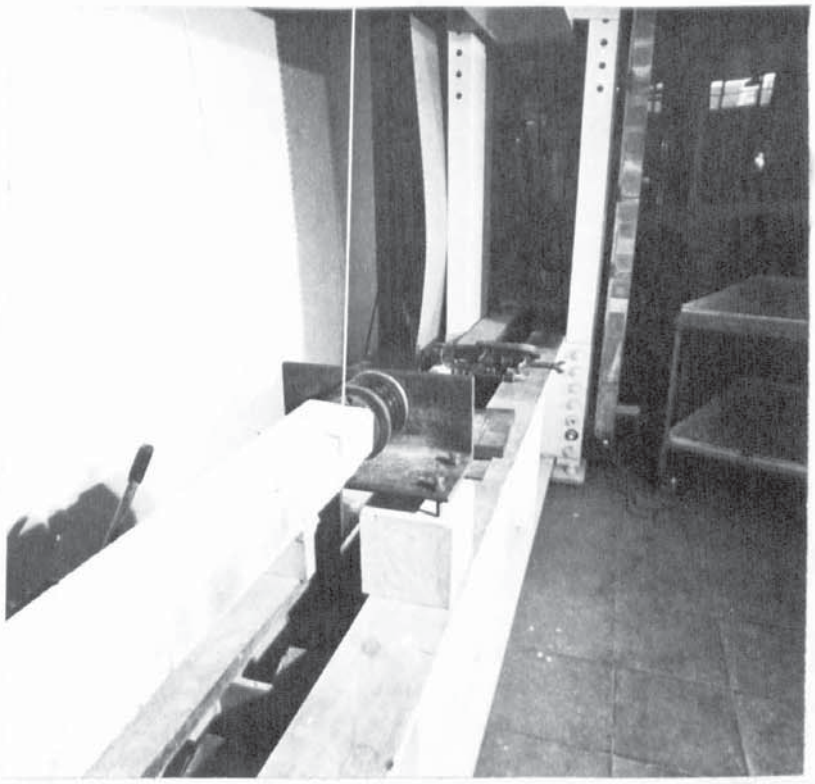

PLATE 5.1 Excitation of longitudinal waves in a suspended brick rod.

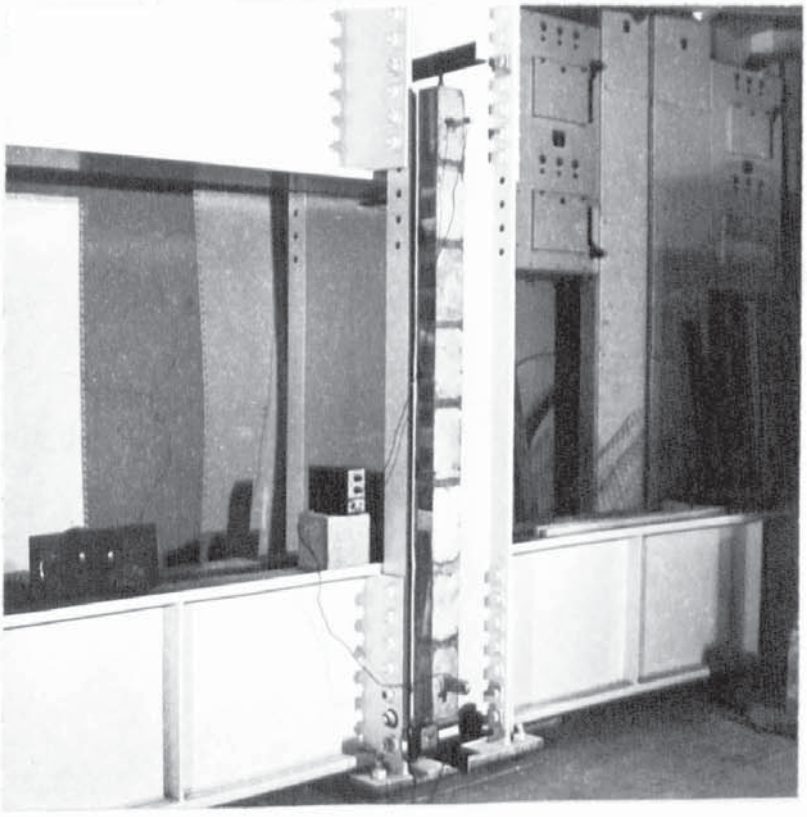

PLATE 5.2 Excitation of torsional waves in a pivoted brick rod.

Fig. 5.1

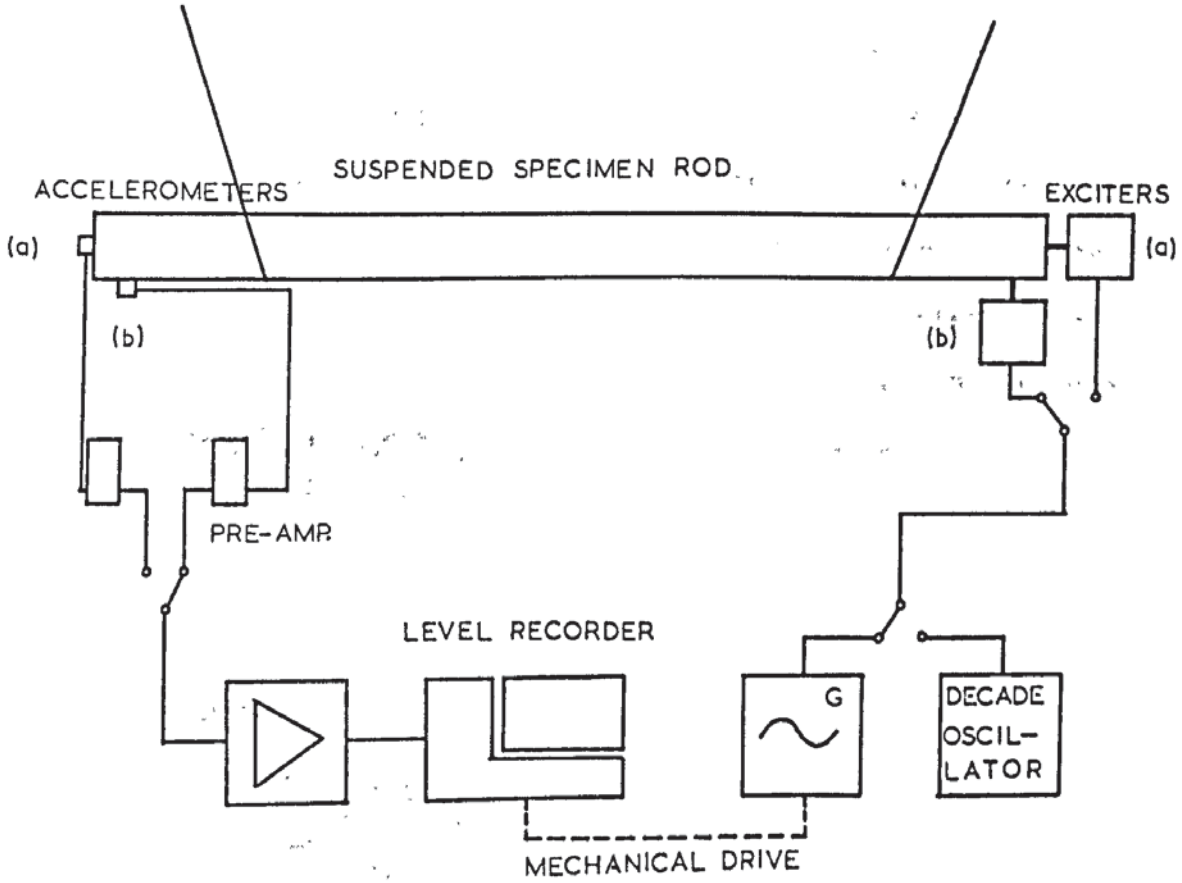

The generation of vibrational modes in a suspended rod.

(a) Longitudinal excitation.

(b) Bending excitation.

5.4.2 The receiver

The acceleration amplitude at any point on the specimen was measured by means of a Brüel and Kjaer (B & K) piezoelectric accelerometer transducer (type 4333) stuck by means of beeswax to the free end of the specimen rod. The accelerometer could be positioned either to measure the longitudinal wave or to measure the bending wave acceleration amplitude (Fig 5.1). The accelerometer signal is passed through a vibration pick-up pre-amplifier (B & K type 2625) and amplified by an audio frequency spectrometer (B & K type 2112) on linear response. The variation of amplitude with frequency could then be plotted logarithmically using a level recorder (B & K type 2305).

5.4.3 The signal source

The signal supplied to the speech coil consisted of an alternating current. The frequency sweep was provided by the drive shaft of the level recorder, driving a sine-random generator (B & K type 1024) which emitted a pure tone, the logarithm of the frequency being made to increase linearly with time. A typical sweep rate for a material of loss factor of the order of 10^{-2} would be approximately one octave per minute. The signal from the generator was amplified using a Quad 50E power amplifier. On obtaining the frequency response of the specimen, the centre frequency of each resonance (and the half-power bandwidth, if desired) was measured accurately, using a decade oscillator (Muirhead K-126-A) reading to 0.1 Hz.

5.5 Torsional waves

Shear vibration, in the form of torsional waves, can be produced in material when the specimen is in the form of a rod. Two methods of excitation were employed.

(1) If the specimen rod is of circular cross-section, it is relatively easy to produce torsional vibration by ensuring that the direction of the driving force is tangential to the cross-sectional circle of the rod. This was done by cementing the speech coil to a projecting aluminium stud (Fig 5.2(a)). The axis of the accelerometer (i.e. the direction of greatest sensitivity) at the other end of the rod is likewise tangential to the cross-sectional circle and is also perpendicular to the axis of the driving force. This ensured that the torsional resonances were not masked by the bending resonances which inevitably resulted, no matter how much care was taken in positioning the driver.

(2) The first method was found unsatisfactory when the specimen was of a rectangular cross-section, such as a brick array. A greater couple is required and this can be produced using two identical speech coils and magnets. The directions of the forces produced, lie parallel to one edge of the cross-sectional rectangle. By reversing the polarity of one coil, relative to the other, the forces produced are thus equal and opposite (Fig 5.2(b)).

Fig. 5.2

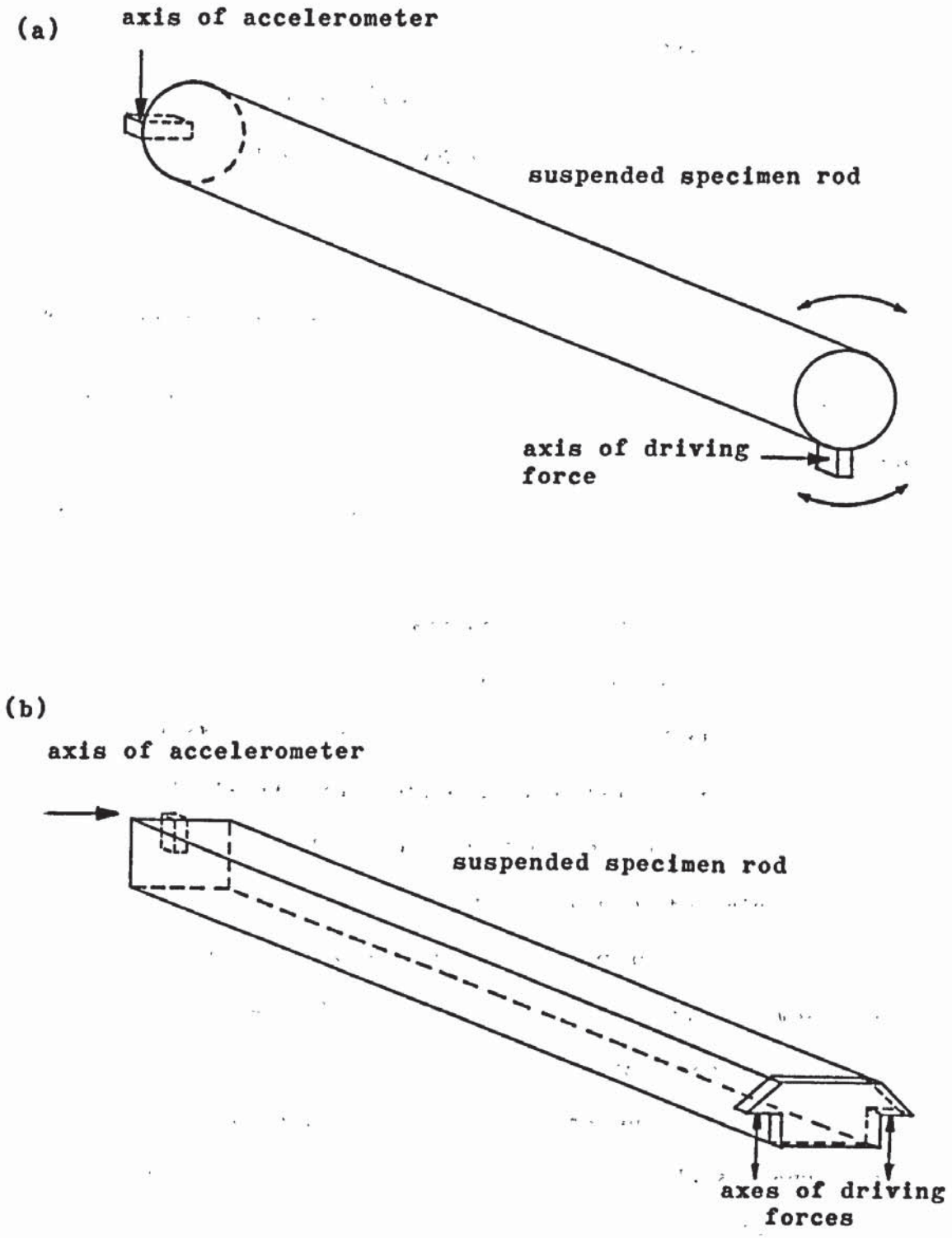

The generation of torsional waves in rods of building material

(a) Circular cross-section.

(b) Rectangular cross-section.

Plate 5.2 illustrates a successful arrangement where torsional waves were excited in a short rod of brickwork, pivoted at the ends.

5.6 Measurement of material loss factor

A description of the methods of assessing the dissipative loss factor in materials has been given in section 3.3. The methods fall into two categories.

(1) Steady-state measurements involve the observation of each vibrational mode for a constant excitation level. At the resonant peak, values of loss factor are calculated from measurements of half-power bandwidth or, by use of the method of Kennedy and Pancu (1949). This involves splitting the accelerometer signal into components in phase with, and in quadrature with the driving signal. As described in section 3.3, when the driving frequency approaches a natural resonance of the specimen, the quadrature component of the accelerometer signal will increase until, at resonance, the signal is completely out of phase with that of the driving signal. The apparatus used in plotting the admittance circle at resonance is illustrated in Figure 5.3.

Figure 5.4 gives an experimental plot of the admittance circle for three resonances, in this case, of a steel

Fig. 5.3.

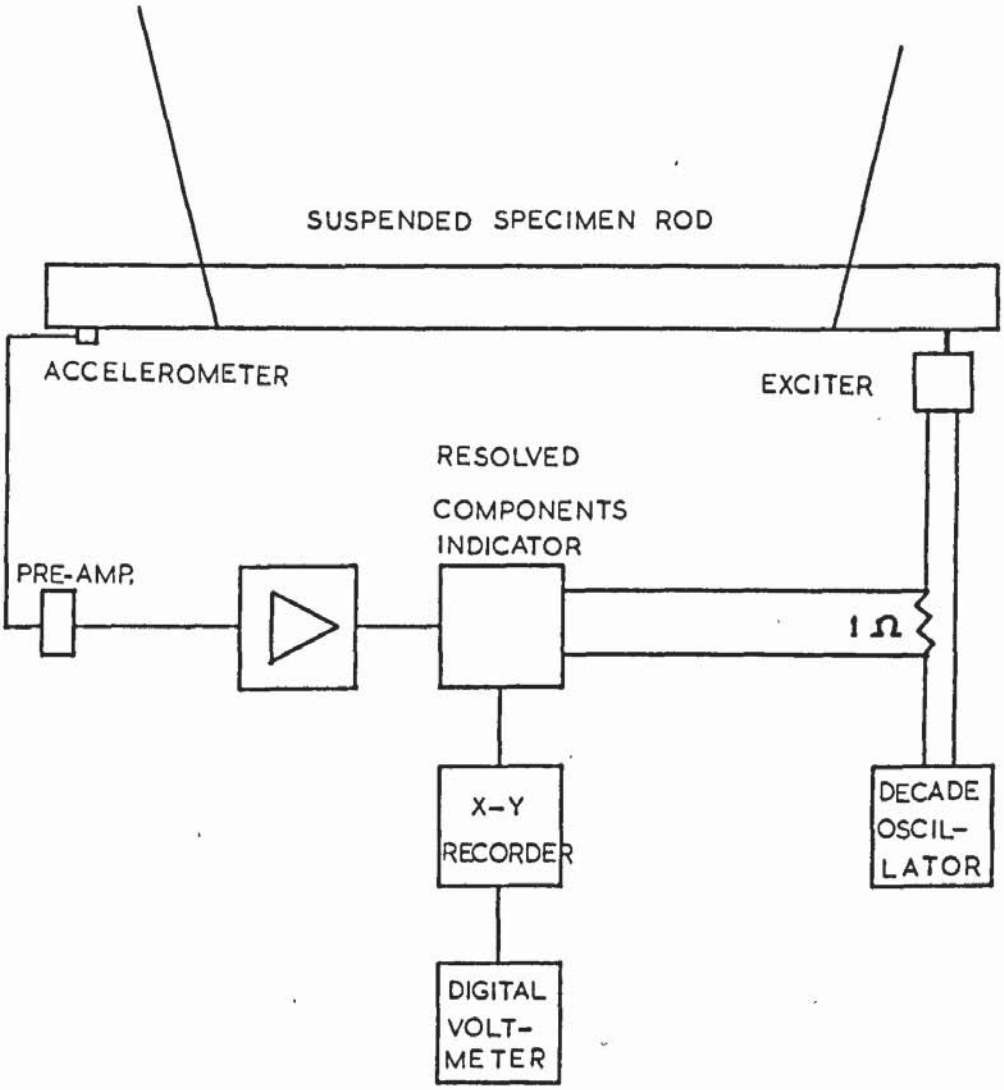

Measurement of loss-factor by the admittance circle method.

Fig. 5.4

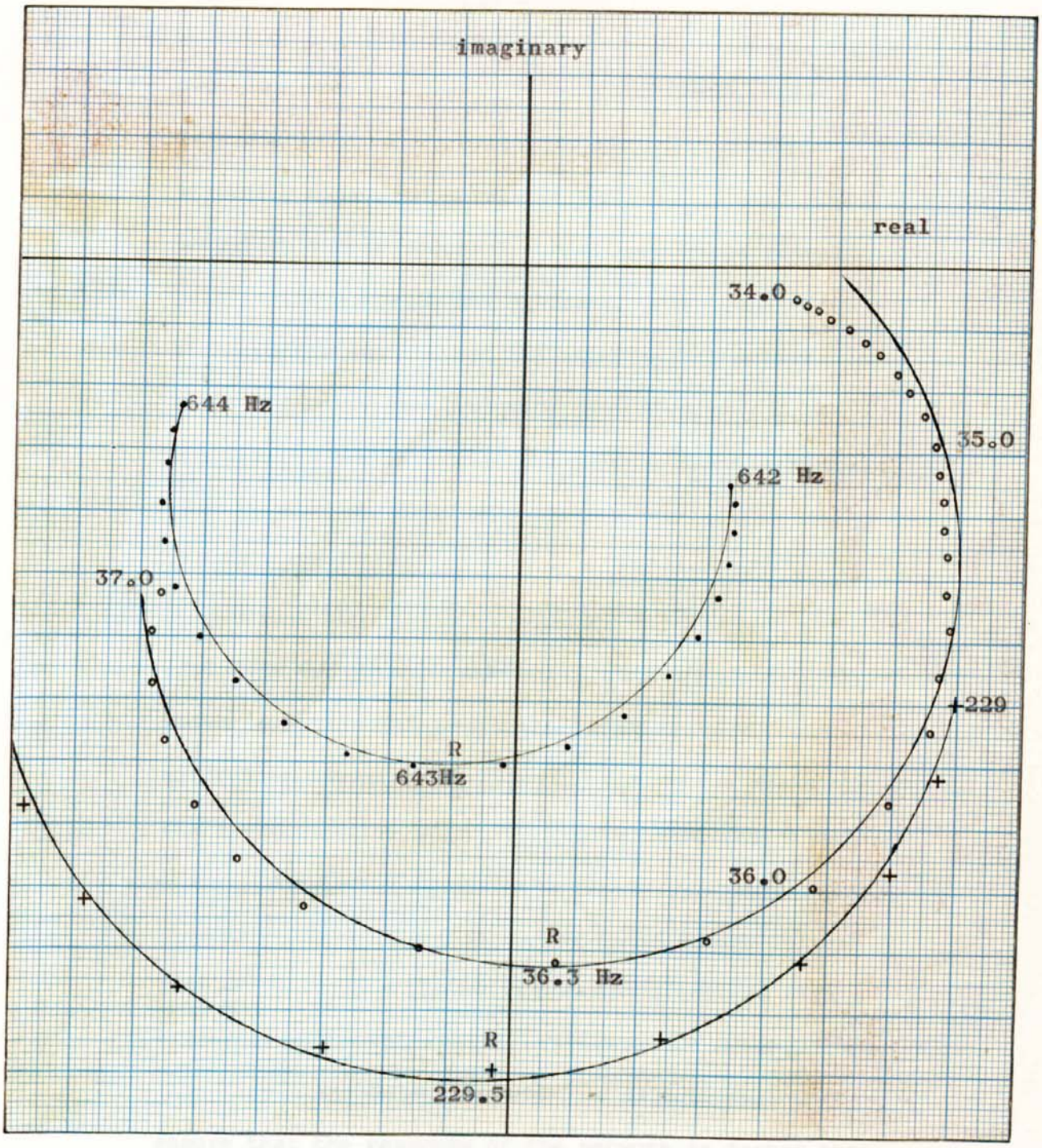

Admittance circle plot of three resonance frequencies for a steel rod of length 0.7 m.

rod. As shown in Figure 3.4(c), the ideal locus is a circle which is symmetric about the negative imaginary axis, and passes through the origin. This situation rarely occurs in practice and the resonance point could occur in any quadrant. Also, the best-fit circle drawn through the experimental points above and below the resonance (the frequency range was usually the half-power bandwidth) did not always pass through the origin.

(2) On removing the source of excitation, the vibration amplitude decays with respect to time, the rate of which is determined by the loss factor. The excitation signal can be a pure tone, as in the steady-state experiments, or can be narrow bandwidth random noise. The latter is produced either by fixed bandwidth warble tones or by one-third octave filters from white noise. The accelerometer signal is also filtered to remove noise and partials and if amplitude decay rates are being measured, it is important to ensure that the response of the network is faster than that of the signal decay. For the spectrometer used (B & K type 2112), full filter network response was stated to occur in three cycles of the centre frequency.

Thus, at 100 Hz, the response time is 10^{-2} seconds, and at 10 kHz, the time is 10^{-4} seconds. These response times are far shorter than the signal decay times

measured (or reverberation times) and it can be assumed that one-third octave filtering of the signal does not mask the transient response.

The decay rates (given in dB/sec) or the reverberation times of materials were measured using three methods (Fig 5.5).

(a) The amplified accelerometer signal could be charted by a high speed level recorder. In measurements, it was ensured that the chart pen speed was at least twice the decay rate being observed. At high frequencies, reverberation times become extremely short and the chart pen speed limits the range of application. The greatest value of loss factor that can be measured by this method was found to be 2×10^{-1} at 100 Hz and 2×10^{-3} at 10 kHz.

(b) To extend the range of application of the level recorder, a scaling technique can be used in which the filtered and amplified accelerometer signal is recorded on magnetic tape and then replayed at a slower speed into the level recorder. The F.M. tape recorder used was a B & K type 7001 which has four tape speeds, ranging from 38.1 mm/sec to 1524 mm/sec. Time-scaling ratios of 2.5, 4, 10, and 40 were possible. As an example, the charting of a reverberation time of 0.2 seconds at 10 kHz is beyond the writing speed of the level recorder alone. By recording the signal magnetically at a tape speed of 1524 mm/sec and then playing back

Fig. 5.5

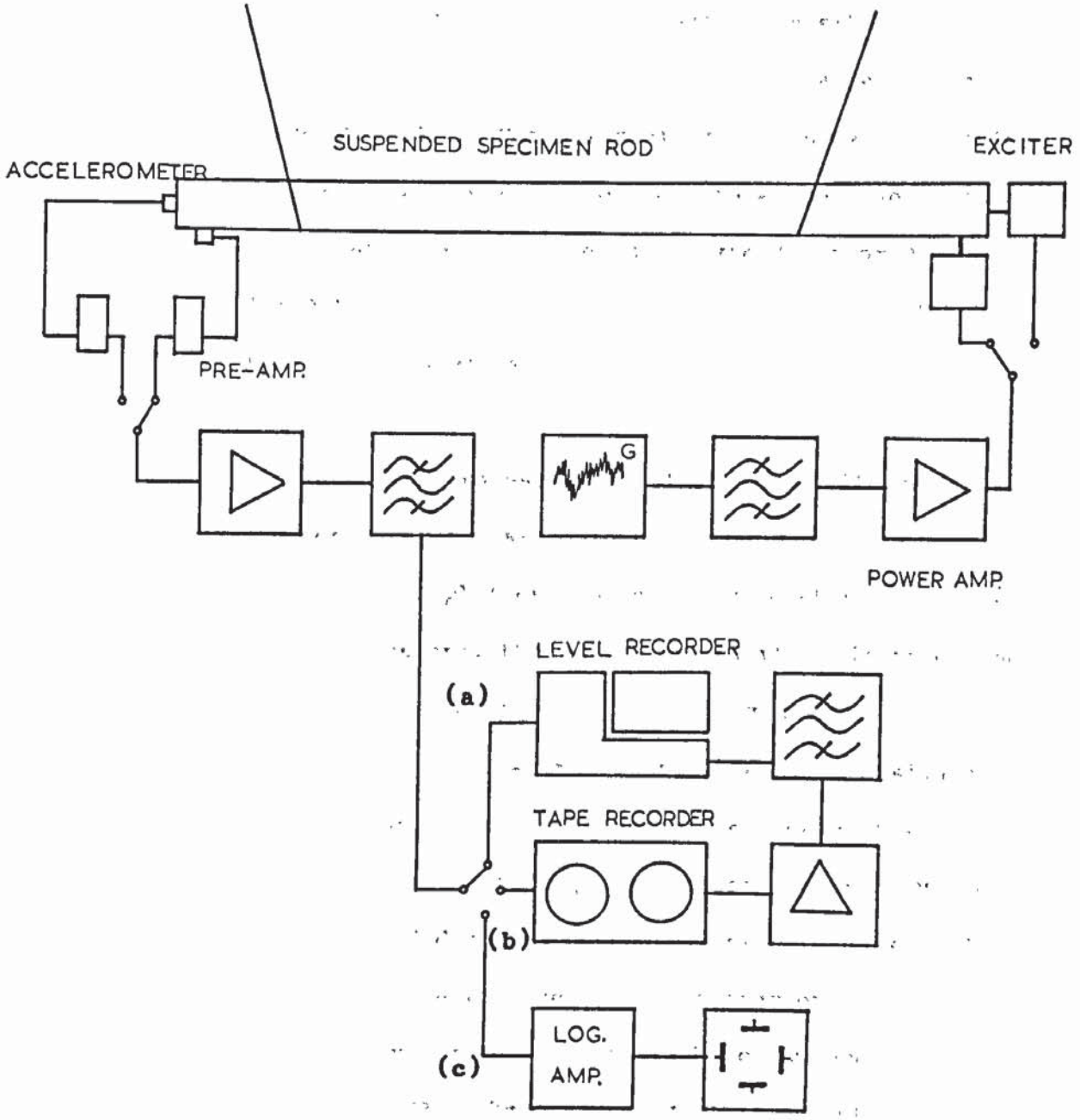

Measurement of loss factor by decay methods.

(a) Level recorder.

(b) Magnetic tape recorder.

(c) Logarithmic amplifier and oscilloscope.

at a speed of 152.4 mm/sec, a decaying signal results, having a frequency of 1 kHz, with a reverberation time of 2 seconds, a value well within the range of the level recorder. Not all scaling ratios were possible as the frequency ranges of each tape speed set limits to the application. The range extended from 0 - 500 Hz for a tape speed of 38.1 mm/sec to 0 - 20 kHz for a speed of 1524 mm/sec.

(c) For fast decay rates, the amplified and filtered accelerometer signal could be passed through a logarithmic amplifier and then displayed on a cathode ray oscilloscope, the time-base of which is triggered by the cut-off of the excitation signal. The logarithmic amplifier was constructed to a design of K F L Lansdowne of the Acoustics Section of the BBC Research Department. It consists of a pair of Mullard OA5 gold bonded diodes connected 'back to back'. The OA5 diodes have voltage/current characteristics which closely approximate to a logarithmic law over an input range of 40 dB. The output signal is unrectified since the time constant of the rectifier required for the lowest frequencies would be comparable with the decay time. This method has the advantage that many decays can be observed within a short time, thereby allowing an average value of the slope of the decaying signal envelope to be obtained quickly and conveniently.

Let the sweep rate be x sec/mm and the vertical amplitude y volts/mm. The y amplifier gives an output proportional to the logarithm of the input voltage. Let the constant of proportionality be K. (In the amplifier constructed, it has a value of 0.32). If the angle of the envelope of the decaying trace from the x axis is θ, the logarithmic decrement which has been defined in section 3.3.1 is calculated as,

$$\delta = \frac{y}{x} \frac{\tan \theta}{K} \frac{1}{v}$$

A circular cursor graduated in tangents of the slope is superimposed on the oscilloscope trace. Thus, by keeping y and x constant, the logarithmic decrement can readily be obtained. The loss factor is then simply calculated from,

$$\eta = \frac{\delta}{\pi}$$

5.7 Reinforced concrete

Concrete rods with various reinforcements were investigated along with their quarter-scale models. The full scale model was of length 5 metres and diameter 0.1 metres. The concrete consisted of one part ordinary portland cement, two parts zone two concreting sand, and four parts 5 mm to 10 mm irregular aggregate. The water content was 0.5.

Three methods of unstressed reinforcement were investigated.

(1) A single ½" diameter steel reinforcing rod running centrally through the concrete.

(2) Four rods of ¼" diameter, symmetrically positioned at an approximate distance of 30 mm from the centre.

(3) A complex reinforcement incorporating two ⅛" diameter steel rods. Each rod was bent into a "square wave" shape, each "step" being of length 1 m and height 70 mm. The planes of the two rod shapes were at right angles to each other. The rods were freely suspended by thin nylon cord (plate5.3) which, it is felt, introduced little additional loss to the system.

Longitudinal excitation

Figure 5.1(a) shows the form of excitation necessary to produce quasi-longitudinal modes. The resonant frequencies ν_n of a mode n is dictated by the rod length L and the wave velocity C_{l2}. The subscript of C_{l2} denotes that the specimen is small in two dimensions thus allowing Poisson expansion and contraction.

The velocity is given as,

$$C_{l2} = \frac{2L}{n} \nu n \qquad \ldots\ldots 5.1$$

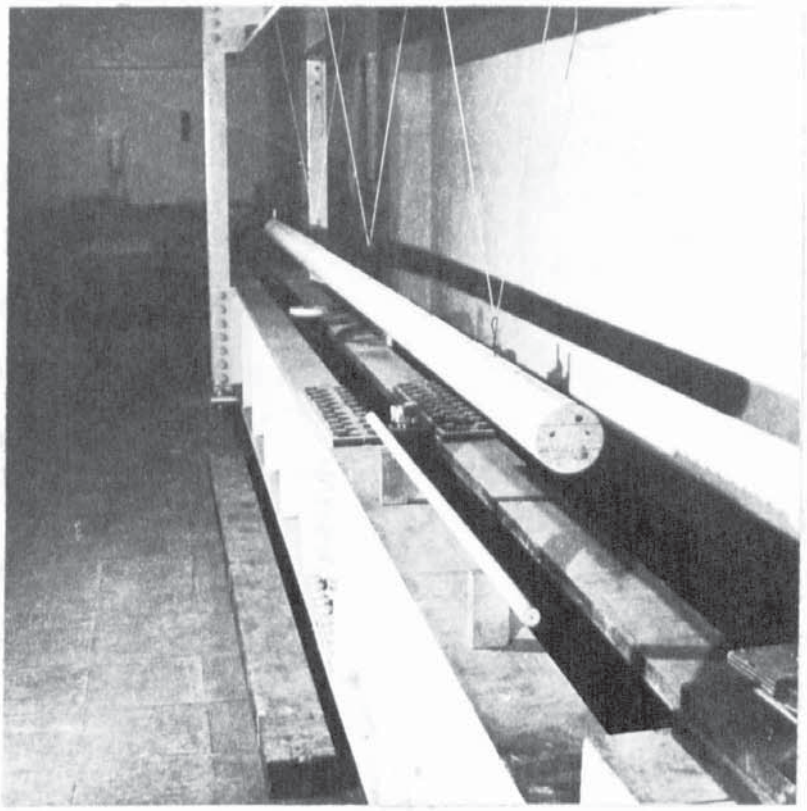

PLATE 5.3 Full scale and quarter scale reinforced concrete rods.

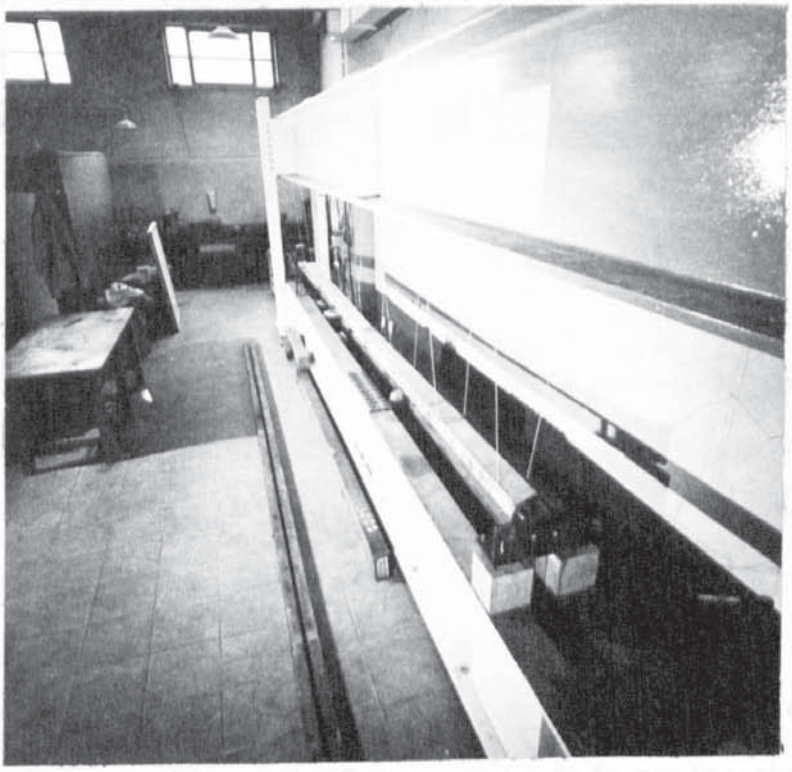

PLATE 5.4 Suspended brickwork rod.

where ν_n is the frequency of the nth mode. The transverse wave velocity is equal to the torsional wave velocity when the specimen cross-section is circular. In the case of a specimen of rectangular cross-section the torsional wave velocity is slower than the transverse wave velocity. For a rod made up of a single array of bricks Cremer (1949) gives the ratio of torsional velocity to transverse velocity as 0.878. The torsional velocity is calculated from an equation similar to that of 5.1 where the mode frequency refers to that of torsional vibration.

The process is the same when calculating bending wavelength with the exception that "end" corrections need to be considered. Figure 5.6 gives the distance of nodes from a free end for each mode of a free-free bar. Experimental values for a steel rod of length 1.915 m are in good agreement with the theory of Rayleigh (1877). It is then a simple matter to calculate the wavelength of the standing bending wave at each bar resonance.

Figure 5.7 illustrates the excitation of the three wave types in a reinforced concrete bar of length 5 m. Fast wave velocities give rise to fundamental modes at higher frequencies than those of slower velocities and, as expected, longitudinal waves are shown to have the greatest velocity, bending waves the smallest, with transverse waves having an intermediate value.

Figure 5.8 gives the longitudinal and transverse wave velocities calculated from equation 5.1, for concrete rods having three types of reinforcement. The mean value is given for each rod and it is

Fig. 5.6

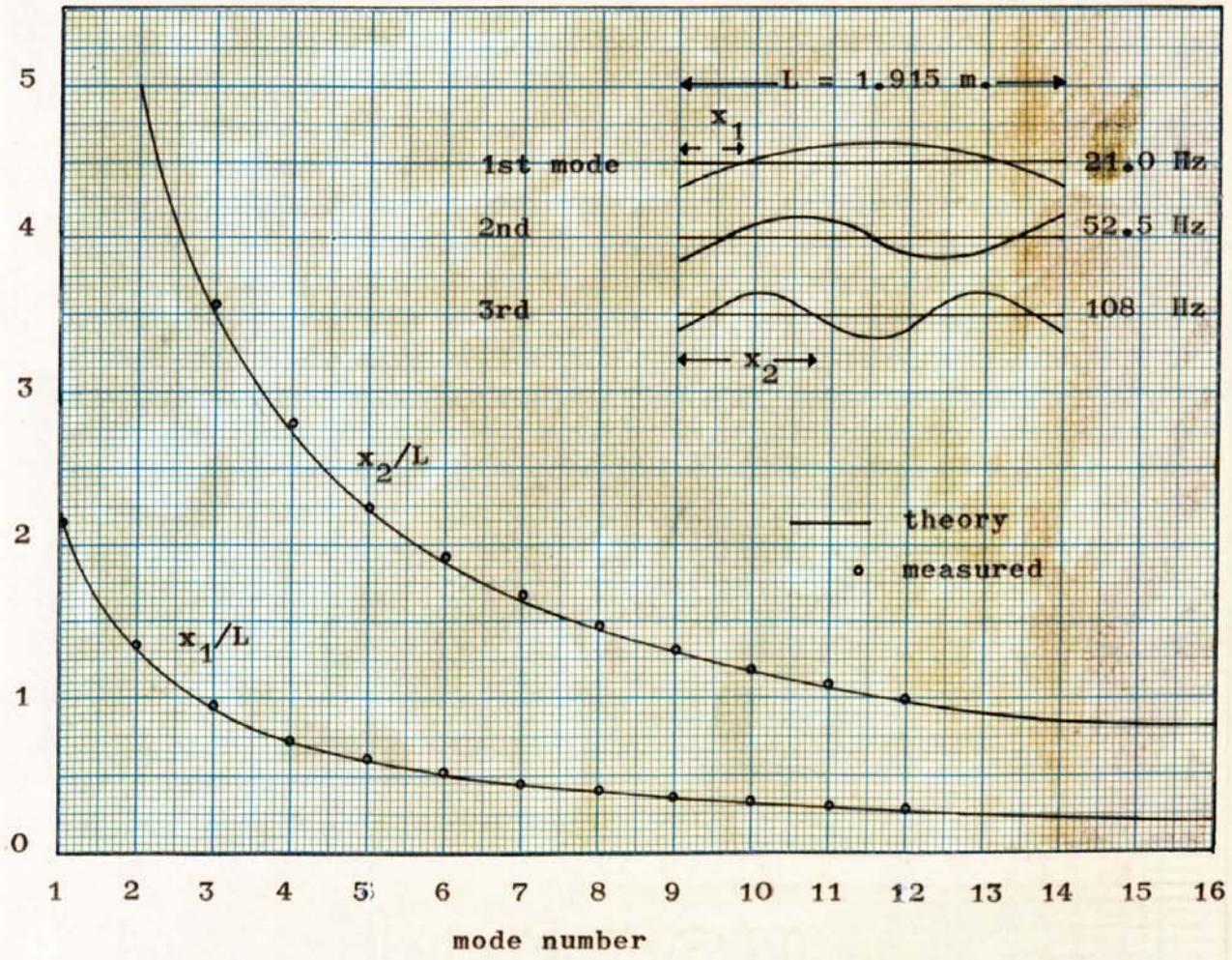

Node positions of a thin rod of steel, freely suspended.

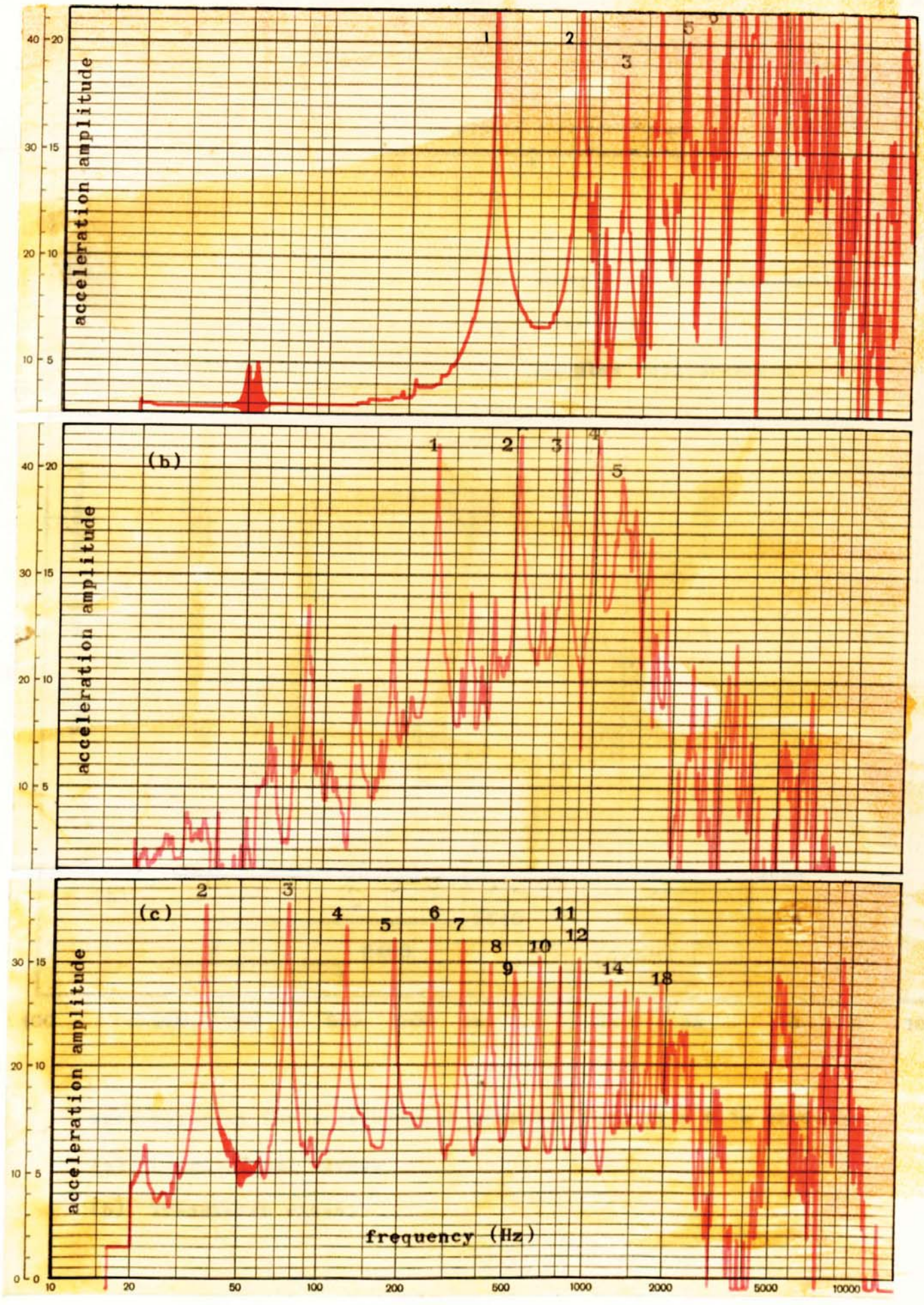

Modes of (single rod) reinforced concrete. 5m. x 0.1m. diameter.

(a) Longitudinal (b) Transverse (c) Bending.

Fig. 5.7

Fig. 5.8

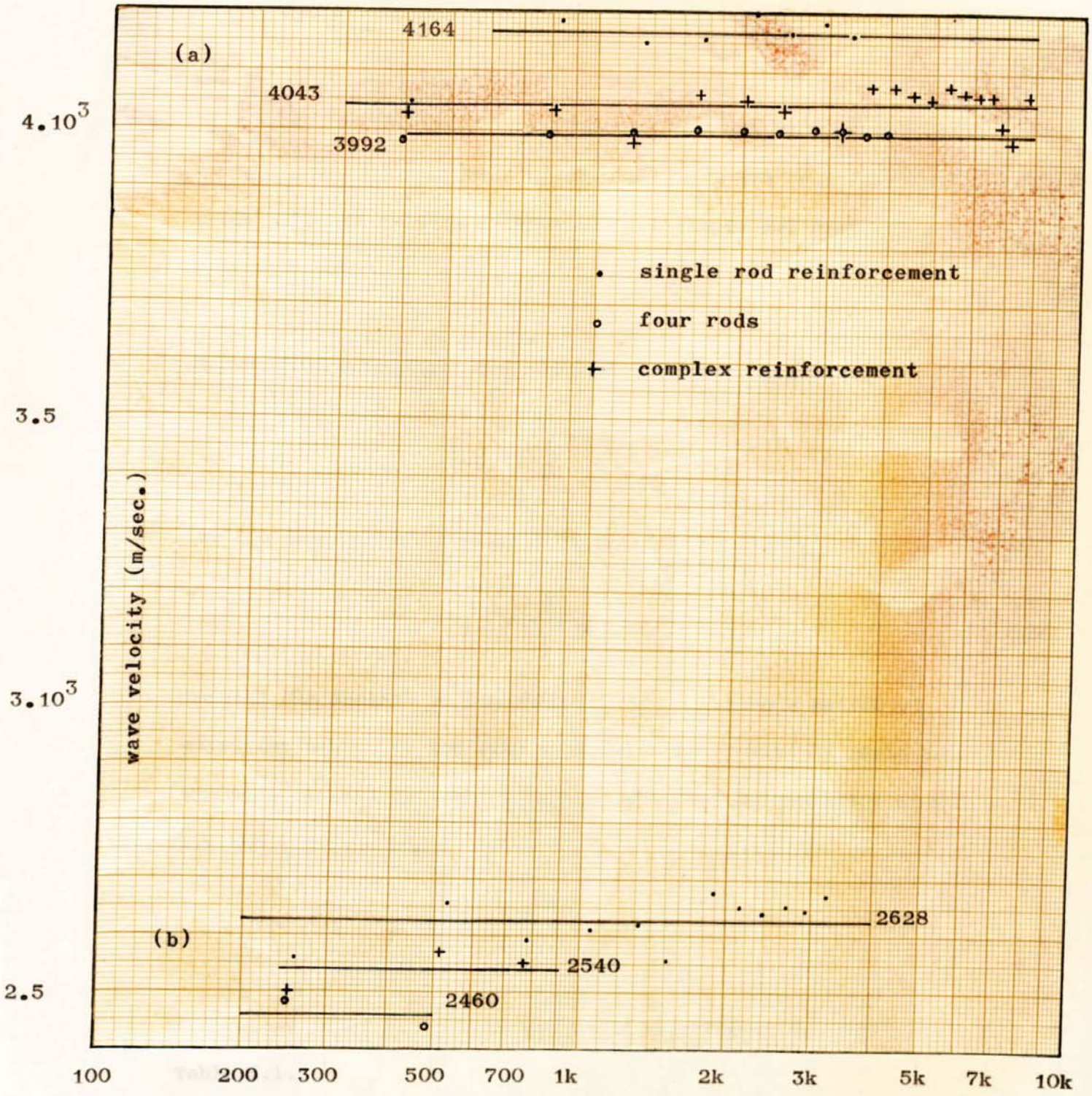

Wave velocity for a reinforced concrete rod. 5m x 0.1m diameter

(a) Longitudinal waves.

(b) Transverse waves.

seen that the rod having the complex reinforcement (which, it is thought, gives the closest approximation to the real situation) gives velocities lying between that of single and four rod reinforcement.

The quasi-longitudinal wave velocity is given by,

$$C_{l2} = \sqrt{\frac{E}{\rho}} \qquad \ldots\ldots\ldots 5.2$$

and the transverse wave velocity by,

$$C_t = \sqrt{\frac{E}{2\rho(1+\mu)}} \qquad \ldots\ldots\ldots 5.3$$

Knowing the density of the concrete it is a simple matter of obtaining values of the dynamic modulus and Poisson's ratio from the wave velocities. The latter is obtained on combining equations 5.2 and 5.3 such that

$$\mu = \frac{1}{2}\left(\frac{C_{l2}}{C_t}\right)^2 - 1 \qquad \ldots\ldots\ldots 5.4$$

The values obtained in this and other experiments are summarised in Table 5.1.

Figure 5.9 gives a plot of measured bending wavelength over a frequency range of 100 Hz to 3.15 kHz. Assuming a value of Young's modulus of 4×10^{10} N/m^2, and a density of 2.5×10^3 Kg/m^2 theoretical curves can be constructed. It is seen that there is agreement between measured values and that predicted using Cremer's modified bending wave theory. (See section 3.5.1.)

Table 5.1 Dynamic constants of common building materials.

Material	Specimen dimensions	c_{l2} m/sec.	c_t m/sec.	$E \times 10^9$ N/m^2	$\rho \times 10^3$ kg/m^3	μ	Loss factor $\times 10^{-2}$		
							η_l	η_t	η_b
Reinforced concrete									
Single rod	5m x 0.1m diam. with $\frac{1}{2}$" rod	4165 ± 15	2628 ± 45	43.0 ± 1.0	2.5 ± 0.05	0.25 ± 0.01	0.88	0.93	1.2
	1.25m x 0.025m diam. with $\frac{1}{8}$" rod	3840 ± 20		35.6 ± 1.2	2.4 ± 0.1				1.2
Four rods	5m x 0.1m diam. with $\frac{1}{4}$" rods	3992 ± 15	2460 ± 15	40.0 ± 1.0	2.5 ± 0.05	0.32 ± 0.01	0.94		0.96
	1.25m x 0.025m diam. with $\frac{1}{16}$" rods	3835 ± 20		36.0 ± 1.8	2.45 ± 0.1				1.21
Complex reinforcement	5m x 0.1m diam.	4043 ± 30	2540 ± 35	41.0 ± 1.4	2.5 ± 0.05	0.26 ± 0.01	1.0	1.14	
Brickwork									
8 brick array	1.84m x 0.105m x 0.08m	2290 ± 80	1377 ± 50	9.7 ± 0.8	1.85 ± 0.03	0.38 ± 0.06	1.0	1.05	1.3
22 brick array	5m x 0.105m x 0.08m	2270 ± 70	1340 ± 40	9.5 ± 0.7	1.85 ± 0.03	0.43 ± 0.05	0.87	1.14	0.8
Model(1:1.5:2.5 w/c=1.1 brick aggragate $\frac{3}{8}$" - $\frac{3}{16}$")	0.64m x 0.025m x 0.02m	2300 ± 25		7.9 ± 0.4	1.7 ± 0.1				
Breeze block									
5 units	2.28m x 0.215m x 0.1m	1933 ± 25	1250 ± 40	4.5 ± 0.3	1.2 ± 0.02	0.2 ± 0.04	0.81	0.77	0.72
Model	0.57m x 0.054m x 0.025	1790 ± 20		4.3 ± 0.3	1.3 ± 0.05		1.3		0.82

Fig. 5.9

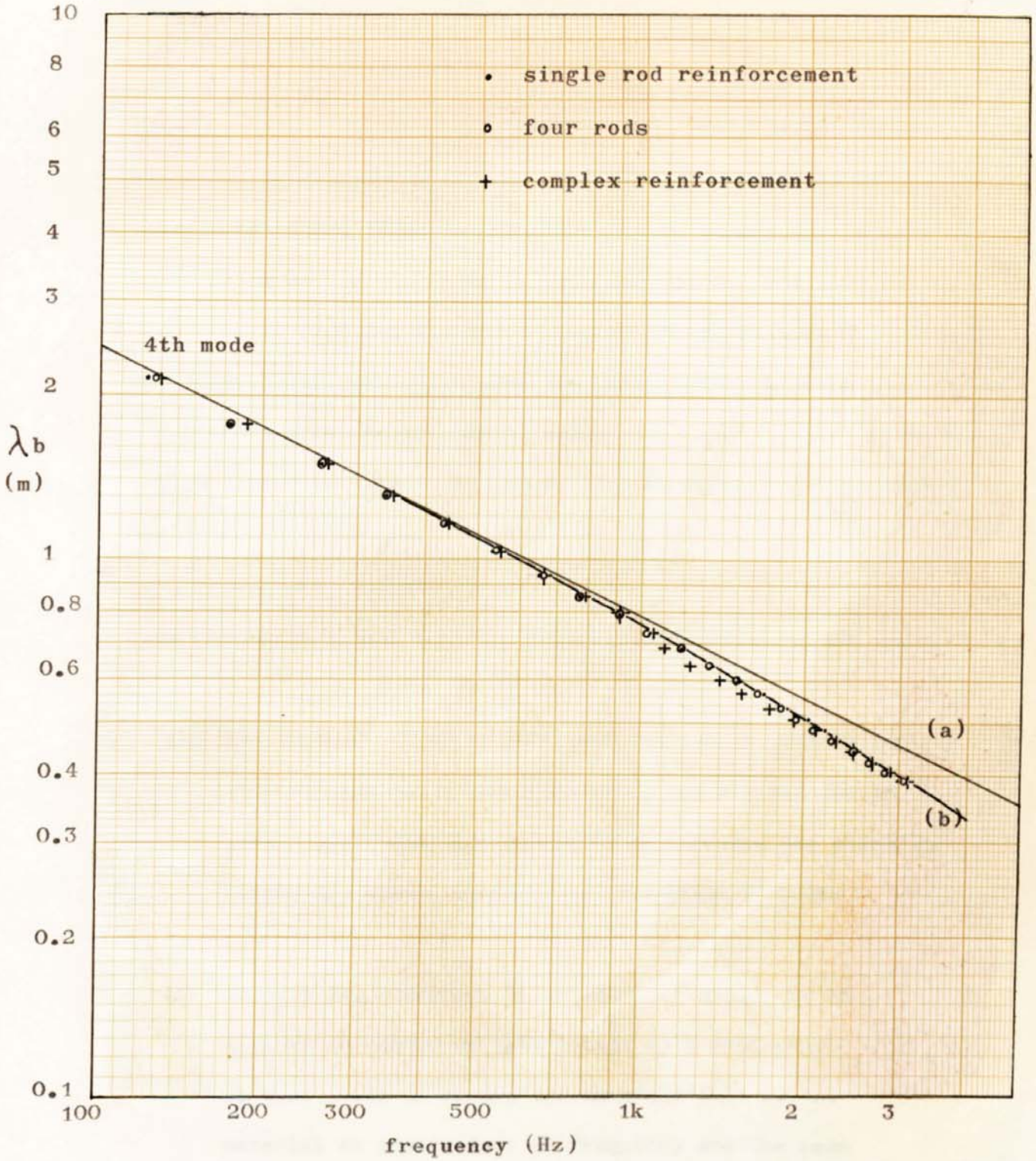

Bending wavelength for reinforced concrete 5m x 0.1m diameter.

(a) Simple bending wave theory.

(b) Cremer's modification.

Figures 5.10 and 5.11 show the measured loss factor of concrete rods for three types of vibration. The method of measurement used most in obtaining these results was that of assessing the rate of decay using any of the three methods described. The process usually consisted of exciting the rod at one of its resonances by a signal of random noise centred at that frequency within a narrow bandwidth. The pre-amplified accelerometer signal is passed through a one-third octave filter to a level recorder, tape recorder, or logarithmic amplifier.

From Figures 5.10 and 5.11 the following observations are made.

(1) The bending, longitudinal, and transverse loss factor have approximately the same value for all reinforced rods. The value for unreinforced concrete are slightly lower than those centred around a value of 0.01.

(2) Despite fluctuations, there does not appear to be systematic change of loss factor with frequency. It is thus valid to regard the internal loss of the material as independent of frequency and the mean value of each set of measured values of loss factor is therefore used to describe the material (Table 5.1).

(3) The loss factors for all wave types are approximately equal.

Attempts were made to produce quarter-scale models of the reinforced

Fig. 5.10

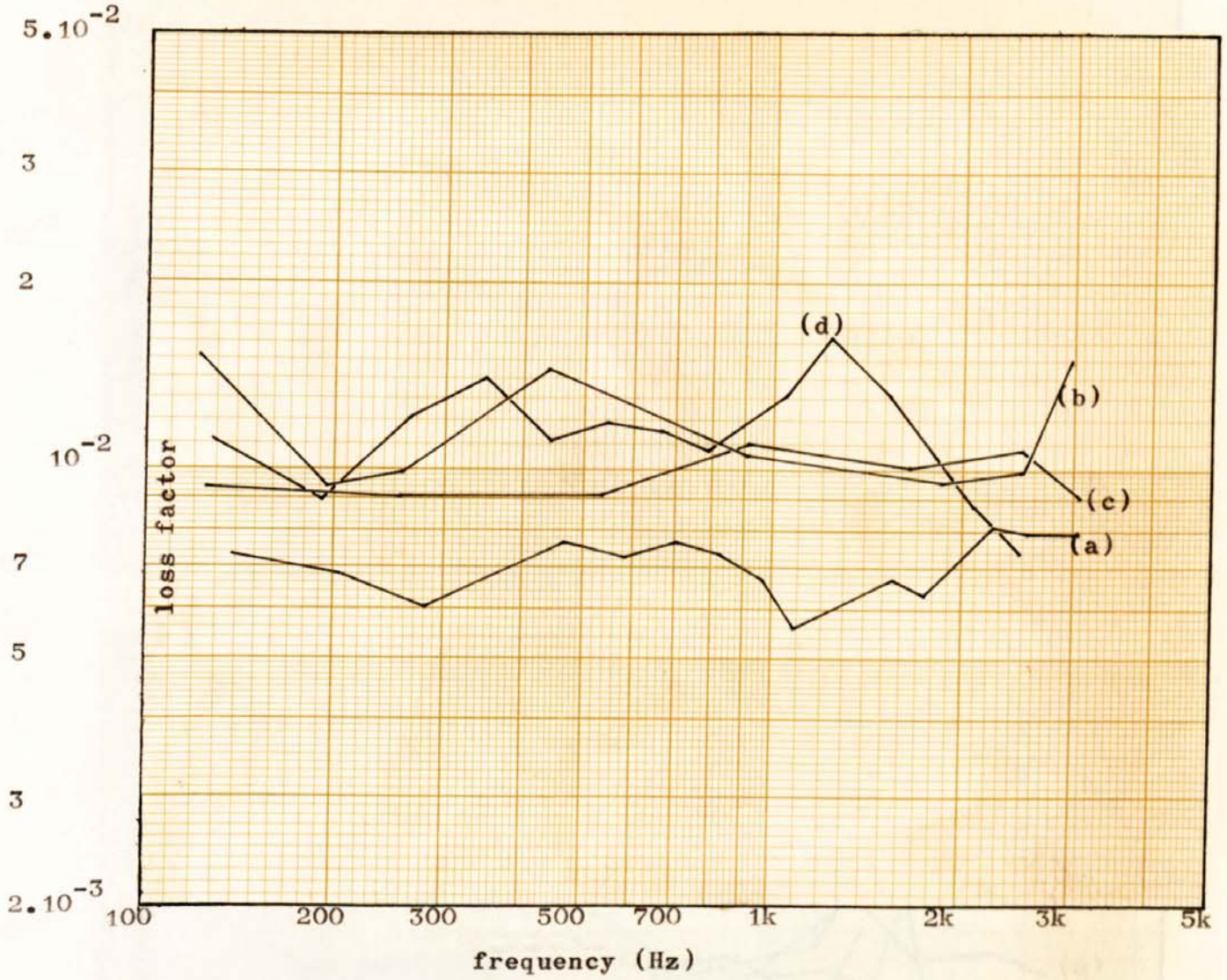

Bending wave loss factor for concrete rods of length 5 metres.

(a) Concrete having no reinforcement.

(b) Single rod reinforcement.

(c) Four rods.

(d) Complex reinforcement.

Fig. 5.11

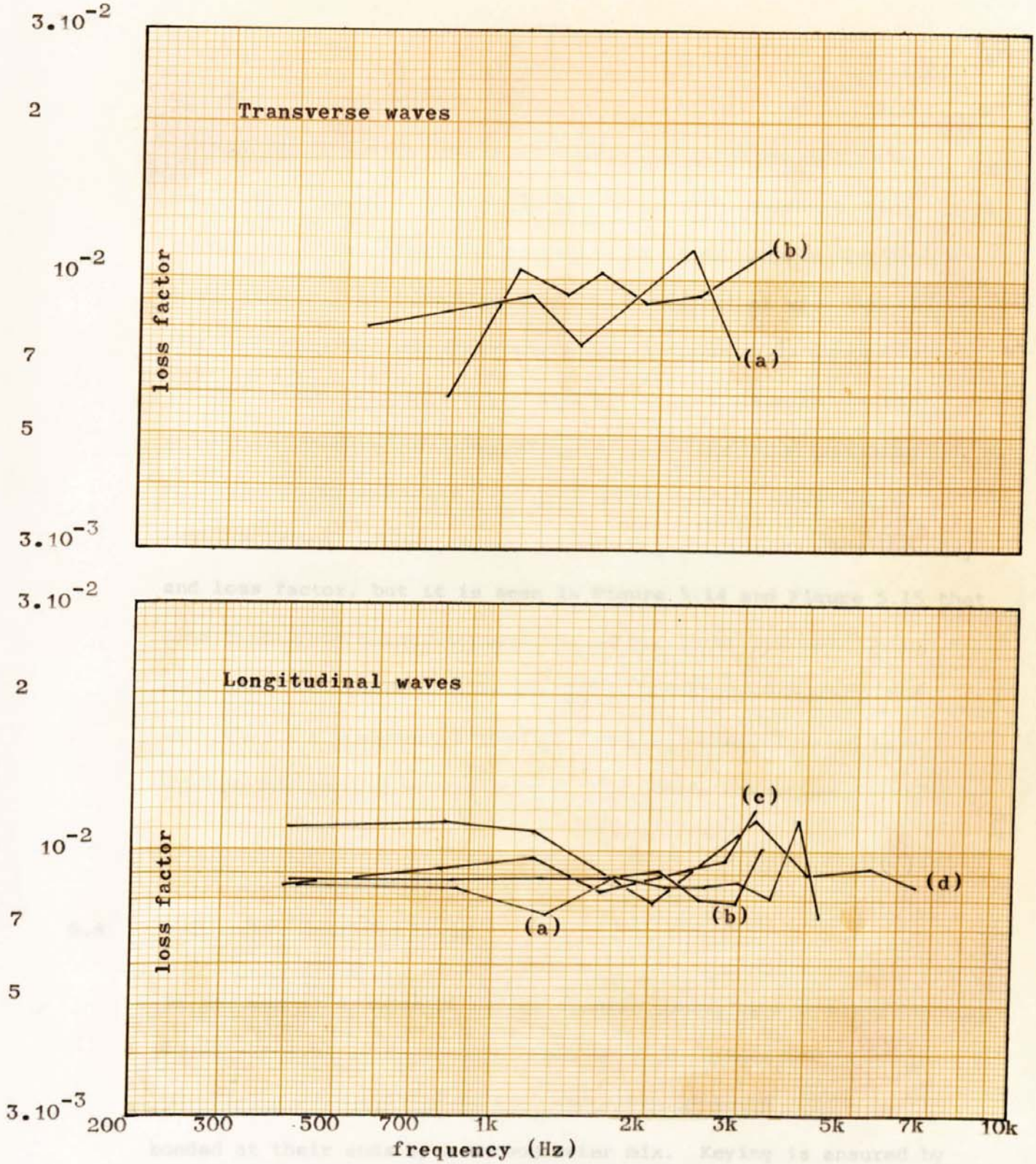

Loss factor for concrete in the form of rods of length 5 metres.

(a) Concrete having no reinforcement.

(b) Single rod reinforcement.

(c) Four rods.

(d) Complex reinforcement.

concrete rods (plate 5.3). The attempts were successful for (1) a single (⅛" diameter) rod reinforcement in a mortar of 1.5:2:3.5 ratio with w/c of 0.55 and (2) four rods ($\frac{1}{16}$" diameter) with the same mortar. In both cases the aggregate is finer than in the full scale mix. Figure 5.12 indicates that the longitudinal wave velocities of the two modes are approximately equal. Figure 5.13 shows that the quarter-scale wavelengths are shorter by approximately 6% than predicted wavelengths using values of building constants measured in the full scale specimens. In most quarter-scale experiments difficulty was encountered in calculating transverse wave velocity and loss factor, but it is seen in Figure 5.14 and Figure 5.15 that good similarity exists between the longitudinal and bending modes of full scale and quarter-scale models of reinforced concrete rods. Note that the frequency scales in the lower diagrams have been shifted two octaves to the left to facilitate comparison.

5.8 Brickwork and breeze block

The methods of assessment of the dynamic parameters of brickwork and breeze block were the same as those used on reinforced concrete. The brick rods consisted of a linear array of bricks (plate 5.4) bonded at their ends by a strong water mix. Keying is ensured by drilling small diameter holes to a depth of 10 mm into the ends of the bricks. The frogs of the bricks were filled by mortar such that one unit of the linear array was regarded as one brick with mortar on the top surface and on one end surface. Figure 5.16 illustrates the resonant modes of an array of twenty-two bricks and Figure 5.17 gives the calculated longitudinal and transverse wave velocities

Fig. 5.12

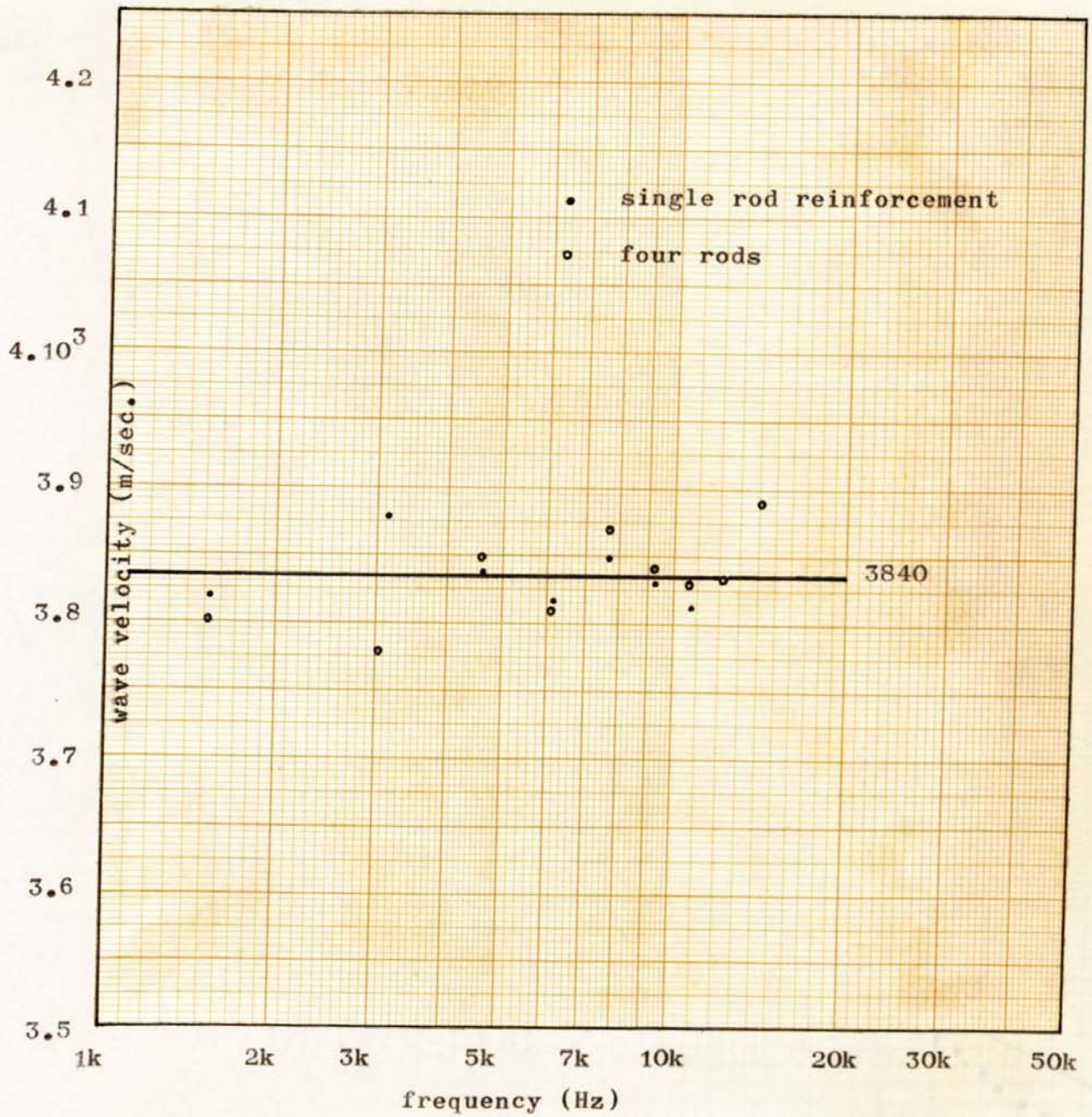

Longitudinal wave velocities for quarter scale reinforced concrete rods. 1.25m x 0.025m diameter.

Fig. 5.13

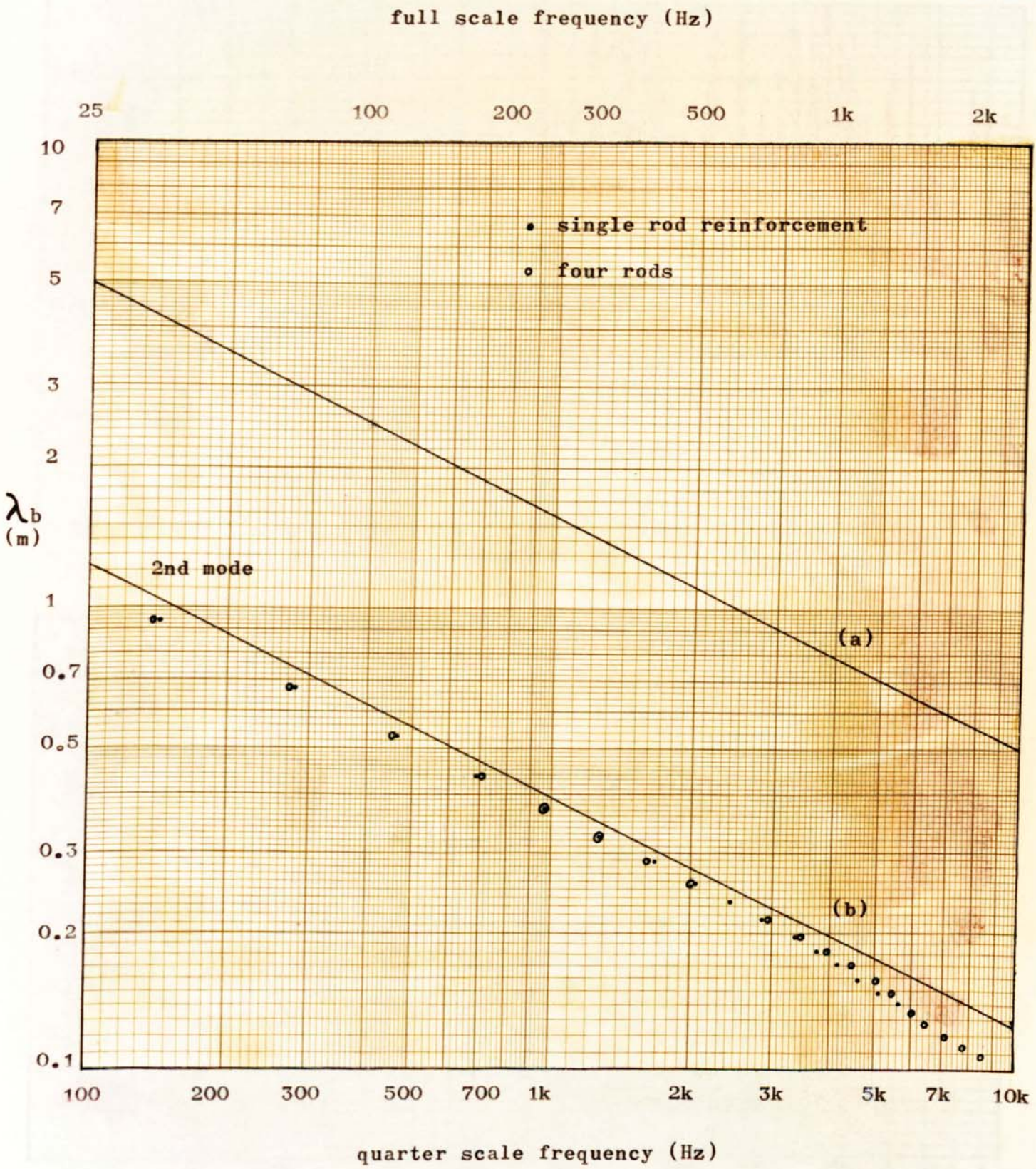

Bending wavelength for quarter scale reinforced concrete rods.

(a) Predicted wavelength for a rod 5m x 0.1m diameter.

(b) Predicted wavelength for a rod 1.25m x 0.025m diameter.

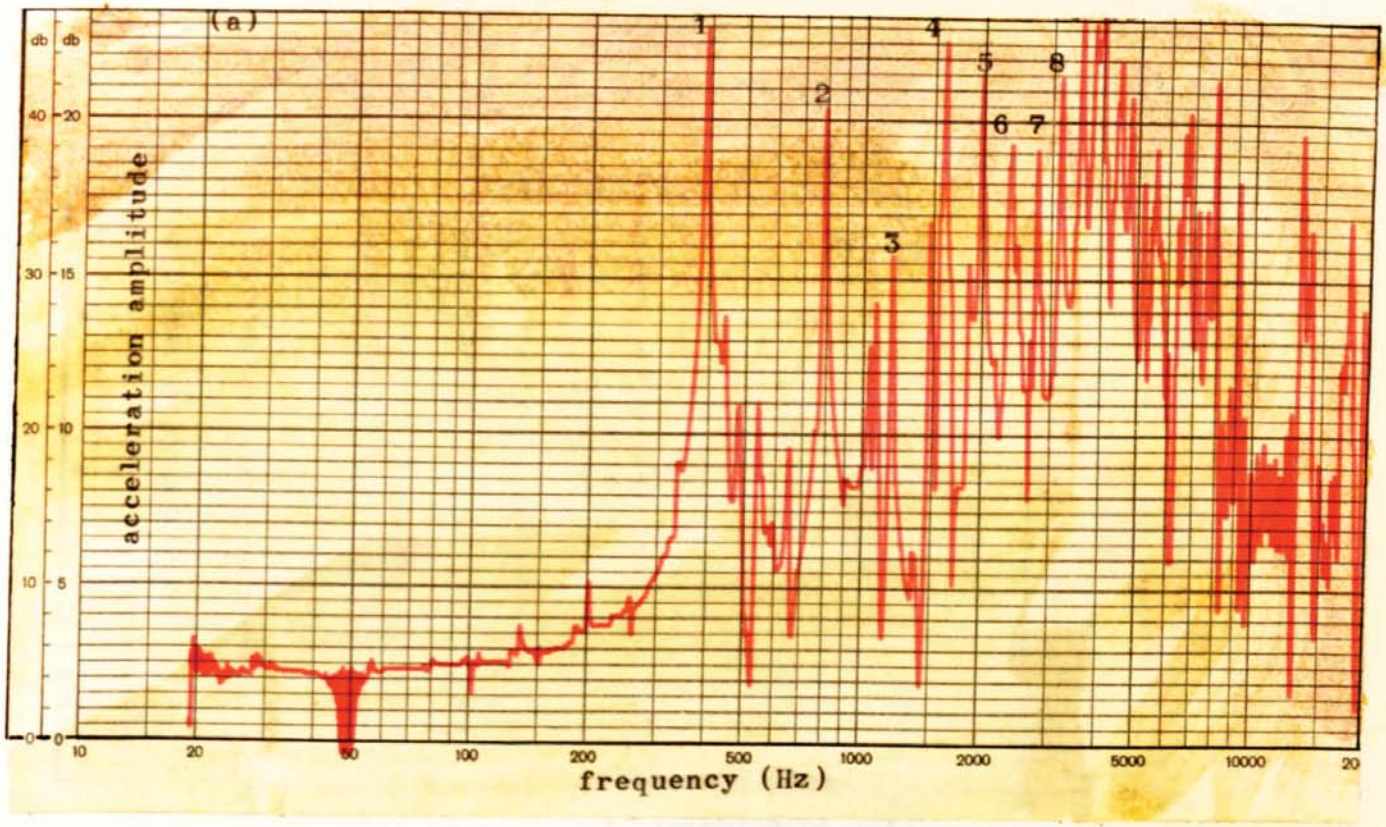

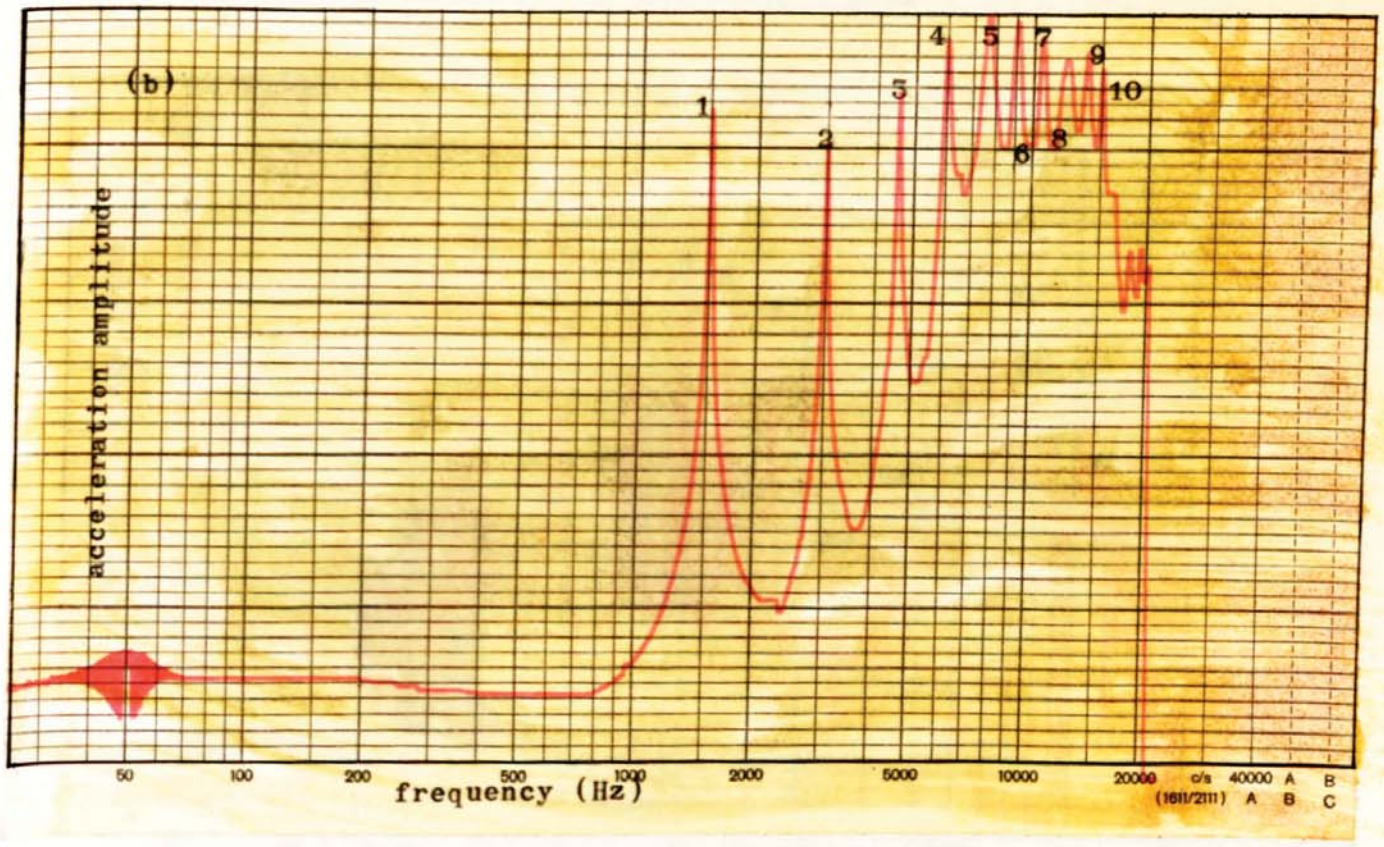

Longitudinal modes of (four bar) reinforced concrete.

(a) Full scale model. 5m. x 0.1m. diameter.

(b) Quarter scale model. 1.25m. x 0.025m. diameter.

Fig. 5.14

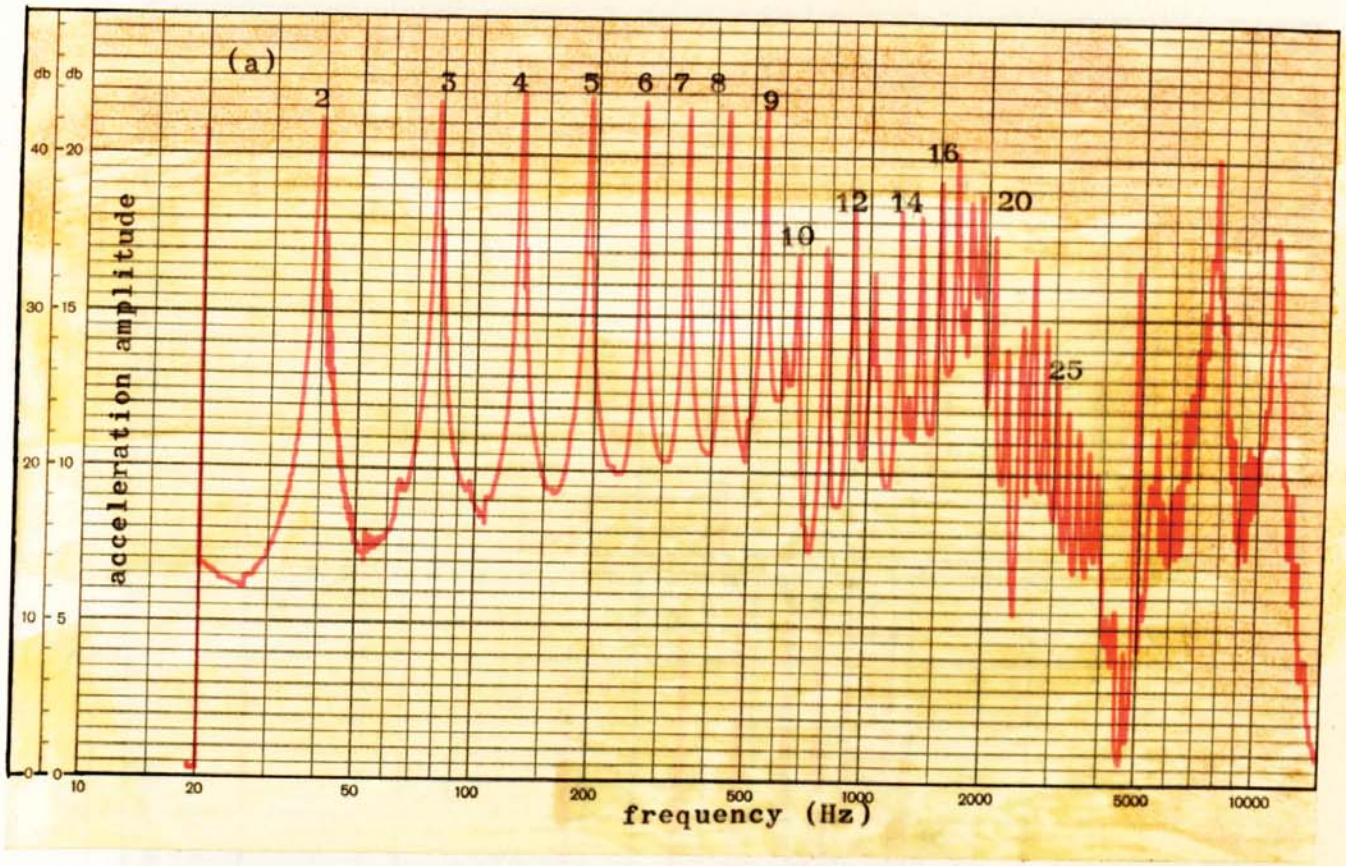

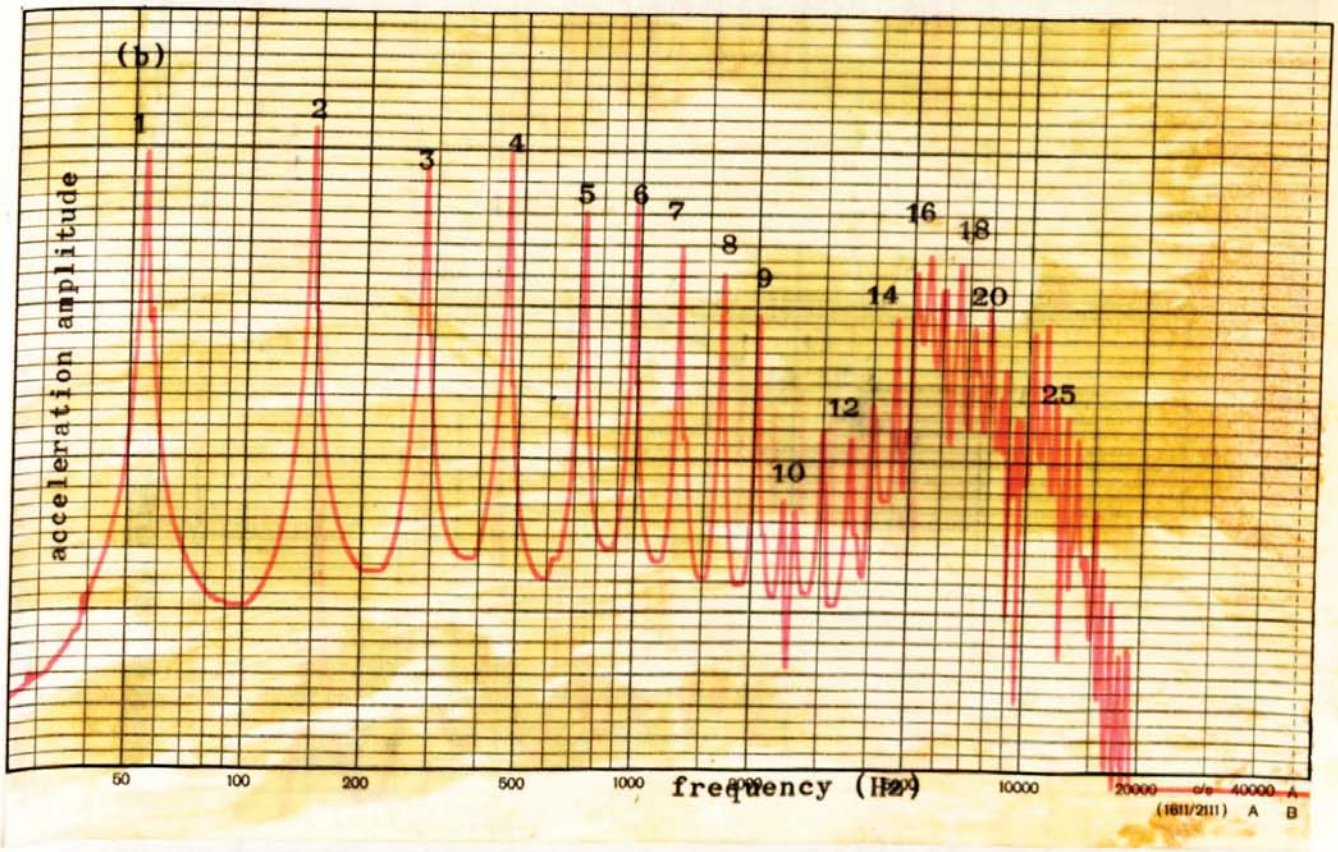

Bending modes of (four bar) reinforced concrete.

(a) Full scale model. 5m. x 0.1m. diameter.

(b) Quarter scale model. 1.25m. x 0.025m. diameter.

Fig. 5.15

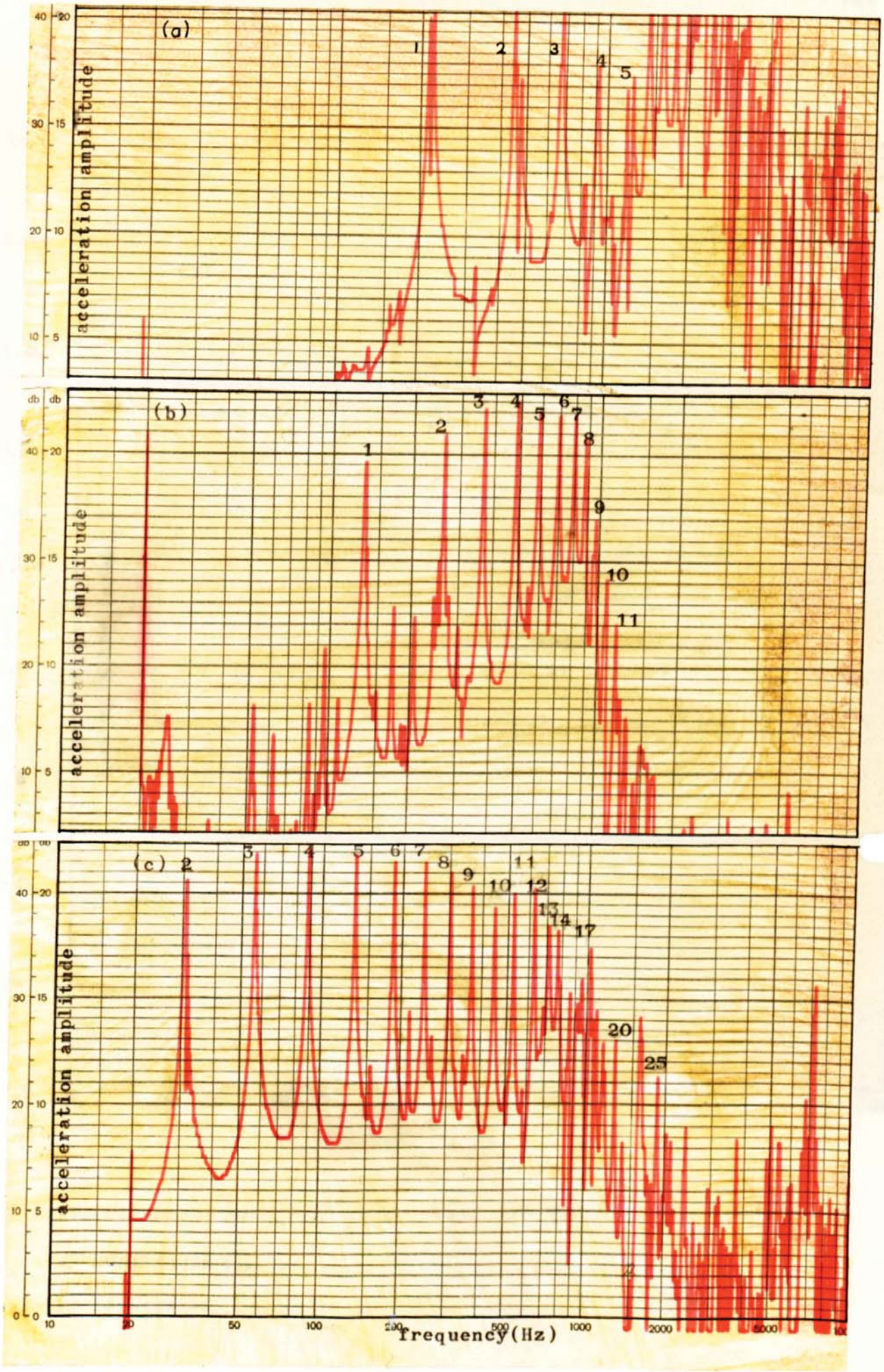

Modes of a (twenty two) brick 'rod' of length 5metres.

(a) Longitudinal (b) Torsional (c) Bending

Fig. 5.16

Fig. 5.17

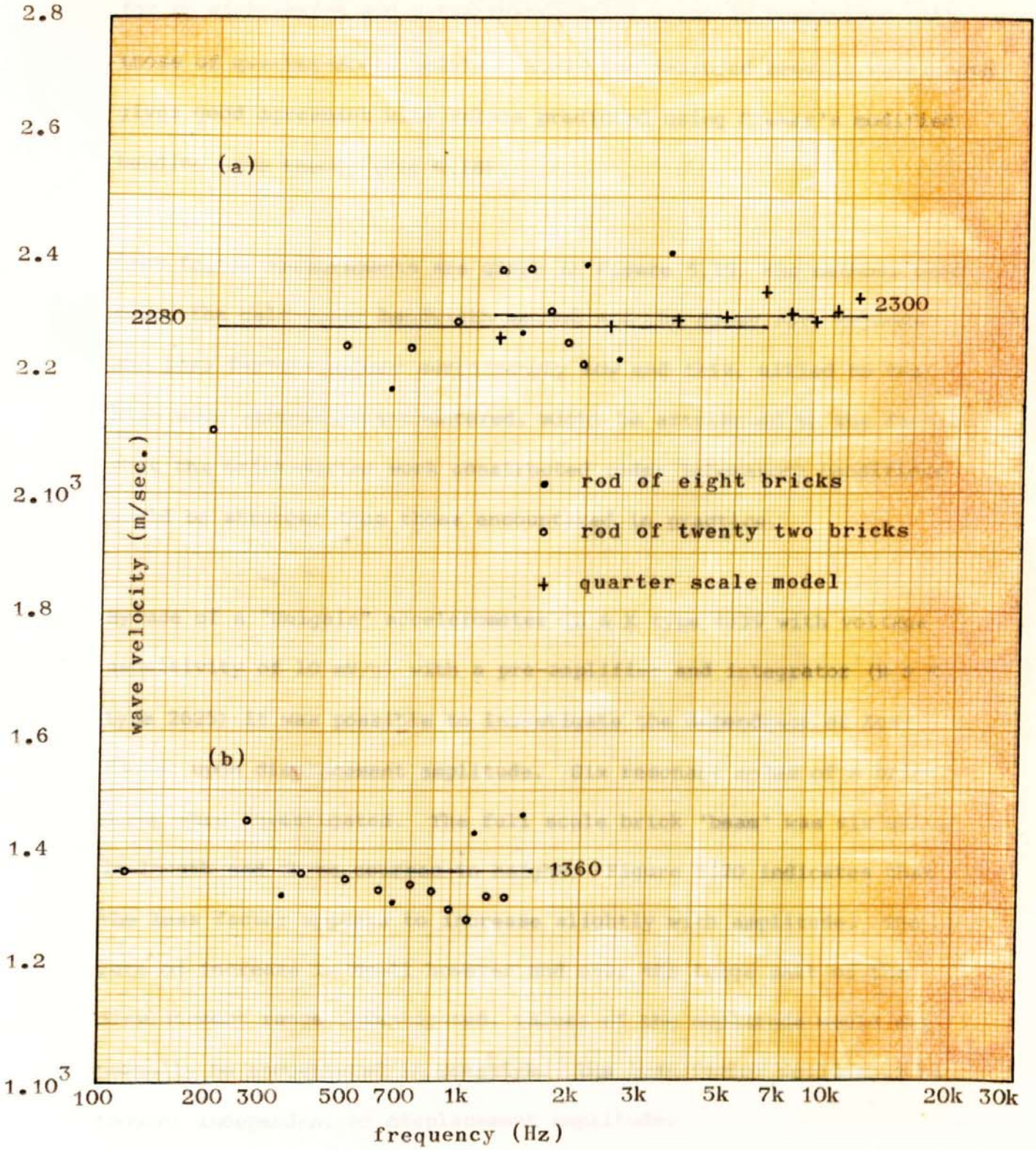

Wave velocity for brick 'rods'; full and quarter scale models.

(a) Longitudinal.

(b) Transverse.

for an eight-brick and a twenty-two-brick array in comparison with those of quarter-scale models. Again the measured bending wavelength gives good agreement with values predicted using Cremer's modified bending wave theory (Fig 5.18).

Loss factor measurements are given in Figure 5.19, the methods used being the half-power bandwidth method and the decay rate methods. The loss factors appear surprisingly low and this, allied to the high wave velocities encountered, might be attributed to the fact that the brick-mortar work constructed under laboratory conditions would be stronger than those encountered in practice.

By use of a "Unigain" accelerometer (B & K type 4339 with voltage sensitivity of 10 mV/g) with a pre-amplifier and integrator (B & K type 2625) it was possible to investigate the dependence of loss factor upon displacement amplitude. Six resonant modes of a brick array were investigated. The full scale brick 'beam' was six units in length and three courses in height. Figure 5.20 indicates that the loss factor appears to increase slightly with amplitude. The rate of increase is small however and over the large part of the displacement range investigated, values of the amplitude would not normally be encountered in practice. The loss factor would thus be thought independent of displacement amplitude.

The construction of quarter-scale modelling of brickwork proved difficult. The method finally adopted was to produce a matrix of brick rubble, sand, and mortar which would give the same density and complex modulus as full scale brickwork. Twelve mixes were

Fig. 5.18

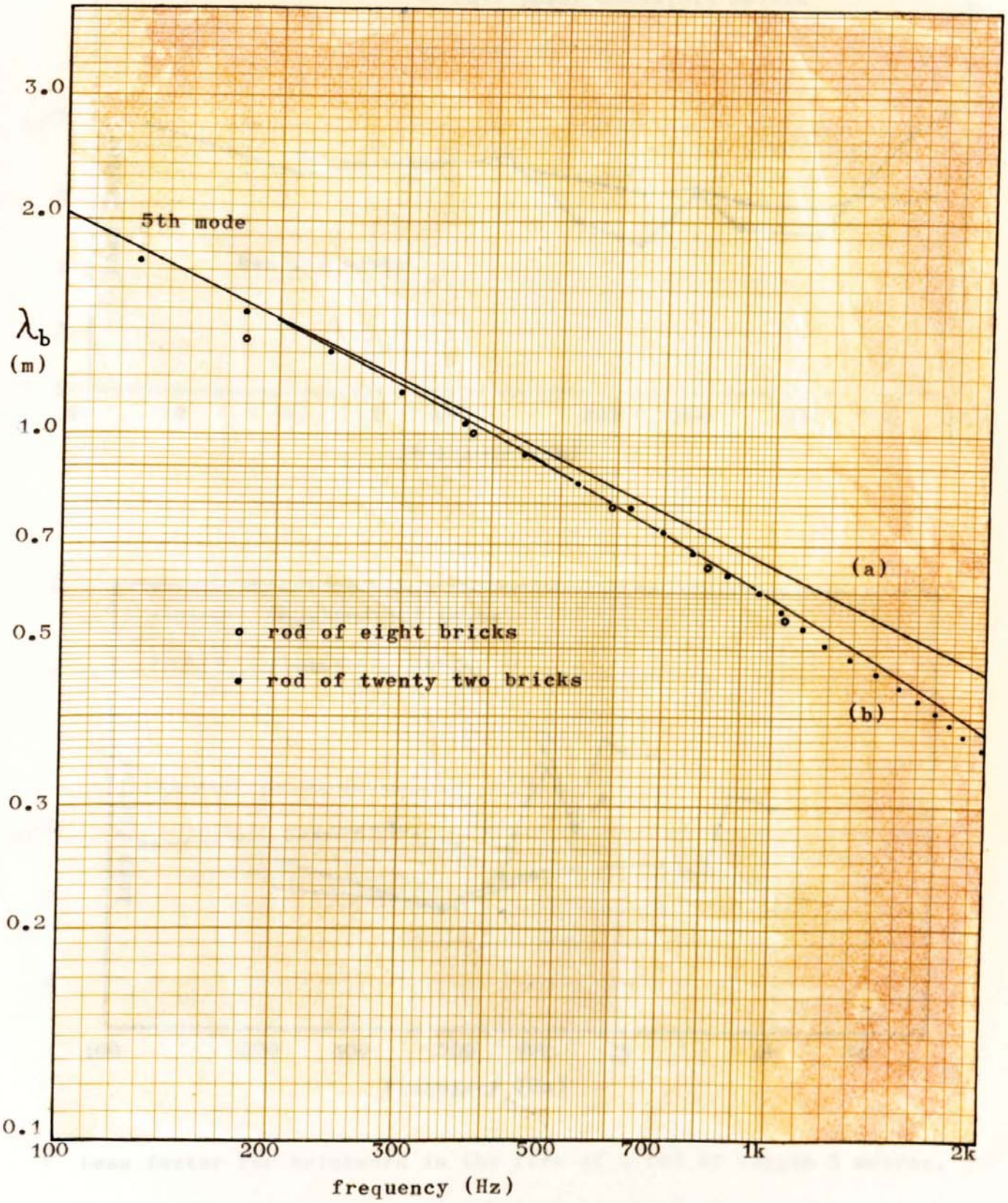

Bending wavelength for brick rods.

(a) Simple theory given by $\lambda_b = \sqrt{(1.8\ c_1\ h/\nu)}$

(b) Cremer's modification given by $\lambda_{mod} = \lambda_b(1 - 3.6(\frac{h}{\lambda_b})^2)$

Fig. 5.19

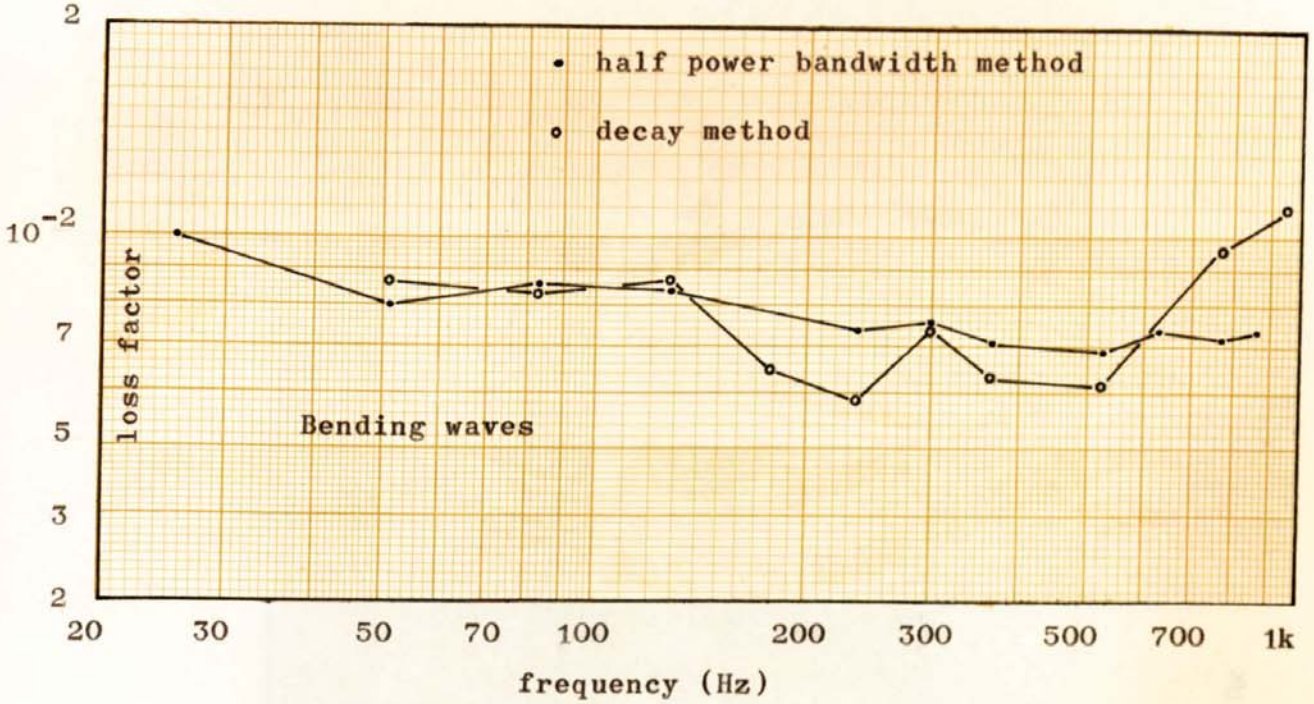

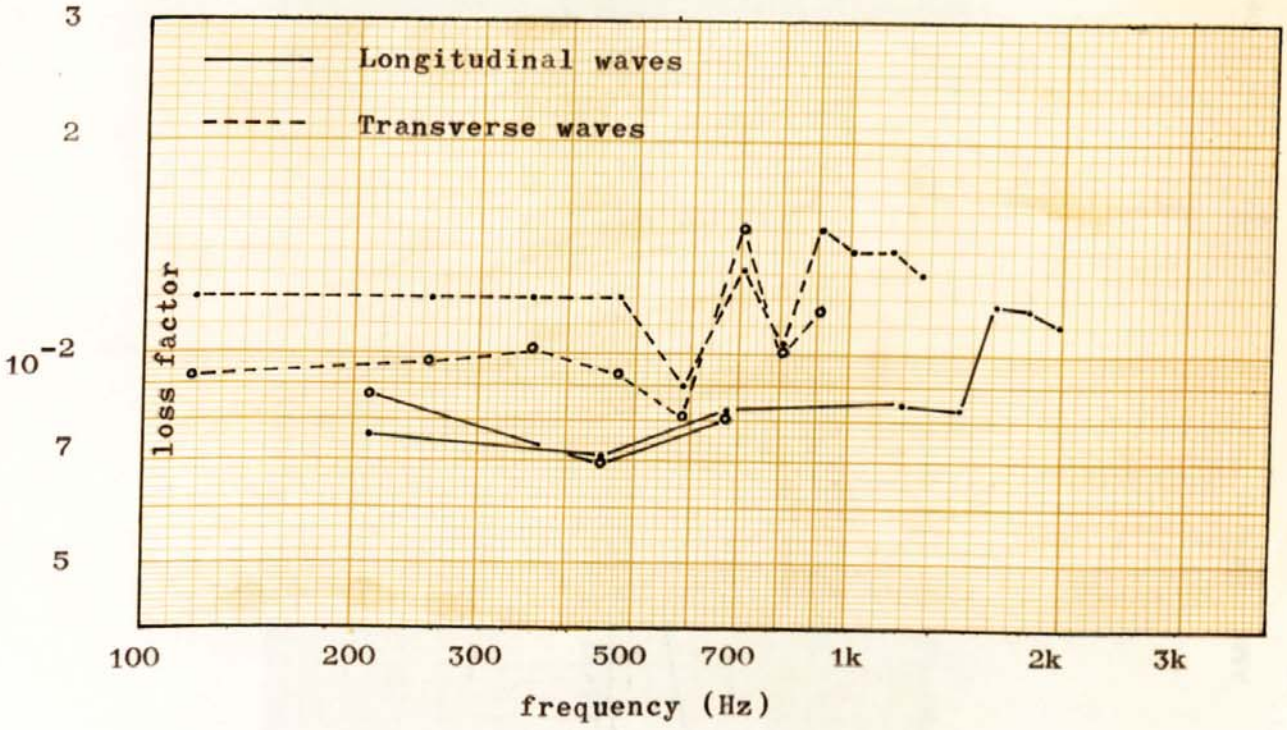

Loss factor for brickwork in the form of a rod of length 5 metres. Methods of measurement are (a) half power bandwidth, and (b) decay methods using chart recorder and tape recorder, and logarithmic amplifier and oscilloscope.

Fig. 5.20

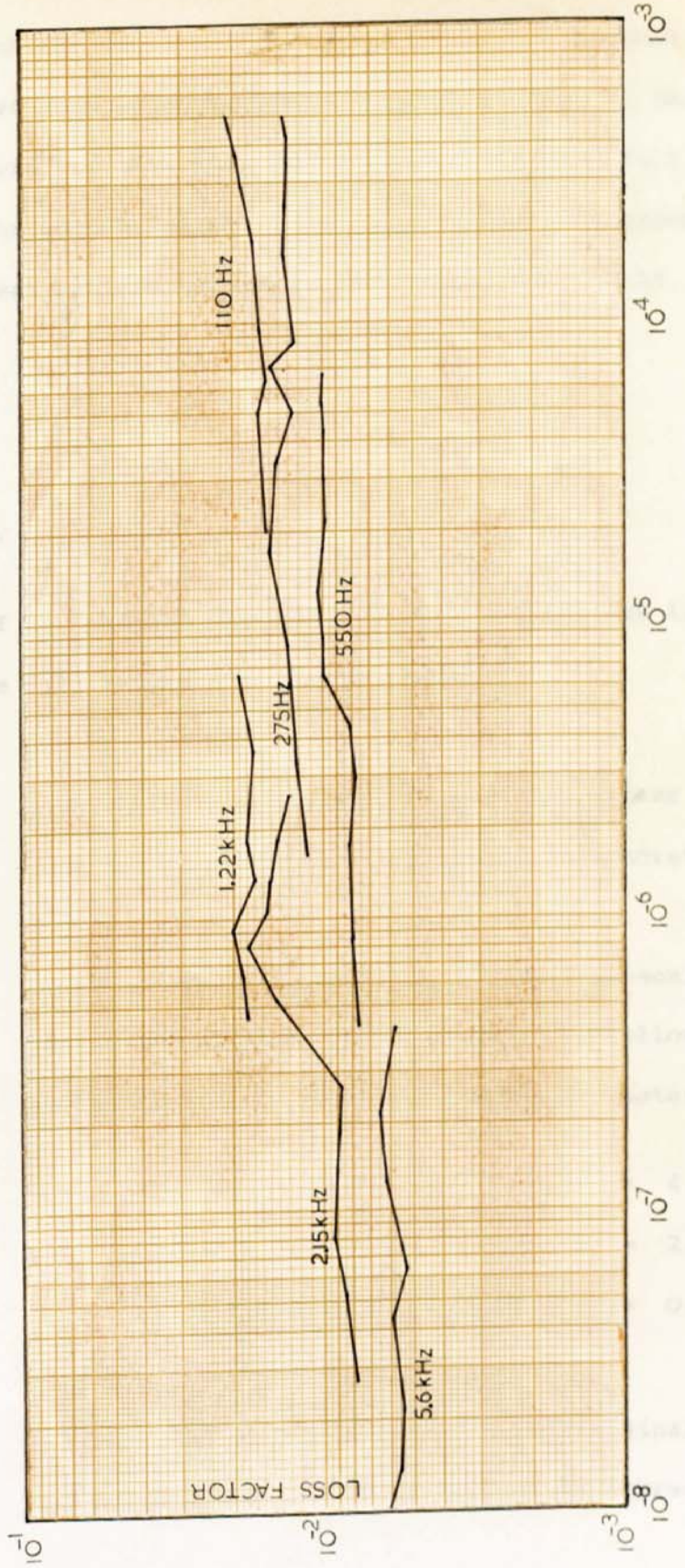

AMPLITUDE DEPENDENCE OF LOSS FACTOR OF BRICKWORK

produced, having varying proportions of these constituents. The final choice was a mix 1:1.5:2.5 with water content 1.1. The aggregate was brick rubble of dimensions 5 to 10 mm. Figure 5.17 and Table 5.1 show that the similarity between full scale and quarter-scale brickwork appears good. The results for breeze block are not discussed but are summarised in Figures 5.21, 5.22, 5.23 and Table 5.1.

5.9 Summary

Some of the results described in this section are listed in Table 5.1 and the following points may be noted.

(1) Wave velocity and loss factor do not appear dependent upon the unstressed reinforcement in concrete.

(2) Consideration of full scale and quarter-scale models of reinforced concrete indicate that the following dynamic parameters can be used to describe the material.

(a)	Young's modulus	$E = 4 \times 10^{10}$ N/m^2
(b)	Density	$\rho = 2.5 \times 10^{3}$ Kg/m^3
(c)	The dynamic poisson's ratio	$\mu = 0.3$

(3) The loss factors of concrete in longitudinal, transverse, and bending wave motion do not differ appreciably.

(4) The loss factor appears independent of frequency and in

Fig. 5.21

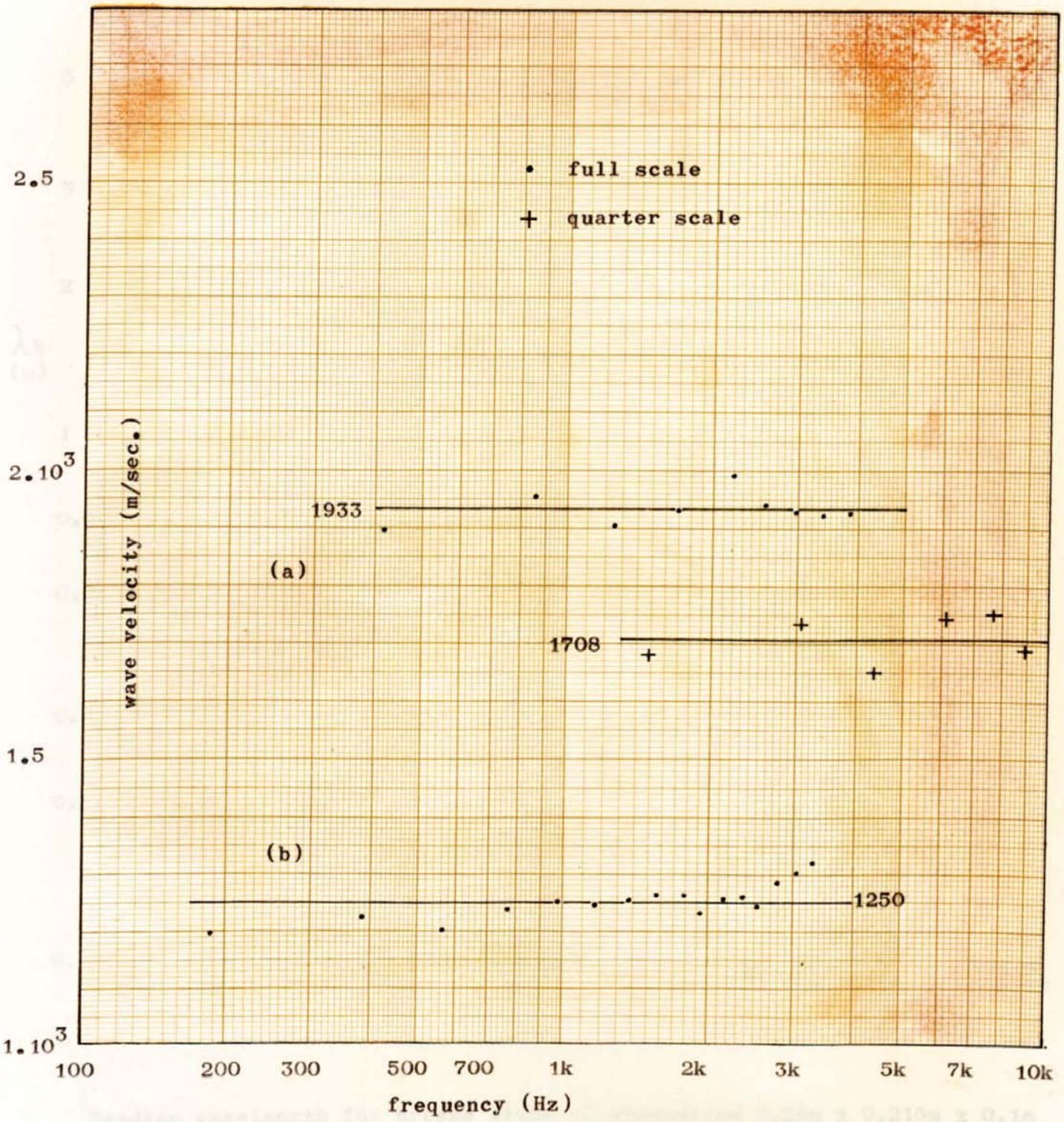

Wave velocity for breeze block of full scale dimensions 2.28 x 0.215 x 0.1 metres, consisting of five units.

(a) Longitudinal waves.

(b) Transverse waves.

Fig. 5.22

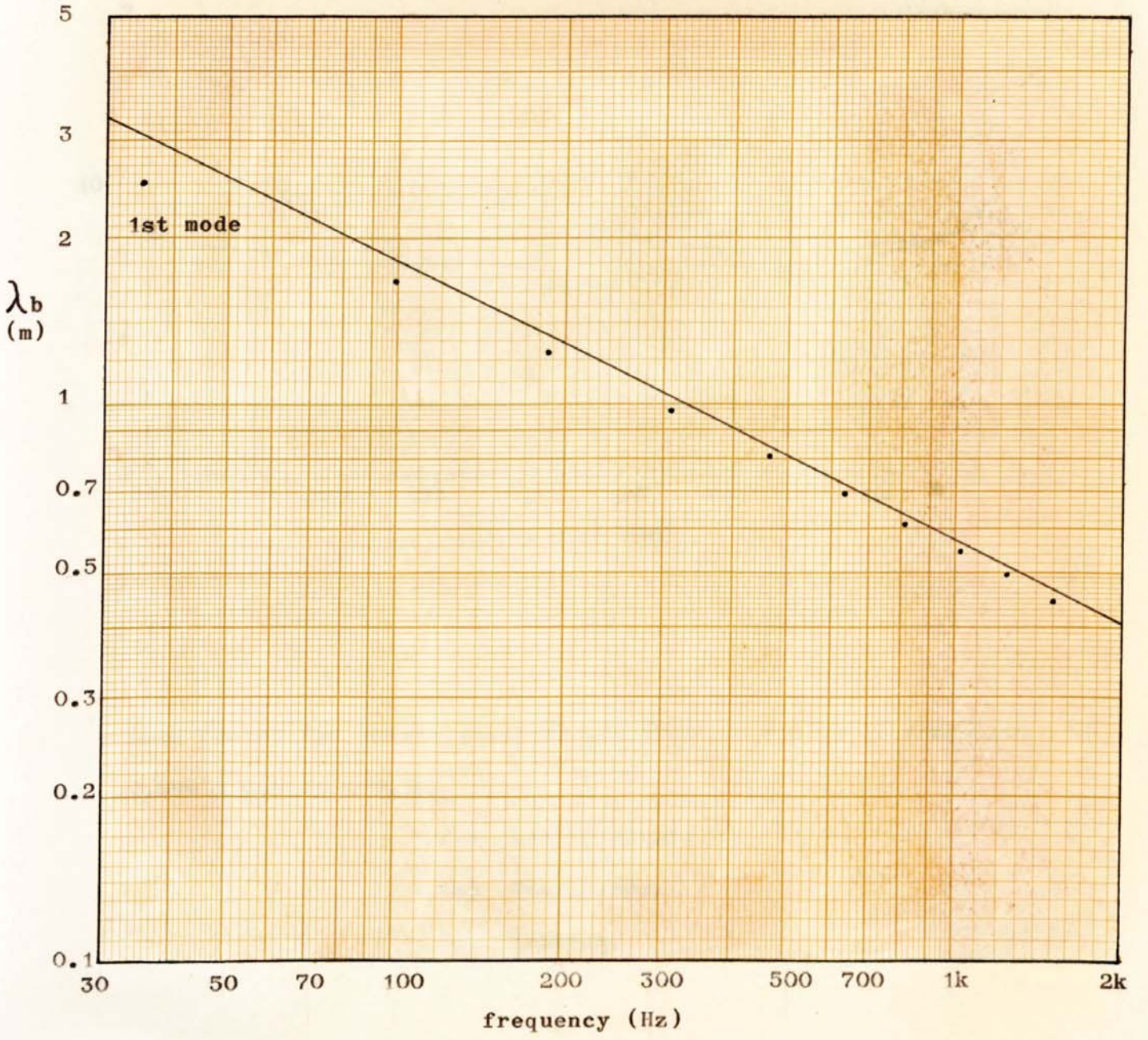

Bending wavelength for breeze block of dimensions 2.28m x 0.215m x 0.1m

Measured values compared to that predicted by simple theory given by

$\lambda_b = \sqrt{(1.8\ c_1\ h\ /\nu)}$.

Fig. 5.23

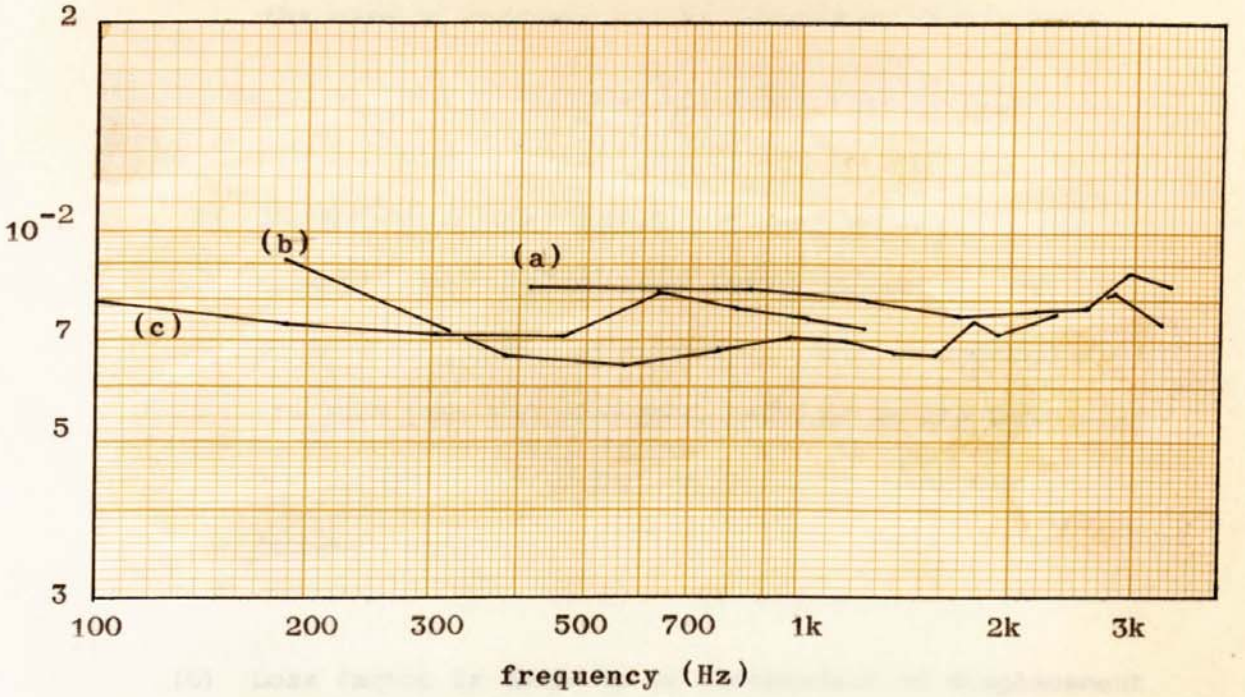

Loss factor for breeze block in the form of a beam of dimensions 2.28m x 0.215m x 0.1m.

(a) Longitudinal.

(b) Transverse.

(c) Bending.

the case of concrete can be assumed to have a value of 0.01.

(5) In brickwork investigated the wave velocities appeared high and the measured loss factor was of the same order as that of reinforced concrete. This is attributed to the fact that the specimens produced in the laboratory had stronger mortar and better keying than the brickwork found on site.

(6) Loss factor is shown to be independent of displacement amplitude over the amplitude range normally encountered in practice.

CHAPTER 6

EXPERIMENTS USING QUARTER-SCALE MODELS

6.1 Introduction

The use of quarter-scale models in assessing the vibrational response of structures has been seen to be valid. It now remains to use these techniques in an experimental verification of the power flow theories, described in Chapter 2. The experiments are in four main categories.

(1) The modal distributions of plates in vibration are measured and compared with the theory. The distribution of pressure wave modes in rectangular rooms was not investigated since the literature provides ample descriptions of this phenomenon, both theoretically (Morse and Bolt (1944), Bolt (1938), Dah-You Maa (1938)) and experimentally (Wente (1938), Hunt (1939), Somerville and Ward (1951)).

(2) The structure-fluid coupling is investigated for the case of rectangular concrete plates. This involved the measurement of radiation loss factor of baffled and unbaffled plates. The influence of edge fixing is also investigated.

(3) Concrete plates, forming junctions, are excited into vibration and the relative bending wave energy of each

plate is measured. The dissipative loss factor of a plate is increased when clad with a visco-elastic material. It is then possible to observe the effect of dissipative loss factor on the vibrational level of a plate, both directly, where the vibration amplitude of the clad plate is measured, and indirectly, where the vibration amplitude of a plate, joined to the clad plate, is measured.

(4) Both structure-fluid and structure-structure couplings are involved when the sound transmission between two model rectangular rooms is investigated. These measurements are described in Chapter 7.

The instrumentation has been designed to measure sound pressure level within rooms and bending wave energy on plates. No attempt is made to measure directly the longitudinal and transverse components of plate vibration. It will be remembered that the plate bending modes only are considered efficiently coupled to the pressure wave modes within a room.

6.2 Instrumentation

Use was made of vibration transducers, signal filters and amplifiers, operational amplifiers and data processing equipment. A description of some of the apparatus has been given in Chapter 5, and the following additional instrumentation is incorporated in the experiments.

6.2.1 The drivers

In these steady-state experiments the mechanical excitation of the plates was provided by electro-magnetic shakers.

The lighter structures, such as the concrete plates forming a junction, were driven by a Ling Altec shaker (model 201). The driver, mounted on a rigid frame, is bolted to the plate, (plate 6.2).

Larger structures, such as the model rectangular rooms require a more powerful source of vibration and this was provided by a Ling Altec shaker (model 407).

The steady-state signal to the driver was provided by a random signal generator (B & K sine random generator type 1024). The signal is filtered by one-third octave band pass filters (B & K type 1615) and amplified by a Quad 50E power amplifier.

The loudspeaker, used to radiate sound into the room in the measurement of radiation loss factor, consisted of an array of five KEF high frequency units (type T.15) mounted in the sides of an enclosed box (plate 6.6). This arrangement results in an approximately omnidirectional sound source at the high frequencies. Low frequency sound is provided by a cone loudspeaker, of 200 mm diameter, radiating from the same box as the high frequency assembly.

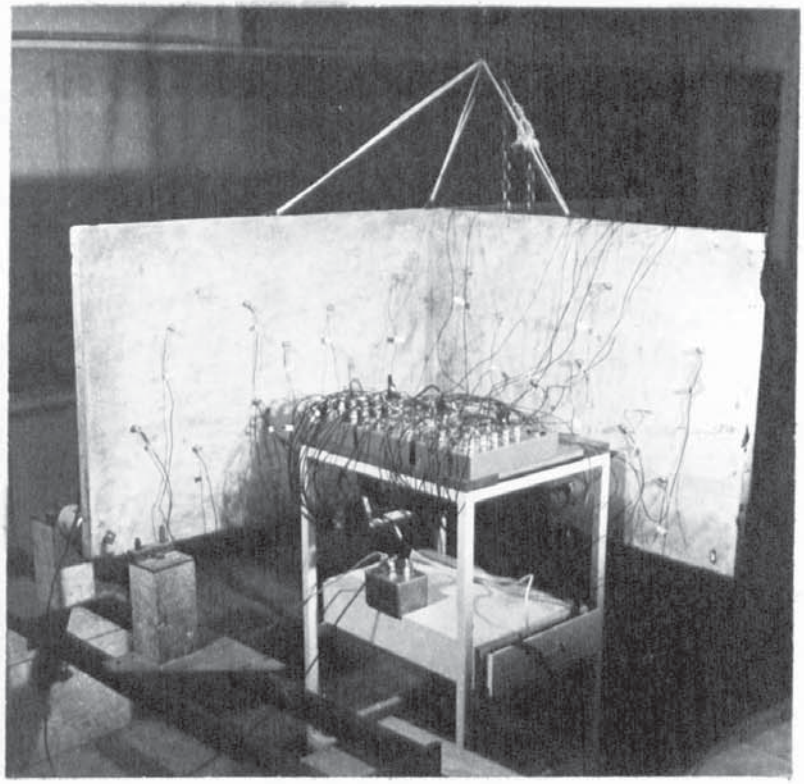

PLATE 6.1 Suspended concrete T-junction with accelerometers in position.

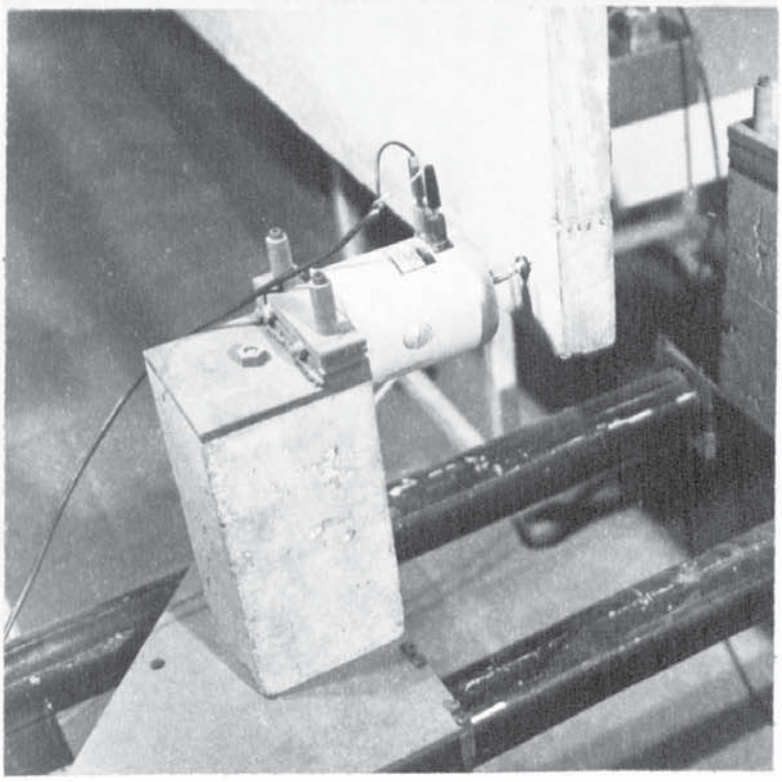

PLATE 6.2 Electro-magnetic shaker.

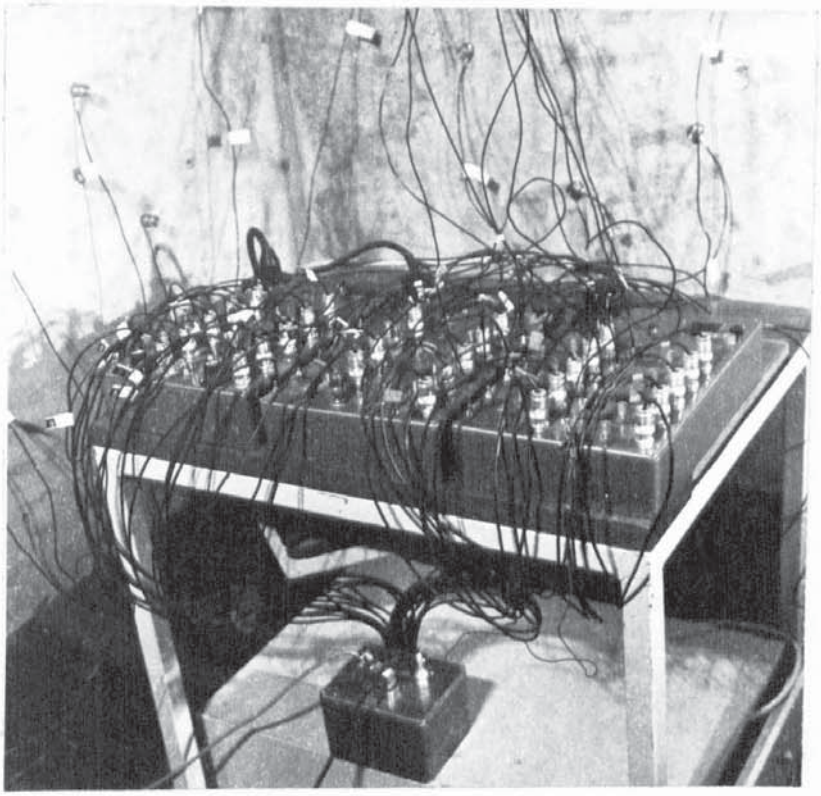

PLATE 6.3 Accelerometer pre-amplifiers and channel selector.

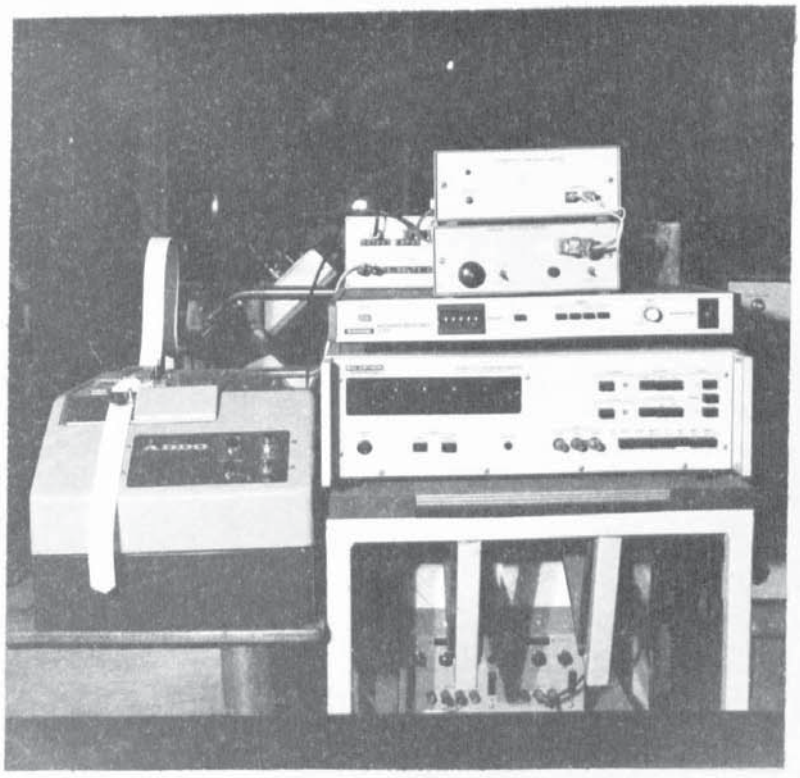

PLATE 6.4 Data processing equipment.

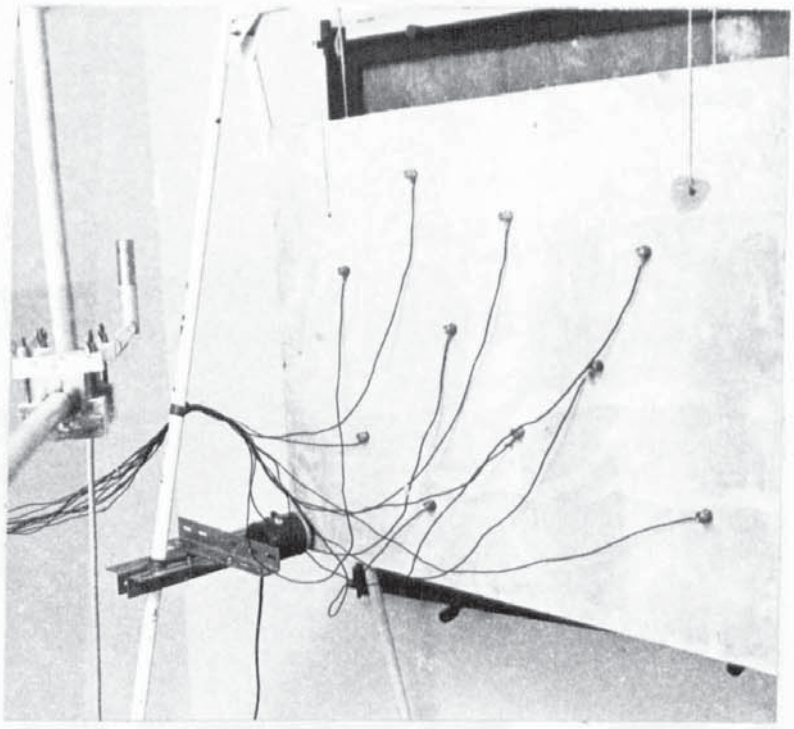

PLATE 6.5 Suspended concrete plate with accelerometers in position.

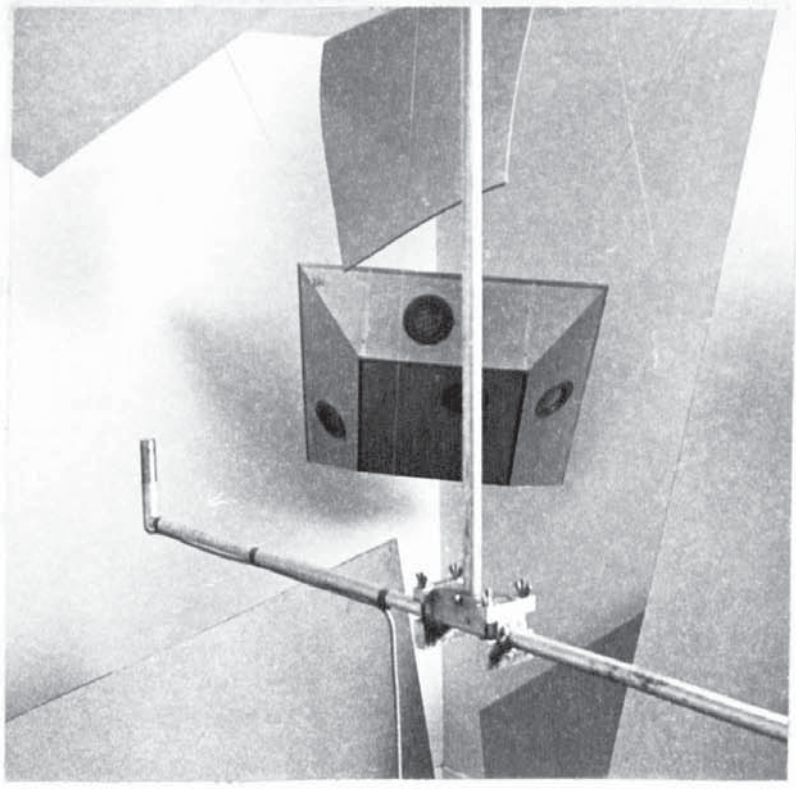

PLATE 6.6 Loudspeaker, condenser microphone, and diffusing sheets in receiver room.

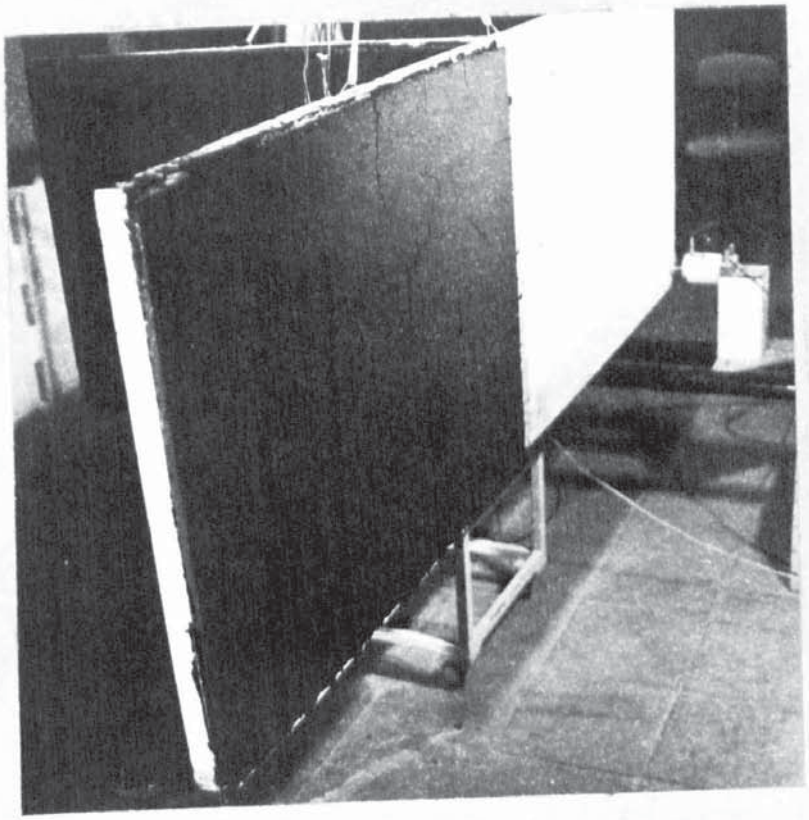

PLATE 6.7 Concrete T-junction with two clad plates.

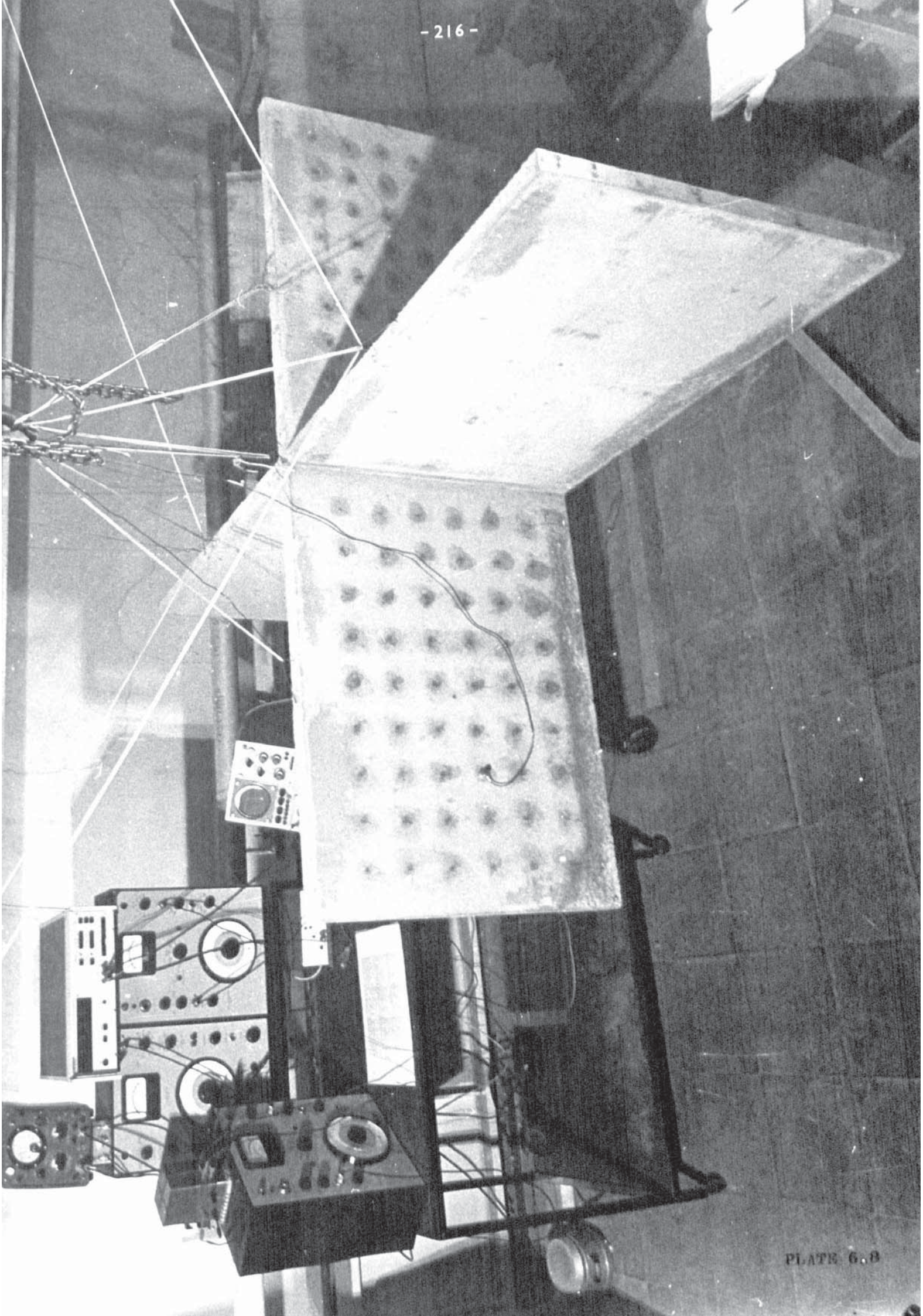

PLATE 6.8

6.2.2 The vibration transducers

Accelerometer transducers were used to measure the acceleration amplitude (and thus the bending wave energy) of the concrete plates. As well as the accelerometers described in Chapter 5 (B & K type 4333) an additional type was used which had the advantage of having a closely controlled sensitivity (10 mV/g $\pm$ 2%). These "unigain" accelerometers (B & K type 4339) proved useful when an absolute value of bending wave energy was required.

It was sometimes necessary to have up to thirty accelerometers with individual variable gain pre-amplifiers to allow the calibration (or standardisation) of the accelerometer sensitivities. The pre-amplifier units were designed and constructed by Lansdowne Associates and are shown in plate 6.3. The gain control on each channel allows a variation of 6 dB in the amplified output signal of nominal gain 10 dB.

Measurement of sound pressure level was made by means of one inch condenser microphones (B & K type 4131) with cathode followers (B & K type 2613), illustrated in plate 6.6.

6.2.3 The channel selector

It was required that, in turn, the signal from each accelerometer pre-amplifier be filtered, amplified, squared, displayed and stored on punched tape. This was made possible by means of a multiplex unit designed and constructed by Martin Ellett of the acoustics research

group (plate 6.4). The unit allowed up to thirty-two channels to be addressed manually or automatically. The automatic switching was sequential, the switching rate being approximately one channel in five seconds. This was long enough to allow for the relatively slow response of the square-law and rectification circuits.

6.2.4 The square-law module

The signal was squared and rectified by means of a circuit of seven "biased" diodes which gave a D.C. output proportional to the square of the A.C. input over a range of 40 dB (Fig 6.1).

6.2.5 Transducer calibration

The accelerometer calibration took two forms.

(1) In measuring the bending wave energy ratio of plates forming junctions it was required that each accelerometer and pre-amplifier have the same sensitivity. An aluminium disc (100 mm diameter, 40 mm thickness) formed a rigid vibration table when bolted to the large electro-magnetic driver. The accelerometers to be calibrated are stuck to this table by means of beeswax. The table is vibrated sinusoidally at the frequency desired and the gain of each pre-amplifier is altered until all accelerometers give the same signal. A check is possible by altering the driver frequency.

Fig. 6.1

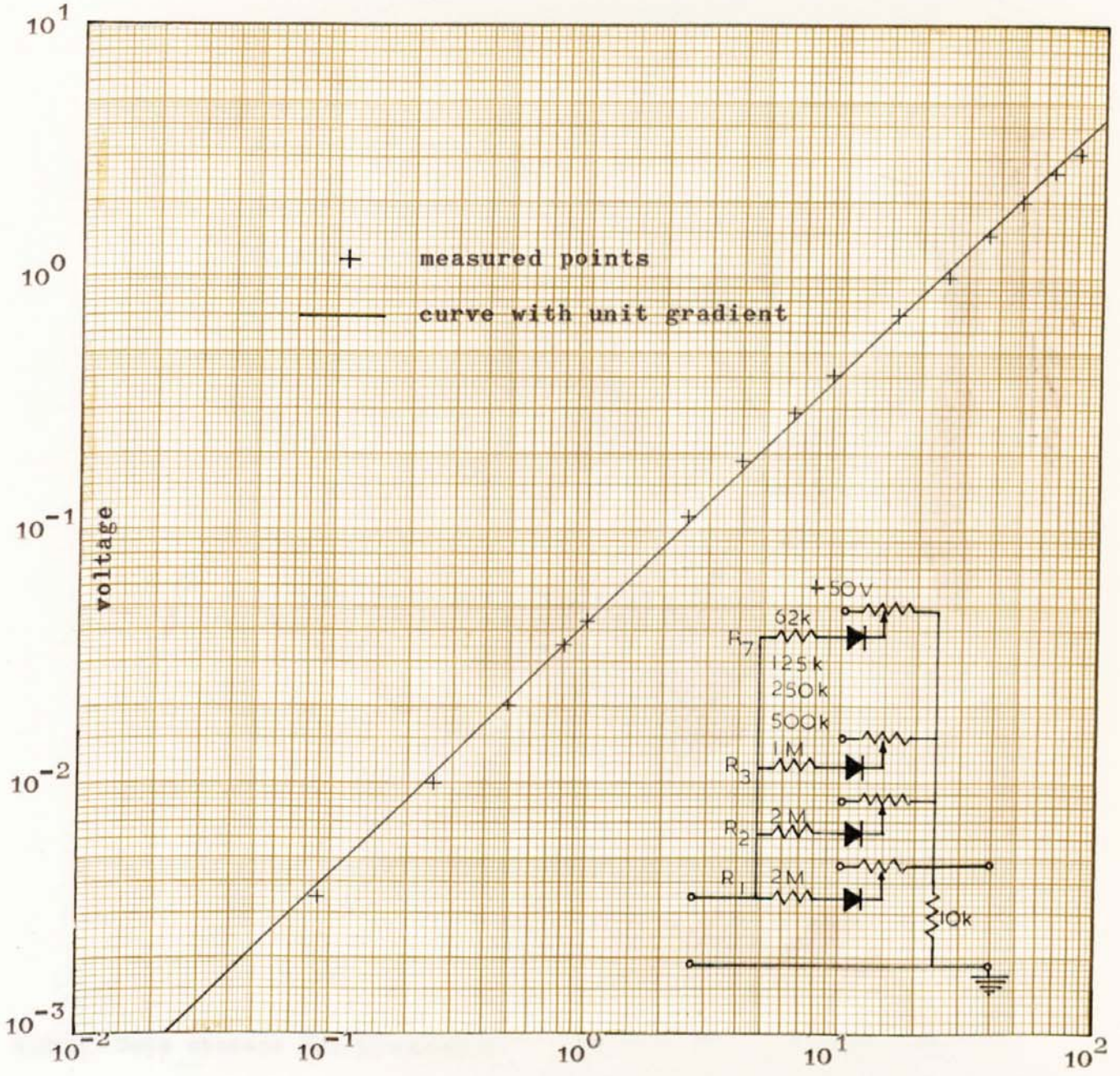

Calibration curve of voltage V against mean square acceleration $\langle a^2 \rangle$ where the constant K, given in $\langle a^2 \rangle = K\,V$, equals $24.15\,[m/sec^2]^2/volts$. Also shown are the biased diodes of the square law device.

(2) In making measurements of the radiation loss factor of plates, it is necessary to calculate the absolute bending wave energy of a plate, or more specifically, the mean square of the acceleration amplitude. A calibration curve is therefore required, showing the output of the digital voltmeter (plus amplifiers, square-law module etc) against the mean square of the table acceleration amplitude. The latter is obtained by use of one or more "Unigain" accelerometers, the pre-amplifiers of which, have zero again (B & K type 2625). The accelerometer sensitivities are known and it is a simple matter to calculate the acceleration amplitude. Figure 6.1 gives a plot of measured voltage (displayed by the digital voltmeter) against the mean square acceleration. A line of unit gradient gives a reasonable approximation over a range of nearly 40 dB, the constant of proportionality in this case, being 24.13 $(m/sec^2)^2$/volt.

6.2.6 Data storage and processing

The data displayed by the D.V.M is stored on tape by means of a Solartron-Schlumberger recorder drive unit (type A290) and tape punch (Addo type 5). The punch is synchronised to the channel selector. Plate 6.3 and plate 6.4 show the main components of the signal processing circuit.

6.3 Statistical considerations

In all experiments it was required that the vibrational response be averaged with respect to time and also with respect to space. The former is characterised by the mean square or the root mean square (R.M.S) of the signal. Most of the apparatus used to measure the vibrational response have rectifying and smoothing circuits which give a direct reading of R.M.S. It is therefore necessary only to say that when a measurement of accelerometer or microphone signal at one position is made, the resultant parameters are the mean square or the root mean square response.

The spatial average of the response is obtained by a sampling process involving many microphone or accelerometer positions. The sampling of the pressure wave field is described in section 6.5. However, it is important at this point to gauge the variation of measured bending wave energy over a plate surface. The measurement of bending wave energy at a point on a plate is described fully in section 6.6. The measurements allowed the mean and standard deviation of a number of accelerometer readings to be calculated, e.g. those obtained from plates forming a cross-junction or a corner junction. For the model cross-junction, in which one plate was mechanically excited, readings were obtained at thirty-five accelerometer positions on each plate. For each plate a plot of normalised standard deviation of the bending wave energy $\sigma_b/\langle E_b \rangle$ was made against frequency (Fig 6.2 and Fig 6.3). The same parameter was plotted for twelve accelerometer readings per plate for a corner junction (Fig 6.4). From the graphs the following observations can be made.

Fig. 6.2

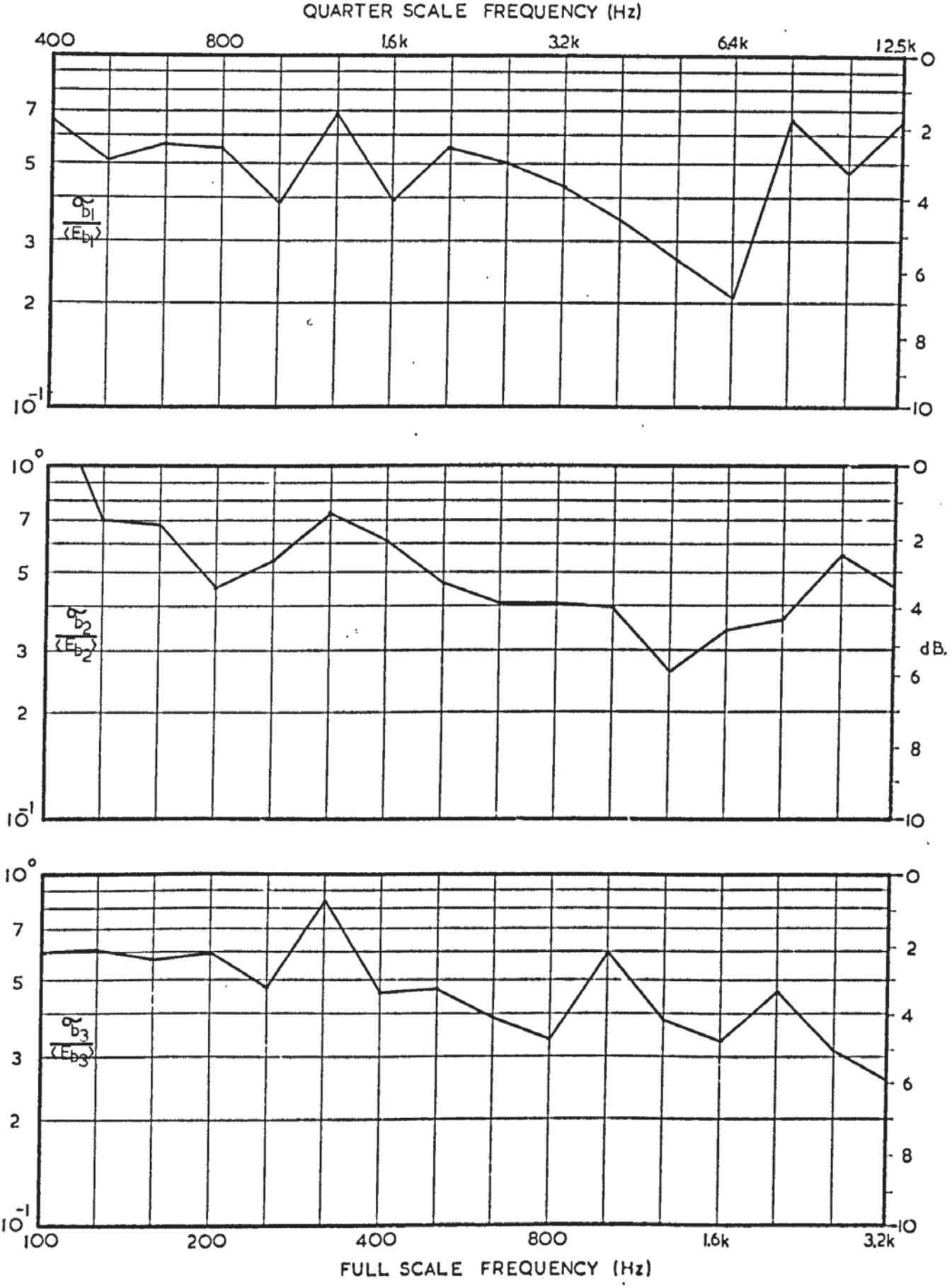

Ratio of standard deviation to mean bending wave energy on concrete plates forming a cross junction where a thick plate is excited mechanically.

Fig. 6.3

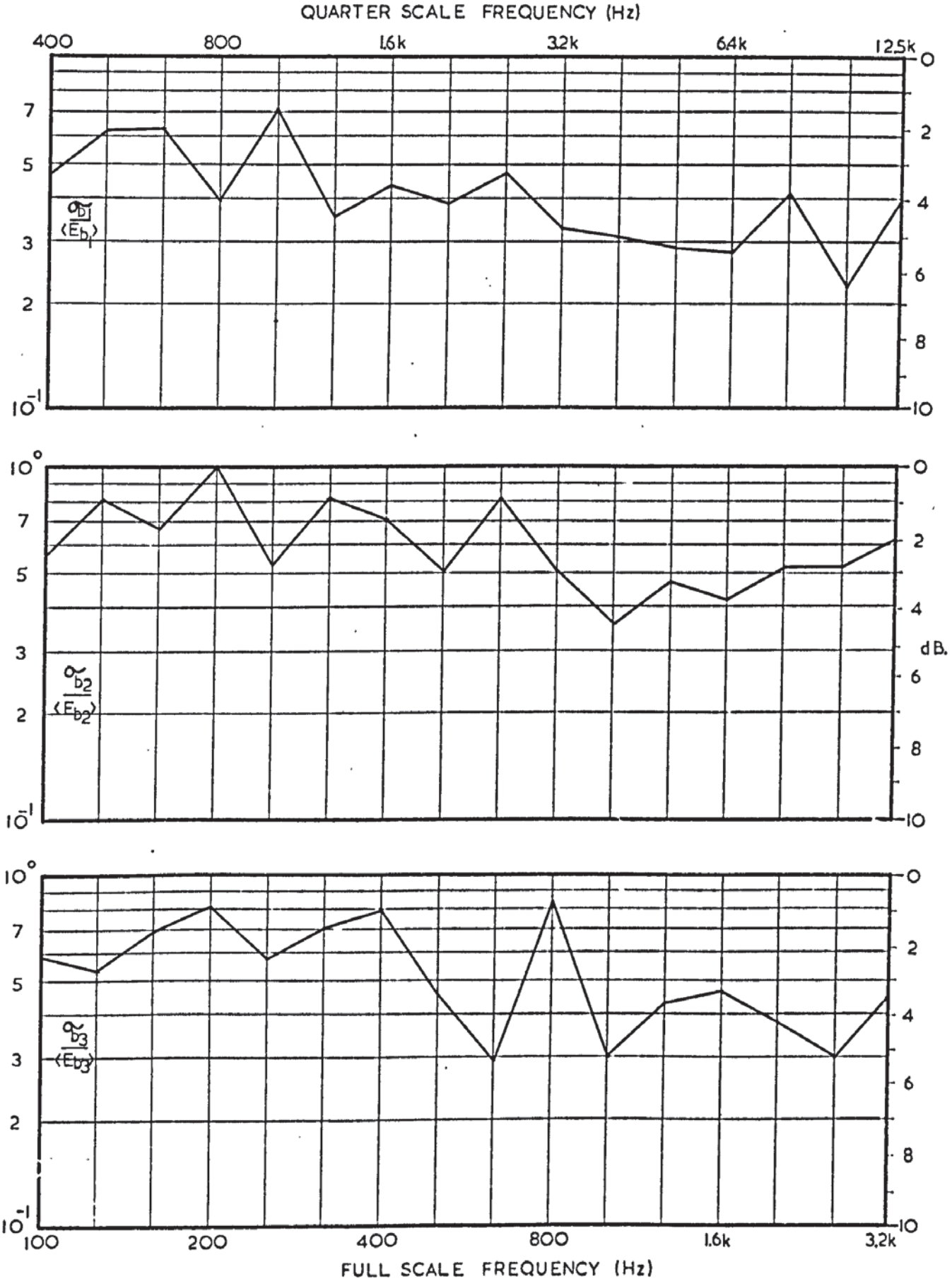

Ratio of standard deviation to mean bending wave energy on concrete plates forming a cross junction in which the thin plate is excited mechanically.

Fig. 6.4

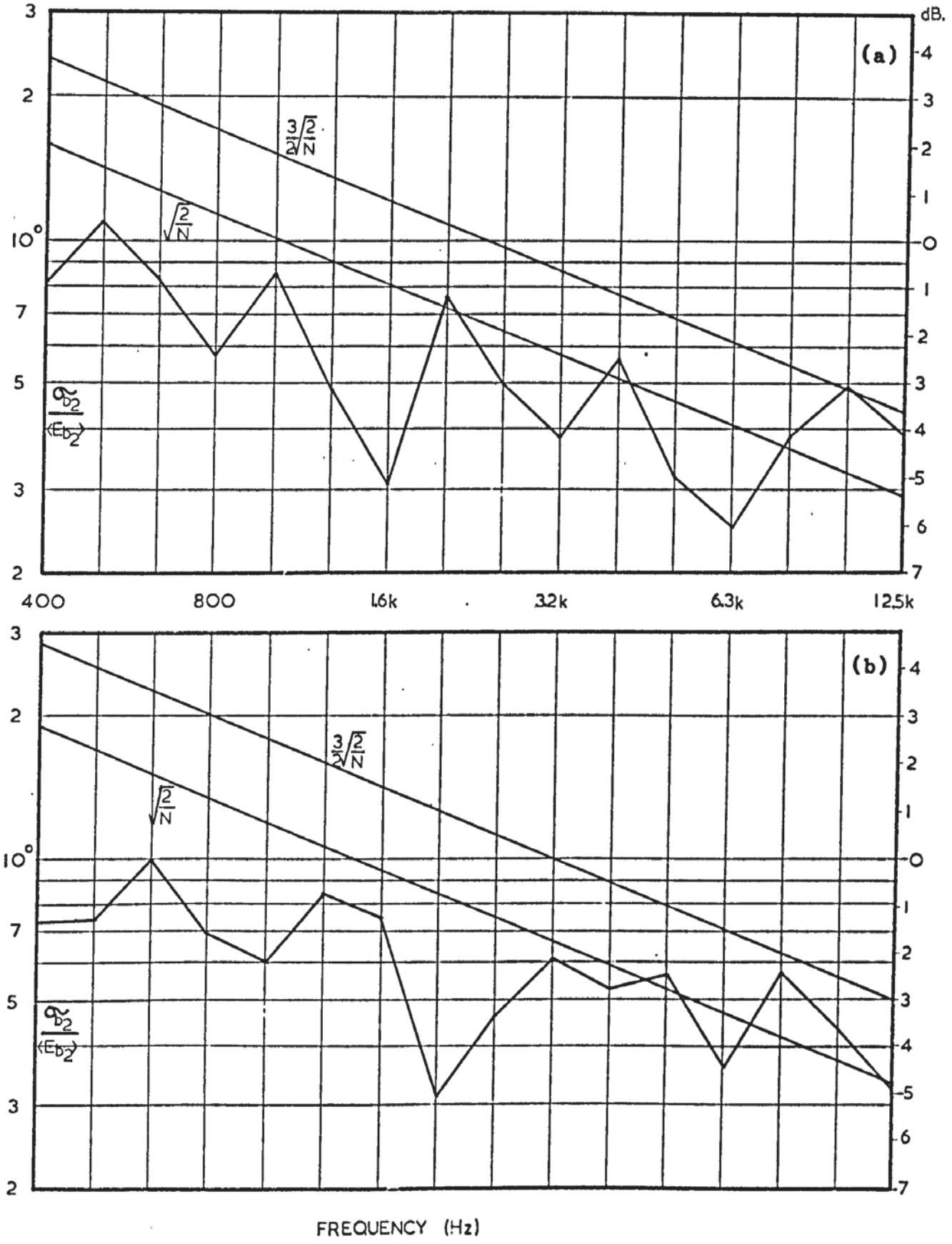

Comparison of measured normalised standard deviation to predicted values of Stearn for a corner junction where,

(a) the thicker plate is excited and measurements are on the thin,

(b) the thin plate is excited and measurements are on the thick plate.

(1) Over the (quarter-scale) frequency range the normalised standard deviation is less than unity.

(2) There is, in general, a decrease with rise of frequency. The high frequency value is often 50% or less than the maximum value which occurs at the low frequencies.

This decrease is to be expected since at the higher frequencies, more modes are generated within a one-third octave bandwidth and the bending wave field becomes more diffuse. If the field was ideally diffuse, then the parameter $\sigma_b/\langle E_b \rangle$ would assume a zero value.

(3) Stearn (1969) has shown that for thin plates and shells and for a fairly high modal density N (ten or more modes per bandwidth) the parameter $\sigma_b/\langle E_b \rangle$ can be predicted as lying between a lower limit $\sqrt{\frac{2}{N}}$ and an upper limit $\frac{3}{2}\sqrt{\frac{2}{N}}$ Figure 6.4 shows that, except at the highest frequencies, the measured values lie below those predicted by Stearn and also over the whole frequency range the gradient is smaller.

To summarise, the spatial variation of plate bending wave energy, as represented by the normalised standard deviation, decreases with increasing frequency from an approximately unit value to a dimensionless value of 0.3 - 0.5. The gradient is small and one might postulate a single number as describing the spatial variation over the whole frequency range. This is given as 0.7 ± 0.3.

The mean of n accelerometer readings will be expected to have a standard deviation smaller by a factor of $1/\sqrt{n}$. Therefore to reduce the value to one fifth of the R.M.S amplitude it is necessary to use at least fifteen accelerometers distributed about a test piece.

In experimentally assessing the spatial average bending wave energy of a plate, two methods were adopted.

(1) The experiments were initiated when few accelerometers and pre-amplifiers were available. The spatial average was obtained by altering the measuring position of a single accelerometer many times. This process was time consuming and introduced two problems, the first of which concerned the mounting of the accelerometer. The accelerometer adhered to the plate surface by means of beeswax and it was found that readings of acceleration amplitude were affected by the degree of adhesion. The constant need to remount the accelerometer cast doubts as to whether an adequate adhesion was being attained each time. The second problem resulted from the long time periods required for a set of readings. This introduced the problem of "drift" in the driver signal which would result in a different overall vibration level at the end of a run from that at the beginning. This problem was eliminated to some extent by having a monitoring accelerometer mounted at the driving point. In this way the power input could be kept reasonably constant.

(2) With the introduction of more accelerometers, pre-amplifiers and automatic switching, it was possible to speed up the process and ensure firmer mounting of the accelerometers. The optimum number of accelerometer points on a plate was set at fifteen. If the number was less, the run is repeated with the accelerometer positions altered and the mean value of energy ratio or radiation loss factor is calculated. In measuring vibrational energy of the plates forming two rectangular rooms, four accelerometers were available for each plate. Thus, the experiment is repeated four or five times and the mean value obtained.

6.4 Modal density

The method of measurement of bending and longitudinal modal distribution of concrete plates is essentially the same as that for the distributions in concrete rods, described in Chapter 5. A freely suspended reinforced concrete plate (1 m x 0.75 m x 0.038 m) is driven by a small shaker supplied by a sinusoidal current which increases slowly in frequency from 100 Hz to 12.5 kHz.

For bending mode measurement, the driver was attached, normal to the plate surface, near one corner. The plate response is measured by an accelerometer, fixed in a position near the corner diagonally opposite to that of the driver. The accelerometer signal, after amplification is recorded by means of a level recorder. The process then consisted of counting the resonant peaks lying between any two

frequency intervals and to plot the total number of modes lying below each frequency. This method of visual assessment is allied to use made of the human ear. Experienced listeners in the laboratory were able to locate all of the low and mid frequency resonances of the plate as the driver frequency increased. The plot, on Figure 6.5 is of the number of modes lying below any frequency (forming the abscissa). The observed values are compared with two theoretical predictions.

(1) The simple, thin plate theory, described in section 3.3.2 gives fair agreement with observation, even at the higher frequencies. It must be stated however that mode counting becomes increasingly difficult at higher frequencies. This problem is eased to a certain degree by reducing the sweep rate of the driver, and increasing the level recorder paper speed as the frequency increases.

(2) A more exact predicted modal distribution was computed using Warburton's (1953) theory for a freely suspended thin plate. By this theory a fundamental frequency, corresponding to the 1,1 mode of 142 Hz was predicted; this gave reasonable agreement with the observed value of 145 Hz.

In measurement of the longitudinal modal distribution the axes of the shaker and the accelerometer are in the plane of the suspended plate. They are again positioned diametrically opposite each other and their axes

Fig. 6.5

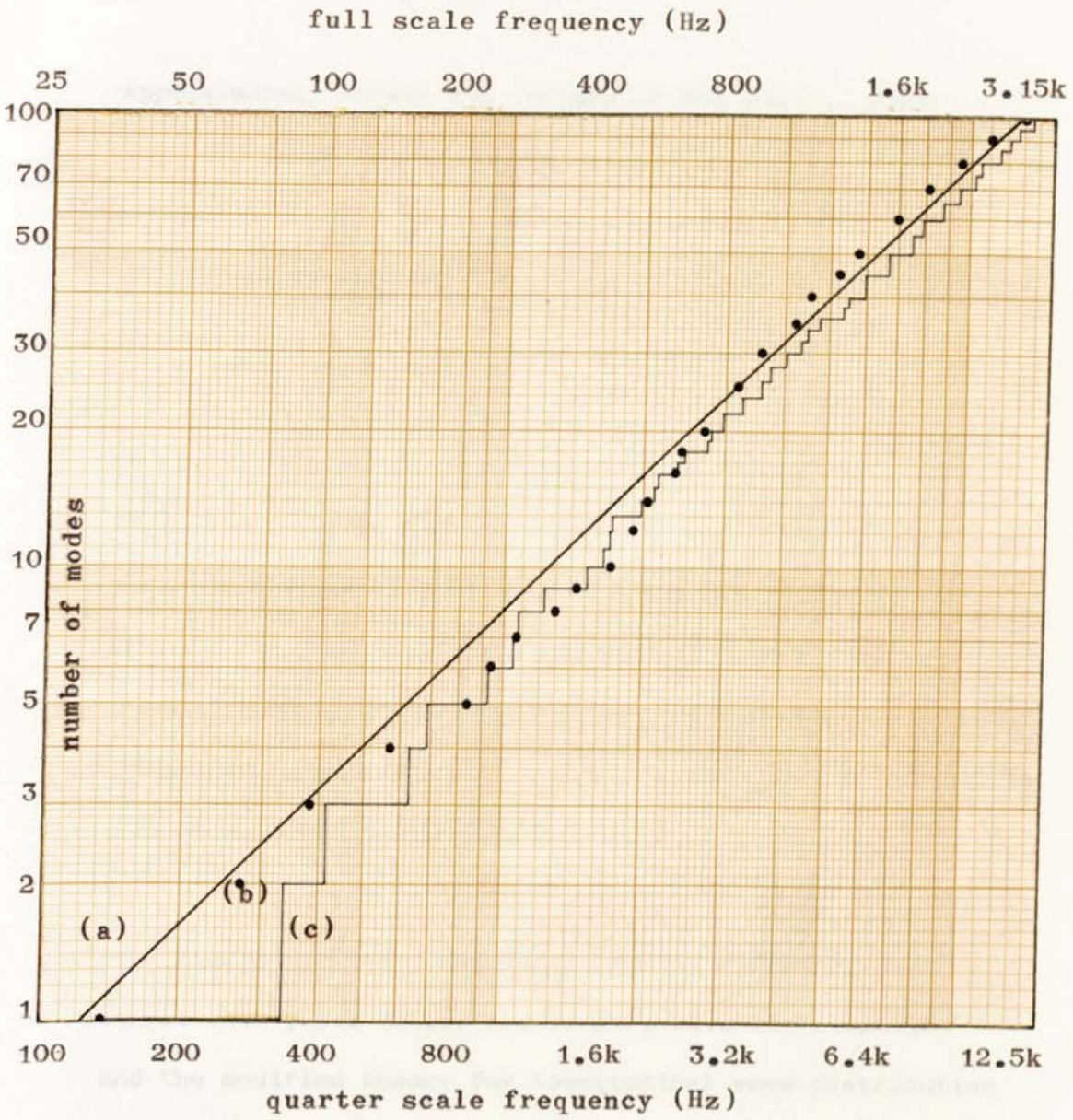

The bending modes of a concrete plate with free edges.

(a) Simple theory, where modal density $n_b = S_p\sqrt{3}\,/(c_l h)$.

(b) Quarter scale measurements.

(c) Modal distribution from the theory of Warburton (1954).

approximately bisect the corners of the plate. Thus, the components of the shaker force are able to excite all longitudinal modes and the components of the accelerometer axis of greatest sensitivity are able to read them.

As would be expected the modal spacing was greater than that of the bending waves and it was a simple task to plot the observed number of modes against frequency, (Fig 6.6). The result is compared with the simple and corrected theory of non-dispersive waves in two dimensions (section 3.3.3) and it is seen that the corrected theory gives fair agreement.

To summarise, these model experiments indicate that the simple thin plate theory for bending wave distribution and the modified theory for longitudinal wave distribution give fair agreement with observed values.

6.5 Radiation loss factor of concrete plates

In section 2.9 energy balance equations were derived to describe the structure-fluid coupling loss factor η_p^r of a plate radiating sound into a room. These expressions are now used in the experimental evaluation of this parameter. The experiment is illustrated in Figure 6.7.

Fig. 6.6

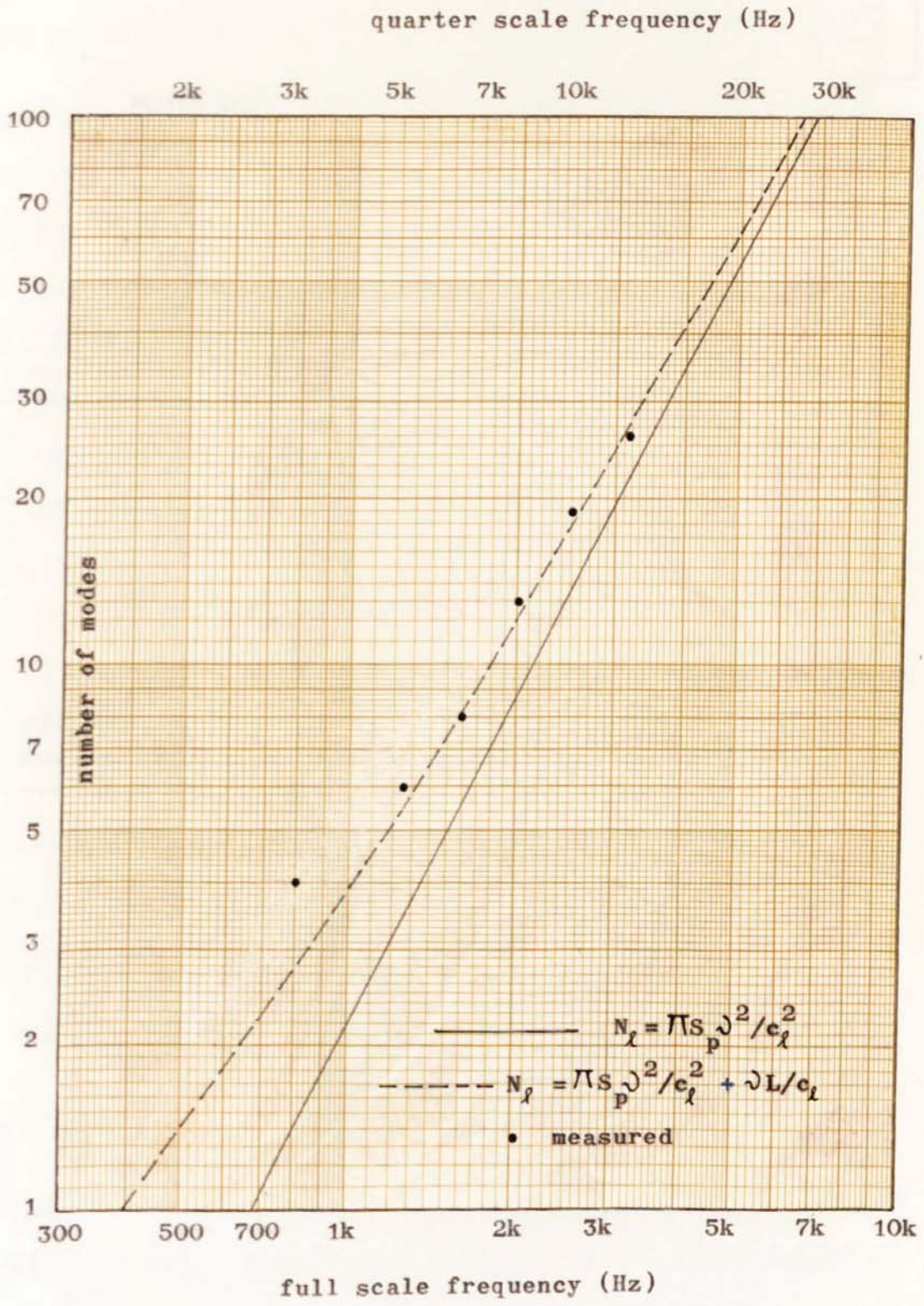

Longitudinal modal density for a concrete plate of quarter scale dimensions 1m x 0.75m x 0.038m.

Fig. 6.7

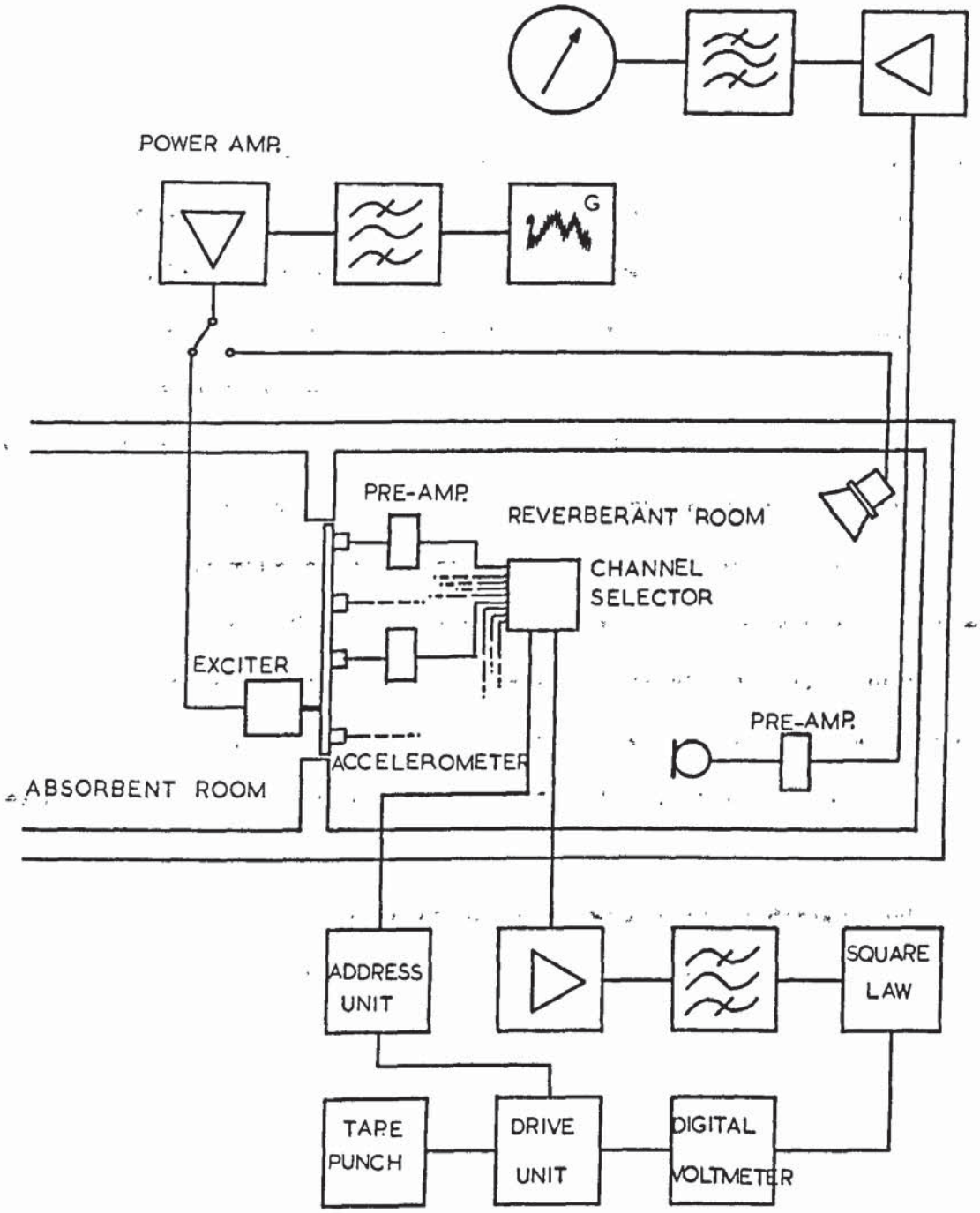

Measurement of radiation loss factor of a baffled panel.

6.5.1 The room

The room, shown in plate 6.6, is one of two rectangular rooms, forming a small transmission suite. The volume is 19.27 m^3 and the wall surfaces are of hard plaster. Suspended within it are hardboard sheets of various sizes and curvature. The total area of the sheets was twice that of the floor area and they were randomly distributed as suggested in British Standard 3638. In addition, the field was sampled at ten microphone positions, the microphone being mounted on a rotatable boom (plates 6.5 and 6.6). In experiment, the difference between the maximum and minimum of the ten microphone readings was approximately 6 dB at 100 Hz, 5 dB at 400 Hz, and 2 dB at 12.5 kHz. Thus, it is fair to assume the sound pressure field to be diffuse in the mid and high frequencies.

The second room of the transmission suite was heavily damped and could be assumed to absorb all sound energy above 400 Hz radiated by a panel in the aperture.

6.5.2 The plate

The model reinforced concrete plates were of length 1 m and breadth 0.75 m. Different plates were used in different configurations in order to assess the influence on radiation loss factor of the following

(1) Two plate thicknesses were considered, that of 0.038 m and 0.05 m; corresponding to full scale thicknesses of

0.15 m and 0.2 m respectively. In subsequent discussions they will be termed the thin plate and thick plate respectively.

(2) The plate edges were either free or fixed. The first condition was obtained by simply suspending the plate by nylon wires (plate 6.5). The second condition was obtained by casting a concrete plate inside a concrete "frame" of depth 130 mm and width 100 mm along the top and bottom edges, and 220 mm width along the side edges. The weight of the plate was less than one third the weight of the frame which was thus thought sufficiently massive. The "framed" plate was placed in the aperture with its surface flush with that of the room wall.

(3) The plates, when freely suspended, could either radiate sound into 4π space, (plate 6.5) or if placed in the transmission suite aperture, could be considered as radiating in 2π space. In the aperture the plate was suspended at two points and the air gap around it was sealed with thin rubber tubing and sealing tape.

(4) The plate could either be directly excited, by an electromagnetic driver (plate 6.5), or indirectly excited by a loudspeaker within the reverberant room (plate 6.6).

6.5.3 Measurement procedure

Irrespective of whether the plate is directly or indirectly excited the two parameters to be calculated are the room pressure wave energy E_r and the plate bending wave energy E_b.

6.5.3.1 Pressure wave energy E_r

The mechanically driven plate or the loudspeaker (either of which is supplied by a random noise signal through a one-third octave filter and power amplifier) results in a steady-state pressure field within the room. For each frequency the mean square pressure $\langle p^2 \rangle$ is obtained from ten microphone readings. The room energy is then calculated from the expression,

$$E_r = \frac{\langle p^2 \rangle}{\rho_o c_o^2} V \qquad \ldots\ldots\ldots 6.1$$

where V is the room volume, ρ_o the air density, and C_o the airborne sound velocity.

6.5.3.2 Bending wave energy E_b

At the same time as the sound pressure is being recorded manually, the signals from ten calibrated accelerometers, placed on the plate surface, are processed and logged. Thus, for each frequency the spatial average mean square acceleration $\langle a^2 \rangle$ is calculated. The expression for plate bending energy is,

$$E_b = M_p \langle v^2 \rangle$$

Where M_p is the plate mass and $\langle v^2 \rangle$ is the mean square velocity amplitude in the direction of the thickness. A reasonable approximation is possible if it is assumed that,

$$\langle a^2 \rangle = \omega^2 \langle v^2 \rangle$$

ω is the centre frequency of the bandwidth. Thus, the plate energy is given as

$$E_b = \frac{M_p}{\omega^2} \langle a^2 \rangle \qquad \ldots\ldots\ldots 6.2$$

Both sets of measurements are repeated for different accelerometer and microphone positions.

6.5.3.3 Radiation loss factor η_b^r

In section 2.9 the ratios of the energies E_b, E_r are given in terms of the internal loss factors of room and plate, the ratio of the modal densities n_b / n_r and the radiation loss factor η_b^r. From the energy balance equations 2.53 and 2.54 and from the equality 2.56, the following relationships result. If the plate only is excited then,

$$\eta_b^r = \frac{\eta_r}{E_b/E_r - n_b/n_r} \qquad \ldots\ldots\ldots 6.3$$

If the room only is (loudspeaker) excited then,

$$\eta_b^r = \frac{\eta_b}{(E_r/E_b)(n_b/n_r) - 1} \qquad \ldots\ldots\ldots 6.4$$

when the plate lies within the room, i.e. radiates from both

surfaces, or when the plate is baffled i.e radiates into the room from one surface.

$$\eta_b^r = \frac{\eta_b}{(E_r/E_b)(n_b/n_r) - 2} \qquad \ldots\ldots\ldots 6.5$$

The factor of 2 is explained when one considers the plate within the transmission suite aperture. It can be seen that half the power radiated or re-radiated by the plate is lost to the highly absorbent second room (Fig 6.7).

6.5.3.4 Room and plate parameters

Figure 6.8 gives the values of the parameters found on the right hand side of equations 6.3 - 6.5. The modal density ratio n_b/n_r is calculated from expressions given in section 3.2. The various internal loss factors are obtained from the rate of decay of pressure or bending wave amplitude, on removing the source of excitation (section 5.6). The reverberation time of the room is a mean value obtained from ten microphone positions. The loss factor for the two freely suspended plates of different thicknesses is given. It is seen that the value of η_b lies somewhat below that of the value measured from reinforced concrete in the form of rods.

6.5.4 Results

The results of the experiments are given in Figures 6.9 to 6.15. On each graph is given the predicted value of Maidanik (1962) for

Fig. 6.8

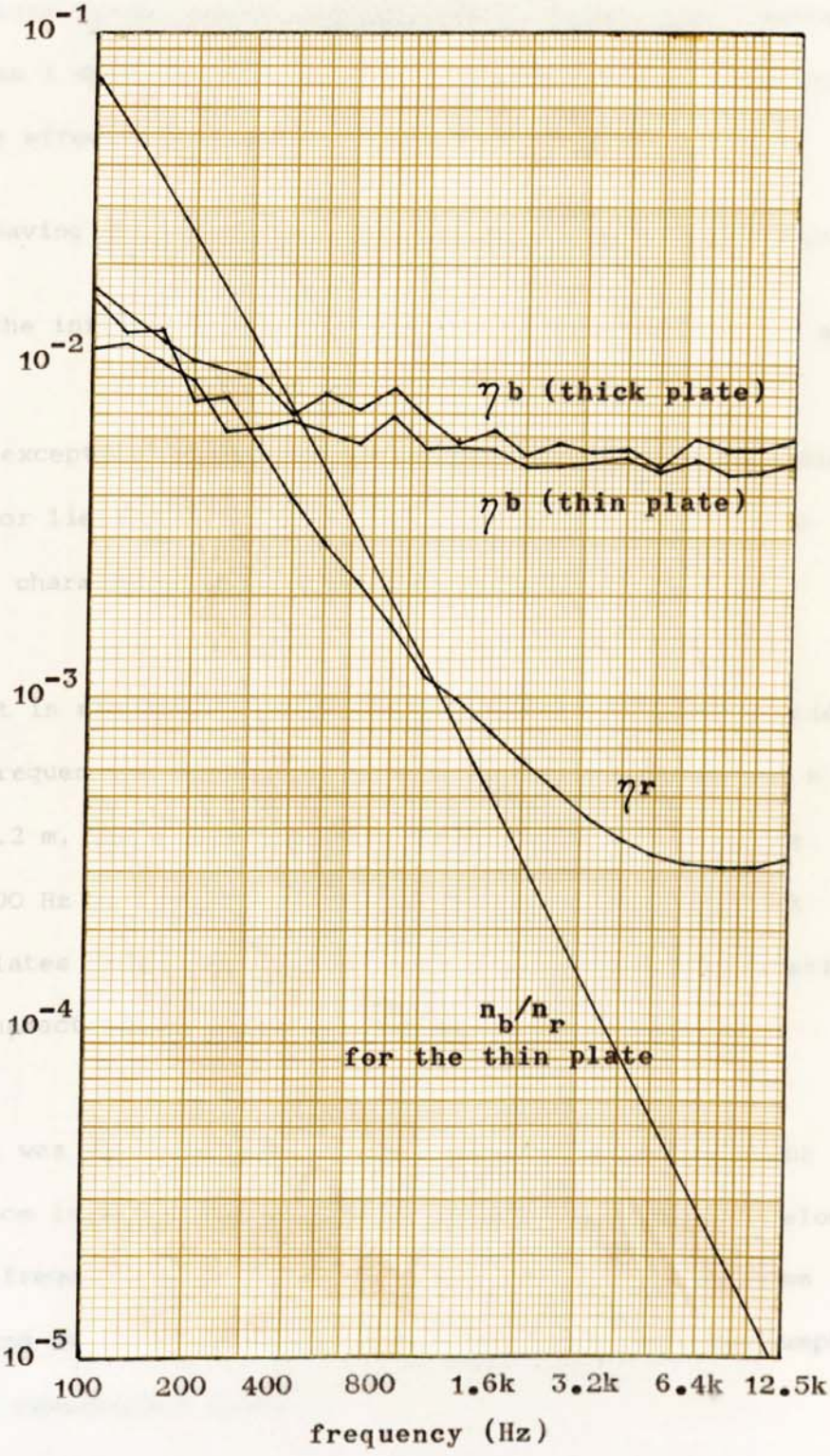

Internal loss factors and ratio of modal densities of model concrete plates and reverberant room.

a thin plate having simply supported edges. The upper (dotted) curve lies 3 dB above the lower curve and is reproduced in order to gauge the effect of

(1) having edge conditions which given bending reflection, and

(2) the influence of radiation into 4π rather than 2π space.

With the exception of Figure 6.12 all measured values of radiation loss factor lie within the supercritical region of the plate radiation characteristics. There are two reasons for this.

(1) It is shown in section 3.1.2 that the critical coincidence frequencies of plates, of full scale thickness 0.15 m and 0.2 m, lie below the frequency range of interest i.e. 100 Hz to 3.15 kHz. We are therefore concerned with plates or wall surfaces which have piston like radiation characteristics.

(2) It was thought that the dimensions of the reverberent room in general prevented meaningful measurements below a frequency of 400 Hz. The modal density of the room (and that of the plate) is too low to allow the assumption of reverberant fields.

Figure 6.9 gives the result of a thin plate (of thickness 0.038 m), freely suspended within the room. Although, in experiment a sharp increase in the radiated power is detected at the predicted critical coincidence frequency the measured radiation loss factor lies well

Fig. 6.9

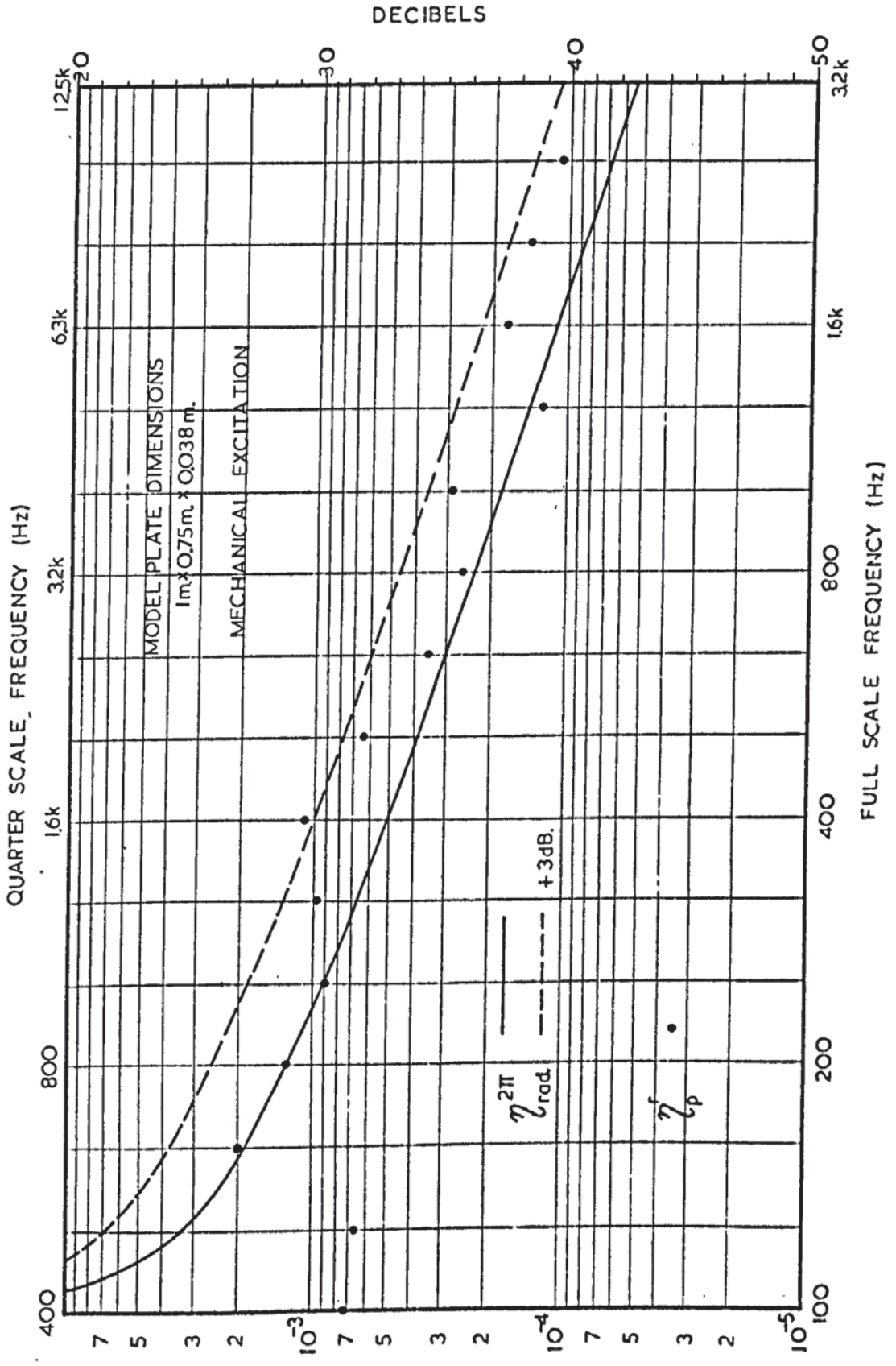
DECIBELS
20
30
40
50
12.5k
6.3k
3.2k
1.6k
800
400
200
100
3.2k
1.6k
800
400
QUARTER SCALE FREQUENCY (Hz)
FULL SCALE FREQUENCY (Hz)
MODEL PLATE DIMENSIONS
1m x 0.75m x 0.038 m.
MECHANICAL EXCITATION
+3dB.
$\eta^{2\pi}_{rad.}$
η^{f}_{p}
10^{-3}
10^{-4}
10^{-5}
7
5
3
2

below that predicted. Over most of the frequency range however, the experimental points lie above the solid line. This might be expected if a simple energy flow model is considered. At the higher frequencies, and for narrow bandwidth noise, ignoring edge effects, phase may be ignored and the radiation loss factor in 4π space may be thought equal to twice that into 2π space. This would correspond to points lying 3 dB above the predicted value of $\eta_{rad}^{2\pi}$.

Fig 6.10 illustrates a repeat of the experiment, using the thicker plate. There is more scatter in the points but again they lie above the solid line.

On disconnecting the mechanical driver and supplying sound power to the room by means of a loudspeaker a resultant bending wave field is produced upon the plate within the room. The radiation loss factor may then be calculated from equation 6.5. Figure 6.11 gives the results for a thin plate suspended within the room. It is seen that measured values are greater than those obtained from mechanical excitation by 1 dB to 4 dB.

The process of mechanical and acoustic excitation was repeated for plates freely suspended within the transmission suite aperture. In this situation the plate is regarded as radiating into 2π space. Figure 6.12 gives the measured values for the thin plate and it is seen that the points agree quite well with theory (solid line) over much of the frequency range, with a tendency to fall below the line at the highest frequency. As would be expected, the values of η_b^r shown in Figure 6.9 lie from 2 dB to 3 dB higher than the values in

Fig. 6.10

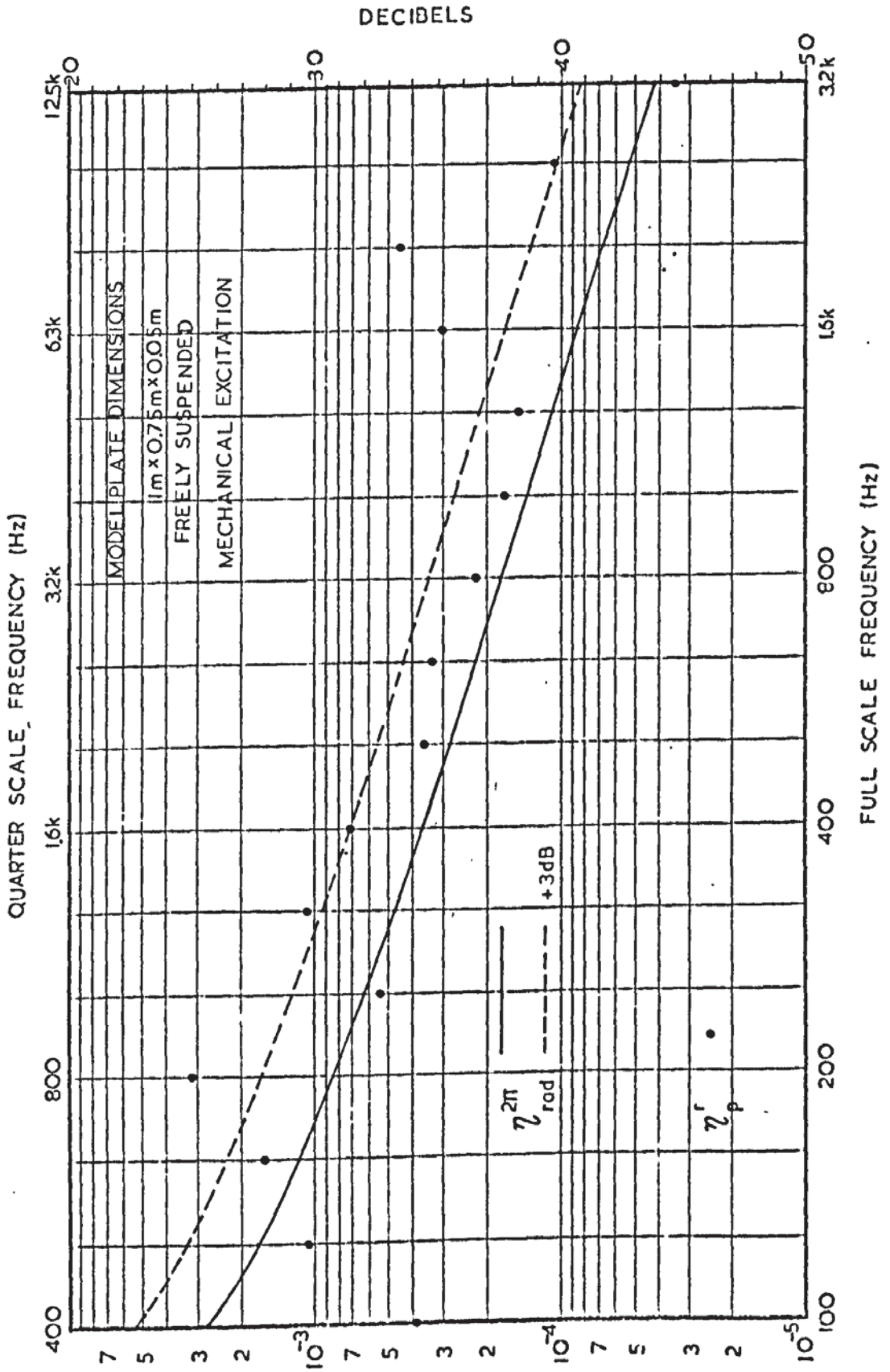
DECIBELS
20
30
40
50
125k
63k
32k
16k
8k
4k
32k
16k
8k
4k
2k
1k
500
250
125
MODEL PLATE DIMENSIONS
1m × 0.75m × 0.05m
FREELY SUSPENDED
MECHANICAL EXCITATION
+3dB
$\eta^{2\pi}_{rad}$
η^{r}_{p}
QUARTER SCALE FREQUENCY (Hz)
FULL SCALE FREQUENCY (Hz)

Fig. 6.11

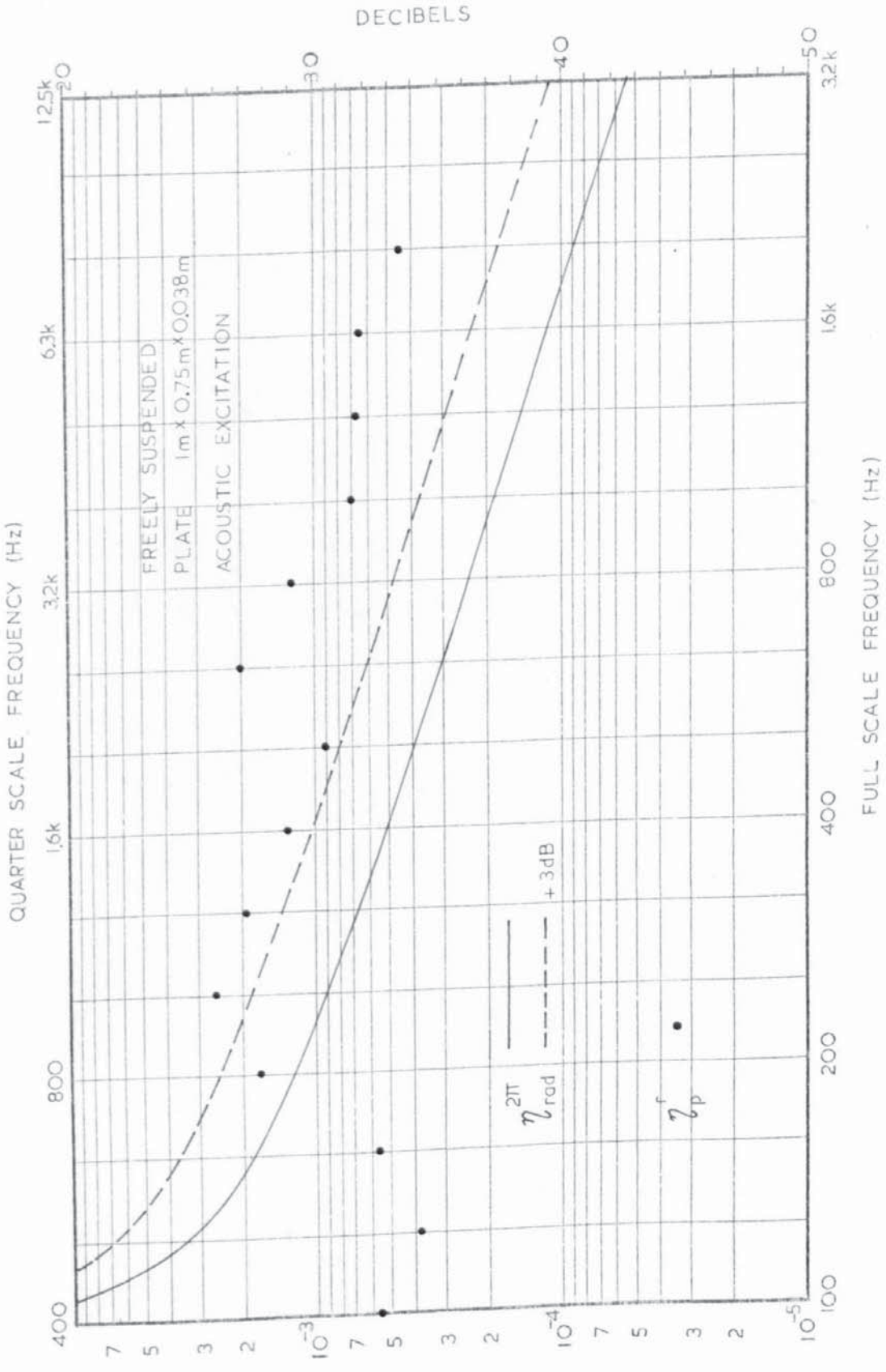
DECIBELS
20
30
40
50
12.5k
6.3k
3.2k
1.6k
800
400
200
100
FREELY SUSPENDED
PLATE 1m x 0.75m x 0.038m
ACOUSTIC EXCITATION
QUARTER SCALE FREQUENCY (Hz)
FULL SCALE FREQUENCY (Hz)
2π η_{rad}
+ 3dB
η_p^f
10^{-3}
10^{-4}
10^{-5}
7
5
3
2

Fig. 6.12

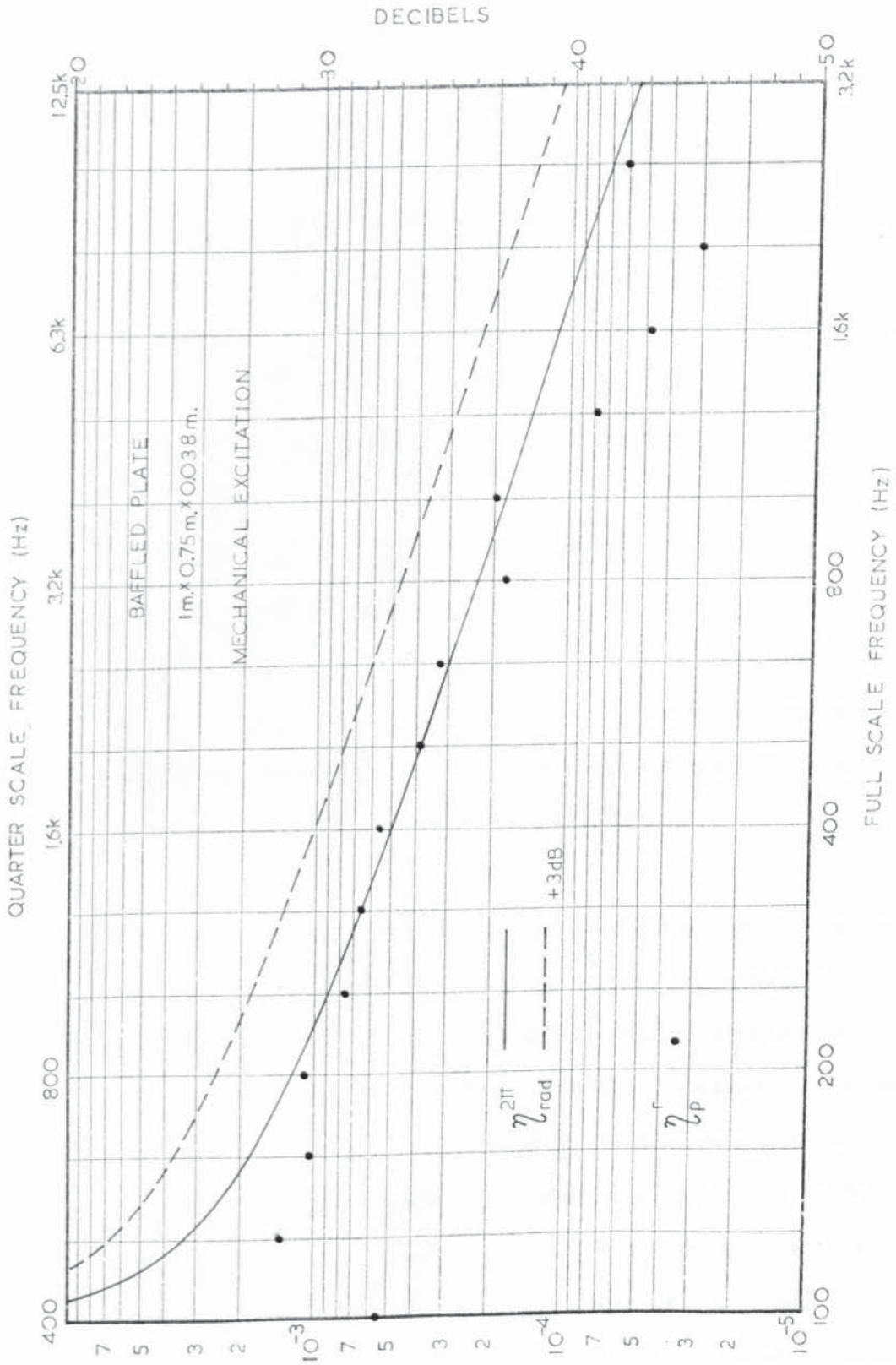
DECIBELS
20
30
40
50
12.5k
6.3k
3.2k
1.6k
800
400
200
100
3.2k
1.6k
800
400
QUARTER SCALE FREQUENCY (Hz)
FULL SCALE FREQUENCY (Hz)
BAFFLED PLATE
1m.X 0.75 m. X 0.038 m.
MECHANICAL EXCITATION
+3dB
$\eta^{2\pi}_{rad}$
η^{r}_{p}
10^{-3}
10^{-4}
10^{-5}
7
5
3
2

Figure 6.12.

Figure 6.13 shows the results of a similar experiment, using the thick plate. It has been stated that each run was repeated with different accelerometer and microphone positions and the mean value taken of the two sets of results. In this graph is shown the maximum, minimum, and mean at each frequency. The observed difference, generally less than 2 dB, is typical of all experiments and thus, only the mean value is indicated in all other results.

Results obtained from the acoustic (indirect) excitation of the baffled, thin plate are given in Figure 6.14. Again there is more scatter and the values are generally higher than those obtained from mechanical excitation. However the results are of the correct order of magnitude and they decrease in value with frequency increase, albeit with a gradient less than that predicted.

Measurements were also made over a frequency range of 100 Hz to 12.5 kHz despite the low frequency limitations which have been discussed. Figure 6.15 illustrates the frequency dependence of η_b^r over the full frequency range. The plate had fixed edges (by means of the concrete frame) and radiated from the transmission suite aperture. Again, results appear reasonable, with the coincidence peak being clearly seen. However it was felt that at the lowest frequencies there was movement from the surfaces surrounding the plate and thus radiation from the frame and the surrounding wall. This would cause an increase in the value of η_b^r.

Fig. 6.13

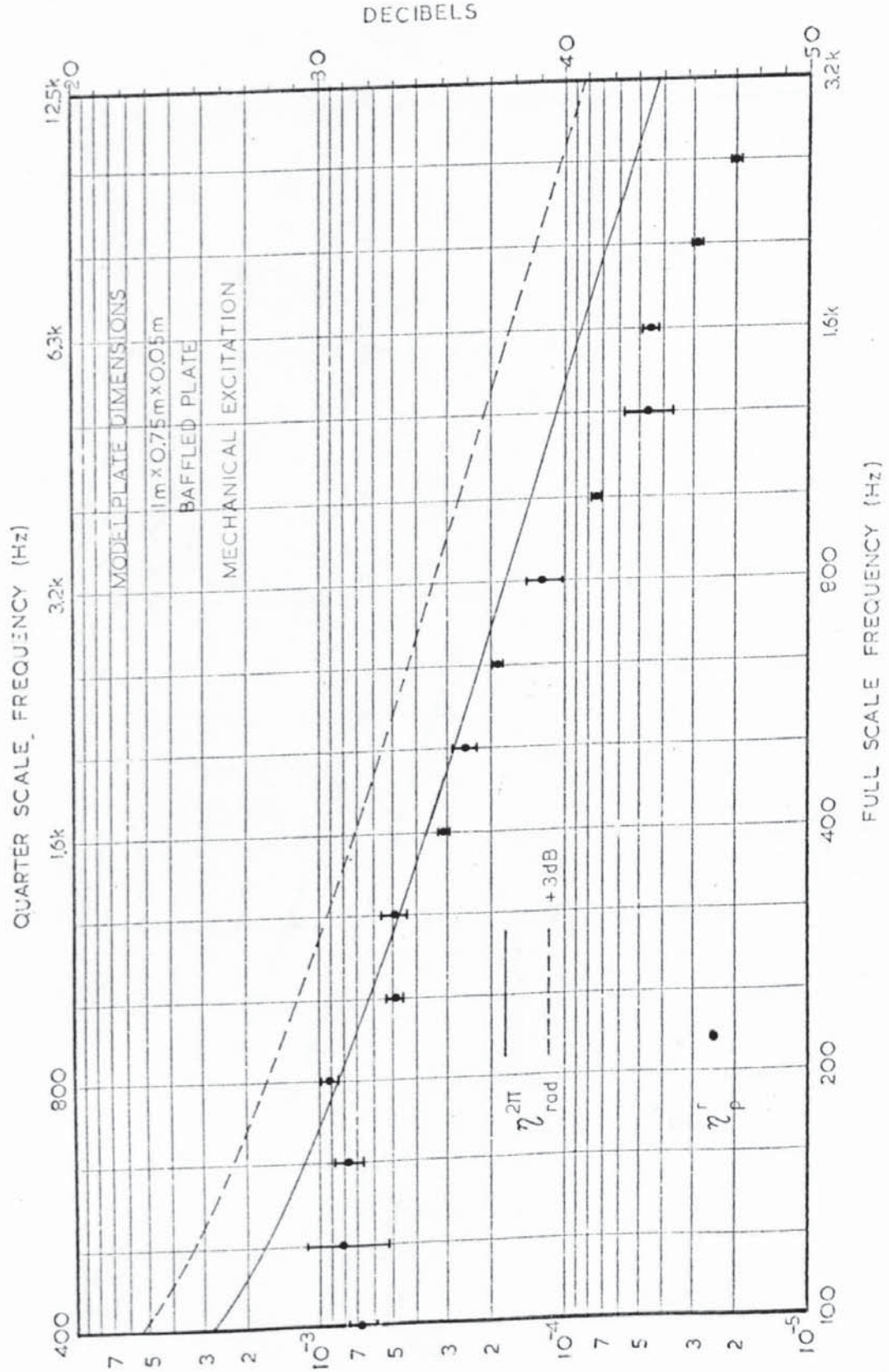
DECIBELS
20
30
40
50
12.5k
6.3k
3.2k
1.6k
800
400
200
100
3.2k
1.6k
800
400
QUARTER SCALE FREQUENCY (Hz)
FULL SCALE FREQUENCY (Hz)
MODEL PLATE DIMENSIONS
1m × 0.75m × 0.05m
BAFFLED PLATE
MECHANICAL EXCITATION
+3dB
$\eta_{rad}^{2\pi}$
η_{p}^{r}
10^{-3}
10^{-4}
10^{-5}
7
5
3
2

Fig. 6.14

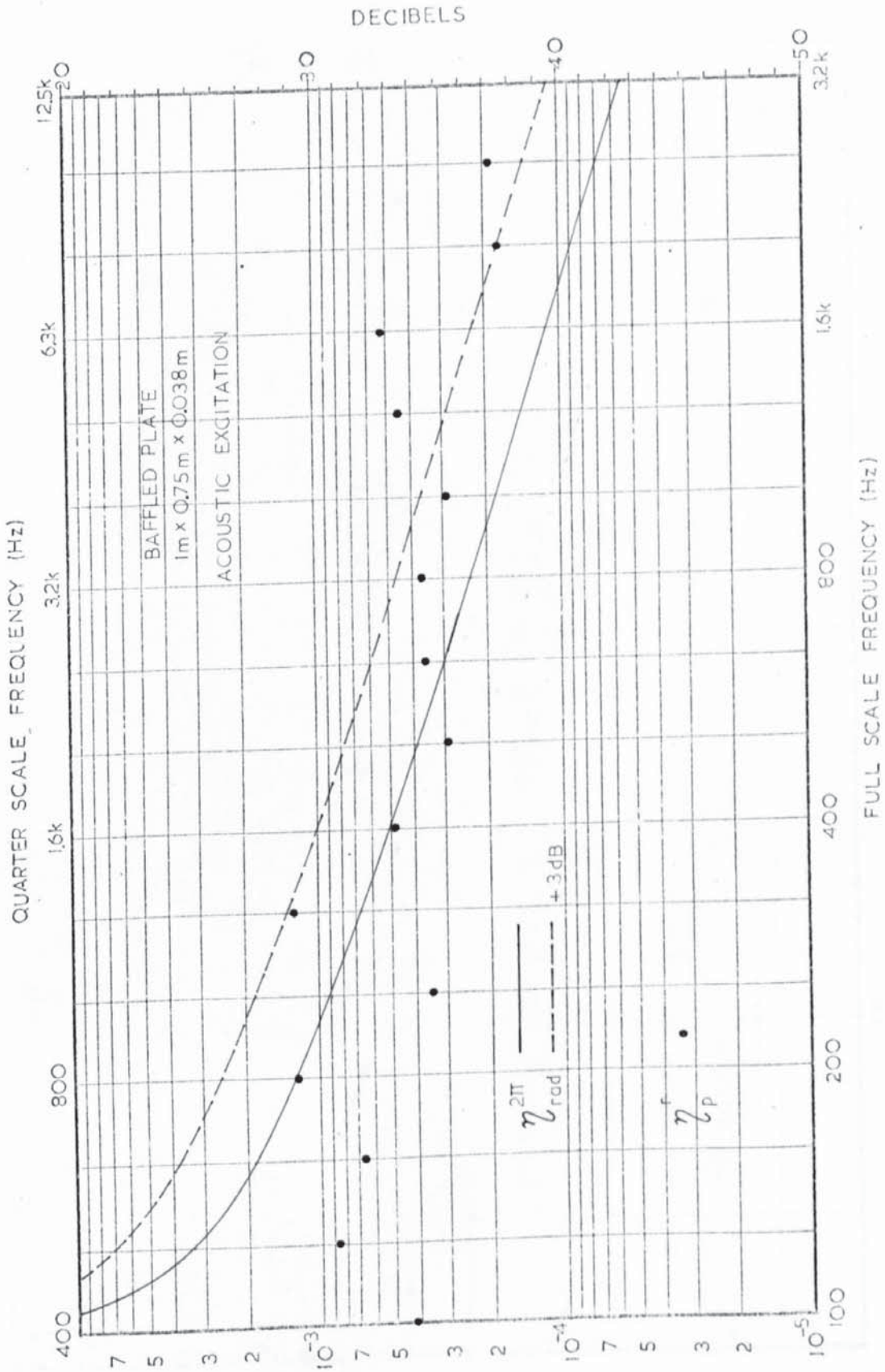
DECIBELS
20
30
40
50
12.5k
6.3k
3.2k
1.6k
800
400
200
100
3.2k
1.6k
800
400
200
100
BAFFLED PLATE
1m x 0.75m x Φ0.038m
ACOUSTIC EXCITATION
+3dB
$\eta_{rad}^{2\pi}$
η_p^r
QUARTER SCALE FREQUENCY (Hz)
FULL SCALE FREQUENCY (Hz)

Fig. 6.15

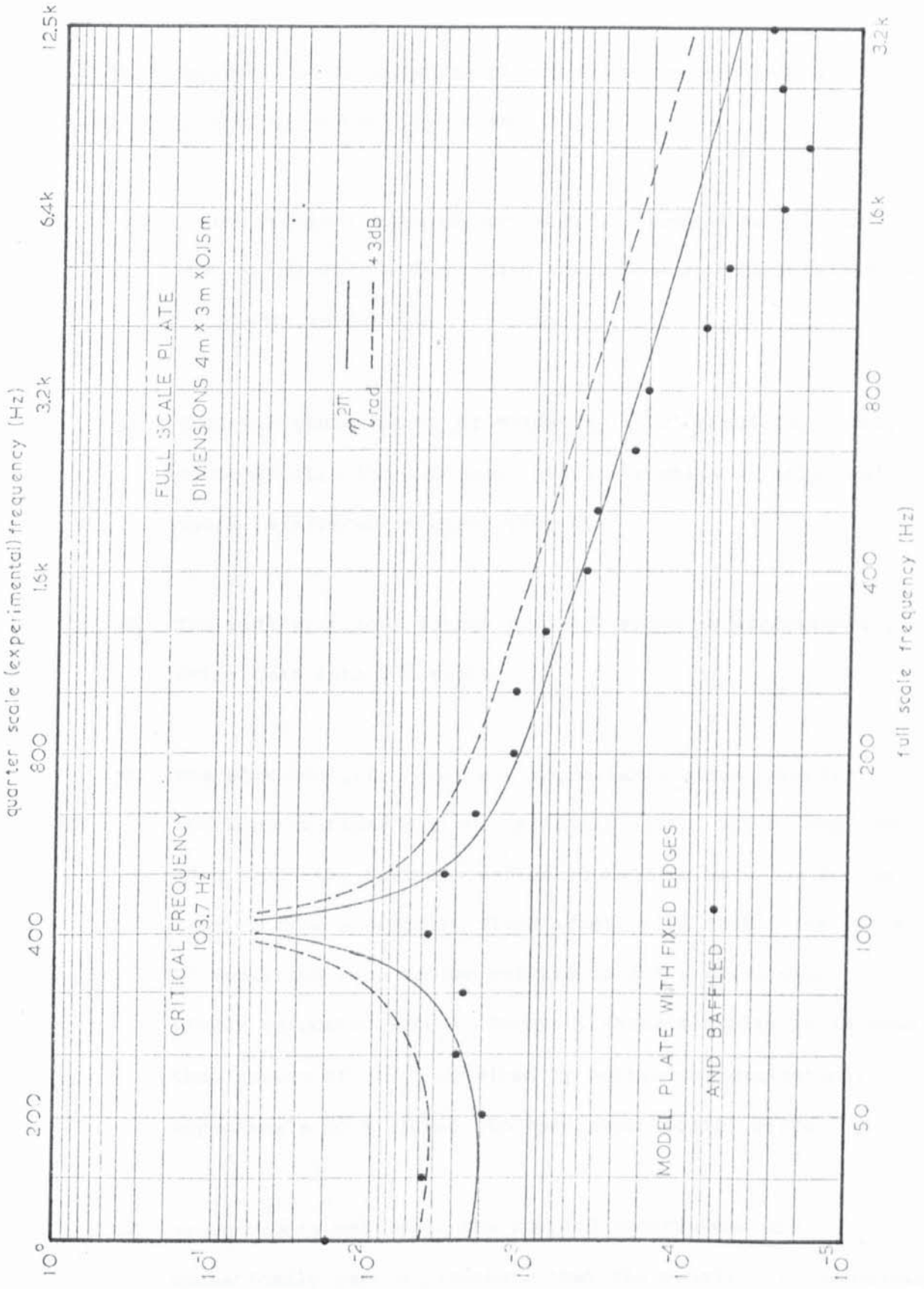
quarter scale (experimental) frequency (Hz)
full scale frequency (Hz)
12.5k
6.4k
3.2k
1.6k
800
400
200
100
50
FULL SCALE PLATE
DIMENSIONS 4m x 3m x 0.15m
$\eta_{rad}^{2\pi}$
+3dB
CRITICAL FREQUENCY
103.7 Hz
MODEL PLATE WITH FIXED EDGES
AND BAFFLED
10^{0}
10^{-1}
10^{-2}
10^{-3}
10^{-4}
10^{-5}

6.5.5 Summary

From experiments with vibrating plates within reverberant rooms the following conclusions may be drawn.

(1) Above critical coincidence, simple energy flow methods are successful in describing the radiation characteristics of plates in bending vibration.

(2) The thin plate theory of Maidanik (1962) predicts, fairly successfully, the radiation characteristics of relatively thick reinforced concrete plates.

(3) The radiation loss factor into 4π space is approximately twice that into 2π space.

(4) The edge condition does not appreciably affect results in the supercritical region. Maidanik (1962) argues that any edge condition giving a reflected bending wave (as in the case of free or rigidly fixed edges) will double the value of radiation loss factor calculated for a plate with simply supported edges. However, experimentally it is seen that values of $\eta_{rad}^{2\pi}$ obtained by mechanical excitation, approximate more closely to the lower (solid) curve.

(5) Measurements made when the coupled sub-systems are acoustically excited indicate that the equality in expression 2.56 can be said to be valid. Experimental points tend to

be higher by 2 to 4 dB than that predicted by the theory but the peaking at coincidence and the subsequent fall off with frequency is seen.

6.6 Bending wave energy ratios of concrete plates forming junctions

In conjunction with theoretical predictions of energy ratios given in section 2.5, measurements were made on quarter-scale models of cross-junctions (plate 6.8), T-junctions (plate 6.1) and corner junctions. The plates were freely suspended by nylon cord and had dimensions of 1 m x 0.75 m. The thicknesses of the plates were 0.038 m for the thin plate and 0.05 m for the thick plate.

The method of obtaining a spatial average of the mean square acceleration amplitude and from it the bending wave energy is the same as described in section 6.5.3.2. The apparatus is illustrated in Figure 6.16.

For the configurations illustrated it might be argued that bending wave energy will be generated on the secondary plates by means of two transmission paths.

(1) Power will flow through the junction from the mechanically excited primary plate.

(2) The primary plate will radiate sound energy which may impinge upon the other plates.

Fig. 6.16

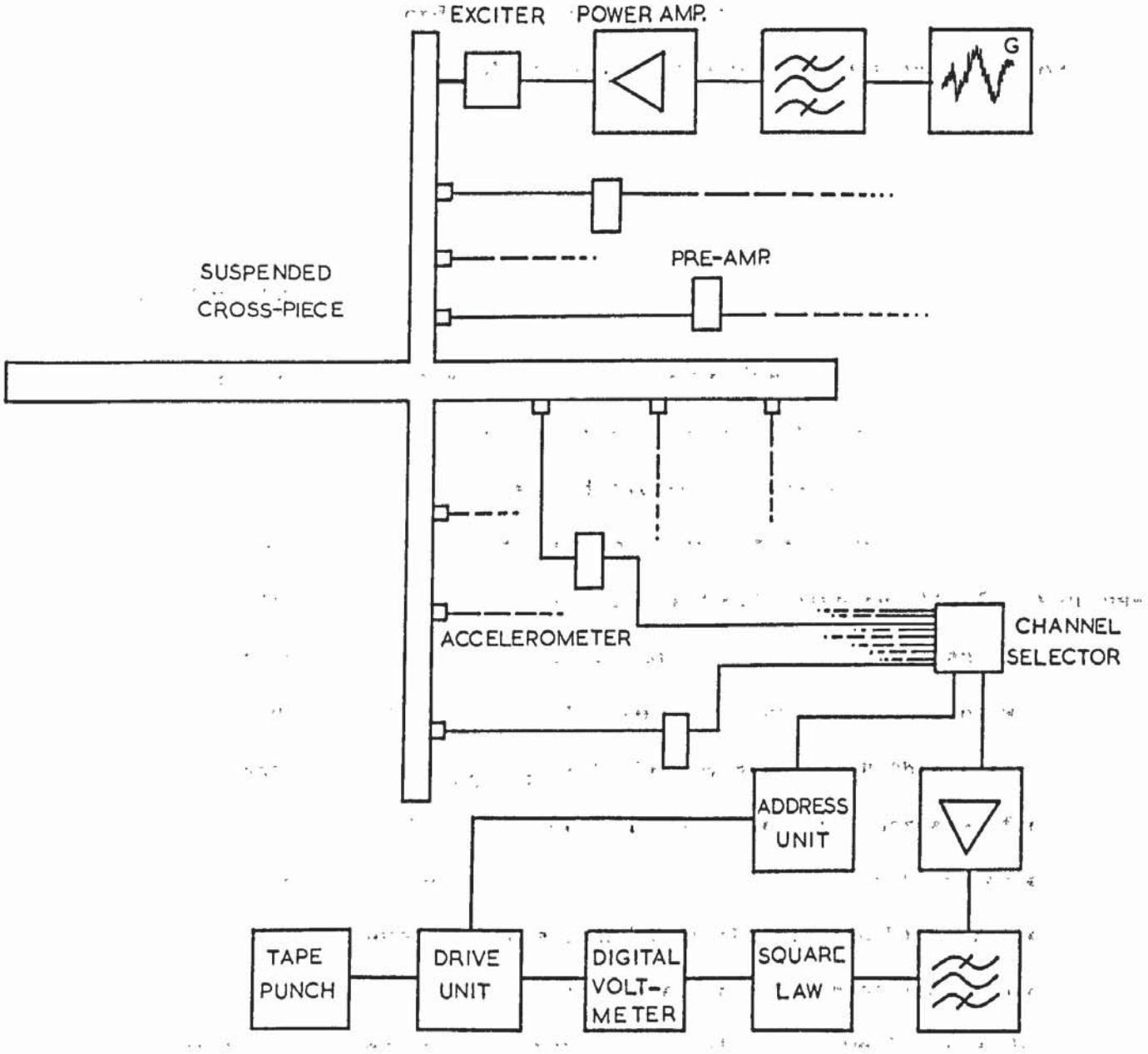

Measurement of bending wave energy ratio of a cross junction.

However the second transmission path is very weak compared with the first, since the coupling between the plate modes and the room (laboratory) modes is small.

6.6.1 Results

The comparison between theory and experiment is given in Figures 6.17 to 6.22. The nomenclature is such that the primary or mechanically excited plate (indicated by the arrow) is termed plate 1, the plate at right angles to it as plate 2, and the plate collinear with it as plate 3. Figures 6.17 and 6.18 give results for a cross-junction where the thick plate and thin plate are mechanically excited, respectively. In Figure 6.17 measurement agrees with theory in that the ratio E_{b3}/E_{b1} is higher by about 3 dB than the ratio E_{b2}/E_{b1}. Also there is a general decrease with increased frequency. In Figure 6.18 the correlation is not so obvious but the experimental results give approximate agreement in the mid and high frequency range. It is seen however in these, and the remaining figures, that in the low frequencies experimental values lie well below those predicted. This is not unexpected since, in this region, modal density (per bandwidth) is low and the assumption of reverberant bending wave fields becomes tenuous.

Figures 6.19 and 6.20 give the results for a T-junction where the thick plate is driven. The bending wave field on each plate was sampled by seven accelerometers and the experiment repeated for another set of accelerometer positions. Indicated is the maximum, minimum, and mean of the two runs. It is seen that at low frequencies

Fig. 6.17

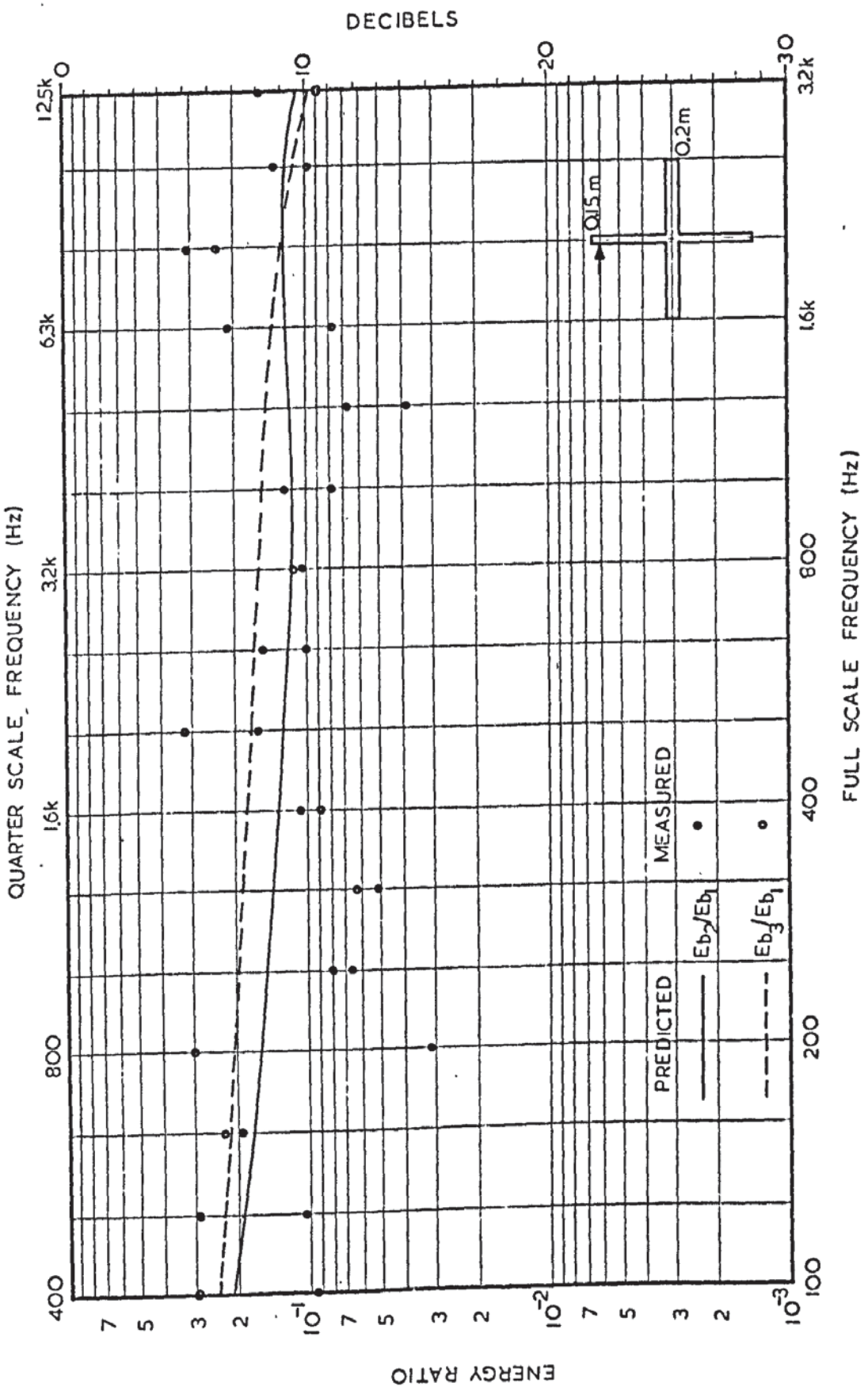
DECIBELS
0
10
20
30
12.5k
6.3k
3.2k
1.6k
800
400
200
100
3.2k
1.6k
800
400
0.2m
0.15m
MEASURED
PREDICTED
E_{b_2}/E_{b_1}
E_{b_3}/E_{b_1}
QUARTER SCALE FREQUENCY (Hz)
FULL SCALE FREQUENCY (Hz)
ENERGY RATIO
10^{-1}
10^{-2}
10^{-3}

Fig. 6.18

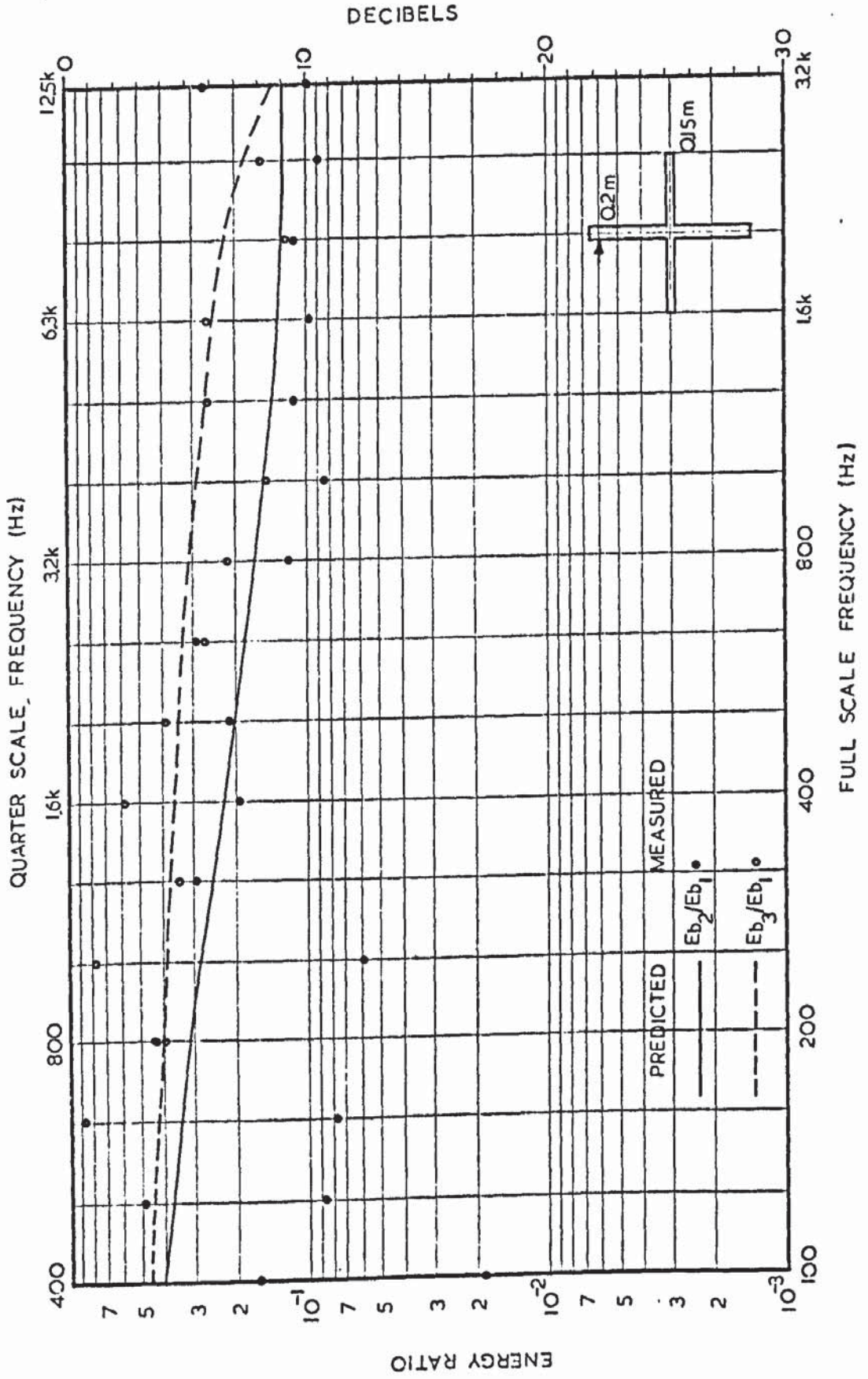
DECIBELS
0
10
20
30
125k
63k
32k
16k
800
400
200
100
32k
16k
800
400
200
100
0.2m
0.15m
PREDICTED
MEASURED
Eb_2/Eb_1
Eb_3/Eb_1
ENERGY RATIO
10^{-1}
10^{-2}
10^{-3}
QUARTER SCALE FREQUENCY (Hz)
FULL SCALE FREQUENCY (Hz)

Fig. 6.19

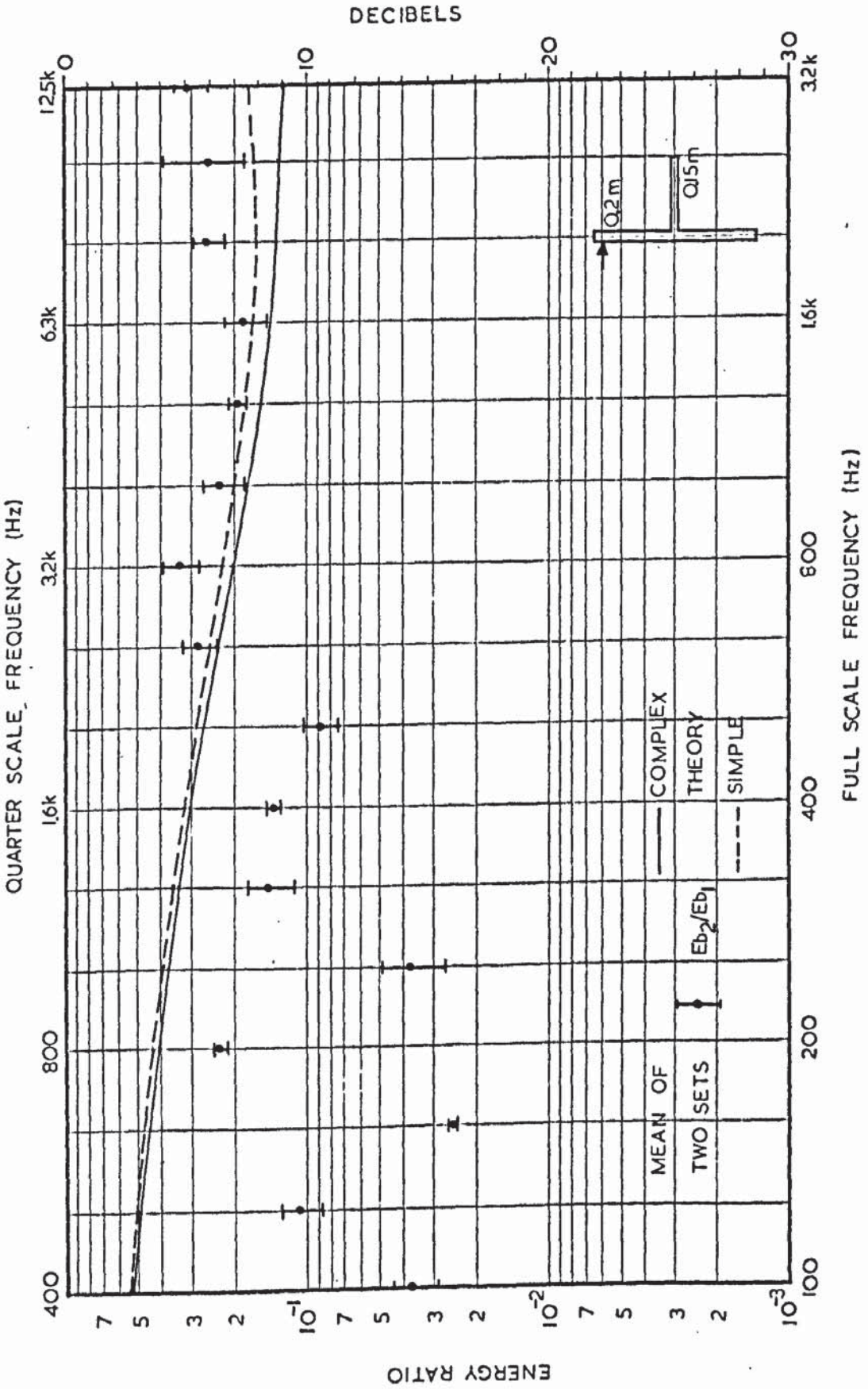
DECIBELS
0
10
20
30
125k
63k
32k
16k
8000
4000
32k
16k
800
400
200
100
QUARTER SCALE FREQUENCY (Hz)
FULL SCALE FREQUENCY (Hz)
ENERGY RATIO
10⁻¹
10⁻²
10⁻³
0.2m
0.15m
COMPLEX
THEORY
SIMPLE
MEAN OF TWO SETS
Eb2/Eb1

Fig. 6.20

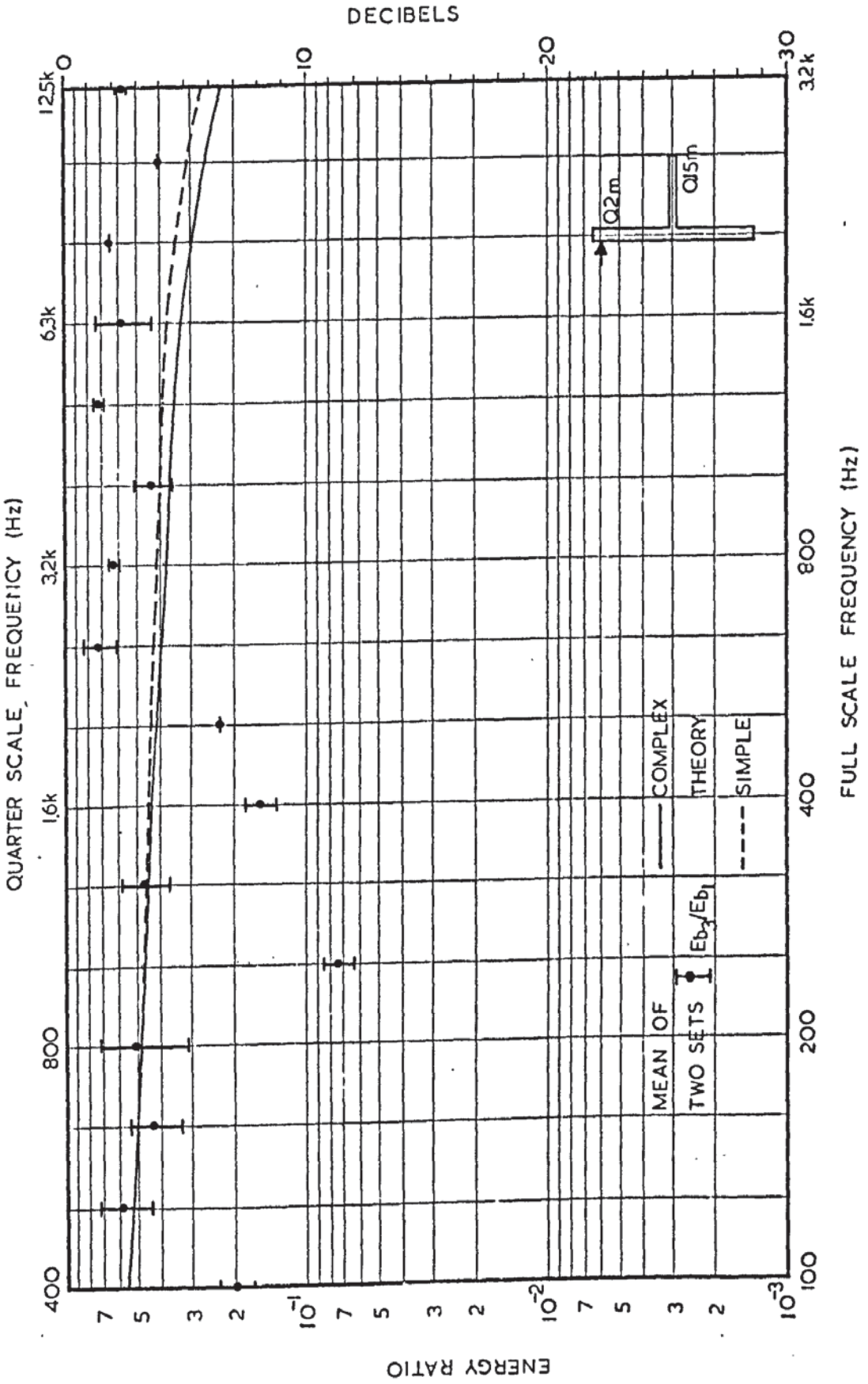
DECIBELS
0
10
20
30
12.5k
6.3k
3.2k
1.6k
800
400
200
100
32k
16k
800
400
200
100
QUARTER SCALE FREQUENCY (Hz)
FULL SCALE FREQUENCY (Hz)
ENERGY RATIO
10⁻¹
10⁻²
10⁻³
7
5
3
2
Q2m
Q5m
COMPLEX
THEORY
SIMPLE
MEAN OF TWO SETS
Eb3/Eb1

the reproducibility is within 3 dB while at the high frequencies this improves, on average, to 2 dB; many points giving less than 1 dB difference in results. The scatter in experimental measurement exceeds the relatively subtle differences observed in the predictions from simple theory and the more complex theory (section 2.6). In both cases the theory can only be said to describe observations at frequencies above 2 kHz (or 500 Hz on the full scale frequency). However the observed values of E_{b3}/E_{b1} give good agreement at several points in the low frequency range.

Figures 6.21 and 6.22 illustrate most clearly the limitations of the theory at low frequencies. Indeed, Figure 6.21 which shows results for a T-junction in which the cantilevered plate is excited, indicates a regular increase in measured energy ratio up to a frequency of 1.6 kHz where a plateau is attained, corresponding (within 3 dB) to the predicted curve. The result for a corner junction, (Fig 6.22) illustrates the same trend.

To summarise, the correlation between experiment and theory for transmission losses through junctions is not as good as that for the radiation loss factor measurements. Agreement can only be said to occur at frequencies above 1.6 kHz quarter-scale frequency. The predictions offered by the theories described in sections 2.5 - 2.8 and Chapter 4, lie within relatively narrow limits; well within the limits set by experimental scatter. However, in the mid and high frequencies, agreement between theory and experiment is often within 2 or 3 dB.

Fig. 6.21

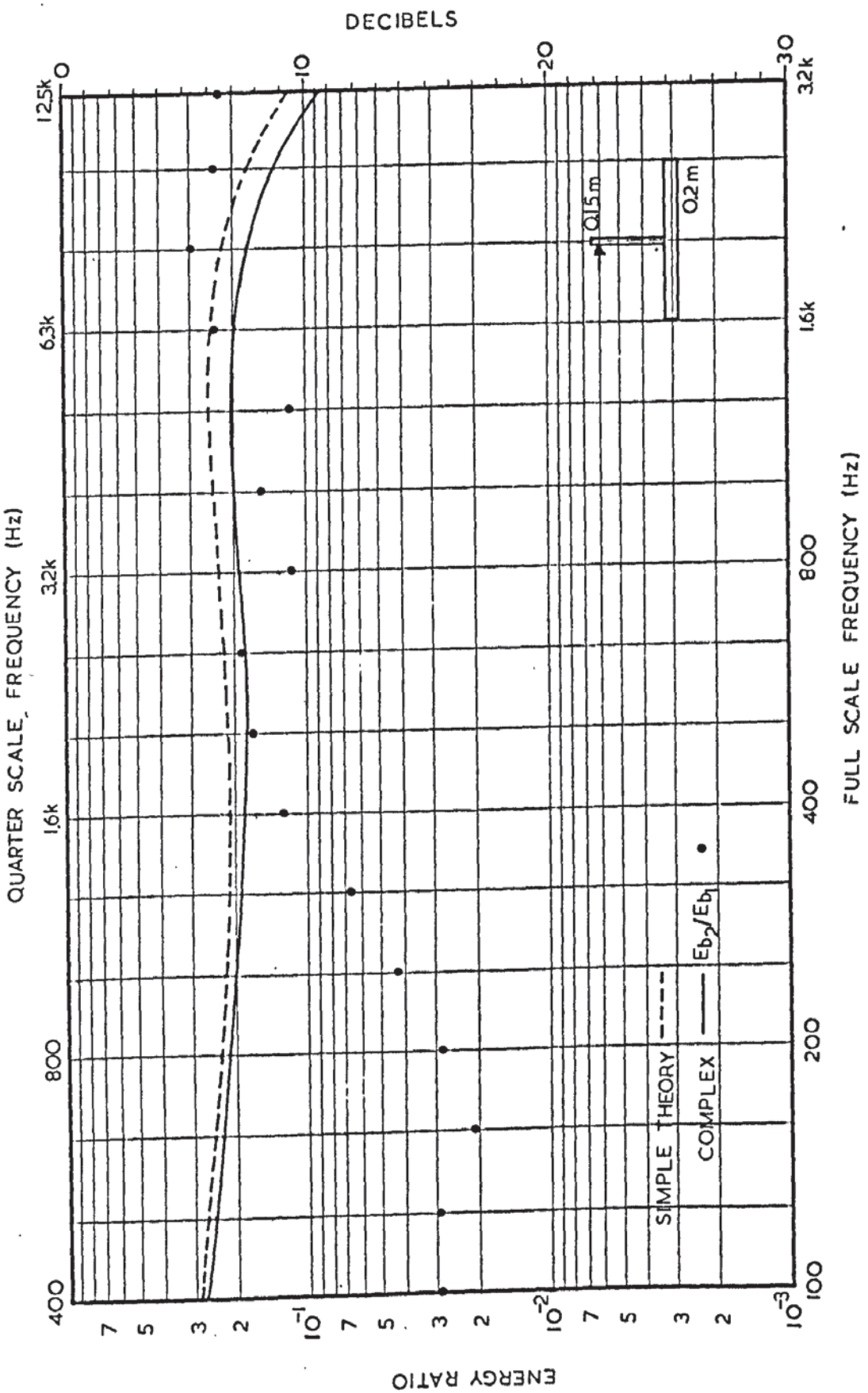
DECIBELS
0
10
20
30
12.5k
6.3k
3.2k
1.6k
800
400
32k
16k
800
400
200
100
QUARTER SCALE FREQUENCY (Hz)
FULL SCALE FREQUENCY (Hz)
0.15m
0.2m
SIMPLE THEORY
COMPLEX
E_{b_2}/E_{b_1}
ENERGY RATIO
7
5
3
2
10^{-1}
10^{-2}
10^{-3}

Fig. 6.22

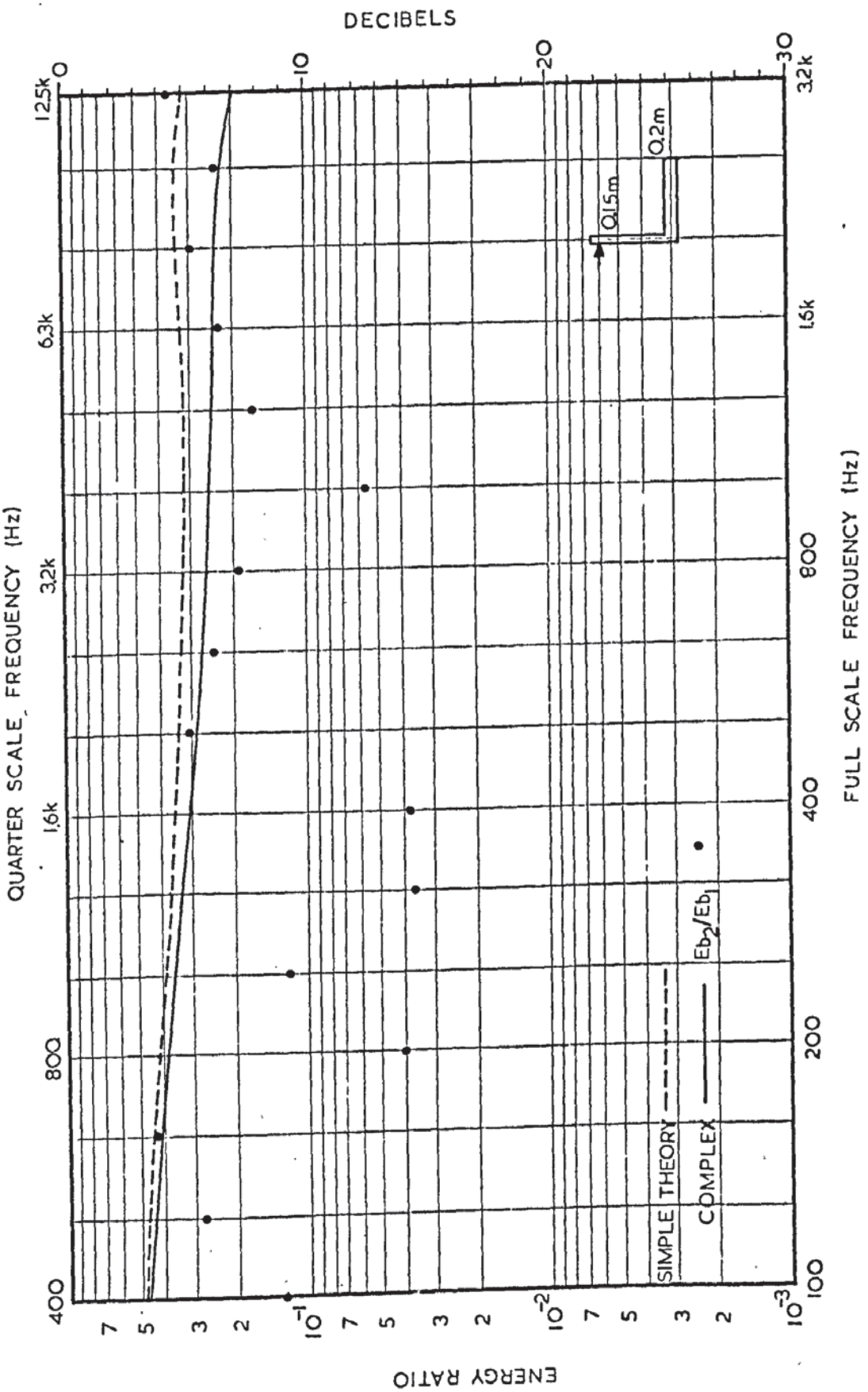
DECIBELS
0
10
20
30
125k
63k
32k
16k
8000
4000
32k
16k
8000
4000
2000
1000
Q15m
Q2m
QUARTER SCALE FREQUENCY (Hz)
FULL SCALE FREQUENCY (Hz)
ENERGY RATIO
SIMPLE THEORY
COMPLEX
Eb2/Eb1

6.6.2 Increase of loss factor by cladding

To investigate the direct and indirect effect of increase of loss factor of plates forming a junction, it was necessary to derive a plate cladding having the following characteristics.

(1) The material is required to have a low bending stiffness so as not to contribute to the stiffness of the plate.

(2) It should be highly dissipative.

Dry sand possesses both properties but problems arise in application to the plate surfaces, which are often vertical. The cladding finally adopted was that of sand, bound in the bitumastic material "Aquaseal". The sand is mixed with the heated aquaseal (in a ratio of approximately 4:1) and is then spread upon the plate surface to a depth of 12-13 mm. On setting, the cladding remains malleable but adheres well to the surface (plate 6.7). Its adhesion is increased by first painting a thin layer of aquaseal on the concrete surface.

The efficiency of the cladding is at the expense of an appreciable increase in weight of the concrete plate. The density of the cladding is measured as 1.7×10^3 Kg/m^3. Thus a layer on the thin plate results in an increase of mass of 23% while a thick plate, when clad, increases in weight by 17%. In measurement therefore a corrected plate mass was incorporated into the bending wave energy calculations.

Figure 6.23 illustrates the loss factor of an unclad and clad concrete plate (dimensions 1 m x 0.75 m x 0.038 m) which is freely suspended.

Fig. 6.23

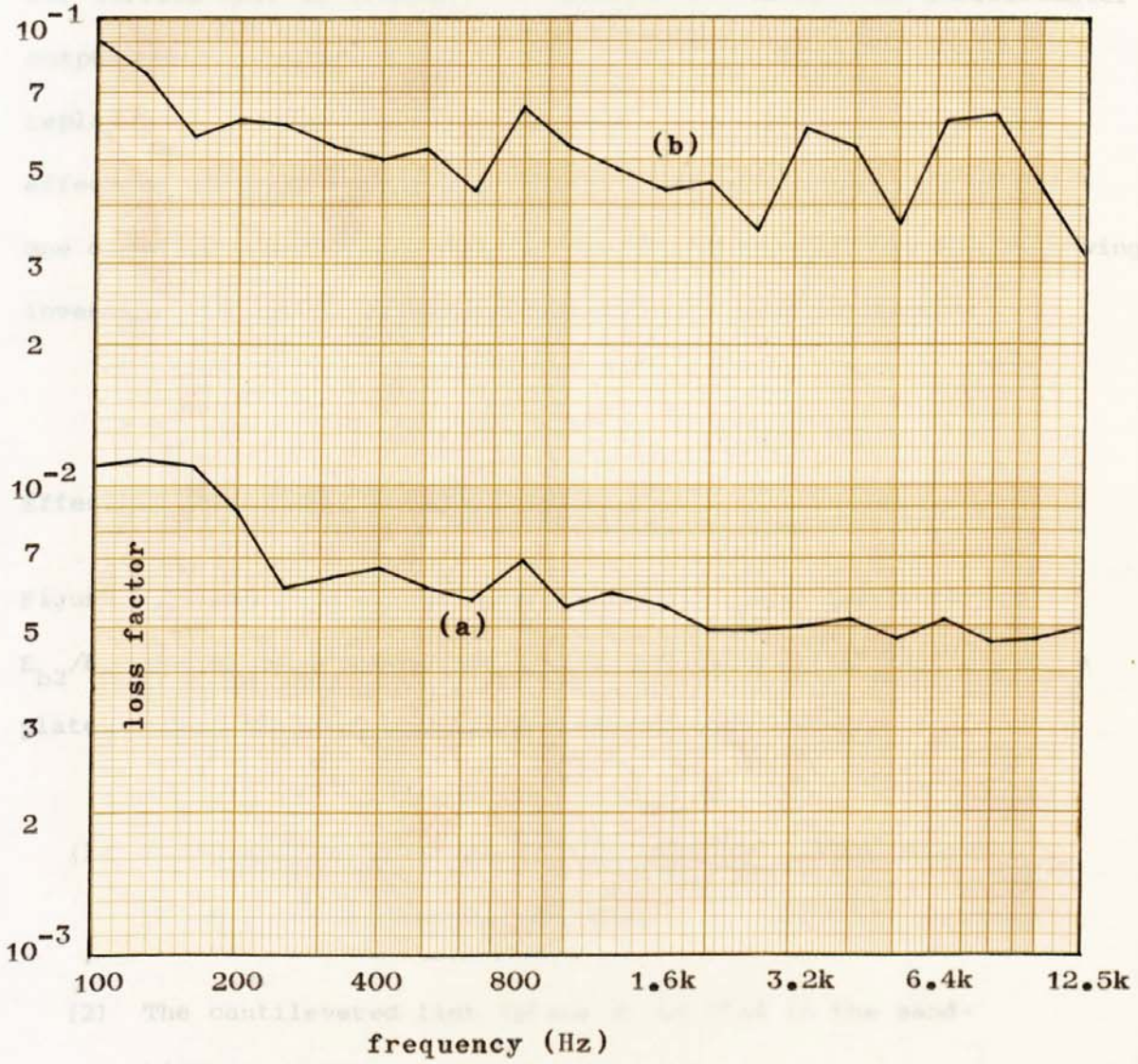

Loss factor of a freely suspended thin concrete plate.

(a) Clean plate.

(b) Clad plate.

One surface only is covered. To measure the decay, the accelerometer outputs were recorded on magnetic tape or high speed tape and replayed at a lower speed for analysis. The cladding causes the effective internal loss factor of the plate to increase by almost one order of magnitude. This was thought sufficient for the following investigation of the effects of increase in this parameter.

6.6.3 Effect of loss factor on energy ratio

Figure 6.24 and Figure 6.25 show the bending wave energy ratios E_{b2}/E_{b1} and E_{b3}/E_{b1} respectively, for a T-junction of thin concrete plates. Four cladding configurations are considered.

(1) Measurements are taken of the bare T-junction where plate 1 is mechanically excited.

(2) The cantilevered limb (plate 2) is clad in the sand-bitumen matrix.

(3) Plate 3 only is clad.

(4) Both plate 2 and 3 are treated.

From the results, the following observations can be made.

(1) The measured energy ratio E_{b2}/E_{b1} is reduced by an amount ranging from 3 dB at the low frequencies, up to 8 dB at the higher frequencies. The reduction is also appreciable for the ratio E_{b3}/E_{b1}. It ranges from 3 dB at low

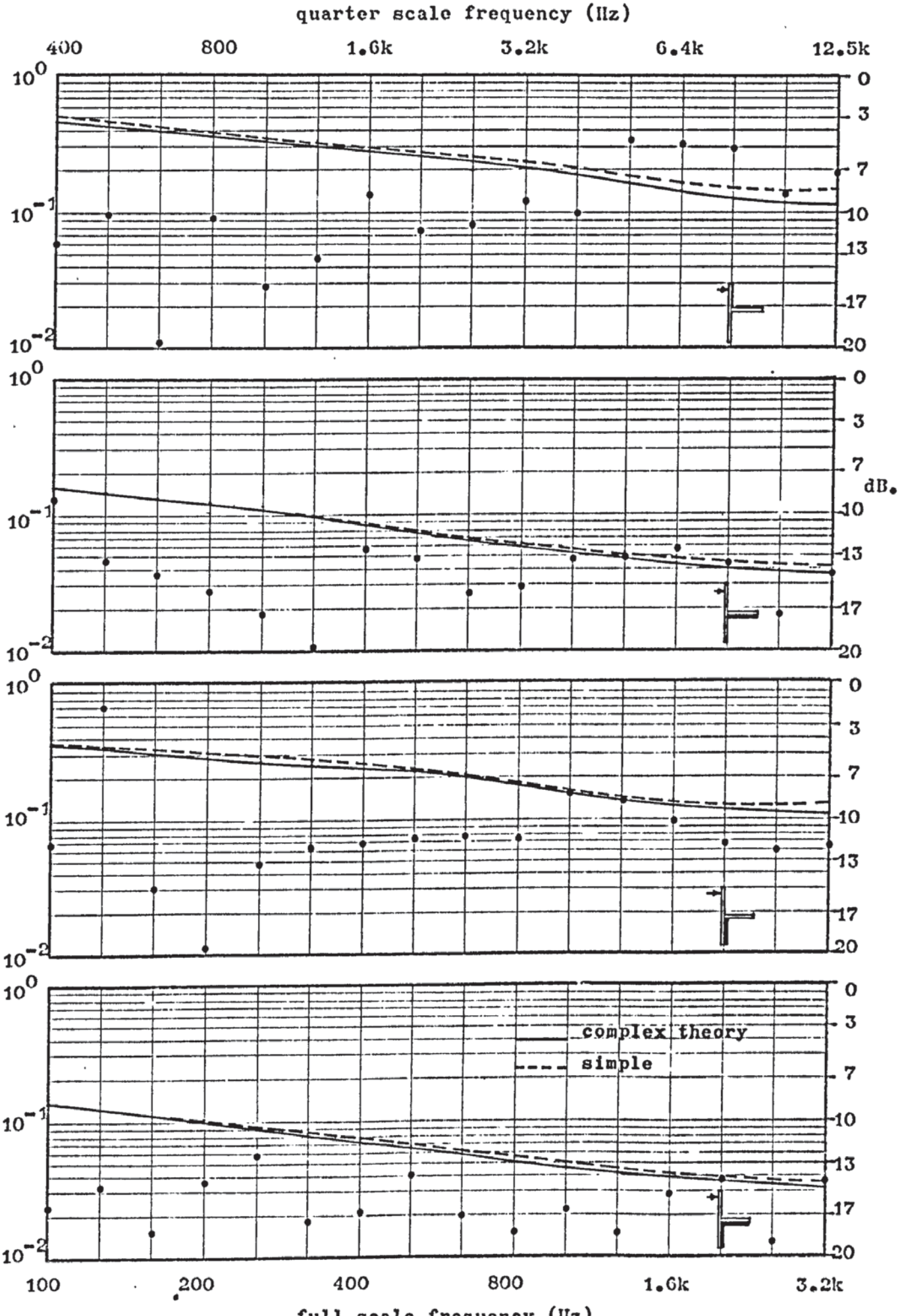

Energy ratio Eb_2/Eb_1 for a T-junction of reinforced concrete with various cladding configurations.

Fig. 6.24

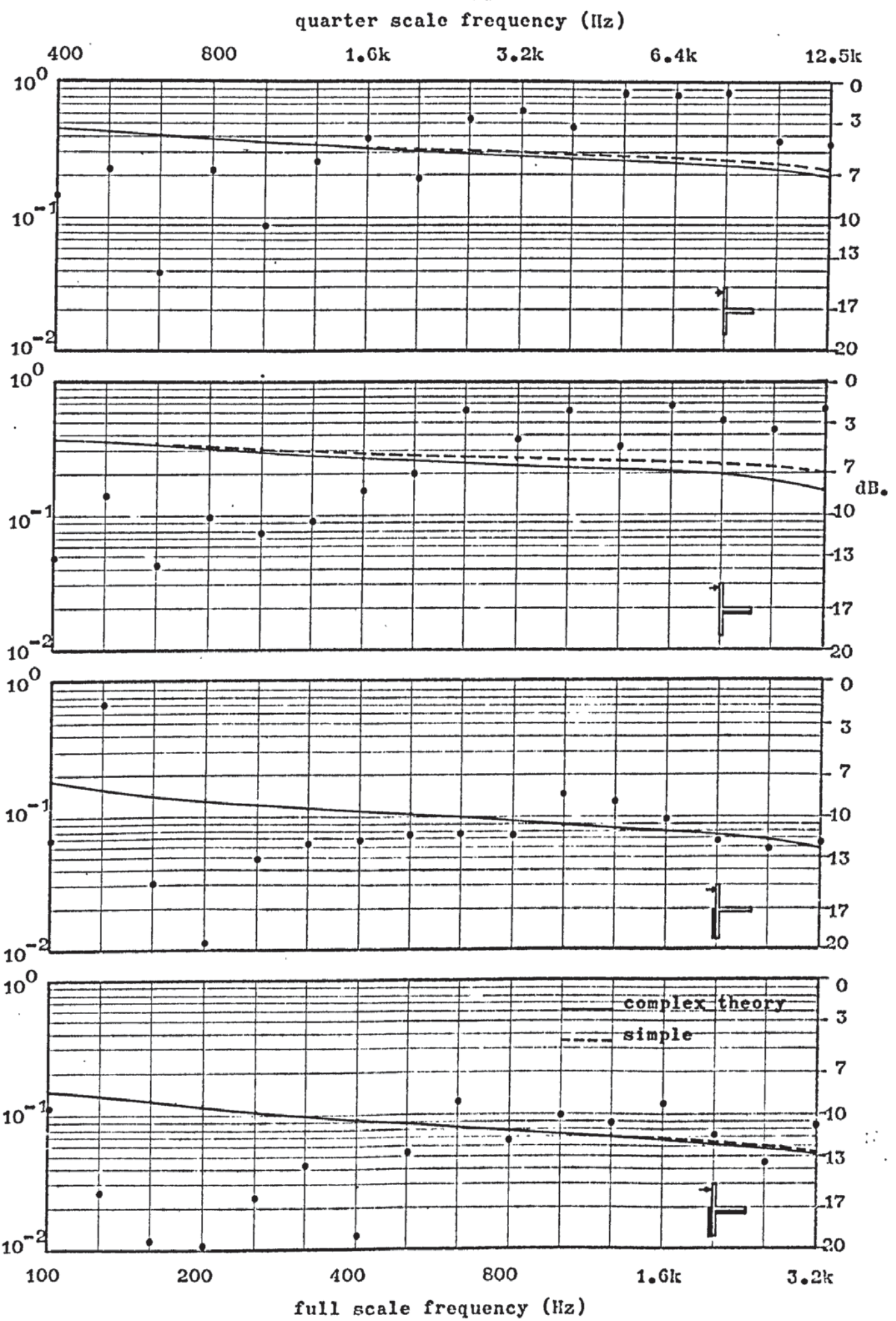

Energy ratio Eb_3/Eb_1 for a T-junction of reinforced concrete with various cladding configurations.

Fig. 6.25

frequencies, to 9 dB at the higher frequencies. The theory gives a predicted reduction in E_{b2}/E_{b1} of 4 dB at 400 Hz, increasing to 5 dB at 12.5 kHz. For the ratio E_{b3}/E_{b1}, the reduction ranges from 3.5 dB at 400 Hz to 5 dB at 12.5 kHz.

(2) Attempts were made to gauge the effect of indirect damping, i.e. the reduction in E_{b2}/E_{b1} when plate 3 only is dad, and the reduction in E_{b3}/E_{b1} when plate 2 only is clad. It is seen that there is an appreciable decrease in E_{b2}/E_{b1} at the high frequencies. Above the frequency of 1.6 kHz the decrease ranges from 0 dB to 4 dB with several points giving higher reductions. The scatter at low frequencies does not allow general comment to be made. It is seen that theory predicts a reduction in E_{b2}/E_{b1} of less than 1 dB. Similarly E_{b3}/E_{b1} is observed to reduce in value, but by the smaller amount of 1-2 dB. This is more in agreement with theory.

(3) Damping of both plate 2 and plate 3 results in appreciable decreases in E_{b2}/E_{b1} and E_{b3}/E_{b1}. The reduction in E_{b2}/E_{b1} at mid and high frequencies, results from both the direct and indirect damping. It has a value of approximately 3 dB at low frequencies, up to 10 dB at the high frequencies. The reduction in E_{b3}/E_{b1} is little affected by damping of plate 2.

From Figure 6.24 and Figure 6.25 the following conclusions are made.

(1) An increase of a magnitude in the loss factor of a plate results in a reduction in bending wave energy ratio of about 6 dB. A plate, at right angles to the source plate, gives a slightly higher reduction than a plate collinear with it.

(2) The decrease in ratio, due to indirect damping, is appreciable only on a plate at right angles to the source plate. At mid and high frequencies, the value is 2-3 dB. The influence of indirect damping on the energy ratio of a plate, collinear with the source plate, is slight.

(3) Direct and indirect damping has a reduced effect at lower frequencies.

6.7 Summary

Quarter-scale model experiments on the sound radiating characteristics of concrete plates and the vibrational energy flow between plates forming structural junctions have shown that there is reasonable agreement between observation and theoretical prediction at the mid and high frequencies. This appears to underline the importance of the vibrational fields in each sub-system having sufficiently high modal densities. Only then can simple power flow techniques be used

with success.

With this in mind a more complex structural system is now considered. Namely that of two rectangular rooms, connected at one corner.

CHAPTER 7

SOUND TRANSMISSION BETWEEN ROOMS

7.1 Introduction

In the investigation of vibrational energy flow between sub-systems, the coupling between plates and that between a plate and the surrounding air have been assessed separately, both theoretically and experimentally. However, when dealing with more complex models, which give a closer approximation to noise transmission in real building structures, it becomes necessary to consider both processes as occurring simultaneously. Thus, as described in Chapter 1, airborne sound impinging upon a wall, will excite it into bending vibration. The wall vibration results in radiation of sound and in the generation of vibrational fields on connected walls which may also radiate energy. The transmission path described is typical of many that contribute to the resultant transfer of noise from one room to another.

The system now considered is that of two rectangular rooms which have a common junction (Fig 7.1). This is a simple approximation to a pair of rooms in a two or three dimensional array of rooms such as occur in a block of flats. The source and receiver room are seen to be on different floor levels and are not directly over each other. Therefore, in this case, any transmission of sound must be by an indirect path.

An important difference between this model and a real situation

Fig. 7.1

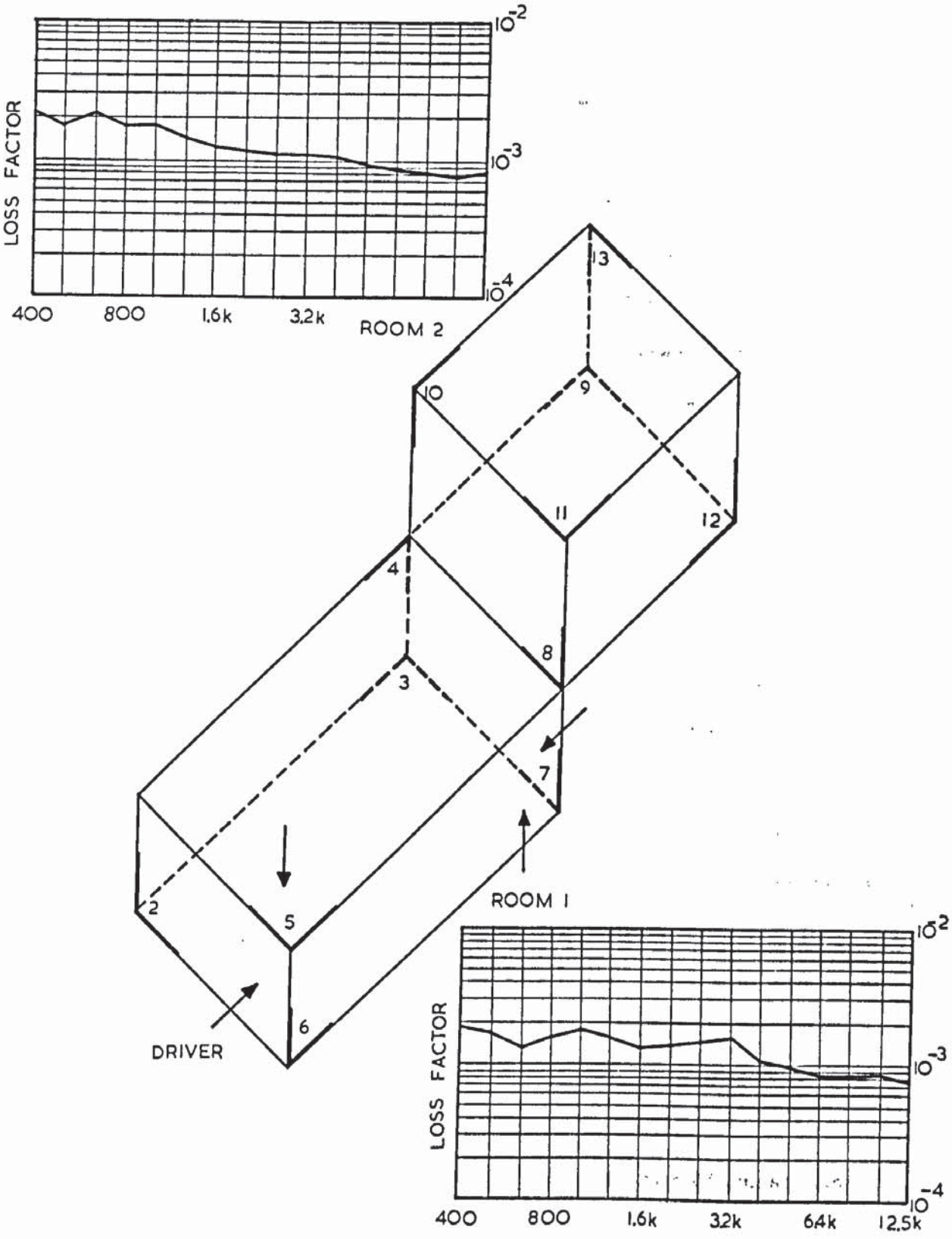

Plate nomenclature for the coupled rooms. The loss factor of each room is also given.

existing in a block of flats, is that many more plates, belonging to adjacent rooms, would be involved in the transfer and dissipation of the vibrational energy. However, the discussion is simplified by considering the two rooms as mechanically isolated, except from each other. The simplicity of the model will allow the assessment of the noise transmission when the source room has steady-state loudspeaker excitation and when some of the plate elements are mechanically driven.

7.2 Energy balance equations

As shown in Chapter 2, each coupled sub-system in a system which receives steady-state excitation is assumed to have vibrational energy flowing in, either directly (such as from a loudspeaker in the room volume), or from connected sub-systems; some energy is internally dissipated and some flows out to the same connected sub-systems. Again, as in section 2, for each plate or air volume, an energy balance equation results in which the L.H.S sums the power internally dissipated or lost to the surrounding plates etc, and the R.H.S sums the power input.

The problem is more complicated than those so far discussed and the following simplifying assumptions are made.

(1) Figure 7.1 shows that the plates can be considered as floor or wall areas, the latter being thinner. Thus, plates 3, 5, 9, and 11 are assumed thick (i.e. 0.2 m full scale dimension) and all other surfaces are

assumed thin. Use is also made of symmetry. Plate 6 and its vibrational field is assumed identical to that of plate 4. Similarly, plate 12 is equal to plate 10 (i.e. 0.15 m full scale dimension).

(2) The internal loss factor of each plate is assumed the same and is also assumed independent of frequency.

(3) Electromagnetic drivers are assumed only to excite plates into bending vibration. Again, the bending modes only are assumed efficiently coupled to the room modes.

(4) As well as generating a pressure wave field within the rooms, the vibrating plates will also radiate outwards. There is therefore the possibility that another transmission path existing between room 1 and room 2. This path is ignored in the following discussion, and it is seen later that it can be eliminated in experimental verification.

(5) A more complex matrix results when longitudinal and transverse components are considered, but in order to simplify the description, the bending wave fields only are considered. Along with graphs of experimental results, predicted values using the complex theory (solid line) and simple theory (dotted line) are given.

(6) The coupling between plate and air η_b^r is assumed to be the radiation loss factor $\eta_{rad}^{2\pi}$. The coupling between

the air and plate η_r^b is calculated using the equation,

$$\eta_r^b = \frac{n_b}{n_r} \eta_{rad}^{2\pi} \qquad \ldots\ldots\ldots 7.1$$

where n_b/n_r is the ratio of modal density to room modal density.

Thus, the pair of rooms given in Figure 7.1 has an associated power flow diagram, given in Figure 7.2. It shows that power flow from room 1 to room 2 is assumed possible only through the coupling of plates 5 and 7 to plates 8 and 9. In experiment, room 1 can be acoustically excited or plates 2, 3, 5, and 7 can be mechanically driven. Assuming the former situation, the energy balance equation for room 1 (air volume) is given as,

$$E_{r1}(\eta_1 + 2(\eta_1^{2b} + \eta_1^{3b} + \eta_1^{4b})) =$$

$$E_{2b}\eta_{2b}^1 + E_{3b}\eta_{3b}^1 + 2E_{4b}\eta_{4b}^1 + E_{5b}\eta_{3b}^1 + E_{7b}\eta_{2b}^1 + \prod_{acoust.}$$

$$\ldots\ldots\ldots 7.2$$

The room loss factor η_1 is shown on Figure 7.1, along with that of room 2. The values were calculated from reverberation time measurements at five microphone positions in model rooms.

Similarly, when a plate is mechanically driven (such as plate 2) the energy balance equation becomes,

$$E_{2b}(\eta_b + \eta_{2b}^{3b} + 2\eta_{2b}^{4b} + \eta_{2b}^{5b} + 2\eta_{2b}^1) =$$

$$E_{3b}\eta_{3b}^{2b} + 2E_{4b}\eta_{4b}^{2b} + E_{5b}\eta_{5b}^{2b} + E_1\eta_1^{2b} + \prod_{mech2} \qquad \ldots\ldots\ldots 7.3$$

Fig. 7.2

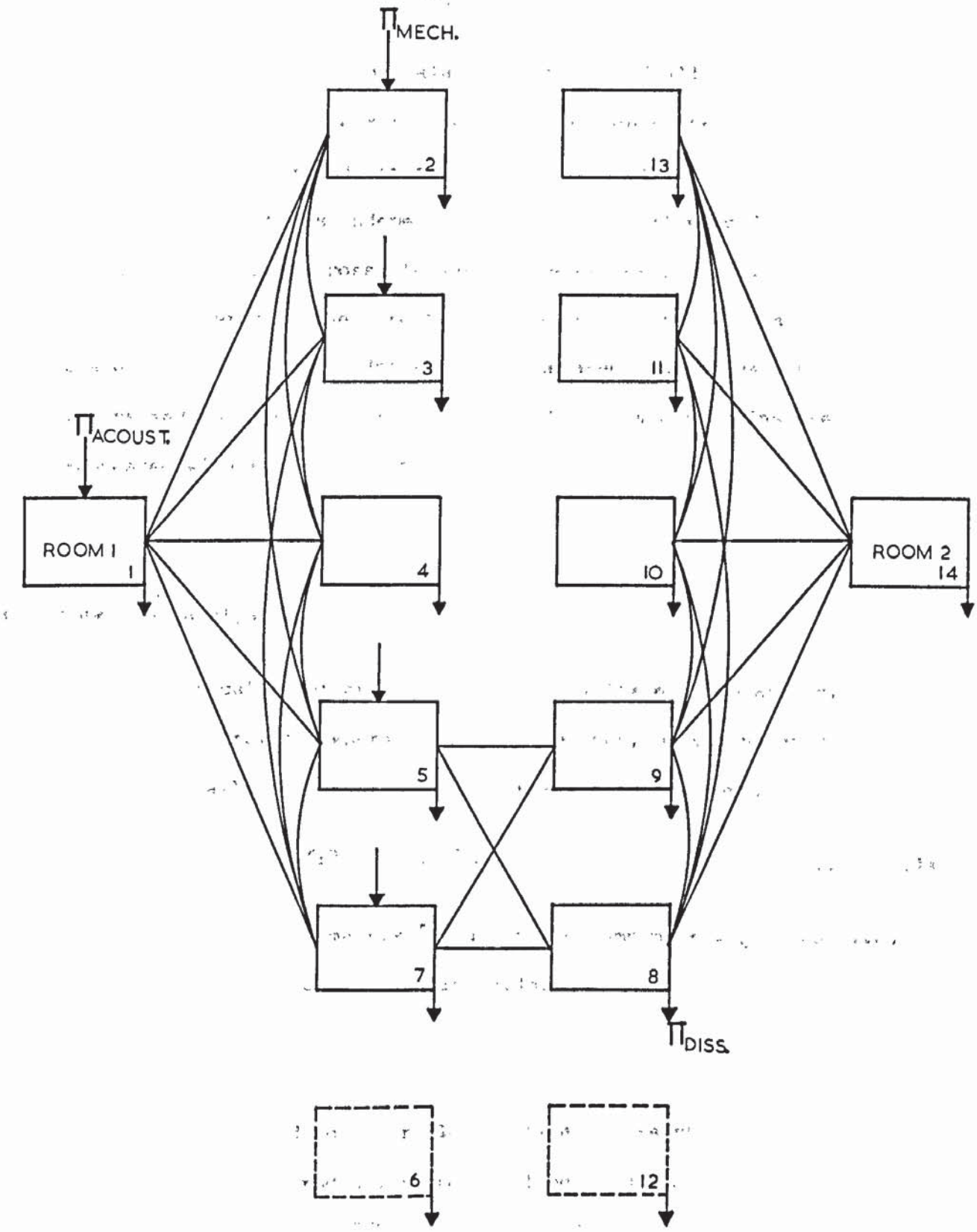

Power flow diagram for two coupled rectangular rooms.

By this method, the energy balance equations of all sub-systems, whether directly or indirectly excited, are generated. As described in Chapter 2, the steady-state energy levels of each sub-system will be expressed in terms independent of the power flowing directly into the system. This is possible when all energies are divided by the generated energy in the directly excited sub-system. Thus, when plate 2 is mechanically driven, the generated bending wave energy is assumed to have unit value and all other plate energies are expressed with respect to it.

7.3 Numerical analysis

In the numerical solution of the set of simultaneous equations, which result from the energy balance equations, matrix notation is used. Initially the equations are expressed in the form,

$$[A]\,[E] = [o] \qquad \ldots\ldots\ldots 7.4a$$

where the coefficient matrix [A] and the column matrix [E] are given in the full expression in equation 7.4b.

Equation 7.4 is equivalent to the statement that no sub-system is directly excited and no power flows between sub-systems. There is much duplication of radiation and coupling loss factor terms in the elements forming matrix [A] in equation 7.4b (i.e. $\eta_{7b}^{3b} = \eta_{2b}^{5b} = \eta_{2b}^{3b}$) and this simplifies notation.

The computational process begins by assigning non-zero values to

$$
\begin{bmatrix}
\eta_{1r}+2(\eta_{1r}^{2b}+\eta_{1r}^{3b}+\eta_{1r}^{4b}) & -\eta_{2b}^{1r} & -\eta_{3b}^{1r} & -2\eta_{4b}^{1r} & -\eta_{3b}^{1r} & -\eta_{2b}^{1r} & 0 & 0 & 0 & 0 & 0 & 0 \\
-\eta_{1r}^{2b} & \eta_b+2(\eta_{2b}^{3b}+\eta_{2b}^{4b}+\eta_{2b}^{1r}) & -\eta_{3b}^{2b} & -2\eta_{4b}^{2b} & -\eta_{3b}^{2b} & 0 & 0 & 0 & 0 & 0 & 0 & 0 \\
-\eta_{1r}^{3b} & -\eta_{2b}^{3b} & \eta_b+2(\eta_{3b}^{2b}+\eta_{3b}^{7b}+\eta_{3b}^{4b}+\eta_{3b}^{1r}) & -2\eta_{4b}^{3b} & 0 & -\eta_{7b}^{3b} & 0 & 0 & 0 & 0 & 0 & 0 \\
-\eta_{1r}^{4b} & -\eta_{2b}^{4b} & -\eta_{3b}^{4b} & \eta_b+2(\eta_{4b}^{2b}+\eta_{4b}^{3b}+\eta_{4b}^{1r}) & -\eta_{3b}^{4b} & -\eta_{2b}^{4b} & 0 & 0 & 0 & 0 & 0 & 0 \\
-\eta_{1r}^{3b} & -\eta_{2b}^{5b} & 0 & -2\eta_{4b}^{5b} & \eta_b+2(\eta_{5b}^{2b}+\eta_{5b}^{4b}+\eta_{5b}^{7b}+\eta_{5b}^{1r}) & -\eta_{7b}^{5b} & -\eta_{7b}^{5b} & 0 & 0 & 0 & 0 & 0 \\
-\eta_{1r}^{2b} & 0 & -\eta_{3b}^{7b} & -2\eta_{4b}^{7b} & -\eta_{5b}^{7b} & \eta_b+\eta_{7b}^{3b}+\eta_{7b}^{8b}+2(\eta_{7b}^{4b}+\eta_{7b}^{5b}+\eta_{7b}^{1r}) & -\eta_{8b}^{7b} & -\eta_{5b}^{7b} & 0 & 0 & 0 & 0 \\
0 & 0 & 0 & 0 & -\eta_{5b}^{7b} & -\eta_{7b}^{8b} & \eta_b+\eta_{8b}^{11b}+\eta_{8b}^{7b}+2(\eta_{8b}^{5b}+\eta_{8b}^{10b}+\eta_{8b}^{2r}) & -\eta_{5b}^{7b} & -2\eta_{8b}^{10b} & -\eta_{11b}^{8b} & 0 & -\eta_{2r}^{8b} \\
0 & 0 & 0 & 0 & -\eta_{5b}^{9b} & -\eta_{7b}^{9b} & -\eta_{7b}^{9b} & \eta_b+\eta_{9b}^{13b}+\eta_{9b}^{5b}+2(\eta_{9b}^{7b}+\eta_{9b}^{10b}+\eta_{9b}^{2r}) & -2\eta_{10b}^{9b} & 0 & -\eta_{13b}^{9b} & -\eta_{2r}^{9b} \\
0 & 0 & 0 & 0 & 0 & 0 & -\eta_{8b}^{10b} & -\eta_{9b}^{10b} & \eta_b+2(\eta_{10b}^{8b}+\eta_{10b}^{9b}+\eta_{10b}^{2r}) & -\eta_{9b}^{10b} & -\eta_{8b}^{10b} & -\eta_{2r}^{10b} \\
0 & 0 & 0 & 0 & 0 & 0 & -\eta_{8b}^{11b} & 0 & -2\eta_{10b}^{11b} & \eta_b+2(\eta_{11b}^{8b}+\eta_{11b}^{10b}+\eta_{11b}^{2r}) & -\eta_{8b}^{11b} & -\eta_{2r}^{9b} \\
0 & 0 & 0 & 0 & 0 & 0 & 0 & -\eta_{9b}^{13b} & -2\eta_{10b}^{13b} & -\eta_{9b}^{13b} & \eta_b+2(\eta_{13b}^{9b}+\eta_{13b}^{10b}+\eta_{13b}^{8b}+\eta_{13b}^{2r}) & -\eta_{2r}^{8b} \\
0 & 0 & 0 & 0 & 0 & 0 & -\eta_{8b}^{2r} & -\eta_{9b}^{2r} & -2\eta_{10b}^{2r} & -\eta_{9b}^{2r} & -\eta_{8b}^{2r} & \eta_{2r}+2(\eta_{2r}^{8b}+\eta_{2r}^{9b}+\eta_{2r}^{10b})
\end{bmatrix}
\begin{bmatrix} E_{1r} \\ E_{2b} \\ E_{3b} \\ E_{4b} \\ E_{5b} \\ E_{7b} \\ E_{8b} \\ E_{9b} \\ E_{10b} \\ E_{11b} \\ E_{13b} \\ E_{2r} \end{bmatrix}
=
\begin{bmatrix} 0 \\ 0 \\ 0 \\ 0 \\ 0 \\ 0 \\ 0 \\ 0 \\ 0 \\ 0 \\ 0 \\ 0 \end{bmatrix}
$$

.....7.4b

the elements in the R.H column of equation 7.4. Thus, if plate 5 is excited directly into bending vibration then all other plate energies are expressed by the ratio E_{bi}/E_{b5}. The equivalent operation is to remove the fifth row (enclosed by dotted lines) from matrix A in equation 7.4 and by moving the fifth column to the R.H.S of the equation, equation 7.4 becomes,

$$\left[A'\right]\left[E/E_{b5}\right] = \begin{bmatrix} a_{1,5} \\ \vdots \\ a_{4,5} \\ a_{6,5} \\ \vdots \\ a_{12,5} \end{bmatrix} \qquad \ldots\ldots 7.5$$

where $a_{i,j}$ are the elements of the coefficient matrix A.

We have now a set of simultaneous equations which are solved using Crout's rule (as in section 4.1 and Appendix II).

Thus, using the initial matrix equation 7.4, a computational routine is evolved where the resultant, relative energy levels of any sub-system can be calculated for the case when any single sub-system is directly excited. Calculation was performed for the case of room 1 being acoustically driven or when plates 2, 3, 5 and 7 are, in turn, mechanically driven.

7.4 Measurement

Experimental measurement involved the use of two model rooms, connected diagonally as shown in plate 7.1. The methods of measurement of plate bending wave energy and room pressure wave energies are as described in Chapter 6. Figure 7.3 gives a diagram of apparatus.

7.4.1 The rooms

The two rooms were constructed from reinforced concrete plates of thickness 0.05 m (plates 3, 5, 9, and 11) and of thickness 0.038 m (for all other plates). The corners of the rooms were produced by keying the edge of each plate and by using a strong grout as an adhesive. The two rooms can be considered as lying on their sides and the whole arrangement is isolated from the floor by rubber pads standing upon concrete cubes (plate 7.3). The rooms were of different dimensions; the source room having internal dimensions of 1.0 m x 0.68 m x 0.76 m and the receiver room dimensions were 0.95 m x 0.75 m x 0.66 m. In measuring the airborne sound transmission between the rooms it was felt necessary to eliminate transmission of energy by outward radiation from the source room. Thus room 1 was screened from room 2 by a large panel bisecting the common corner. The panel was constructed from sheets of urethane and hardboard panels and had a height of 2.5 m and a width of 5 m. Additional damping of any outwardly radiated sound was produced by foam rubber (approximate thickness 50 mm) placed between the source room and the floor area. Despite the laboratory being fairly reverberant it was

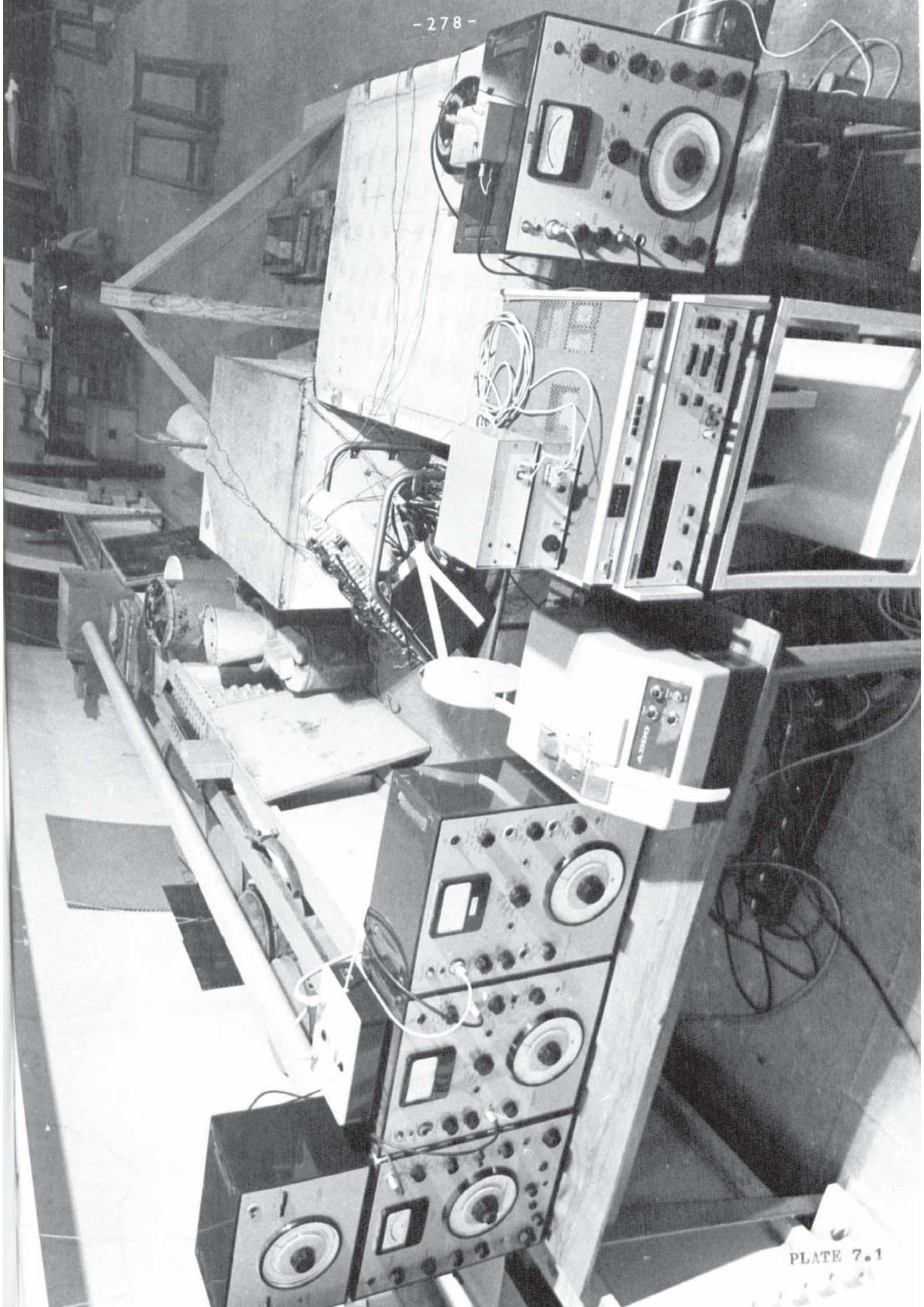

PLATE 7.1

Fig. 7.3

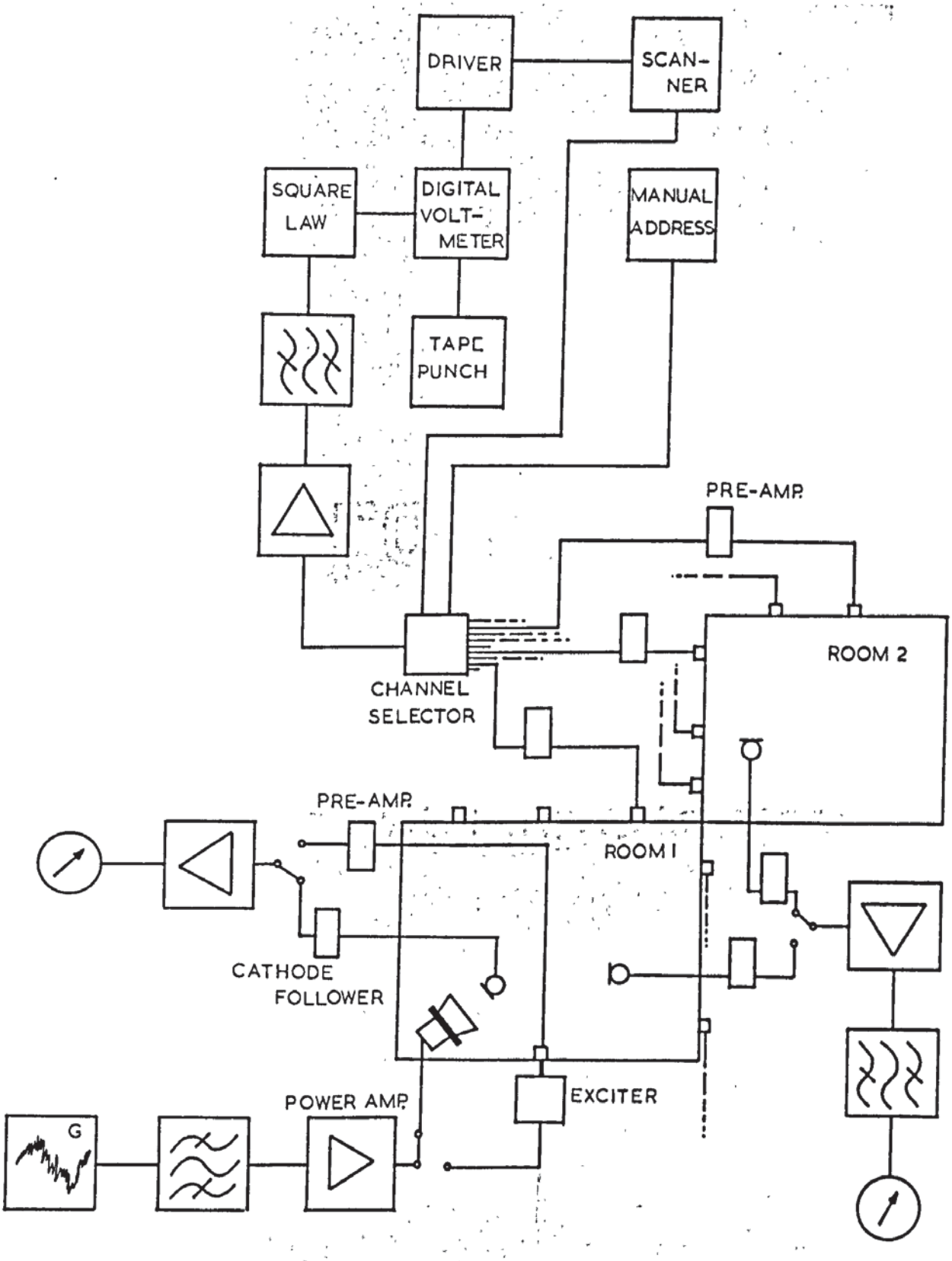

Measurement of noise transmission in connected rooms.

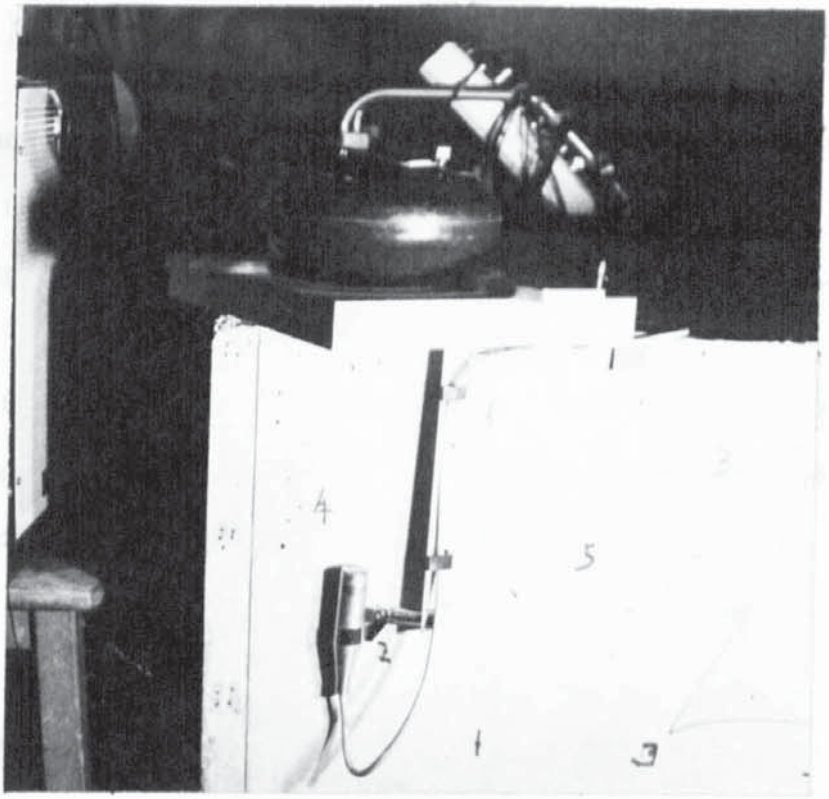

PLATE 7.2 Pressure unit and monitoring condenser microphone.

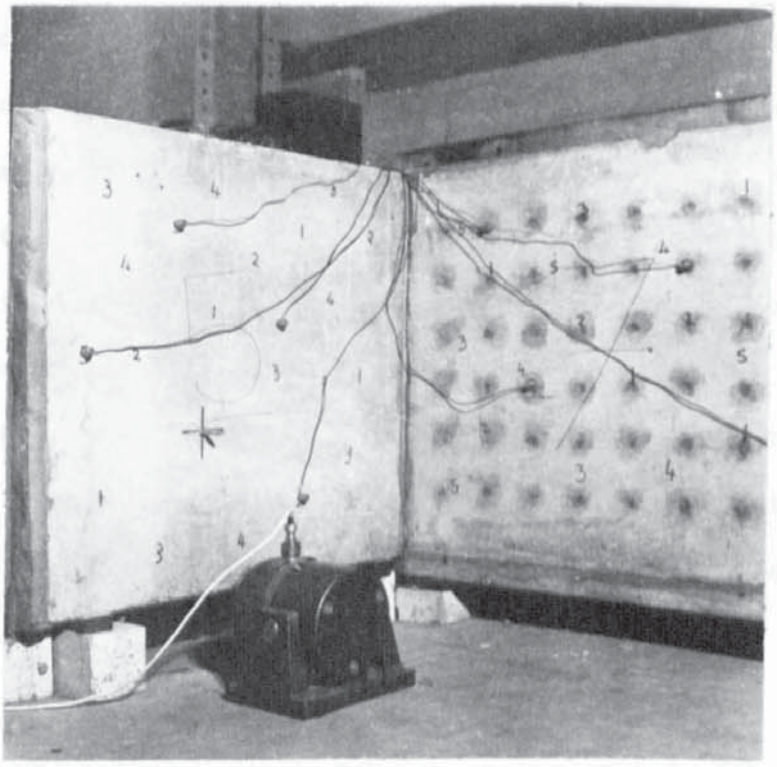

PLATE 7.3 Large electro-magnetic shaker and accelerometers in position.

found that the simple screening reduced the measured energy ratio E_{r2}/E_{r1} by up to 10 dB in the mid and high frequencies. At the frequency of 630 Hz the improvement was still 6 dB.

A small triangular hole in each room allowed the insertion of microphone cable (plate 7.5). The holes were then sealed by wooden pieces of thickness 40 mm.

7.4.2 The drivers

As in previous experiments, mechanical excitation was produced by the large electromagnetic shaker bolted to the plate (plate 7.3).

A steady-state sound field within room 1 was generated by a pressure unit (Vitovox type CN353) positioned outside the room, over a circular aperture in the wooden corner piece. This ensured that the sound source was located as near as possible to a room corner. In this position, the maximum number of room modes are excited within the bandwidth of interest. In order to prevent any vibration of the pressure unit directly generating plate bending fields, the unit was isolated from the corner piece by a seal of rubber tubing. Sound radiation into the laboratory from the unit was eliminated by enclosing it within a box, the inside of which was lined with absorbent material.

Both acoustic and mechanical drivers were supplied with amplified, one-third octave filtered random noise. A microphone on the axis of the pressure unit, at a distance of approximately 200 mm

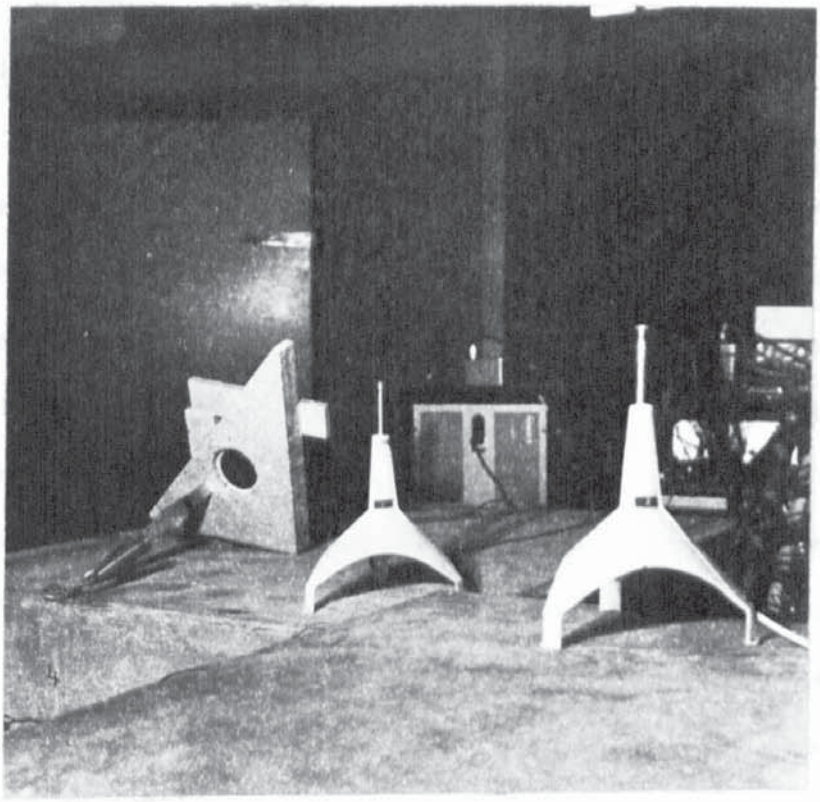

PLATE 7.4 Condenser microphones and stands.

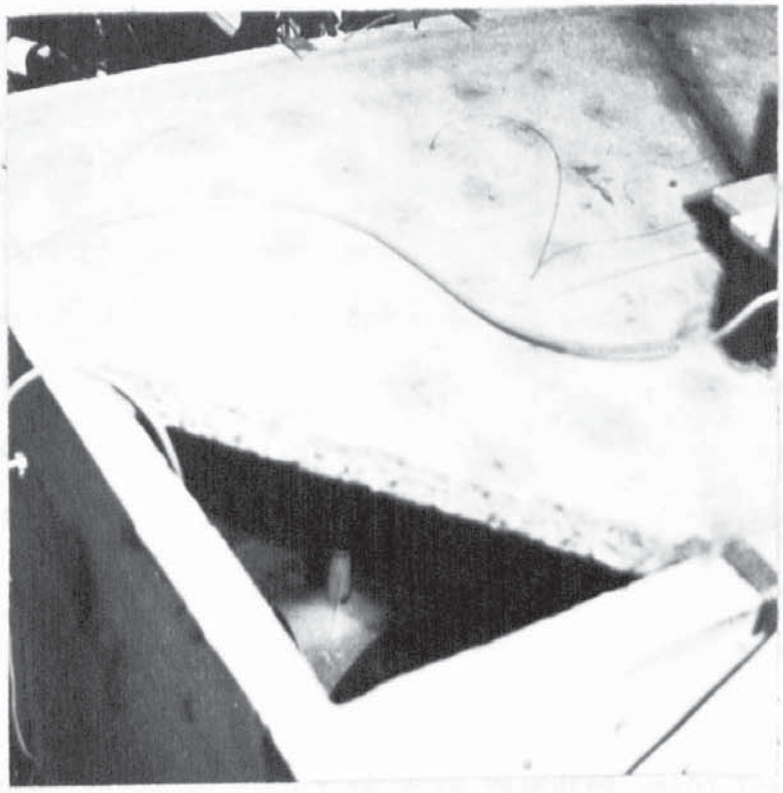

PLATE 7.5 Microphone inside model room.

(plate 7.2), and an accelerometer cemented at the driving point of the mechanical shaker allowed the input power to the system to be monitored. It was found that in the time taken to complete a set of readings little or no drift in power input was observed. The monitoring microphone and accelerometer also allowed any experiment to be repeated. If it was required that the reading at different accelerometer positions be taken, then the same power input could be reproduced. Thus, at 400 Hz the monitoring microphone reading (on a R.M.S meter on slow response) could be reproduced with an accuracy of $\pm$ 1 dB. While at 12.5 kHz the reproducibility was within 0.2 dB.

7.4.3 The vibrational transducers

Figure 7.3 shows that the accelerometer signal circuit is the same as that used in the radiation loss factor measurements and in the measurement of bending energy ratio in plates forming junctions (section 6.6). The bending wave energies of plates 2, 3, 5, 7, 8, 9, 11, and 13, were measured and compared with the predictions. With the thirty-two accelerometer signal channels available, four calibrated accelerometers could be distributed on each plate. The experiment was repeated up to four times for different accelerometer positions to give a total of twenty accelerometer readings for each plate. A typical distribution of accelerometers is seen in plate 7.3.

The pressure fields in each room were measured using the one inch condenser microphones plus cathod followers. Readings at five microphone positions were recorded at each frequency. The microphone

signal is amplified, filtered by a one-third octave bandwidth and then metered. Plate 7.4 illustrates the monitoring microphone, the two sampling microphones and stands, while plate 7.5 shows a microphone in a position in the source room.

7.5 Results

Experimental measurement and values predicted from theory are given in Figures 7.4 - 7.15. In all graphs the solid line represents predicted values from theory where bending, longitudinal, and transverse wave fields are considered. The dotted line gives the predicted values from the simpler theory where bending waves only are considered. The experimental points are the mean values of three to five measurements. This corresponds to between twelve and twenty accelerometer positions per plate.

7.5.1 Acoustic excitation

Loudspeaker excitation of room 1 will result in the direct generation of a pressure field in room 1, and the indirect generation of bending fields on all plates and a pressure field in room 2. For simplicity of interpretation the plate bending wave energies are divided by the bending wave energy of plate 3, i.e. $E_{b3} = 1$.

The plate energies in the source room (Fig 7.4) vary little from each other. As is expected, the deviation of theory from measurement is a maximum at low frequency. In this and in subsequent results it

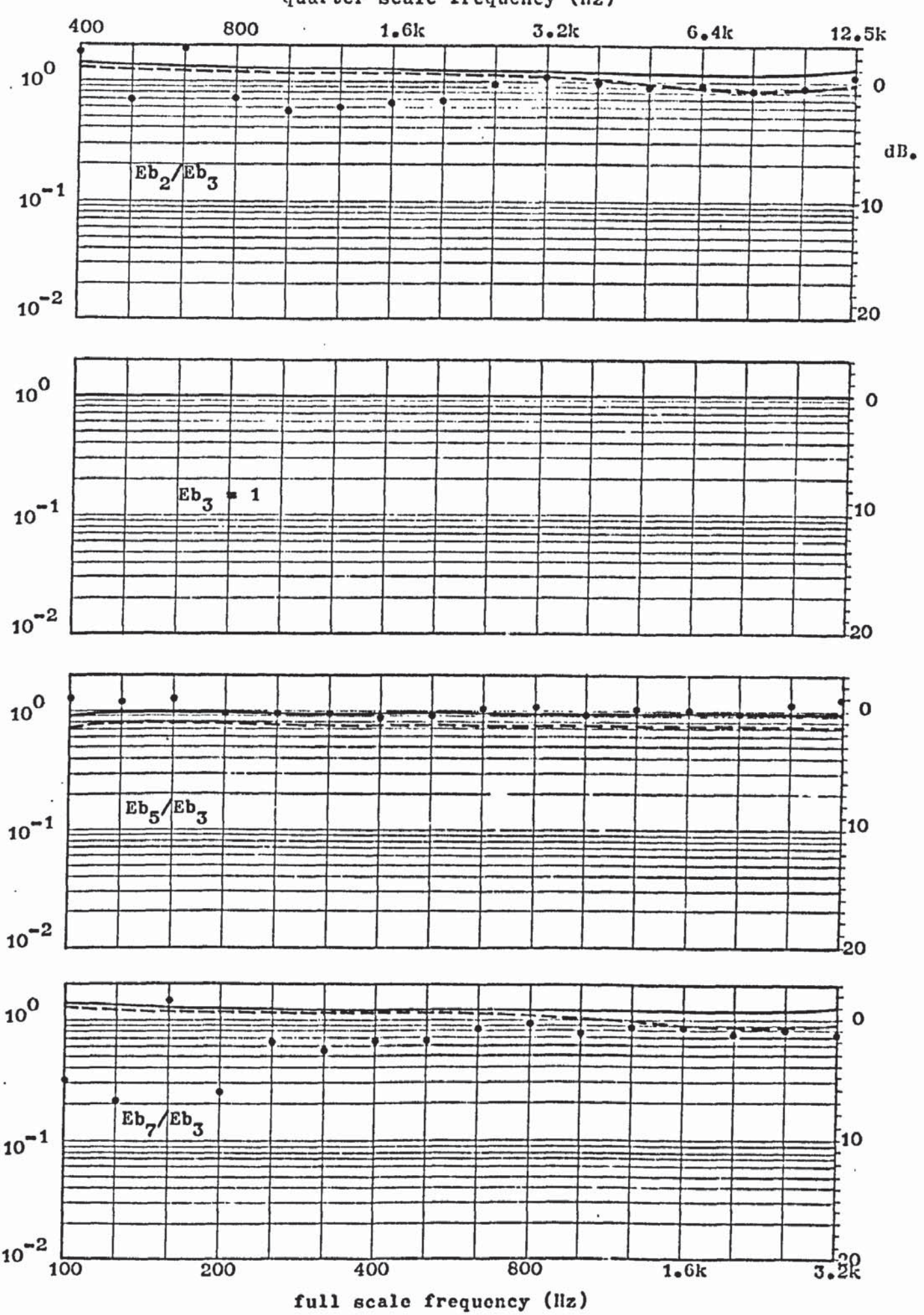

Plate energy ratios of room 1 with respect to plate 3 energy.

Loudspeaker excitation of room 1.

Fig. 7.4

is seen that agreement between measurement and theory can only be considered fair at frequencies above 1.6 kHz in the quarter-scale frequency range.

The following observations are made of the results for the plates forming the receiver room (Fig 7.5).

(1) Theory and experiment indicate a decrease in energy ratio with increase in frequency.

(2) E_{b8}/E_{b3} and E_{b9}/E_{b3} have greater values than those of E_{b11}/E_{b3} and E_{b13}/E_{b3}. This is seen to be the result of vibrational energy having to pass through two plate junctions in the receiver room, before reaching plates 11 and 13. With the exception of E_{b11}/E_{b3}, agreement between predicted and measured values is reasonable. The difference in values predicted using simple and complex theory is in general less than the difference between either and experimental results.

Figure 7.6 presents the frequency dependence of the room pressure ratio E_{r2}/E_{r1} when room 1 is driven by a loudspeaker. In the mid and high frequency range there is seen to be good agreement between simple theory and experiment. The gradient is approximately 10 dB/ octave over most of the frequency range.

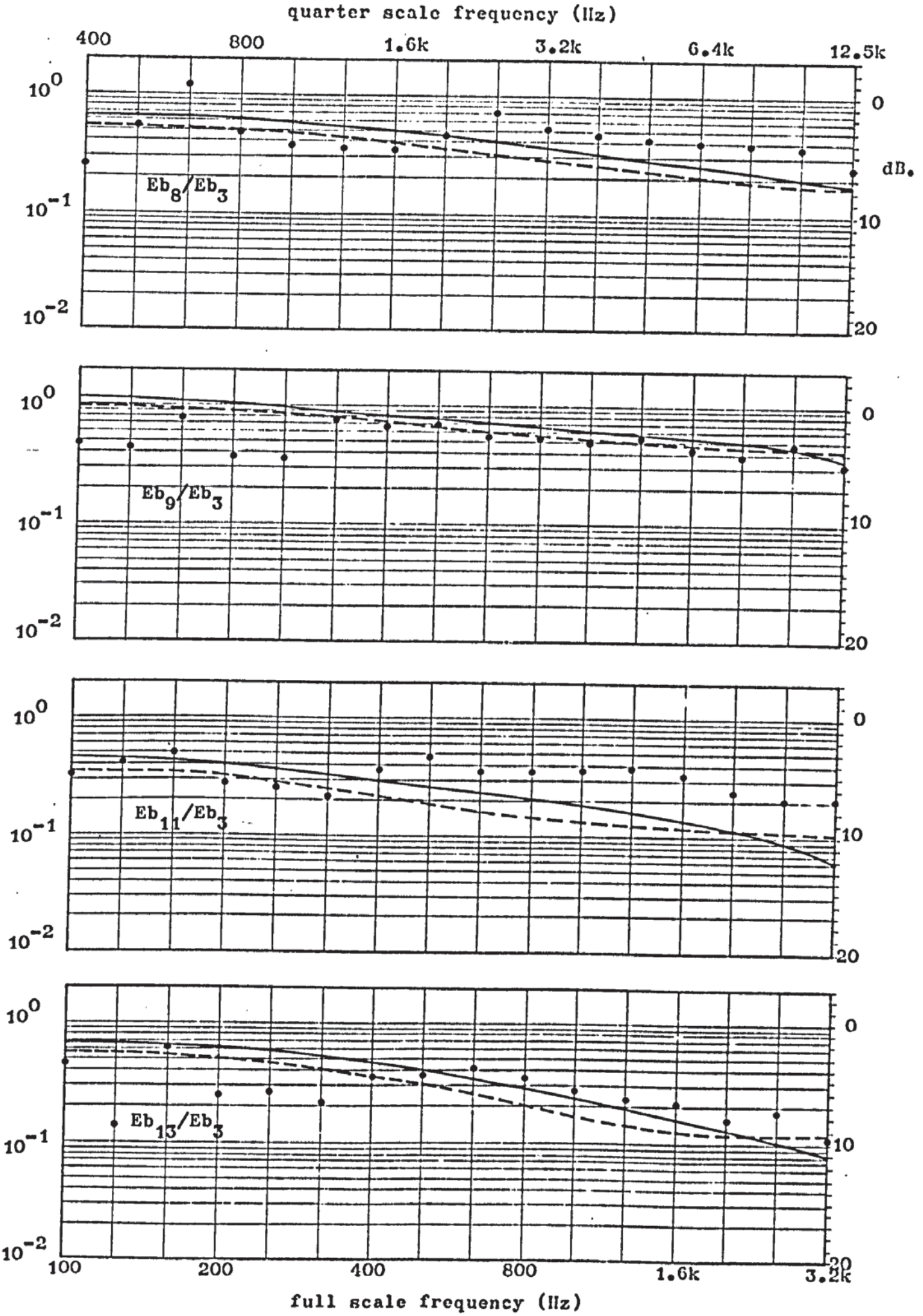

Plate energy ratios of room 2 with respect to plate 3 energy.

Fig. 7.5

Fig. 7.6

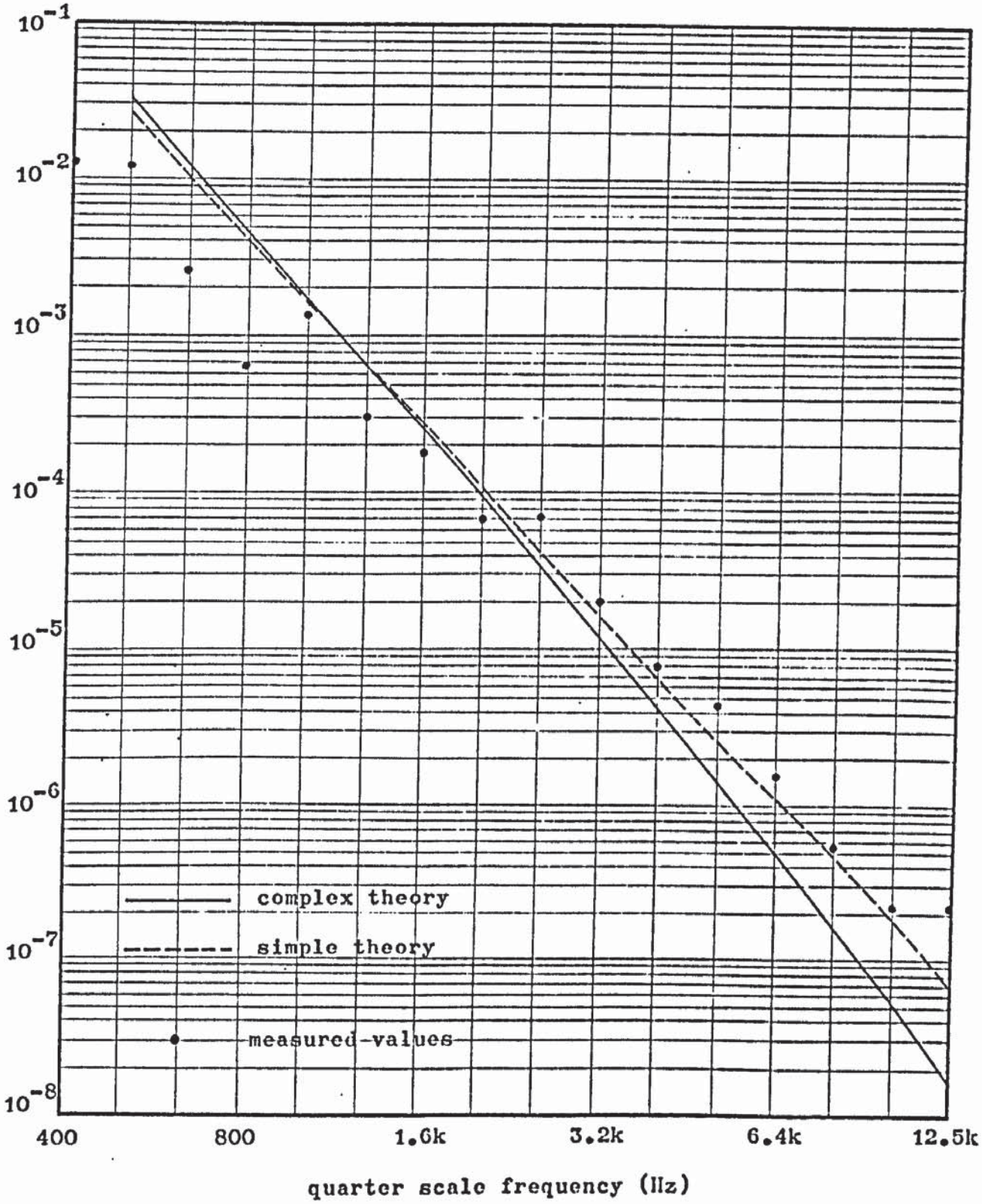

Room energy ratio Er_2/Er_1 when room 1 is acoustically excited.

7.5.2 Mechanical excitation

Figures 7.7 - 7.14 give the bending energy ratios of each plate when plates 2, 3, 5, and 7 are mechanically excited. From the graphs the following observations are made.

(1) Again the theory is seen to break down at frequencies below 1.6 kHz in the quarter-scale frequency range.

(2) In general, although following the measured trend with frequency, the theory gives values lower than that observed. The difference can be as much as 5 dB between the experimental results and values predicted by either theory. This is particularly true of the bending energy of plate 11 which gives consistently high measured values, irrespective of the plate excited.

(3) The decrease in energy ratio with increase in frequency is again seen in both theory and experiment. The line predicted from the more complex theory has a steeper gradient than that of the simple theory or a line (approximately) fitting the measured results. Indeed, at the highest frequencies (5 kHz to 12.5 kHz) the agreement between measurement and simple theory is often better than that with the more complex theory.

(4) The low predicted values may be the result of assigning too low a value to the coupling factor η_r^b i.e. the coupling between the enclosed air volume and the surrounding

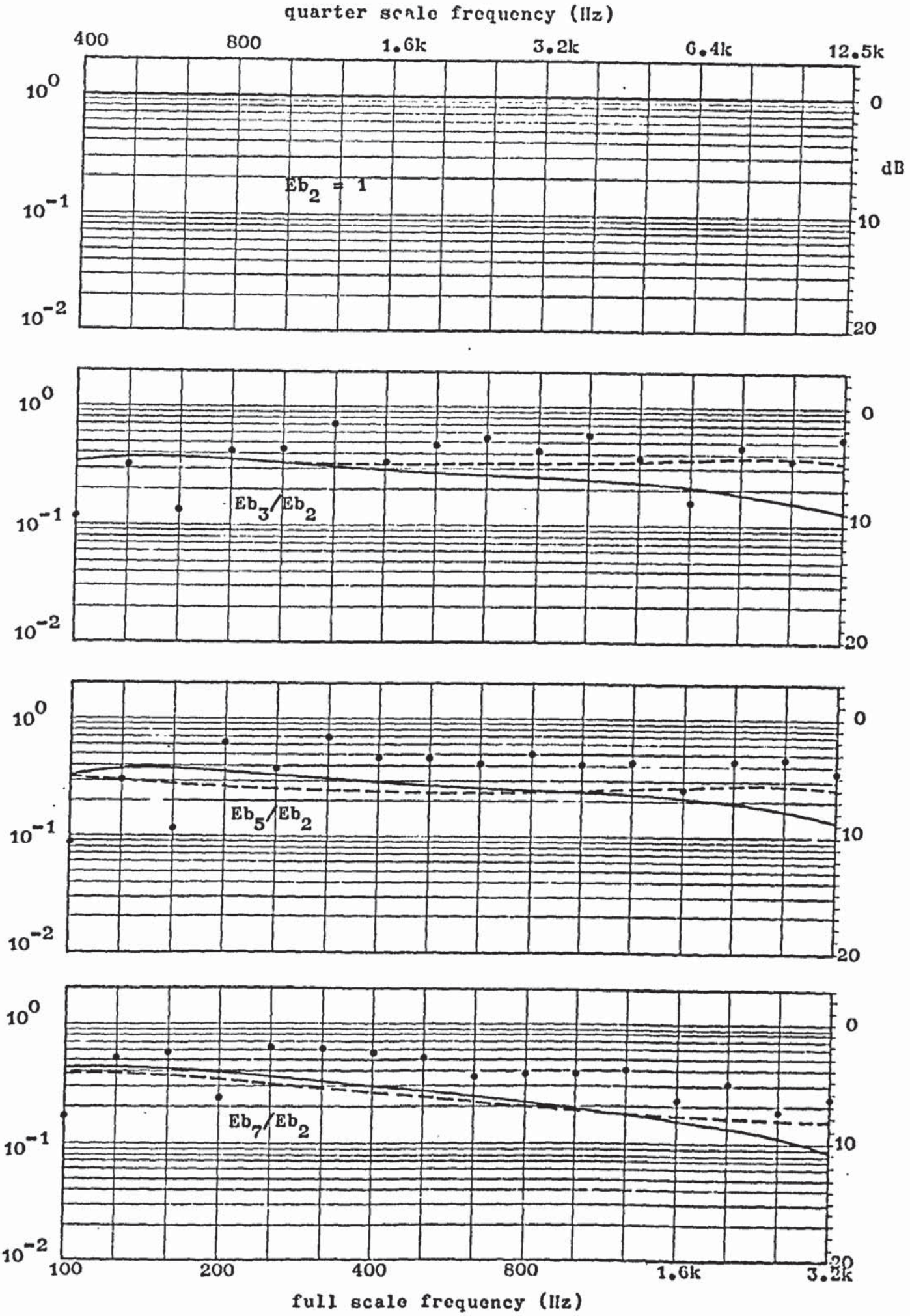

Plate energy ratios of room 1 with respect to plate 2 energy.

Mechanical excitation of plate 2.

Fig. 7.7

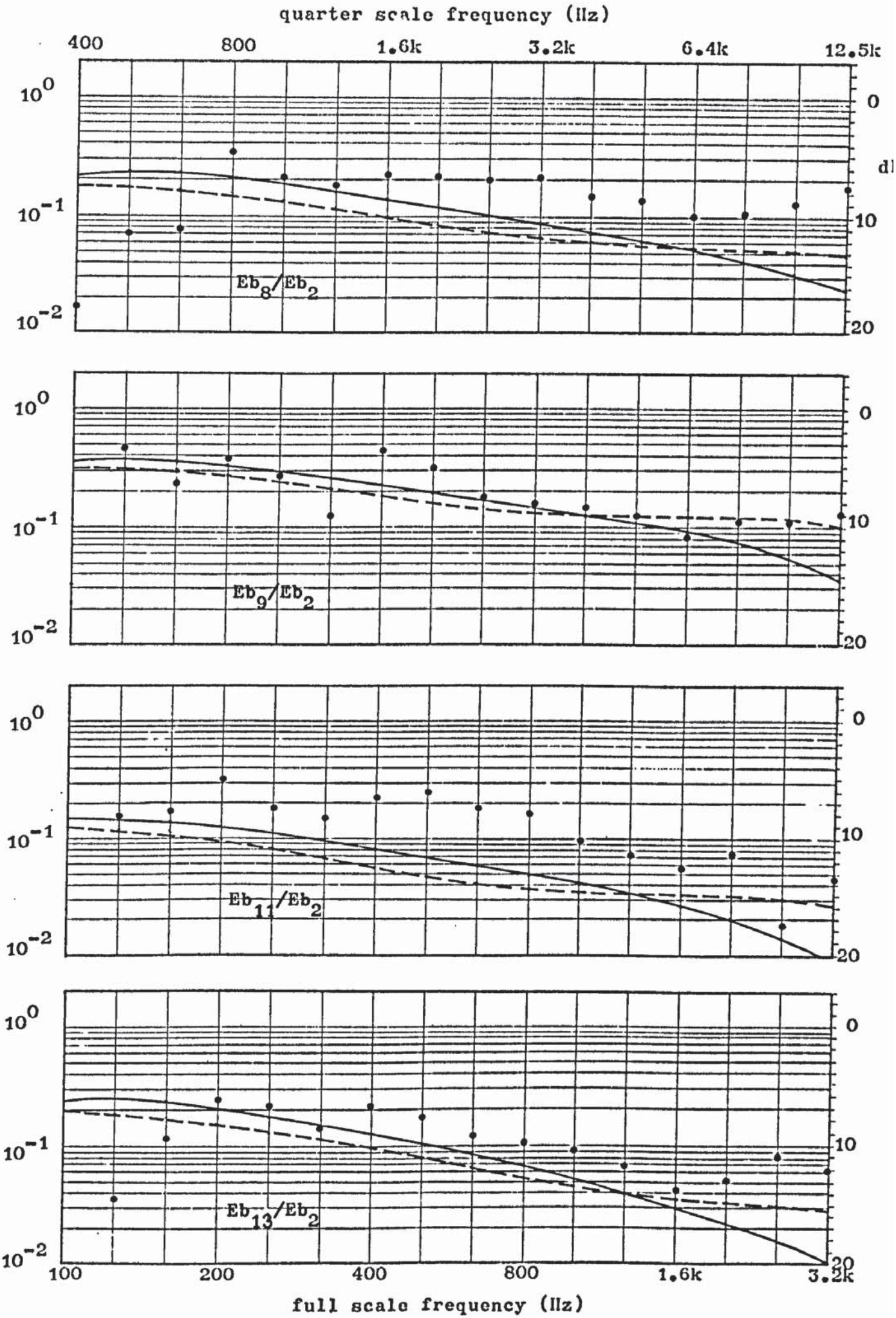

Plate energy ratios of room 2 with respect to plate 2 energy.

Fig. 7.8

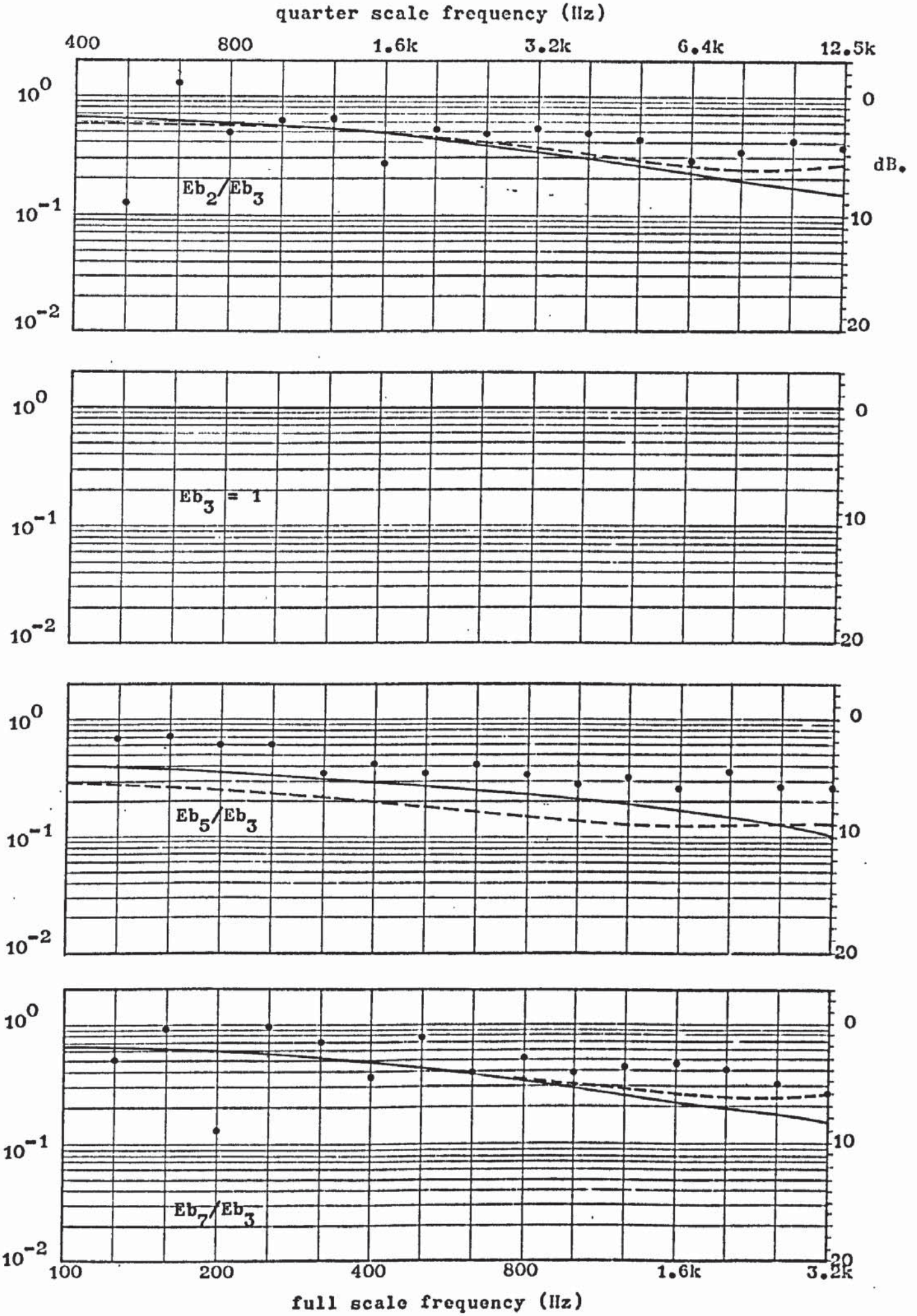

Plate energy ratios of room 1 with respect to plate 3 energy.

Mechanical excitation of plate 3.

Fig. 7.9

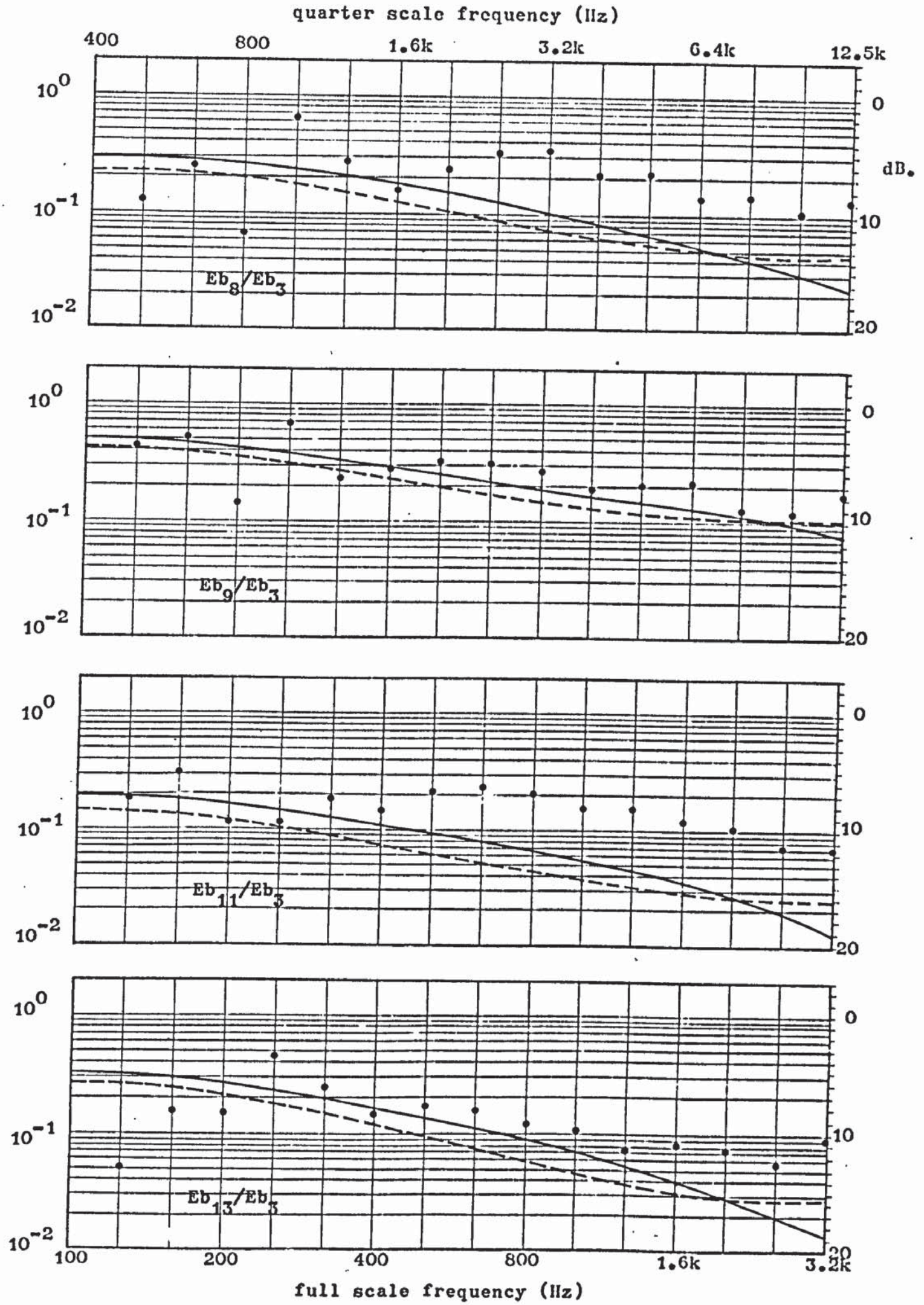

Plate energy ratios of room 2 with respect to plate 3 energy.

Fig. 7.10

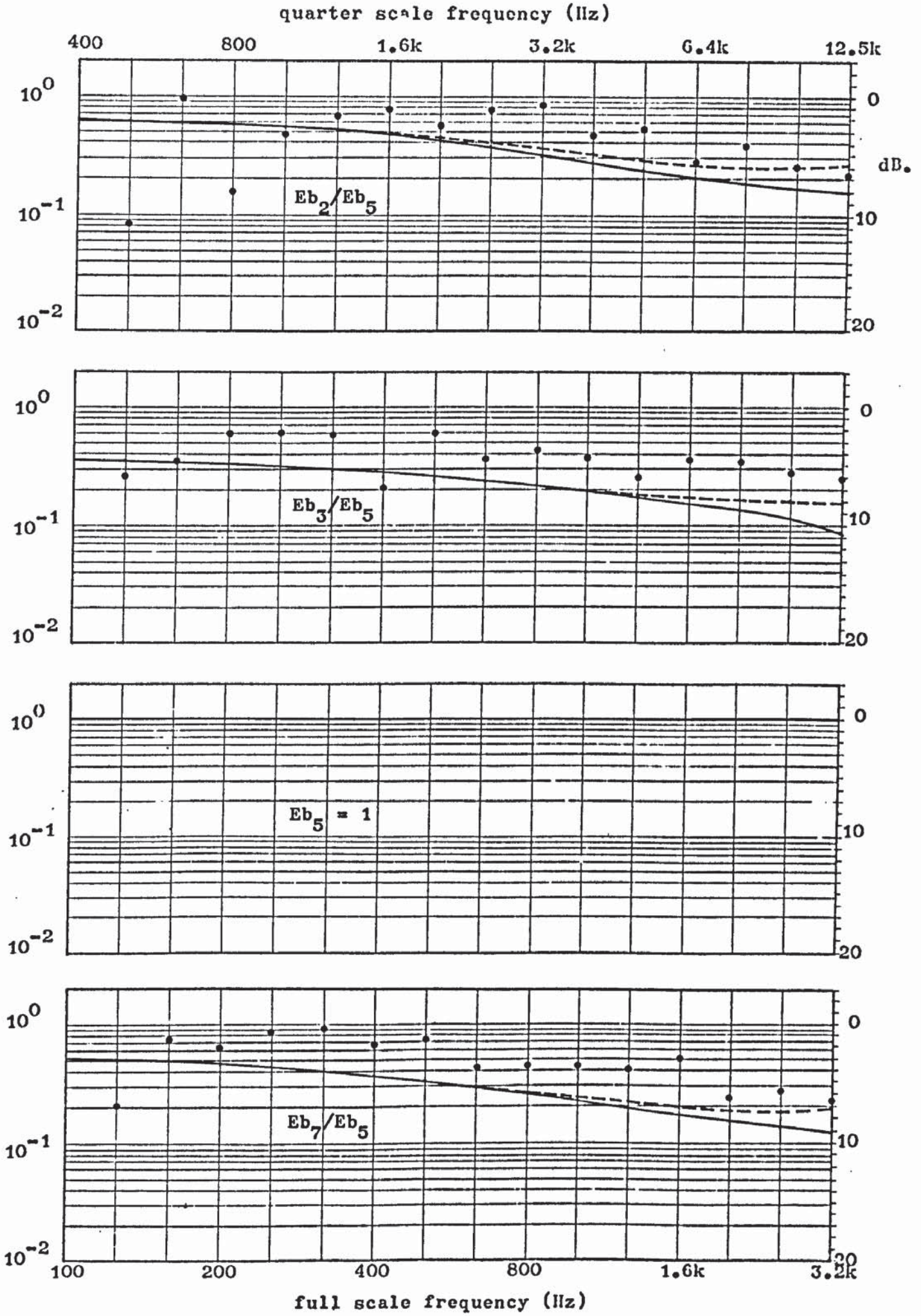

Plate energy ratios of room 1 with respect to plate 5 energy.

Mechanical excitation of plate 5.

Fig. 7.11

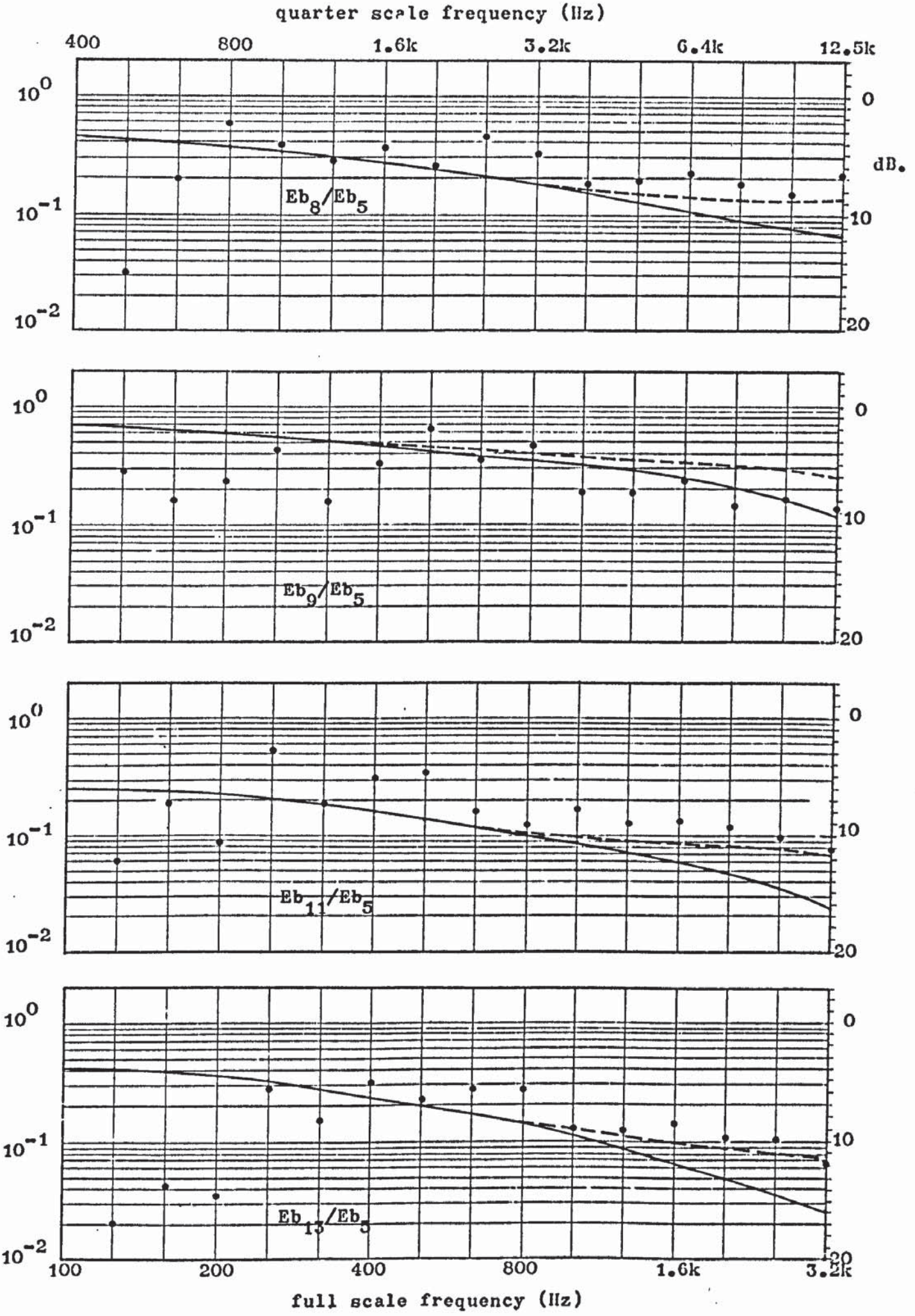

Plate energy ratios of room 2 with respect to plate 5 energy.

Fig. 7.12

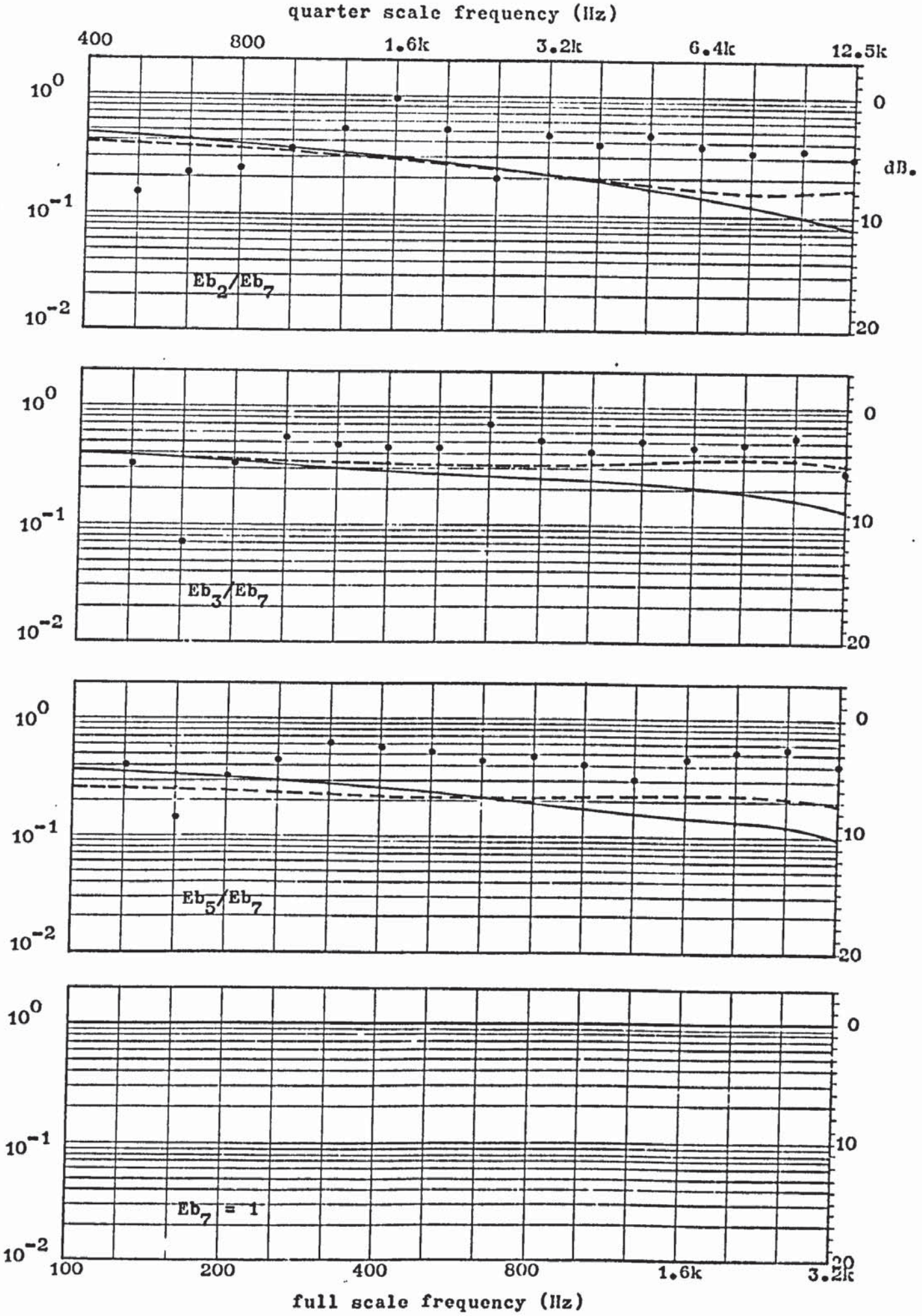

Plate energy ratios of room 1 with respect to plate 7 energy.

Mechanical excitation of plate 7.

Fig. 7.13

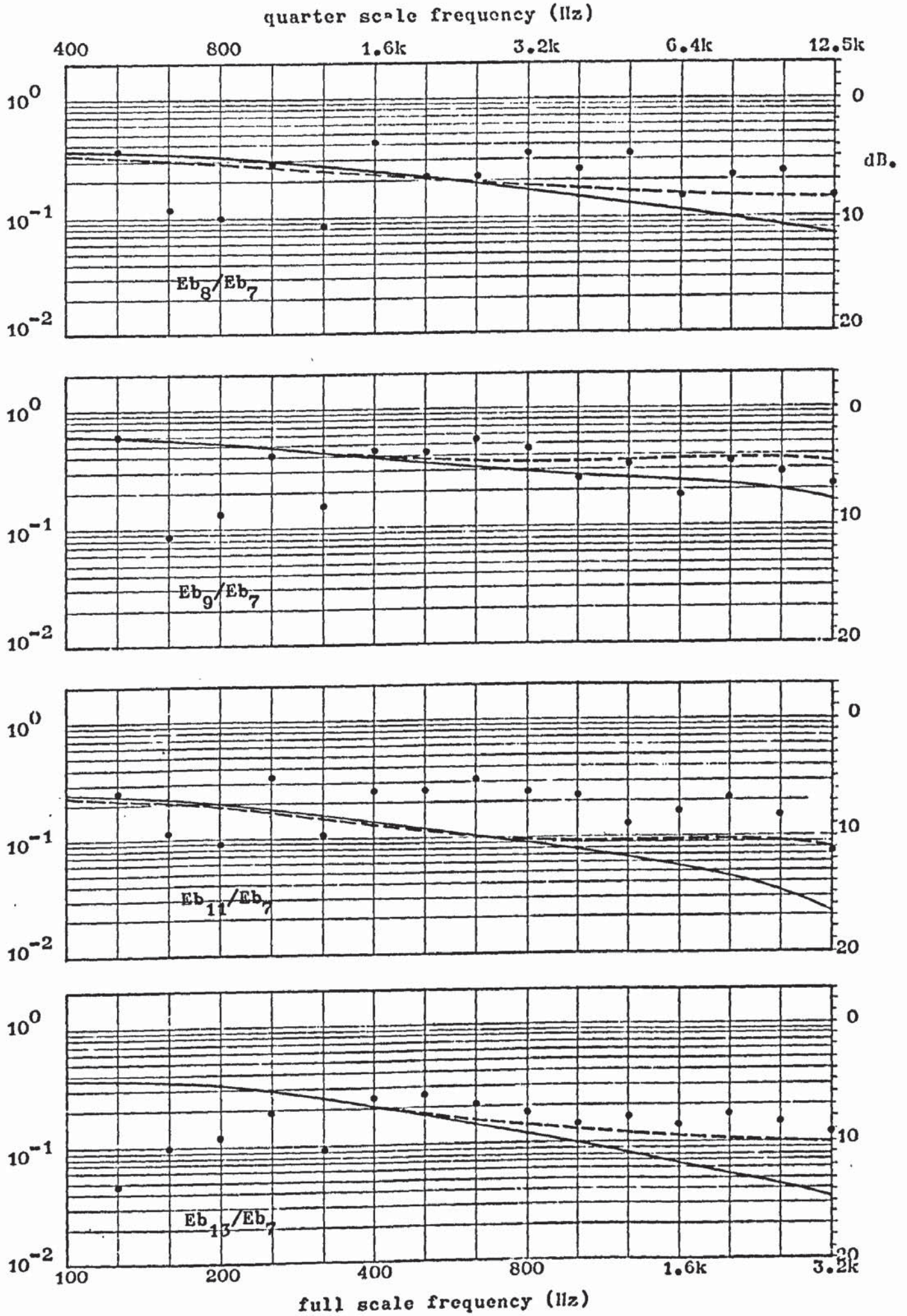

Plate energy ratios of room 2 with respect to plate 7 energy.

Fig. 7.14

plates. It will be remembered that in the measurements of radiation resistance by acoustic excitation (section 6.5.4) the observed values were consistently higher (though of the same order of magnitude) than the theoretical value.

(5) As a result of having transmission paths incorporating two structural discontinuities it would be expected that lower energies would be found on plates 8 and 9 when either plates 2 or 3 are excited than when plates 5 and 7 are excited. Although plate 9 energies are consistently lower (by approximately 3 dB over much of the frequency range) when plates 2 or 3 are excited, the same cannot be said of plate 8. The energy on this thinner plate appears largely independent of the plate mechanically excited in the source room. This again appears to support the theory that the coupling between the pressure modes and the plate bending modes is stronger than initially thought.

The room energy ratio E_{r2}/E_{r1} is also calculated for each excited plate (Fig 7.15). From the mid-frequencies upwards both theory and experiment give a decrease in energy ratio with increase in frequency. The theory and experiment also indicate that the energy ratio is largely independent of which plate is excited. It might be expected that values of E_{r2}/E_{r1} would be lower when plate 2 or plate 3 are excited than when plate 5 or plate 7 is excited. This is seen to be true on plate 5. In general the ratio is insensitive to the

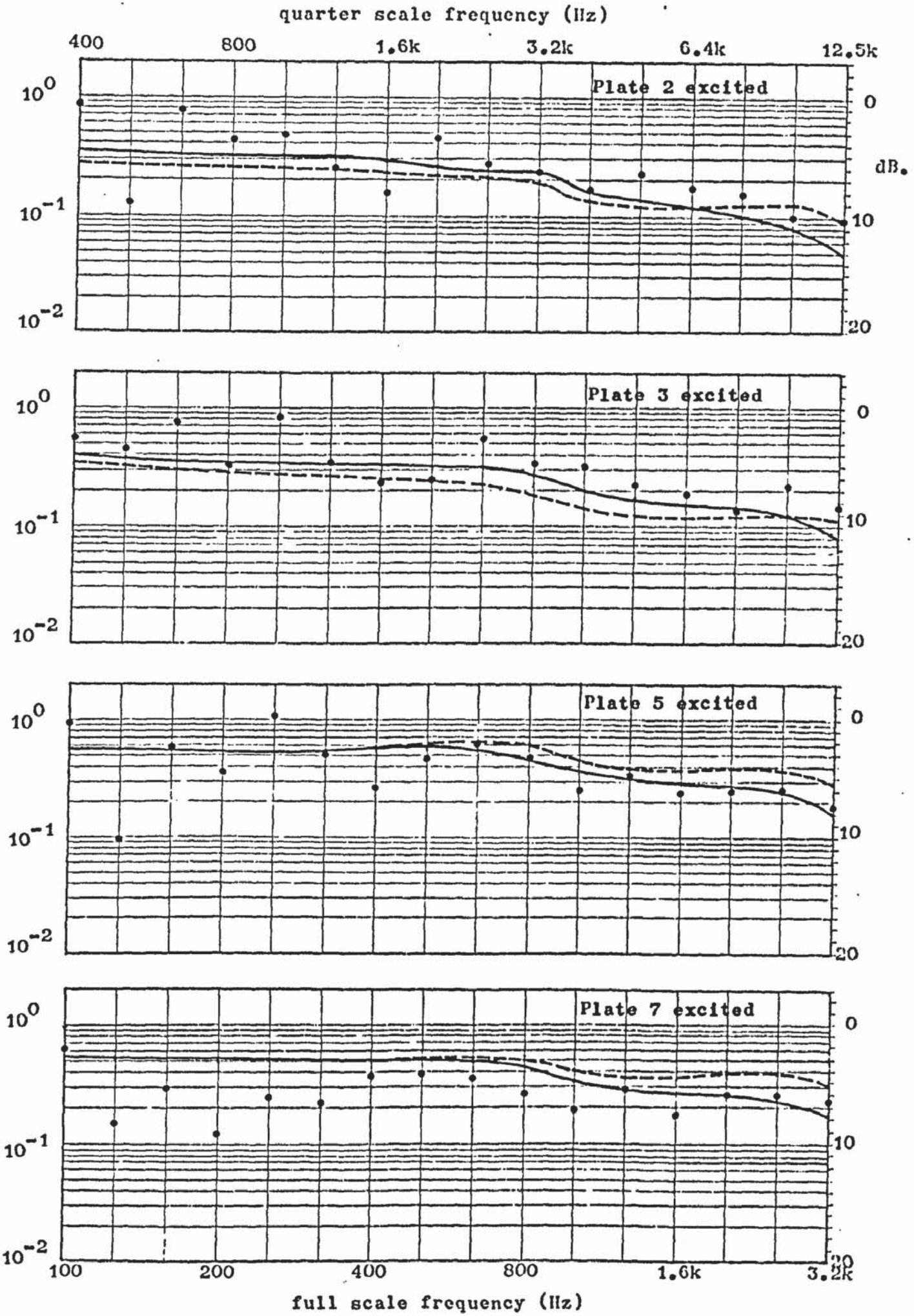

Room energy ratio Er_2/Er_1 when room 1 plates are mechanically excited.

Fig. 7.15

plate excited in the source room.

CHAPTER 8

CONCLUDING REMARKS

8.1 General conclusions

Sound transmission in building structures has been investigated theoretically, by means of power flow techniques, and experimentally, by use of quarter-scale models. From prediction and measurement the following observations are made.

(1) Vibrational energy is transferred readily from one concrete plate to other concrete plates which form a junction. This is particularly true when all plate thicknesses are equal or nearly equal. It is shown that bending, longitudinal, and transverse waves are the main forms of vibrational energy transfer. As well as generating bending waves on all connected plates, an obliquely incident bending wave gives rise to longitudinal and transverse waves on plates at right angles to the source plate, and, to a lesser extent, on plates collinear with the source plate.

At certain angles of incidence, longitudinal and transverse waves are totally reflected and the mechanical impedance of the junction effectively becomes zero. A large transmission of bending wave energy then occurs between collinear plates, i.e. the transmission coefficient γ_{1b}^{3b} gives a peak value which is almost unity at low frequencies.

Contrary to results of Kihlman (1967) the average bending wave transmission coefficient γ_{1b}^{2b} between plates at right angles is seen to be frequency dependent, albeit to a smaller degree than γ_{1b}^{3b}. The coefficient γ_{1b}^{3b} increases with increase in frequency and, except at high frequencies, is greater in value than γ_{1b}^{2b}. A general statement can be made that the most important transmission for the case of bending, longitudinal, or transverse waves incident at cross-junctions or T-junctions of plates of nearly equal thickness in that involving the generation of a wave type on the collinear plate which is the same as that incident, i.e. γ_{1b}^{3b}, γ_{1l}^{3l}, γ_{1t}^{3t}.

(2) From calculated transmission coefficients at junctions of semi-infinite plates, structural coupling loss factors were derived and then entered into energy balance equations, along with internal loss factor and radiation loss factor. These equations describe the power flow between finite plates forming junctions.

It is seen that, for the configurations investigated, consideration of wave types other than bending waves did not appreciably alter the predicted bending wave energy on each plate. The difference between values predicted from this simple theory and those from more complex theory is never more than 2 dB; this is well within experimental error.

In general, predicted and measured values of bending wave energy agreed only in mid and high frequencies. The frequency range of interest was 100 Hz - 3.15 kHz (full scale). At the low frequencies, measured values were generally lower than predicted. This is certainly due to the breakdown of simple power flow concepts at low frequency where all vibrational modal densities are low. In the bandwidth of measurement (one-third octave) one bending mode may predominate and the bending field cannot be assumed to be diffuse.

(3) Power flow methods are used more successfully in describing the radiation characteristics of rectangular, reinforced concrete plates. Thin plate theory of Maidanik (1962) gives fair agreement with experimental results. For the plate thicknesses investigated it is seen that the critical coincidence frequency lies below the frequency range of interest. In this supercritical region, the radiation characteristics are unaffected by edge conditions. Also, the radiation loss factor into 4π space is approximately twice that into 2π space. Therefore, the radiation characteristics of a reinforced concrete plate are independent of situation, i.e. whether it forms part of or all of a surface of a rectangular room or is radiating into 2π or 4π space.

Thus, the sound radiation from a vibrating plate can be described by the radiation loss factor which is entered

into the energy balance equations in the same way as dissipative loss factor. Values of radiation loss factor were obtained from reciprocal experiments in which the plate is indirectly (acoustically) excited. The values obtained were higher than those obtained from direct (mechanical) excitation by about 3 dB.

(4) The validity of using quarter-scale models in experiment has been established. The dynamic constants of full and quarter-scale specimens of reinforced concrete, brickwork, and breezeblock were calculated. Bending, longitudinal, and transverse (torsional) wave velocities of concrete rods are independent of the form of (unstressed) reinforcement. The dissipative loss factor is also independent of the form of reinforcement and gave approximately the same measured value for all three wave types. All these parameters are shown to be independent of frequency and, in the case of brickwork, dissipative loss factor is independent of displacement amplitude.

The dynamic constants assigned to reinforced concrete are given as,

Young's modulus $E = 4 \times 10^{10}$ N/m^2

Density $\rho = 2.5 \times 10^{3}$ Kg/m^3

Poisson's ratio $\mu = 0.3$

Dissipative loss factor $\eta = 0.01$

The measured wave velocities in brickwork were higher than expected, and those of dissipative loss factor were lower than expected. This is thought to be due to the strong mortar mix (and method of keying) employed in the linear arrays of brick produced. In general, structures made in the laboratory had purer constituents, and constructional methods were more exact than those employed on the site. This will tend to increase vibrational wave velocities and reduce the dissipative loss factor.

Structures made from the above building materials can be scaled successfully to a ratio of 4:1. In brickwork, scale models were made from a mix 1:1.5:2.5 with the water content of 1.1. The aggregate is of crushed brick of dimensions 5 mm - 10 mm.

(5) Experiments were carried out on the direct and indirect effect of increase of material loss factor of a concrete plate or plates forming junctions. The loss factor was increased an order of magnitude by cladding the plate with a layer of sand-bitumin mixture. The direct effect of this increase is to reduce the bending wave energy on the clad plate by approximately 6 dB. Indirect damping in which the bending wave energy of a plate is decreased when a connected plate is clad, is appreciable on plates at right angles to the source plate. In mid and high frequencies, it is of the order of 2-3 dB.

The indirect effect on plates collinear to the source plate is slight. This fact would suggest that the reduction in energy on a plate at right angles to the source plate may be the result of increase of mechanical impedance of the junction as well as the increase in internal loss factor of the connected plate. This increase in impedance results from the additional mass of the cladding.

(6) Predicted values from thin plate theory agree fairly well with the measured modal distributions of bending waves on reinforced concrete plates.

A two dimensional analogy to the wave theory of pressure waves in rectangular rooms gives values in agreement with measured longitudinal modal distributions on rectangular concrete plates.

(7) Investigations were carried out on the sound transmission between two rectangular rooms which have a common junction. Again, agreement between predicted values and experiment is found only in the mid and high frequencies. It is seen that the bending wave energy distribution in the receiver room and the room pressure wave energy ratio are largely independent of which surface in the source room is mechanically excited. Theory, in which bending wave transmissions only are considered, gives fair agreement with experiment in the mid and high frequencies.

8.2 Suggestions for further work

In this attempt to apply power flow methods to noise transmission in building structures, several aspects have not been discussed, or at least, only briefly. It is thought however, that the limitations of the method have been pointed out so that it can be applied with some confidence to more complex problems than those so far discussed. The suggested topics for further research thus are as follows.

(1) As well as the bending wave energy on wall and floor surfaces, measurement could also be made of other wave types. The problem is that of differentiating between the bending wave vibration and that of longitudinal and transverse waves. Measurements could be made of the transmission of one wave type into another at junctions.

(2) A direct comparison could be made between a real structure and a quarter-scale model. A suggested configuration would be the adjacent rooms of two semi-detached houses. Measurement would be made, at full scale and quarter-scale, of the airborne sound transmission and the bending wave energy on the wall surfaces.

(3) Energy balance equations can be applied to more complex structures than those discussed. An example would be the investigation of sound transmission between rooms separated by several floors or rooms. It might be thought that the energy balance matrix would rapidly become

intractable. However, it is the very complexity of the problem which allows power flow methods to be applied meaningfully. Sub-systems such as each wall area which so far have been considered separately may be lumped together to form one sub-system. Thus, a rectangular room can be thought of as two coupled sub-systems, i.e. the total floor and wall area and the air volume enclosed. Also if the rooms form part of a two or three dimensional array, as exist in high rise buildings, a reiterative method may further simplify the analysis.

(4) The direct and indirect effect of increase in internal loss factor of materials can be investigated for real situations.

(5) The method so far described is a steady-state method. Impact noise transmission is often of a pulse like nature. Thus the techniques may be modified or replaced in order to describe transient effects.

APPENDIX I

DERIVATION OF IMPEDANCE Z_{lt} AT THE JUNCTION OF SEMI-INFINITE PLATES

The calculations of Cremer (1949) and Kihlman (1967) of the mechanical impedance of a corner junction and cross-junction, respectively, are by similar methods. Cremer's expression has the advantage that the component which gives rise to the longitudinal wave and that which gives rise to the transverse wave are clearly distinguishable. By making the simplifying assumption that the impedance of a junction with a free edge is half that of a junction without a free edge a convenient expression, describing Z_{lt} can be derived using the method of Cremer. The following derivation is thus an abbreviated form of his theory.

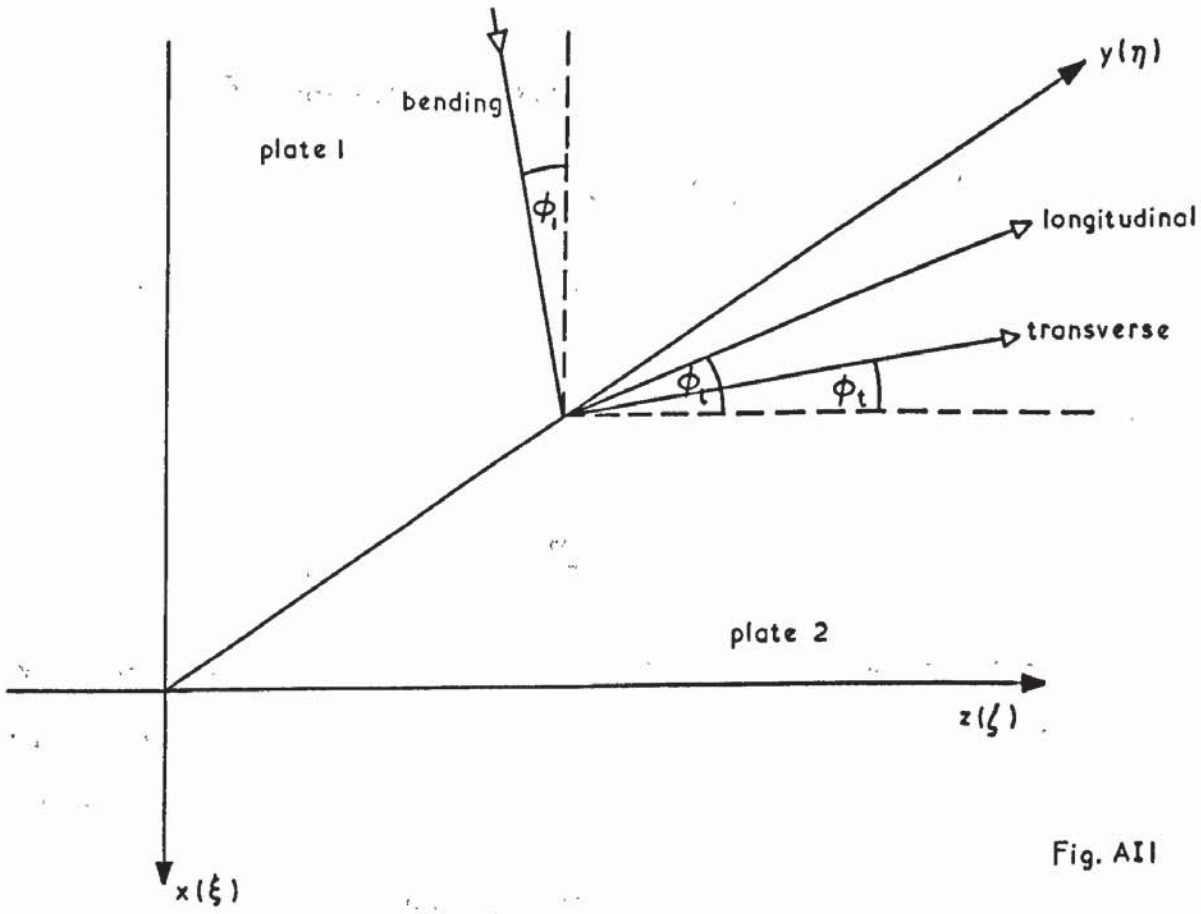

Fig. AII

A bending wave on plate 1, incident at the junction (Fig A I.1) will produce a force which will excite a longitudinal wave in plate 2. Snell's law dictates that this wave leaves the junction at an angle ϕ_l given by

$$K_l \sin\phi_l = K_1 \sin\phi_1 \qquad (1)$$

The force in the wave therefore has components in the y- and z-directions. However, since the driving force has components in the z-direction only, it is necessary to assume the excitation of a transverse wave in which the particle movement is perpendicular to the direction of propagation and parallel to the plane of the plate.

The vortex-free longitudinal wave can be described by a potential function Φ and the source-free transverse wave by a stream function ψ. Cremer expresses these functions as,

$$\Phi = \Phi_o \exp(-iK_1 y \sin\phi_1)\exp(-iz\sqrt{(K_l^2 - K_1^2 \sin^2\phi_1)}) \qquad (2)$$

$$\psi = \psi_o \exp(-iK_1 y \sin\phi_1)\exp(-iz\sqrt{(K_t^2 - K_1^2 \sin^2\phi_1)}) \qquad (3)$$

The displacements of the field are given by,

$$\eta = \frac{\partial\Phi}{\partial y} + \frac{\partial\psi}{\partial z} \qquad (4)$$

$$\zeta = \frac{\partial\Phi}{\partial z} - \frac{\partial\psi}{\partial y} \qquad (5)$$

To obtain the ratio of the quantities ψ_o and Φ_o the condition is assumed that in the yz-plane there are no shearing stresses. According to Cremer (1949, Section I 134b), this condition is given by,

$$\frac{d\zeta}{dy} + \frac{d\eta}{dz} = 0 \qquad (6)$$

Substitution of equations 2, 3, 4, and 5, into equation 6 gives at z = 0,

$$\frac{\psi_o}{\Phi_o} = \frac{-2K_1 \sin\phi_1 \sqrt{(K_l^2 - K_1^2 \sin^2\phi_1)}}{(K_t^2 - 2K_1^2 \sin^2\phi_1)} \qquad (7)$$

The particle velocity which results on plate 2 can be expressed as,

$$(V_z)_{z=0} = i\omega\zeta_{z=0} = i\omega\left[\frac{d\Phi}{dz} - \frac{d\psi}{dy}\right]_{z=0} \qquad (8)$$

Substituting equations 2, 3, and 7 into equation 8 gives

$$(V_z)_{z=0} = \omega\left[(K_l^2 - K_1^2\sin\phi_1) + \frac{2K_1^2\sin^2\phi_1\ (K_l^2 - K_1^2\sin^2\phi_1)}{(K_t^2 - 2K_1^2\sin^2\phi_1)}\right]\Phi_o \qquad (9)$$

The force in the z-direction is obtained from the stress σ_z . A general expression for stress is given by Timoshenko and Goodier (1951) as,

$$\sigma_z = \frac{E}{(1+\mu)}\left[\frac{d\zeta}{dz} + \frac{\mu}{1-2\mu}\left(\frac{d\xi}{dx} + \frac{d\eta}{dy} + \frac{d\zeta}{dz}\right)\right] \qquad (10)$$

where E is the Young's modulus of the material and μ is the Poisson's ratio.

If it is assumed that the stress is zero in the x-direction, a similar expression to equation 10 yields,

$$\frac{d\xi}{dx} = -\frac{\mu}{(1-\mu)}\left(\frac{d\eta}{dy} + \frac{d\zeta}{dz}\right) \qquad (11)$$

Substitution of equation 11 into equation 10 gives,

$$\sigma_z = \frac{E}{(1-\mu^2)}\left(\frac{d\zeta}{dz} + \mu\frac{d\eta}{dy}\right) \qquad (12)$$

Equation can now be expressed in terms of Φ_o by substituting equations 2, 3, 4, 5, and 7. The Poisson ratio inside the bracket in equation 12 can be expressed in terms of the longitudinal and transverse wave number as follows,

$$\mu = 1 - \frac{2k_l^2}{K_t^2} \tag{13}$$

The final expression of stress in the z-direction thus becomes,

$$(\sigma_z)_{z=0} = \frac{-E}{(1-\mu^2)} \frac{K_l^2}{K_t^2} \left[(K_t^2 - 2K_1^2\sin^2\phi_1) + \frac{4K_1^2\sin^2\phi_1 \sqrt{(K_t^2 - K_1^2\sin^2\phi_1)} \sqrt{(K_l^2 - K_1^2\sin^2\phi_1)}}{(K_t^2 - 2K_1^2\sin^2\phi_1)} \right] \Phi_o \tag{14}$$

The expression for impedance is,

$$Z_{lt} = \left(\frac{F_z}{V_z}\right)_{z=0} = -\left(\frac{\sigma_z h}{V_z}\right)_{z=0} \tag{15}$$

Inserting equations 9 and 14 into equation 15,

$$Z_{lt} = \frac{E K_l^2 h}{\omega (1-\mu^2) K_t^4} \left[\frac{(K_t^2 - 2K_1^2\sin^2\phi_1)^2}{\sqrt{(K_l^2 - K_1^2\sin^2\phi_1)}} + 4K_1^2\sin^2\phi_1 \sqrt{(K_t^2 - K_1^2\sin^2\phi_1)} \right] \tag{16}$$

The two terms in equation 16 indicate the subdivision of energy into the two wave components.

The first term has a square root as a denominator which becomes imaginary at an angle at which no longitudinal wave is transmitted. Instead of a

transmitted progressive wave, a rapidly decaying near field is produced. In describing this component of the impedance at angles greater than this critical angle the convention is adopted of substituting $-i\sqrt{(K_1^2\sin^2\phi_1 - K_t^2)}$ for $\sqrt{(K_t^2 - K_1^2\sin^2\phi_1)}$ in the first term of equation 16. Therefore, this term describes the energy transmitted as a longitudinal wave.

Similarly, the second term in equation 16 becomes imaginary when the limiting angle for transverse waves is exceeded and this term describes energy transmitted as a transverse wave. The transverse component which is compliance is subtracted from the longitudinal component which is a reactance above the critical angle for transverse waves. An angle therefore is attained at which the two terms cancel and the impedance effectively becomes zero. It is seen that at this angle this phenomenon is accompanied by large values of transmission coefficient of bending waves in plate 1 into bending waves in plate 3.

APPENDIX II

THE SOLUTION OF A SERIES OF LINEAR SIMULTANEOUS EQUATIONS BY CROUT'S METHOD

The following sub routine is complete or can be used dynamically as part or a larger programme.

```
'Begin'
'Integer' M, I, J, K;
M: = read;
'Comment'  This gives the number of equations to be solved;
'Begin'
'Real' 'Array'  X [ 1:M, 1:M + 1 ] ,  A [ 1:M ] ;
'For' I: = 1 'step' 1 'until' M 'do'
'For' J: = 1 'step' 1 'until' M + 1 'do'
X [ I, J ] : = read;
'Comment'  The elements may either be read into the programme, as above,
           or result from the calculation in a preceding sub routine;
'For' I: = 2 'step' 1 'until' M + 1 'do'
X [ 1, I ] : = X [ 1, I ] /X [ 1, 1 ] ;
'Comment'  X [ 1, 1 ]  is non zero;
'For' J: = 2 'step' 1 'until' M 'do'
'Begin'
        'For' I: = J 'step' 1 'until' M 'do'
        'For' K: = 1 'step' 1 'until' J - 1 'do'
        X [ I, J ] : = X [ I, J ]  - X [ I, K ] * X [ K, J ] ;
        'For' I: = J + 1 'step' 1 'until' M + 1 'do'
```

```
'Begin'
        'For' K: = 1 'step' 1 'until' J - 1 'do'
        X[J, I]: = X[J, I] - X[J, K] * X[K, I];
        X[J, I]: = X[J, I]/X[J, J];
        'end';
'end';
        A[M]: = -X[M, M + 1];
        'For' I: = M - 1 'step' -1 'until' 1 'do'
        'Begin'
                A[I]: = -X[I, M + 1];
                'For' K: = M 'step' -1 'until' I + 1 'do'
                A[I]: = A[I] - X[I,K]*A[K];
        'end';
        'Comment' The solution is given by the array A and can now be
                  output by any convenient method;
```

APPENDIX III

TABLES OF TRANSMISSION COEFFICIENTS, AS FUNCTIONS OF FREQUENCY, FOR CROSS-JUNCTIONS, T-JUNCTIONS, AND CORNERS OF REINFORCED CONCRETE PLATES

Table 1 Crossjunction h_1 = 0.2m h_2 = 0.15m

Hz.	γ_{lb}^{2b}	$\gamma_{lb}^{2l,t}$	γ_{lb}^{3b}	$\gamma_{lb}^{3l,t}$	γ_{ll}^{2b}	$\gamma_{ll}^{2l,t}$	γ_{ll}^{3b}	$\gamma_{ll}^{3l,t}$	γ_{lt}^{2b}	$\gamma_{lt}^{2l,t}$	γ_{lt}^{3b}	$\gamma_{lt}^{3l,t}$
100	4.75×10^{-2}	9.04×10^{-3}	1.12×10^{-1}	6.53×10^{-4}	2.54×10^{-2}	5.14×10^{-4}	4.2×10^{-3}	6.42×10^{-1}	2.26×10^{-2}	5.27×10^{-4}	4.12×10^{-3}	5.22×10^{-1}
125	4.81	1.09×10^{-2}	1.19	8.24	2.8	6.4	4.66	6.35	2.49	6.71	4.67	5.16
160	4.77	1.48	1.21	1.17×10^{-3}	3.08	7.96	5.15	6.27	2.74	8.55	5.28	5.08
200	4.84	1.69	1.23	1.46	3.38	9.86	5.68	6.18	3.01	1.09×10^{-3}	5.99	5.0
250	4.87	2.19	1.33	1.97	3.69	1.22×10^{-3}	6.23	6.09	3.29	1.4	6.8	4.92
315	4.91	2.71	1.41	2.58	4.02	1.5	6.8	5.98	3.59	1.8	7.4	4.82
400	4.97	3.37	1.48	3.41	4.35	1.83	7.37	5.86	3.88	2.32	8.82	4.71
500	5.07	3.98	1.57	4.45	4.69	2.23	7.93	5.73	4.18	3.02	1.01×10^{-2}	4.59
630	5.26	5.09	1.66	6.12	5.03	2.69	8.44	5.59	4.46	3.94	1.15	4.46
800	5.51	6.13	1.79	8.24	5.35	3.22	8.87	5.43	4.7	5.2	1.33	4.32
1k	5.91	7.48	1.91	1.13×10^{-2}	5.65	3.82	9.2	5.26	4.9	6.94	1.53	4.17
1.25	6.56	9.24	2.01	1.62	5.9	4.49	9.37	5.07	5.0	9.42	1.78	4.02
1.6k	7.54	1.14×10^{-1}	2.1	2.34	6.08	5.24	9.34	4.86	5.0	1.31×10^{-2}	2.08	3.85
2k	9.01	1.44	2.13	3.51	6.16	6.09	9.08.	4.63	4.85	1.86	2.44	3.68
2.5k	1.11×10^{-1}	1.83	2.08	5.52	6.1	7.05	8.54	4.37	4.57	2.74	2.85	3.52
3.15	1.4	2.31	1.92	7.0	5.88	8.22	7.69	4.08	4.28	3.97	3.13	3.35

Table 2 Crossjunction $h_1 = 0.15m$ $h_2 = 0.2m$

Hz.	γ^{2b}_{lb}	γ^{2l}_{lb}	γ^{3b}_{lb}	$\gamma^{3l,t}_{lb}$	γ^{2b}_{ll}	$\gamma^{2l,t}_{ll}$	γ^{3b}_{ll}	$\gamma^{3l,t}_{ll}$	γ^{2b}_{lt}	$\gamma^{2l,t}_{lt}$	γ^{3b}_{lt}	$\gamma^{3l,t}_{lt}$
100	3.93×10^{-2}	4.21×10^{-3}	3.03×10^{-2}	1.26×10^{-3}	3.8×10^{-2}	4.66×10^{-4}	7.8×10^{-3}	6.05×10^{-1}	3.33×10^{-2}	4.61×10^{-4}	7.38×10^{-3}	4.89×10^{-1}
125	3.97	4.89	3.25	1.51	4.16	5.77	8.57	5.94	3.65	5.77	8.2	4.79
160	4.0	6.71	3.47	2.13	4.55	7.11	9.38	5.81	3.98	7.22	9.09	4.68
200	3.99	8.82	3.76	2.87	4.94	8.75	1.02×10^{-2}	5.68	4.34	9.02	1.01×10^{-2}	4.56
250	4.05	1.07×10^{-2}	4.11	3.71	5.35	1.07×10^{-3}	1.11	5.53	4.7	1.13×10^{-3}	1.11	4.43
315	4.13	1.36	4.6	5.0	5.76	1.31	1.2	5.37	5.07	1.41	1.22	4.28
400	4.24	1.71	4.96	6.64	6.17	1.6	1.29	5.19	5.44	1.76	1.34	4.12
500	4.48	2.19	5.54	9.15	6.56	1.94	1.38	5.0	5.79	2.19	1.47	3.94
630	4.8	2.73	6.21	1.24×10^{-2}	6.91	2.34	1.46	4.79	6.1	2.73	1.6	3.75
800	5.28	3.41	6.86	1.7	7.21	2.82	1.54	4.56	6.37	3.41	1.73	3.54
1k	6.07	4.48	7.86	2.4	7.42	3.37	1.59	4.31	6.55	4.25	1.86	3.32
1.25	7.19	5.58	8.74	3.47	7.53	4.0	1.63	4.04	6.63	5.3	1.99	3.08
1.6k	8.72	7.17	9.71	5.1	7.47	4.73	1.64	3.75	6.56	6.62	2.09	2.84
2k	1.08×10^{-1}	9.29	1.06×10^{-1}	7.69	7.22	5.56	1.61	3.44	6.31	8.29	2.17	2.58
2.5k	1.32	1.22×10^{-1}	1.12	1.16×10^{-1}	6.75	6.52	1.55	3.1	5.84	1.04×10^{-2}	2.2	2.32
3.15	1.48	1.51	1.2	1.55	5.99	7.66	1.45	2.73	5.14	1.3	2.16	2.08

Table 3 T-junction h_1 = 0.2m h_2 = 0.15m

Hz.	γ_{lb}^{2b}	$\gamma_{lb}^{2l,t}$	γ_{lb}^{3b}	$\gamma_{lb}^{3l,t}$	γ_{ll}^{2b}	$\gamma_{ll}^{2l,t}$	γ_{ll}^{3b}	$\gamma_{ll}^{3l,t}$	γ_{lt}^{2b}	$\gamma_{lt}^{2l,t}$	γ_{lt}^{3b}	$\gamma_{lt}^{3l,t}$
100	7.06×10^{-2}	3.04×10^{-2}	1.55×10^{-1}	2.58×10^{-4}	3.18×10^{-2}	7.59×10^{-4}	1.63×10^{-3}	6.7×10^{-1}	2.69×10^{-2}	8.68×10^{-4}	1.86×10^{-3}	5.51×10^{-1}
125	7.07	3.65	1.59	3.27	3.54	9.48	1.83	6.65	2.98	1.12×10^{-3}	2.17	5.47
160	7.08	4.43	1.64	4.23	3.92	1.18×10^{-3}	2.05	6.61	3.3	1.46	2.55	5.43
200	7.11	5.28	1.69	5.43	4.34	1.46	2.29	6.55	3.63	1.92	3.02	5.39
250	7.16	6.3	1.76	7.0	4.79	1.81	2.56	6.49	3.98	2.53	3.59	5.34
315	7.21	7.45	1.84	9.06	5.26	2.23	2.86	6.43	4.35	3.36	4.32	5.28
400	7.28	8.78	1.94	1.18×10^{-3}	5.75	2.72	3.17	6.36	4.71	4.52	5.25	5.22
500	7.37	1.03×10^{-1}	2.06	1.54	6.24	3.3	3.51	6.28	5.07	6.17	6.46	5.15
630	7.51	1.2	2.2	2.04	6.72	3.98	3.85	6.19	5.38	8.58	8.07	5.08
800	7.7	1.39	2.36	2.72	7.17	4.75	4.2	6.09	5.63	1.22×10^{-2}	1.03×10^{-2}	5.01
1k	7.99	1.62	2.53	3.7	7.55	5.62	4.53	5.99	5.77	1.8	1.34	4.93
1.25k	8.44	1.89	2.73	5.11	7.84	6.59	4.82	5.87	5.74	2.79	1.81	4.85
1.6k	9.12	2.19	2.92	7.22	7.99	7.68	5.05	5.75	5.47	4.62	2.6	4.78
2k	1.02×10^{-1}	2.58	3.1	1.05×10^{-2}	7.95	8.91	5.19	5.62	4.93	8.59	4.12	4.73
2.5k	1.18	3.08	3.22	1.6	7.67	1.04×10^{-2}	5.2	5.48	4.11	2.1×10^{-1}	8.4	4.73
3.15	1.41	3.8	3.26	2.58	7.09	1.22	5.03	5.33	3.56	3.35	1.27×10^{-1}	4.73

Table 4 T-junction where incident wave is on the cantilevered plate $h_1 = 0.15m$ $h_2 = 0.2m$

Hz.	γ_{lb}^{2b}	$\gamma_{lb}^{2l,t}$	γ_{ll}^{2b}	$\gamma_{ll}^{2l,t}$	γ_{lt}^{2b}	$\gamma_{lt}^{2l,t}$
100	5.7×10^{-2}	3.72×10^{-3}	3.63×10^{-2}	1.0×10^{-6}	3.33×10^{-2}	4.61×10^{-4}
125	5.69	4.67	4.01	2.0	3.65	5.77
160	5.73	5.9	4.41	3.0	3.98	7.22
200	5.81	7.4	4.84	5.0	4.34	9.02
250	5.96	9.31	5.3	7.0	4.7	1.13×10^{-3}
315	6.3	1.17×10^{-2}	5.77	9.0	5.07	1.41
400	6.73	1.46	6.26	1.3×10^{-5}	5.44	1.76
500	7.45	1.84	6.74	1.7	5.79	2.19
630	8.59	2.3	7.22	2.3	6.1	2.73
800	1.01×10^{-1}	2.87	7.66	2.8	6.37	3.41
1k	1.19	3.59	8.04	3.1	6.55	4.25
1.25k	1.39	4.53	8.32	3.0	6.63	5.3
1.6k	1.55	5.82	8.46	2.1	6.56	6.62
2k	1.58	7.84	8.39	7.0×10^{-6}	6.31	8.29
2.5k	1.44	1.13×10^{-1}	8.04	1.0×10^{-5}	5.84	1.04×10^{-2}
3.15k	1.14	1.72	7.33	1.49×10^{-4}	5.14	1.3

Table 5 T-junction h_1 = 0.15m h_2 = 0.15m

Hz.	γ_{lb}^{2b}	$\gamma_{lb}^{2l,t}$	γ_{lb}^{3b}	$\gamma_{lb}^{3l,t}$	γ_{ll}^{2b}	$\gamma_{ll}^{2l,t}$	γ_{ll}^{3b}	$\gamma_{ll}^{3l,t}$	γ_{lt}^{2b}	$\gamma_{lt}^{2l,t}$	γ_{lt}^{3b}	$\gamma_{lt}^{3l,t}$
100	9.35×10^{-2}	1.98×10^{-2}	1.04×10^{-1}	4.18×10^{-4}	3.67×10^{-2}	9.53×10^{-4}	3.07×10^{-3}	6.62×10^{-1}	3.11×10^{-2}	9.75×10^{-4}	3.09×10^{-3}	5.44×10^{-1}
125	9.36	2.42	1.06	5.35	4.08	1.2×10^{-3}	3.45	6.56	3.45	1.25×10^{-3}	3.54	5.39
160	9.36	2.97	1.08	6.87	4.53	1.51	3.88	6.5	3.81	1.6	4.07	5.34
200	9.38	3.61	1.11	8.87	5.01	1.9	4.36	6.44	4.19	2.06	4.69	5.29
250	9.4	4.38	1.15	1.14×10^{-3}	5.52	2.38	4.89	6.36	4.6	2.67	5.44	5.23
315	9.43	5.32	1.2	1.48	6.06	2.98	5.48	6.28	5.03	3.47	6.32	5.16
400	9.48	6.41	1.26	1.92	6.63	3.73	6.13	6.19	5.47	4.54	7.4	5.08
500	9.55	7.68	1.33	2.5	7.2	4.65	6.84	6.09	5.9	5.99	8.7	5.0
630	9.67	9.24	1.42	3.31	7.75	5.78	7.59	5.98	6.32	7.98	1.03×10^{-2}	4.91
800	9.85	1.10×10^{-1}	1.53	4.4	8.27	7.16	8.39	5.86	6.68	1.08×10^{-2}	1.23	4.81
1k	1.01×10^{-1}	1.31	1.66	5.93	8.7	8.82	9.21	5.73	6.97	1.48	1.5	4.7
1.25	1.06	1.56	1.81	8.1	9.02	1.08×10^{-2}	1.0×10^{-2}	5.59	7.11	2.09	1.83	4.59
1.6k	1.13	1.87	1.98	1.13×10^{-2}	9.15	1.31	1.07	5.44	7.07	3.05	2.29	4.47
2k	1.24	2.23	2.15	1.62	9.05	1.59	1.13	5.28	6.78	4.66	2.96	4.36
2.5k	1.4	2.68	2.31	2.41	8.65	1.91	1.17	5.11	6.2	7.61	4.02	4.26
3.15k	1.62	3.26	2.42	3.76	7.91	2.28	1.17	4.93	5.35	1.37×10^{-1}	5.92	4.17

Table 6 T-junction where incident wave is on the cantilevered plate h_1 = 0.15m h_2 = 0.15m

Hz.	γ_{lb}^{2b}	$\gamma_{lb}^{2l,t}$	γ_{ll}^{2b}	$\gamma_{ll}^{2l,t}$	γ_{lt}^{2b}	$\gamma_{lt}^{2l,t}$
100	8.99×10^{-2}	4.29×10^{-3}	2.47×10^{-2}	1.0×10^{-6}	2.54×10^{-2}	4.84×10^{-4}
125	8.95	5.4	2.74	2.0	2.8	6.1
160	8.9	6.81	3.04	2.0	3.08	7.7
200	8.88	8.54	3.36	4.0	3.38	9.73
250	8.87	1.07×10^{-2}	3.7	5.0	3.69	1.23×10^{-3}
315	8.94	1.35	4.07	7.0	4.01	1.55
400	9.09	1.69	4.47	1.0×10^{-5}	4.34	1.97
500	9.4	2.14	4.89	1.4	4.66	2.5
630	9.96	2.69	5.31	1.7	4.97	3.18
800	1.08×10^{-1}	3.39	5.15	2.1	5.26	4.06
1k	1.22	4.27	6.17	2.2	5.5	5.21
1.25k	1.42	5.39	6.57	2.0	5.67	6.72
1.6k	1.67	6.83	6.92	1.1	5.73	8.74
2k	1.97	8.75	7.17	2.0×10^{-6}	5.67	1.15×10^{-2}
2.5k	2.24	1.16×10^{-1}	7.28	3.3×10^{-5}	5.45	1.53
3.15k	2.33	1.64	7.19	2.84×10^{-4}	5.06	2.08

Table 7 $h_1 = 0.15m$ $h_2 = 0.2m$ Corner junction

Hz.	γ_{1b}^{2b}	$\gamma_{1b}^{2l,t}$	γ_{1l}^{2b}	$\gamma_{1l}^{2l,t}$	γ_{1}^{2b}	$\gamma_{1}^{2l,t}$
100	1.62×10^{-1}	1.3×10^{-2}	4.71×10^{-2}	1.23×10^{-3}	4.01×10^{-2}	1.2×10^{-3}
125	1.61	1.63	5.21	1.55	4.43	1.52
160	1.59	2.05	5.75	1.96	4.87	1.94
200	1.58	2.56	6.32	2.47	5.34	2.48
250	1.57	3.21	6.93	3.11	5.84	3.18
315	1.56	4.04	7.55	3.93	6.35	4.08
400	1.57	5.05	8.19	4.96	6.87	5.27
500	1.59	6.31	8.81	6.24	7.38	6.84
630	1.64	7.93	9.38	7.87	7.85	8.95
800	1.74	9.94	9.86	9.91	8.25	1.18×10^{-2}
1k	1.89	1.25×10^{-1}	1.02×10^{-1}	1.25×10^{-2}	8.55	1.58
1.25k	2.12	1.56	1.03	1.57	8.68	2.16
1.6k	2.46	1.97	1.02	1.97	8.59	3.01
2k	2.9	2.48	9.74×10^{-2}	2.46	8.22	4.34
2.5k	3.4	3.13	8.85	3.08	7.53	6.5
3.15k	3.73	4.11	7.54	3.83	6.54	1.01×10^{-1}

Table 8 Corner junction h_1 = 0.15m h_2 = 0.15m

Hz.	γ_{lb}^{2b}	$\gamma_{lb}^{2l,t}$	γ_{ll}^{2b}	$\gamma_{ll}^{2l,t}$	γ_{lt}^{2b}	$\gamma_{lt}^{2l,t}$
100	2.05×10^{-1}	1.47×10^{-2}	3.67×10^{-2}	9.53×10^{-4}	3.11×10^{-2}	9.75×10^{-4}
125	2.04	1.83	4.08	1.2×10^{-3}	3.45	1.25×10^{-3}
160	2.02	2.31	4.53	1.51	3.81	1.6
200	2.0	2.87	5.01	1.9	4.19	2.06
250	1.98	3.59	5.52	2.38	4.6	2.67
315	1.96	4.51	6.06	2.98	5.03	3.47
400	1.94	5.63	6.63	3.73	5.47	4.54
500	1.91	7.03	7.2	4.65	5.9	5.99
630	1.9	8.82	7.75	5.78	6.32	7.98
800	1.89	1.11×10^{-1}	8.27	7.16	6.68	1.08×10^{-2}
1k	1.92	1.39	8.7	8.82	6.97	1.48
1.25k	1.99	1.75	9.02	1.08×10^{-2}	7.11	2.09
1.6k	2.13	2.23	9.15	1.31	7.07	3.05
2k	2.37	2.84	9.05	1.59	6.78	4.66
2.5k	2.74	3.65	8.65	1.91	6.2	7.61
3.15k	3.27	4.75	7.91	2.28	5.35	1.37×10^{-1}

REFERENCES

BERANEK L L and WORK G A (1949): "Sound transmission through multiple structures containing flexible blankets", J Acoust Soc Am 21 (4) p 419.

BERENDT R D and WINIZER G E (1964): "Sound insulation of wall, floor, and door constructions", Nat Bur Stand, Monograph.

BERT C W (1973): "Material damping", J Sound Vib 29 (2) p 129.

BHATTACHARYA M C and CROCKER M J (1969/70): "Forced vibration of a panel and radiation of sound into a room", Acustica 22 p 275.

BHATTACHARYA M C and MULHOLLAND K A (1971): "Forced vibration of a panel and radiation of sound into a room cavity", Acustica 24 p 354.

BHATTACHARYA M C, GUY R W, and CROCKER M J (1971): "Coincidence effect with sound waves in a finite plate", J Sound Vib 18 (2) p 157.

BHATTACHARYA M C, MULHOLLAND K A, and CROCKER M J (1971): "Propagation of sound energy by vibration transmission via structural junctions", J Sound Vib 18 (2) p 221.

BOLT R H (1939): "Frequency distribution of eigentones in a three-dimensional continuum", J Acoust Soc Am 10 p 228.

BRANDT O (1954): "Some measurements on lightweight double walls", Acustica 4 p 270.

BRILLOUIN J (1952): "Problemes de rayonnement en acoustique du batiment", Acustica 2 p 65.

BRITISH STANDARD 2750 (1956): "Recommendations for field and laboratory measurement of airborne and impact sound transmission in buildings"

BRITISH STANDARD 3638 (1963): "Method for the measurement of sound absorption coefficients (I.S.O) in a reverberation room"

BUDRIN S V and NIKIFOROV A S (1964): "Wave transmission through assorted plate joints", Sov Phys Acoust 9 (4) p 333.

BURD A N (1964): "Correlation techniques in studio testing", Radio Electron Engr 27 (5) p 389.

BURD A N (1968): "The measurement of sound insulation in the presence of flanking paths", J Sound Vib 7 (1) p 13.

CRANDALL S H and LOTZ R (1971): "On the coupling loss factor in statistical energy analysis", J Acoust Soc Am 49 (1) Pt 2 p 352.

CREMER L (1942): "Theorie der Schall dämmung dünner Wände bei Schrägen Einfall", Akustiche Zeitschrift 7 p 81.

CREMER L (1948): "The propagation of structure-borne sound", Dept Sci Ind Res Rep No 1 Ser B.

CREMER L (1954): "Berechnung der wirkung von schallbrücken", Acustica 4 p 273.

CREMER L and HECKL M (1967): "Körperschall", Berlin: Springer-Verlag.

CROCKER M J and PRICE A J (1969): "Sound transmission using statistical energy analysis", J Sound Vib 9 (3) p 469.

CUMMINGS A and MULHOLLAND K A (1968): "The transmission loss of finite sized double panels in a random incidence sound field", J Sound Vib 8 (1) p 126.

DAVIES H G (1972): "Exact solutions for the response of some coupled multimodal systems", J Acoust Soc Am 51 (1) Pt 2 p 387.

DAVIES H G (1972): "Power flow between two coupled beams", J Acoust Soc Am 51 (1) Pt 2 p 393.

DAVIES H G (1973): "Random vibration of distributed systems strongly coupled at discrete points", J Acoust Soc Am 54 (2) p 507.

DYER I (1960): "Moment impedance of plates", J Acoust Soc Am 32 (10) p 1290.

DONATO R J (1972): "Sound transmission through a double-leaf wall", J Acoust Soc Am 51 (3) Pt 1 807.

EICHLER E (1964): "Plate-edge admittances", J Acoust Soc Am 36 (2) p 344.

EICHLER E (1965): "Thermal circuit approach to vibrations in coupled systems and the noise reduction of a rectangular box", J Acoust Soc Am 37 (6) p 995.

EIJK J and KASTELEYN M L (1955): "A method of measuring flanking transmission in flats", Acustica 5 p 263.

EXNER M L and BOHME W (1953): "Messung der Körperschalldämmung bei biegewellen", Acustica 3 p 105.

EYRING C F (1930): "Reverberation time in dead rooms", J Acoust Soc Am 1 p 217.

FAHY F J and WEE R B S (1968): "Some experiments with stiffened plates under acoustic excitation", J Sound Vib 7 (3) p 431.

FAHY F J (1969): "Vibration of containing structures by sound in the contained fluid", Jnl Engng Ind 91 (4) p 939.

FAHY F J (1969): "Vibration of containing structures by sound in the contained fluid", J Sound Vib 10 (3) p 490.

FORD R D, LORD P and WALKER A W (1967): "Sound transmission through sandwich constructions", J Sound Vib 5 (1) p 9.

FORD R D, LORD P and WILLIAMS P C (1967): "The influence of absorbent linings on the transmission loss of double-leaf partitions", J Sound Vib 5 (1) p 22.

GERSCH W (1969): "Average power and power exchange in oscillators", J Acoust Soc Am 46 (5) Pt 2 p 1180.

GOFF K W (1955): "An analogue electronic correlator for acoustic measurements", J Acoust Soc Am 27 (2) p 223.

GÖSELE K (1953): "Schallabstrahlung von platten die zu biegeschwingungen augeregt sind", Acustica 3 p 243.

GÖSELE K (1965): "Uber prüfstände zur messung der luftschalldämmung von wänden und decken", Acustica 15 p 317.

GÖSELE K (1968): "Zur luftschalldämmung von einschaligen wänden und decken", Acustica, 20 p 334.

GREENE D C (1961): "Vibration and sound radiation of damped and undamped flat plates", J Acoust Soc Am 33 (10) p 1315.

HART F D, SHAH K C (1971): "Compendium of modal densities for structures", NASA Contractors Report CR - 1773.

HARWOOD H D and BURD A N (1973): "Acoustic scaling of studios and concert halls", Acustica 26 (6) p 330.

HECKL M (1959): "Schallabstrahlung von platten bei punktförmiger anregung", Acustica 9 (5) p 371.

HECKL M (1960): "Die schalldämmung von homogenen einfachwänden endlicher fläche", Acustica 10 (2) p 98.

HECKL M A (1962): "Measurement of absorption coefficients on plates", J Acoust Soc Am 34 (6) p 803.

HECKL M and RATHE E J (1963): "Relationship between the transmission loss and the impact - noise isolation of floor structures", J Acoust Soc Am 35 (11) p 1825.

HECKL M A (1964): "Investigations on the vibrations of grillages and other simple beam structures", J Acoust Soc Am 36 (7) p 1335.

HINSCH H (1960): "Verkettete mechanische impedanzen zur messung der Körperschalldämmung an ecken und Kreuzförmigen stoss-stellen (modell-versuche)", Acustica 10 (4) p 287.

HUDSON R R and MULHOLLAND K A (1971): "The measurement of high transmission loss (the brick wall experiment)", Acustica 24 p 251 (5).

HUNT F V (1939): "Investigation of room acoustics by steady-state transmission measurements", J Acoust 10 (3) p 216.

INGEMANSSON S (1969): "The effects of connections on the sound reduction factor of double walls. Investigations on models.", National Swedish Building Research Summaries 1969.

JOSSE R and LAMURE C (1964): "Sound transmission through a simple partition", Acustica 14 p 266.

KENNEDY C C and PANCU C D F (1947): "Use of vectors in vibration measurement and analysis", J Aero Sci 14 (11) p 603.

KHABBAZ G R (1970): "Comparison of mechanical coupling factor by two methods", J Acoust Soc Am 47 p 392.

KIHLMAN T (1967): "Transmission of structure-borne sound in buildings. A theoretical and experimental investigation.", Publication by Nat. Swedish Inst for Building Research. Report 9: 1967 UDC 699.844.

KIHLMAN T (1967): "Sound radiation into a rectangular room. Applications to airborne sound transmission in buildings", Acustica 18 (1) p 11.

KIHLMAN T (1970): "Report on the influence of boundary conditions in the reduction index", Chalmers Technical Report, ISO/TC43/SC2/WG2.

KIHLMAN T (1970): "Sound transmission in building structures of concrete", J Sound Vib 11 (4) p 435.

KOST A (1967): "Modelluntersuchungen zur theorie der einfachwand", Acustica 18 (6) p 342.

KUHL W and KAISER H (1952): "Absorption of structure-borne sound in building materials without and with sand-filled cavities", Acustica 2 (4) p 179.

KURTZE G, TAMM K and VOGEL S (1955): "Modellversuche zur biege wellendämmung an ecken", Acustica 5 (4) p 223.

KURTZE G and BOLT R H (1959): "On the interaction between plate bending waves and their radiation load", Acustica 9 p 238.

KURTZE G and WATTERS B G (1959): "New wall design for high transmission loss or high damping", J Acoust Soc Am 31 (6) p 739.

LAZAN B J: "Damping of materials and members in structural mechanics" New York: Pergamon Press.

LONDON A (1941): "Measurements of sound transmission loss in the field", J Res Natn Bur Stand 26 p 419.

LONDON A (1950): "Transmission of reverberant sound through double walls", J Acoust Soc Am 22 (2) p 270.

LOTZ R, CRANDALL S H (1973): "Prediction and measurement of the proportionality constant in statistical energy analysis of structures", J Acoust Soc Am 54 (2) p 516.

LYON R H and MAIDANIK G (1962): "Power flow between linearly coupled oscillators", J Acoust Soc Am 34 (5) p 623.

LYON R H (1963): "Noise reduction of rectangular enclosures with one flexible wall", J Acoust Soc Am 35 (11) p 1791.

LYON R H and EICHLER E (1964): "Random vibration of connected structures", J Acoust Soc Am 36 (7) p 1344.

LYON R H and SCHARTON T D (1965): "Vibrational energy transmission in a three-element structure", J Acoust Soc Am 38 (2) p 253.

LYON R H and SCHARTON T D (1966): J Acoust Soc Am 39 p 755.

DAH-YOU MAA (1939): "Distribution of eigentones in a rectangular chamber at low frequency range", J Acoust Soc Am 10 p 235.

MAIDANIK G (1962): "Response of ribbed panels to reverberant acoustic fields", J Acoust Soc Am 34 (6) p 809.

MARTIN R and MULLER H W (1956): "Uber Körperschalluntersuchungen in Wohnbauten", Acustica (Akustische Beihefte) 6 p 89.

MERCER C A, REES P L and FAHY F J (1971): "Energy flow between two weakly coupled oscillators subject to transient excitation", J Sound Vib 15 (3) p 373.

MEYER E, PARKIN P H, OBERST H, and PURKIS H J (1951): "A tentative method for the measurement of indirect sound transmission in buildings", Acustica 1 p 17.

MINDLIN R D (1951): "Influence of rotatory inertia and shear on flexural motions of isotropic, elastic plates", I Appl Mech 73 p 31.

MORSE P and BOLT R H (1944): "Sound waves in rooms", Review of Modern Physics 16 p 137.

MORSE P M and INGARD K V (1968): "Theoretical acoustics", McGraw Hill.

MUGIONO (1955): "Messungen der reflexion von biegewellen an queschnittssprüngen auf stäben", Acustica 5 (3) p 182.

MULHOLLAND K A, PARBROOK H D, CUMMINGS A (1967): "The transmission loss of double panels", J Sound Vib 6 (3) p 324.

NELSON H M (1971): "A universal dispersion curve for flexural wave propagation in plates and bars", J Sound Vib 18 (1) p 93.

NELSON H M (1972): "The modal density for flexural vibration of thick plates and bars", J Sound Vib 25 (2) p 255.

NEWLAND D E (1966): "Comment on 'Vibrational Energy Transmission in a three-element structure' ", J Acoust Soc Am 39 p 755.

NEWLAND D E (1966): "Calculation of power flow between coupled oscillators", J Sound Vib 3 (3) p 262.

NEWLAND D E (1968): "Power flow between a class of coupled oscillators", J Acoust Soc Am 43 (3) p 553.

NILSSON A C (1971): "Sound transmission between two rectangular rooms", Chalmers Technical Report 71-01.

NOLL G G (1971): "Frequency dependency of complex elastic constants of some building materials between approximately 5 and 100 kHz", Acustica 24 p 93.

PARKIN, PURKIS, and SCHOLES (1960): "Field measurement of sound insulation between dwellings", National Building Studies Research Paper No 33.

PAUL M (1968): "Die messung von transmissionsgraden bei schallübertritt von stäben auf platten", Acustica 20 (1) p 36.

PEUTZ V M A (1954): "Some fundamental measurements on single and double plate structures", Acustica 4 p 281.

PISARENKO G S (1962): "Dissipation of energy during mechanical vibration", Academy of Sciences of the Ukraine S.S.R Kiev.

PRICE A J and CROCKER M J (1970): "Sound transmission through double panels using statistical energy analysis", J Acoust Soc Am 47 (3) Pt 1 p 683.

PURKIS H J and PARKIN P H (1952): "Indirect sound transmission with joist and solid floors", Acustica 2 (6) p 237.

PUTT R A (1970): "Sound transmission and prestressed concrete", Final year project in the Department of Building, Aston University.

RAES A C (1955): "Tentative method for the measurement of sound transmission losses in unfinished buildings", J Acoust Soc Am 27 p 98.

RAYLEIGH J W S (1877): "The theory of sound", Dover Publications, New York.

REICHARDT von W and RICHTER U (1970): "Unterschieduche transmissionsgrade für die Biegewellenübertragung an einer recktwinkligen Wandecke in Abhängigkeit von der Durchtrittsricktung", Acustica 23 p 16.

ROMANOV V N (1969): "Investigation of a plate T-junction in a diffuse flexural wave field", Sov Phys Acoust 15 p 234.

RUPPRECHT J (1958): "Körperschallausbreitung in baukörpen aus homogon und zusammengesetzten baustoffen", Acustica 8 p 19.

SCHARTON T D and LYON R H (1968): "Power flow and energy sharing in random vibration", J Acoust Soc Am 43 (6) p 1332.

SCHLOSS F and READER W T (1967): "Measurements of the effect of geometric scale on structural impedance and radiated sound", J Acoust Soc Am 41 (5) p 1193.

SCHMIDT R (1934): "Dämpfungsmessungen an schallwellen in festen Körpen", Ing Arch 5 p 352.

SCHOCH A and FEHER K (1952): "The mechanism of sound transmission through single leaf partitions investigated using small scale models", Acustica 2 (5) p 189.

SEWELL E C (1970): "Transmission of reverberent sound through a single-leaf partition surrounded by an infinite rigid baffle", J Sound Vib 12 (1) p 21.

SEWELL E C: "Two dimensional solution for transmission of reverberant sound through a double partition", J Sound Vib 12 (1) p 33.

SHARP B H S and BEAUCHAMP J W (1969): "The transmission loss of multilayer structures", J Sound Vib 9 (3) p 383.

SMITH P W (1964): "Coupling of sound and panel vibrations below the critical frequency", J Acoust Soc Am 36 (8) p 1516.

SNOWDON J C (1968): "Vibration and shock in damped mechanical systems", Wiley Inc, New York.

SOMERVILLE T and WARD F L (1951): "Investigation of sound diffusion in rooms by means of a model", Acustica 1 (1) p 40.

STEARN S M (1970): "Spatial variation of stress, strain and acceleration in structures subject to broad frequency band excitation", J Sound Vib 12 (1) p 85.

TIMOSHENKO S (1921): "On the correction for shear of the differential equation for transverse vibrations of prismatic bars", Phil Mag 41 series 6 p 744.

TIMOSHENKO S (1940): "Theory of plates and shells", McGraw-Hill Book Company Inc, New York.

TIMOSHENKO S and GOODIER J N (1951): "Theory of elasticity", McGraw-Hill Book Company 2nd ed, New York.

UNGAR E E and SCHARTON T D (1967): "Analysis of vibration distributions in complex structures", Shock Vibr Bull. 36 (5) p 41.

UTLEY W A and MULHOLLAND K A (1967): "Measurement of transmission loss using vibration transducers", J Sound Vib 6 (3) p 419.

UTLEY W A (1968): "Single leaf transmission loss at low frequencies", J Sound Vib 8 (2) p 256.

VÉR I L (1971): "Relation between the normalised impact sound level and sound transmission loss", J Acoust Soc Am 50 (6) Pt 1 p 1414.

WARBURTON G B (1953): "The vibration of rectangular plates", Proc Inst Mech Engrs 168 p 371.

WARD F (1963): "The accelerometer pick-up as a diagnostic tool in noise studies in buildings", BBC Research Department Report No B.078, serial number 1963/37.

WATERHOUSE R V (1954): "Transmission of reverberant sound through walls", Acustica 4 p 290.

WATTERS B G (1959): "The transmission loss of some masonry walls", J Acoust Soc Am 31 (7) p 898.

WATTERS B G (1959): "The transmission loss of some masonry walls" J Acoust Soc Am 31 (7) p 898.

WENTE E C (1935): "Characteristics of sound transmission in rooms", J Acoust Soc Am 7 p 123.